UAB
Universitat Autònoma de Barcelona

Role of p38α in UVB-induced melanoma development, progression and immune response regulation

Paula Granado Martínez

ADVERTIMENT. L'accés als continguts d'aquesta tesi queda condicionat a l'acceptació de les condicions d'ús establertes per la següent llicència Creative Commons: https://creativecommons.org/licenses/?lang=ca

ADVERTENCIA. El acceso a los contenidos de esta tesis queda condicionado a la aceptación de las condiciones de uso establecidas por la siguiente licencia Creative Commons: https://creativecommons.org/licenses/?lang=es

WARNING. The access to the contents of this doctoral thesis it is limited to the acceptance of the use conditions set by the following Creative Commons license: https://creativecommons.org/licenses/?lang=en

PhD Thesis

Role of p38α in UVB-induced melanoma development, progression and immune response regulation

Presented by:

Paula Granado Martínez

PhD Program in Biochemistry, Molecular Biology and Biomedicine

Biochemistry and Molecular Biology Department

Universitat Autònoma de Barcelona (UAB)

2024

THESIS DIRECTOR	PhD CANDIDATE	ACADEMIC TUTOR
Dr. Juan Ángel Recio Conde	Paula Granado Martínez	Dr. José Miguel Lizcano de Vega

“Questions of science,
science in progress”

Coldplay – The scientist

ACKNOWLEDGMENTS

Es increíble que este capítulo de mi vida haya llegado a su fin. Han pasado tantas cosas. Sin duda, todas las alegrías, penas, risas, torpezas, issues, lágrimas, pocas horas de sueño, experiencias y amistades que me llevo conmigo han hecho de mi la persona que soy hoy. Y no podría estar más orgullosa de cada una de estas cosas. Aunque los obstáculos que me he ido encontrando por el camino a veces no me permitieron disfrutar plenamente del momento, a día de hoy puedo decir que ha sido una de las mejores experiencias de mi vida. Y, sin duda, no podría haberlo logrado sola.

Se que he sido muy pesada estos últimos seis años, por ello no podía faltar agradecer a todas aquellas personas que me han acompañado en este viaje llamado tesis. Quien bien me conoce sabe que las palabras no son lo mío. Aun así, me he esforzado mucho para que se me deshiele este corazoncito y agradeceros todo lo que habéis hecho por mí.

Quiero empezar dando las gracias a **Kelle**, por confiar en mi desde el primer día. Gracias por haberme dado la oportunidad de convertirme en la científica que soy hoy. Por haberme dado la autonomía que he tenido durante todos estos años. Por haberme ayudado siempre que lo he necesitado, incluso durante mi ausencia por esa rodilla rota que había que arreglar. Por haberme enseñado todo lo que has podido y haberme hecho pensar mucho, siempre con criterio científico. Por haber dejado en mis manos a todos esos ratones con total confianza. Gracias por haber hecho que esta (dura) experiencia haya sido mucho más fácil y llevadera.

Evidentemente, todo este trabajo no podría haberlo realizado sin la ayuda y apoyo de todo el Kelle's lab. **Yuxin**, gracias por dejarme enseñarte durante el máster y haberte atrevido a seguir con una parte de este proyecto. **Roberto**, gracias por haberme dejado enseñarte todo mi conocimiento ratonil y haber estado siempre tan dispuesto a todo. Estoy súper convencida de que los dos acabaréis con una tesis increíble. En especial, gracias a **Kim**, por haberme enseñado prácticamente todo lo que he aprendido en este laboratorio, por haberme ayudado y apoyado siempre. Me siento muy afortunada de haberte conocido y poder considerarte mi amiga. Te admiro, por tu trabajo, pero también por lo buena persona y generosa que eres. Creo que, si hubiera pedido una compañera de lab hecha a medida, no habría sido mejor que tú. De verdad que no sé qué hubiéramos hecho ni mis células ni yo todos estos años sin ti.

Mª José, **Pedro Fuentes**, **Pedro J. Guijarro** y **Yoelsis**, gracias por acogerme desde el principio cuando llegué al VHIR siendo casi una niña. Por todos esos cafés eternos que nos hacíamos sin falta a las 10:30 de la mañana.

Si a alguien tengo que darle las gracias por haber hecho que hasta me apetezca venir a trabajar es a mis niñas del 204 y 211. A las autoras de la futura revista "Nature Issues", comisión de festividades oficial del VHIR y fundadoras del OncoBar para ahogar las penas después de semanas durísimas. A las personas con las que puedes estar un viernes a las 9 p.m. en cultivos escuchando la misma música que escuchamos el miércoles anterior a las 4 a.m. en Razzmatazz. **Marta**, mi vecina de laboratorio y de casa. Gracias por todas las risas que nos has dado, espero nunca perder todos tus stickers, siempre serán mis favoritos. Por estar siempre dispuesta a ayudar, ya sea con un western o con montarte un disfraz improvisado. Por saber siempre cuándo una necesita un Boldú o un kínder bueno para superar un día horrible. Prometo no volver a darte un ratón por muy tranquilo que parezca, y espero poder compartir muchos más desayunos de kiwi, tostada y café contigo. **Elena**, mi farmacéutica de confianza y compi de skincare independientemente de la hora y las condiciones en las que lleguemos. Gracias por todos tus consejos y por todos esos momentos haciendo lo que más nos gusta: criticar. Que sé que se nos nota todo en la cara, pero es que es inevitable. Por tu capacidad de organización, es increíble como puedes reservar unos vuelos y un hotel con cancelación gratuita en un minuto. Junto con Marta, gracias por poner todo vuestro empeño en que el ambiente de este edificio haya cambiado por completo desde que llegasteis. Gracias por convertir vuestro laboratorio en El Corte Inglés y haber traído el espíritu navideño, de Halloween, de la llegada de la primavera o del verano, e incluso St. Patrick's day. Habéis conseguido que estos últimos años hayan sido divertidísimos. **Sara**, siempre serás parte del 203. Gracias por ser tan sabia siempre, preguntarte a ti a veces es mejor que preguntarle a Google, es increíble la información que almacenas en esa cabeza. Me alegra saber que a pesar de que no pudieras quedarte en nuestro lab, estás a tan solo una puerta de distancia y con las mejores compañeras que te podría haber tocado. **Almu**, la mami de este grupo. Gracias por ser tan generosa, por alimentarnos con esos cinnamon rolls dignos del Demasié y con esas carrilleras que tardabas 6 horas en preparar hasta que te hicimos el mejor regalo de tu vida: la olla exprés. Siempre me ha sorprendido la de cosas que sabes de la vida, y es que me ha encantado nutrirme de todas ellas, de cada moraleja o consejo que sacabas de cada una. **Marina**, la creadora del VHIR Bang. Creo que eres con la persona que más horas he pasado en cultivos, ya fuera pasando células, infectando, transfectando o mirando en el microscopio si había bacterias, hongos o *cell bubbling*. Tampoco vamos a negar que a veces simplemente bailábamos. Ha sido un placer ser tu casi-postdoc de confianza. Espero que ahora mi título pase a ser tu postdoc de confianza.

Gracias también a todos los estudiantes de máster que han pasado por nuestros laboratorios, pero sobre todo a la multitud que ha pasado por el 204. A pesar de que han sido capaces de hacer que esto pareciera un circo, con inundaciones, incendios y mutaciones, también he aprendido mucho de todos (haciendo hincapié en el desarrollo de mi paciencia). En especial, a **Sonia** y **Mire**, que a pesar de ser de las primeras másters que nos abandonaron, habéis seguido en mi vida todos estos años, preocupándoos y apoyándome siempre. Estoy segura de que llegaréis muy lejos, aunque sea verdes fluorescentes y escribiendo trabajos enteros en menos de 24 horas. A **Rocío**, gracias por todas las risas que nos hemos echado y que han hecho que el tiempo pasara mucho más rápido durante tus distintas estancias por aquí. Gracias también a **Claudia** y a **Aldo**, por traer el espíritu italiano al VHIR y hacer las mejores pizzas, tiramisú y pasta carbonara de todos los tiempos.

Del lab 204 no puedo dejarme a **Stefan**, que después de llevar más de medio año preguntándome como voy con la tesis se alegrará de ver que por fin la acabé. Gracias por preocuparte tanto siempre, por tu generosidad y la ayuda durante todos estos años.

Gracias a todos mis compañeros de doctorado del edificio Collserola. Por todos esos VHIRetiros de destrucción que hemos vivido juntos y nos han acercado tanto. A los kinasos, en especial a **Sergio**, **Nora**, **Idoia** y **María**. Llegasteis para acaparar la sala de revelado y os convertisteis en unos imprescindibles en este edificio. A **Hugo**, por seguir rellenando nuestro álbum de selfies cada vez que salimos de fiesta. A **Jordi**, por seguir compartiendo muchos años más tu pasión por la música, prometo llevarte al siguiente concierto de Melendi. A **Bea**, porque algún día conseguiremos que Carlos Cuevas sepa que existimos. A **Álvaro**, por todas esas colaboraciones locas que se les ocurrían a nuestros jefes y que nunca se han llegado a hacer, y por traer a **Chemita** a mi vida, que ya es uno más en este edificio. Seguiremos diciendo que es el hijo de Andrés. También gracias al resto de compañeros, sobre todo a **Anna Deàs**, **Marta Barber**, **Adri**, **Marta Miera** y **Anna** y **Clàudia** mini kinasas. Porque todos habéis puesto un pedacito de vosotros para que este camino fuera más llevadero y divertido.

Siguiendo con el edificio Collserola, gracias a todos los celadores, pero en especial a **Andrés**, por insistir en que me vaya a casa cuando me ve más tarde de las 19 h, por consentirnos siempre y preocuparse de que todo esté bien. **Eulàlia**, gracias por hacer que este edificio funcione. Desde luego, con todos los percances que ha habido, esta tesis no hubiera salido adelante si tú no hubieras estado tan encima de que todo funcione bien.

No me puede faltar agradecer también a toda esa gente que ha cuidado de mis ratones durante todos estos años. Desde **Iván** en el PRBB, hasta **Eva** y **Cris** del Cellex. Gracias por mantener todas mis colonias, por los avisos de cada parto y de cada tumor. Hacer esto hubiera sido muchísimo más difícil y costoso sin vosotros.

También tengo que agradecer a **Herena** y **Carmen Espejo** todo el empeño y esfuerzo que han puesto en el diseño de los paneles de citometría y en introducirme en este mundo tan complejo de la inmunología. Gracias por cederme el uso del citómetro hasta las tantas de la noche como si fuera mío.

Pasando de la parte científica (aunque no mucho), el apoyo por parte de todas mis niñas de @mossos fuera del laboratorio ha sido fundamental. Porque como buenas chicas polifacéticas que somos, hemos compartido viajes, deportes, festivales y comidas que acaban convirtiéndose en cenas y fiesta, pero también lloros y preocupaciones. Pero sin duda, no podría haber llegado hasta aquí sin vosotras. **Sandra**, gracias por el coworking clandestino en el estabulario, pero también por la paz, tranquilidad y cariño que me has transmitido. **Marta**, gracias por ponerme los pies en la tierra muchas veces. Por seguir aquí siempre a pesar de todo lo que te conseguimos sacar de quicio. Aunque no lo creas, dice mucho de lo gran amiga que eres. **Laia**, gracias por no rajarte de nuestra amistad. Debajo de esa faceta de "Musso" has demostrado ser una amiga increíble, generosa y siempre dispuesta a ayudar. Que ganas de volver a invadir tu casa de Lloret. **Mercé**, gracias por ser el punto de unión de este grupo. Por compartir el primer puesto de persona torpe conmigo y por todas las crónicas y desdichas de tu vida que han conseguido sacarme siempre una sonrisa. Por tu generosidad y tus buenos consejos, aunque a veces desearía un botón de x0.5 para poder escucharlos mejor. **Ana**, antes que darte las gracias quiero pedirte perdón. Perdón por haber tenido que aguantar horas y horas de conversaciones sobre tesis varias. Piensa que ya quedamos menos, en nada acaba tu pesadilla. Y ahora gracias. Por ser tan buena y preocuparte tanto siempre. Eres de esas personas con las que siempre puedo contar, que transmites una confianza increíble para poder abrirme de corazón. Doy gracias porque sigas en mi vida desde aquella conversación de OT. **Ángela**, gracias por no decir nunca que no a un plan, por todos los cubatas compartidos y todas las risas que me has sacado. Quién nos diría que sería en Barcelona y no en Castellón donde nos teníamos que conocer. Gracias por tu gran corazón y por ser de esas amigas que quieres conservar toda la vida. Por dejarme entrar en tu vida, amigos, casa y familia. Soy muy afortunada de tenerte en mi vida. **María**, tan despistada y aun así te haces querer tanto. Gracias por tu serenidad, tu paz y por intentar siempre sacar el mejor lado de las cosas. Que ganas de

tener más tiempo libre y poder volver a pintar cuadros juntas. **Lily**, gracias por todas las risas, fiestas y planes random que me han hecho evadirme un poquito del estrés de estos años. Que ganas de seguir contándole a todo el mundo lo divertido que fue nuestro viaje a la Costa Brava. **Triana**, es muy fuerte que lo que empezó con unas tímidas copas en mi casa post-COVID haya seguido hasta el día de hoy. Gracias por haber compartido el sufrimiento de una tesis conmigo y haberme apoyado durante todos estos años. **Alicia**, gracias por ser siempre tan alegre y positiva. A tu lado se van todas las penas. **Clara**, gracias por transmitirme toda tu bondad y tranquilidad, por preocuparte tanto y consolar tan bien. Estoy muy agradecida de que de ser "la novia de un amigo de Marina" hayas pasado a ser mi amiga. **Belén**, gracias por ser mi compitrueno. A pesar de haber sido la última en llegar, lo has hecho por todo lo alto. Que bien saber que siempre se puede contar contigo.

A mis makumbas. Ya es 2024 y no os veo en las Olimpiadas. **David**, que gran descubrimiento contigo. Que grandes momentazos me has dado estos últimos años, todavía me sigo riendo de algunos cuando me acuerdo. De verdad, que agradecida estoy a la vida de poder llamarte amigo. **Andrés**, gracias por ser tan buena persona. Aunque la vida (llamémosla Marina) nos juntara por primera vez hace 10 años, este último año me has demostrado que siempre se puede contar contigo. Gracias por todo el apoyo. **Antonio**, mi amigo y mejor compi de piso. No vamos a nombrar lo que aprecio tu tranquilidad. Gracias por preocuparte tanto siempre, aunque a veces demasiado. Por muchos más viajes a Beni en coche (y que se te olvide cobrarme), muchas más mañanas de playa y series sin acabar. Gracias por llegar a mi vida y hacerme volver a sentirme en casa.

A mis chicos y chicas de Camp Hot. **Toni**, gracias por aparecer con tu locura en mi vida y por juntarnos con este grupo tan maravilloso. Quién iba a decir que esta chica de Castellón que te cayó tan mal en aquel correbars iba a acabar siendo tu amiga. Gracias por darme los mejores vídeos que tengo en mi galería, de esos que le alegran un día triste a cualquiera. **Marcus**, gracias por haberme hecho sentir joven a pesar de considerarme una octogenaria. **Leandre**, gracias por ser tan bueno, por ser mi coach deportivo y motivarme siempre con todo. **Jose** y **Alex**, gracias por hacerme reír tanto, sois increíbles. **Irene** y **Aldara**, gracias por aportar siempre vuestro punto de locura y hacerme sentir que no ha pasado el tiempo cuando os veo.

Gracias a los de toda la vida, **Carlota**, **Álvaro**, **Javi**, **Younes**, **Yolanda**, **María**, **Camila**, **Celia**, **Víctor** y **Paula**, por hacerme sentir siempre en casa. Por haber confiado en mi desde

que tengo uso de razón y haberme repetido cien mil veces que llegaría lejos. Que ganas de celebrar la primera boda del grupo.

Andrea, gracias por haber estado siempre. Por haber empezado esta aventura a mi lado y que, aunque la vida acabara separándonos de casa, hayas seguido siempre aquí. **Lau**, no podría olvidarme de ti. Que, aunque no hablemos tanto, estoy muy agradecida de saber que siempre puedo contar contigo. **Carlos**, **Titi** y **Albert**, porque estos años han sido duros para todos, pero que agradecida estoy de saber que siempre vais a estar ahí para todo lo que necesite. **Rubén** y **Riera**, gracias por ese viaje que hicimos en el momento que más necesitaba y por hacerme sentir que Lleida siempre será mi casa.

Marina, mi Maro, qué voy a decirte que no sepas. Se que no son dos caras dedicadas solamente a ti como esperabas, pero espero que pueda reflejar lo importante que has sido para mí, no solo durante estos años de tesis, sino desde los inicios prehistóricos de mi formación científica. Llegaste a mi vida hace casi 11 años (socorro) en la calurosa estepa catalana, y desde entonces no nos hemos separado. Empezaré dándote las gracias simplemente por aparecer en mi vida. Por todos esos momentos de clases, prácticas, trabajos, apuntes en catalán con *bacterias del sol* y *serums suspitosos*, repasos de nombres de bacterias a las 5 a.m. porque se nos quedaba mejor, de muchos bolis de los que se borran acabados, mucho barro en Agrònoms de Ferro, noches en los Vins y LaNuit, días de estudio mano a mano en el Rectorat o Medicina, miles de tropiezos en la misma grieta, visitas a urgencias por mis torpezas y millones de momentos en los que no podía ni respirar de la risa. Nos convertimos en biotecnólogas viviendo los mejores años de nuestras vidas. Pero no acabó ahí, y es que estos 7 años que llevamos en Barcelona no han sido para menos. Aquí estamos, a punto de convertirnos en doctoras. Sin duda, todo este camino no hubiera sido lo mismo sin ti. Gracias por haber seguido compartiendo tu día a día conmigo y por tenerme siempre en cuenta. Gracias por ser mi mayor apoyo siempre, por poder contártelo todo y saber dar los mejores consejos del mundo. Gracias por escucharme cuando llego a casa queriendo matar a alguien, y también por saber cuándo simplemente necesito que estemos en silencio en el sofá. Gracias por alegrarte siempre de las cosas buenas que me pasan y por haber estado a mi lado en los peores momentos de mi vida. Gracias por seguirme el rollo cuando me dan venazos de locura y apreciar mis comidas como si fuera un chef con estrella Michelin. Por ser la persona más desastre en la cocina que conozco, la más exagerada que existe y la que más me hace reír del universo. Por muchos más años compartiendo la vida juntas, llena de risas que cortan la respiración y de sustos que casi te matan; de viajes, de fiestas, de tardes y noches de sofá, peli

y manta; de Santander, de Benicàssim, de Barcelona. Como una vez puse de título en una foto juntas: “Que sí, que la vida puede dar muchas vueltas, pero quien de verdad te quiere, las da contigo”.

A mis segundos padres, **Yolanda**, **Fede**, **Javi**, **Lola**, **Mari Loli**, **Ángel**, **Rosana** y **Quique**. Gracias por haberme apoyado siempre y haberos preocupado tanto por mi como lo haría mi familia (si es que no lo sois ya).

Por último, y más importante, gracias a mi familia, a mis padres, hermano, tíos, primos y abuela. Llegar hasta aquí hubiera sido imposible sin vuestro apoyo. **Papá**, gracias por apoyarme en todas mis decisiones, creer siempre en mí más de lo que yo soy capaz y estar siempre tan orgulloso de mí. **Gonzalo**, gracias por ser el mejor hermano que podría tener, por ser tan cariñoso y generoso conmigo, aunque me llames okupa cada vez que voy a casa. **Mamá**, sé que allá donde estés, estarás muy orgullosa de que lo haya logrado. Si he llegado hasta aquí, es también gracias a ti.

INDEX

ACKNOWLEDGMENTS **3**

INDEX **13**

ABBREVIATIONS **19**

SUMMARY **25**

INTRODUCTION **31**

1. Skin cancer. **33**

1.1. Classification and epidemiology. 33
1.2. Risk factors. 33
1.2.1. Environmental factors: ultraviolet (UV) radiation. 34
1.2.2. Genetic factors. 35

2. Melanoma. **35**

2.1. Classification. 35
2.2. Melanoma tumor progression and staging. 36
2.3. Main alterations in melanoma. 37
2.3.1. MAPK pathway alterations. 38
2.3.2. PI3K/AKT pathway alterations. 40
2.3.3. Other pathways alterations. 41
2.4. Treatment of melanoma. 41
2.4.1. Targeted therapy. 42
2.4.2. Immune response in melanoma and immunotherapy. 44
2.4.2.1. Anti-tumor immune response and immune evasion mechanisms. 44
2.4.2.2. Immune-based therapies. 47
2.4.2.2.1. Immune checkpoint inhibitors (ICIs). 48
2.4.2.2.2. Cancer vaccines. 49
2.4.2.2.3. Adoptive cell therapy (ACT). 50

3. Mitogen-activated protein kinase (MAPK) pathways. **51**

3.1. Classification. 51
3.2. p38 MAPK pathway. 52
3.2.1. The p38 MAPK family. 52
3.2.2. Pathway activation and signal transduction. 54
3.2.3. Downstream substrates of p38α. 56
3.2.4. p38α in cancer. 57
3.2.4.1. Role of the p38 MAPK pathway in the response to stress stimuli. 58
3.2.4.2. Role of the p38 MAPK pathway in the inflammatory cytokine response. 60
3.2.4.3. Role of the p38 MAPK pathway in oncogene-induced senescence. 60
3.2.4.4. Role of the p38 MAPK pathway in tumor growth and progression. 62
3.2.5. p38α as a therapeutic target. 63

HYPOTHESIS AND OBJECTIVES **67**

RESULTS **73**

p38α is altered in human cutaneous melanoma and is associated to a poor survival of patients. 75
p38α is involved in melanocyte survival, proliferation and stress response. 79
Absence of *p38α* expression in melanocytes is associated with a delay in melanoma development, a higher tumor multiplicity and reduced tumor size in a UVB-induced *Braf*^{V600E} melanoma mouse model. 82
Smaller size of *B;p38α* tumors correlates with a decreased proliferation of melanoma cells. 85
Absence of *p38α* in tumor cells results in increased and prolonged cytotoxic immune response in *Braf*^{V600E} mouse melanoma tumors. 86
Tumors lacking *p38α* exhibit an enhanced activity and recruitment of NK and NK-T cells. 91
Lack of *p38α* in tumor cells favors the accumulation of polymorphonuclear over monocytic MDSCs and decreases the recruitment of macrophages and activated DCs. 93
Gene expression analysis confirmed the role of p38α in the modulation of the tumor microenvironment and the anti-tumor immune response by tumor cells. 96
p38α mediates the expression of cytokines and chemokines that are critical for the modulation of the anti-tumor immune response. 101
p38α expression by tumor cells determines the response to PD-1 immune checkpoint blockade. 106
Absence of *p38α* expression in tumor cells recapitulates a good prognosis signature to immune checkpoint blockade in humans. 109

DISCUSSION **115**

CONCLUSIONS **133**

MATERIALS AND METHODS **137**

Cell culture and treatments. 139
Immunohistochemistry. 139
Lentiviral infection for p38α knockdown. 140
Cell proliferation and viability assay. 141
Immunoblotting. 141
Mouse model and UVB irradiation. 142
Mouse genotyping. 143
Mouse melanoma cell lines generation. 144
Immunophenotyping. 144
Gene expression analysis. 146
Quantitative Reverse Transcription Polymerase Chain Reaction (RT-qPCR). 147
Cytokines array. 148
In vivo immunotherapy. 149
Statistical analysis. 149

SUPPLEMENTARY INFORMATION **151**

BIBLIOGRAPHY **171**

ABBREVIATIONS

#	
6-4PP	Pyrimidine-pyrimidone (6-4) photoproducts
α-MSH	α-melanocyte-stimulating hormone
A	
ACT	Adoptive cell therapy
AF	Alexa Fluor
AJCC	American Joint Committee on Cancer
AKT	Protein kinase B
ANGPT	Angiopoietin
AP-1	Activator protein 1
APC	Allophycocyanin
APCs	Antigen-presenting cells
AR	Amphiregulin
ARAF	ARAF serine/threonine kinase
ASK1	Apoptosis signal-regulating kinase 1
ATF	Cyclic AMP-dependent transcription factor
B	
Bax	Bcl-2 associated X protein
BCC	Basal cell carcinoma
Bcl-2	B-cell lymphoma 2
BMK1	Big MAP kinase 1
BRAF	BRAF serine/threonine kinase
BSA	Bovine serum albumin
BV	Brilliant violet
C	
C/EBP	CCAAT/enhancer binding protein
CAR-T	Chimeric antigen receptor T-cell
CCL	C-C motif chemokine ligand
CCR	C-C motif chemokine receptor
CD	Cluster of differentiation
CD206	Mannose receptor C-type 1
CD62L	L-selectin
CDK4	Cyclin-dependent kinase 4
CDKN2A	Cyclin-dependent kinase inhibitor 2A
CHI3L1	Chitinase 3-like 1
CHK	Checkpoint kinase
COT/TPL2/MAP3K8	Mitogen-activated protein kinase kinase kinase 8
CPD	Cyclobutene pyrimidine dimer
CRAF	CRAF serine/threonine kinase
CREB	Cyclic AMP-responsive element-binding protein
CSF	Colony-stimulating factor
CST3	Cystatin C
CTL	Cytotoxic T lymphocyte
CTLA-4	Cytotoxic T-lymphocyte-associated protein 4
CXCL	C-X-C motif chemokine ligand
CXCR	C-X-C motif chemokine receptor
Cy	Cyanine

D		
	DC	Dendritic cell
	DCT	L-dopachrome tautomerase
	DKK-1	Dickkopf-1
	DLK1	Dual-leucine zipper-bearing kinase 1
	dLN	Draining lymph node
	DMEM	Dulbecco's Modified Eagle Media
	DNA	Deoxyribonucleic acid
	DUSP	Dual-specificity phosphatase
E		
	EDTA	Ethylenediaminetetraacetic acid
	EGF	Epidermal Growth Factor
	ELK1	ETS domain-containing protein
	EMEM	Eagle's Minimum Essential Media
	EMT	Epithelial-mesenchymal transition
	ER81	ETS-related protein 81
	ERK	Extracellular signal-regulated kinase
	ETS1	Protein C-ets-1
F		
	F4/80	Mouse homolog of epidermal growth factor (EGF)-like module-containing mucin-like hormone receptor-like 1
	FAMMM	Familial atypical multiple mole-melanoma
	FBS	Fetal bovine serum
	FC	Fold change
	FDA	Food and Drug Administration
	FGFR	Fibroblast growth factor receptor
	FITC	Fluorescein isothiocyanate
	FoxP3	Forkhead box P3
G		
	GADD153/CHOP	Growth arrest and DNA damage inducible gene 153
	GAPDH	Glyceradehyde-3-phosphate dehydrogenase
	GAS 6	Growth Arrest Specific
	GDP	Guanosine diphosphate
	GFP	Green fluorescent protein
	GNA11	G protein subunit alpha 11
	GNAQ	G protein subunit alpha Q
	GO	Gene ontology
	GPCR	G-protein coupled receptor
	GTP	Guanosine triphosphate
H		
	HBP1	HMG-box transcription factor 1
	HGF	Hepatocyte Growth Factor
	HMGN1	Non-histone chromosomal protein HMG-14
	HRP	Horseradish peroxidase
I		
	I-A/I-E	Major histocompatibility complex type II
	ICI	Immune checkpoint inhibitor
	IFN	Interferon
	IGF1R	Insulin-like growth factor receptor
	IHC	Immunohistochemistry
	IL	Interleukin

	IPRES	Innate αPD-1 Resistance
J		
	JNK	c-Jun NH2-terminal kinase
K		
	KIT	Kit tyrosine kinase
L		
	LAG-3	Lymphocyte activation gene-3
	LDL R	Low Density Lipoprotein Receptor
	LIF	Leukemia inhibitory factor
	LPS	Lipopolysaccharide
	Ly6C	Lymphocyte antigen 6 complex, locus C
	Ly6G	Lymphocyte antigen 6 complex, locus G
M		
	MAPK	Mitogen-activated protein kinase
	MAPKAPK2/MK2	Mitogen-activated protein kinase-activated protein kinase 2
	MAS	Melanoma-asrtocytoma syndrome
	MC1R	Melanocortin 1 receptor
	Mcl-1	Myeloid leukemia 1
	MDA	Melanoma differentiation antigen
	MDSC	Myeloid-derived suppressor cell
	MEF	Myocyte enhance factor
	MEK	Mitogen-activated protein kinase kinase
	MEKK	MAPK/ERK kinase kinase
	MET/HGFR	Hepatocyte growth factor receptor
	MHC	Major histocompatibility complex
	MITF	Microphthalmia-associated transcription factor
	MLK3	Mixed-lineage kinase 3
	MMP	Matrix metalloproteinase
	MRP	Proliferin
N		
	NER	Nucleotide excision repair
	NF1	Neurofibromin 1
	NFκB	Nuclear factor-kappa-B
	NGS	Next-generation sequencing
	NK	Natural killer
	NP-40	Nonidet P-40
	NRAS	Neuroblastoma RAS viral oncogene homolog
O		
	OIS	Oncogene-induced senescence
	OPN/SPP1	Osteopontin
P		
	PAX6	Paired box protein 6
	PBS	Phosphate-buffered saline
	PCR	Polymerase chain reaction
	PD-1	Programmed cell death protein 1
	PD-L1	Programmed cell death ligand 1
	PDGFR	Platelet-derived growth factor receptor
	PE	Phycoerythrin
	PerCP	Peridinin-chlorophyll-protein complex

PGE2	Prostaglandin E2
PI3K	Phosphatidylinosito 3-kinase
PMCA4b	Plasma membrane Ca^{2+} pump isoform 4b
POSTN	Periostin
PP2A	Protein phosphatase 2A
PRAK	p38-regulated/activated protein kinase
PTEN	Phosphatase and tensin homolog
PTX	Pentraxin
PVDF	Polyvinylidene difluoride
R	
RARα	Retinoic acid receptor α
RARRES2	Chemerin
RB1	Retinoblastoma-associated protein
RFP	Red fluorescent protein
RNA	Ribonucleic acid
ROS	Reactive oxygen species
RPMI	Roswell Park Memorial Institute
RTK	Receptor tyrosine kinase
S	
SAPK	Stress-activated protein kinase
SCC	Squamous cell carcinoma
SDS	Sodium dodecyl sulfate
SDS-PAGE	SDS-polyacrylamide gel electrophoresis
shRNA	Short hairpin RNA
STAT	Signal transducer and activator of transcription
T	
TAA	Tumor-associated antigen
TAB1	Transforming growth factor-β-activated kinase 1-binding protein 1
TAK1	Transforming growth factor-β-activated kinase 1
TAO	Thousand-and-one amino acid
TBS	Tris-buffered saline
TCGA	The Cancer Genome Atlas
TCR	T-cell receptors
TERT	Telomerase reverse transcriptase
TGF-β	Transforming growth factor-β
Th	T helper
TIDE	Tumor Immune Dysfunction and Exclusion
TIGER	Tumor Immunotherapy Gene Expression Resource
TIGIT	T cell immunoreceptor with immunoglobulin and ITIM domains
TIL	Tumor-infiltrating lymphocyte
TIM-3	T cell immunoglobulin and mucin-domain containing-3
TNF	Tumor necrosis factor
TNFSF4/OX40-L	Tumor necrosis factor ligand superfamily member 4
TNM	Tumor, node, metastasis
TP53	Tumor suppressor p53
TPL2	Tumor progression loci 2
Treg	Regulatory T cell
TRP	Tyrosinase-related protein
TSA	Tumor-specific antigen

U		
	UV	Ultraviolet
V		
	VEGF	Vascular endothelial growth factor
	VEGFR	Vascular endothelial growth factor receptor
	VISTA	V-domain immunoglobulin suppressor of T cell activation
W		
	WB	Western blot
Z		
	ZAK1	Leucine zipper and sterile-α-motif kinase 1
	ZAP70	Zeta-chain associated protein kinase 70 kDa

SUMMARY

SUMMARY

Melanoma, the most aggressive form of skin cancer, remains challenging to treat due to the lack of clear biomarkers of response or resistance to current therapies and its complex interactions with the immune system. Understanding the molecular mechanisms underlying melanoma progression and response to immunotherapy is critical for the development of effective therapeutic strategies.

In this study, we have investigated the role of p38α, a key signaling molecule, in melanoma development and progression, and its impact on the tumor microenvironment (TME) and response to immunotherapy. This study provides novel insights into the dual role of p38α in UVB-induced *Braf*^{V600E} melanoma development and progression. Using mouse models, our results suggest that p38α may act as a tumor suppressor in the melanocyte transformation induced by *Braf*^{V600E} oncogene activation and UVB irradiation but may facilitate melanoma tumor growth and progression. Analysis of the tumor-infiltrating immune cells demonstrates that p38α contributes to melanoma progression by regulating anti-tumor immunity, impairing cytotoxic immune responses, and modulating the recruitment and activity of immunosuppressive myeloid cells. Our findings reveal differential gene expression profiles between tumors with and without p38α expression, particularly in immune-related processes. Tumor cells regulate the expression of a number of inflammatory molecules through p38α that may potentially impact the anti-tumor immune response and the TME. In addition, we show that the absence of p38α in tumor cells leads to a more favorable response to PD-1 blockade, suggesting that targeting p38α could enhance the efficacy of immunotherapy in melanoma patients. A p38α-associated gene signature identified in this study correlates with a good response to immunotherapy in melanoma patients, highlighting the translational potential of our findings.

In conclusion, our study provides valuable insights into the role of p38α in melanoma development, progression and immunotherapy response. Targeting p38α may represent a promising therapeutic approach to enhance the anti-tumor immune response and improve patient outcomes in melanoma.

RESUMEN

El melanoma, la forma más agresiva de cáncer de piel, sigue siendo difícil de tratar debido a la falta de biomarcadores claros de respuesta o resistencia a las terapias actuales y a sus complejas interacciones con el sistema inmunitario. Comprender los mecanismos moleculares que subyacen a la progresión del melanoma y la respuesta a la inmunoterapia es fundamental para el desarrollo de estrategias terapéuticas eficaces.

En este estudio, hemos investigado el papel de p38α, una molécula de señalización clave, en el desarrollo y la progresión del melanoma, y su impacto en el microambiente tumoral (MAT) y la respuesta a la inmunoterapia. Este estudio aporta nuevos conocimientos sobre la doble función de p38α en el desarrollo y la progresión del melanoma *Braf*^{V600E} inducido por UVB. Utilizando modelos de ratón, nuestros resultados sugieren que p38α puede actuar como supresor tumoral en la transformación de melanocitos inducida por la activación del oncogén *Braf*^{V600E} y la irradiación UVB, pero puede facilitar el crecimiento y la progresión del tumor de melanoma. El análisis de las células inmunitarias que infiltran el tumor demuestra que p38α contribuye a la progresión del melanoma regulando la inmunidad antitumoral, perjudicando las respuestas inmunitarias citotóxicas y modulando el reclutamiento y la actividad de las células mieloides inmunosupresoras. Nuestros resultados revelan perfiles de expresión génica diferenciales entre tumores con y sin expresión de p38α, particularmente en procesos relacionados con la inmunidad. Las células tumorales regulan la expresión de una serie de moléculas inflamatorias a través de p38α que pueden potencialmente impactar en la respuesta inmune antitumoral y en el MAT. Además, mostramos que la ausencia de p38α en las células tumorales conduce a una respuesta más favorable al bloqueo de PD-1, lo que sugiere que dirigirse a p38α podría mejorar la eficacia de la inmunoterapia en pacientes con melanoma. Una firma génica asociada a p38α identificada en este estudio se correlaciona con una buena respuesta a la inmunoterapia en pacientes con melanoma, destacando el potencial traslacional de nuestros hallazgos.

En conclusión, nuestro estudio proporciona información valiosa sobre el papel de p38α en el desarrollo del melanoma, la progresión y la respuesta a la inmunoterapia. Dirigirse a p38α puede representar un enfoque terapéutico prometedor para potenciar la respuesta inmunitaria antitumoral y mejorar los resultados de los pacientes con melanoma.

RESUM

El melanoma, la forma més agressiva de càncer de pell, continua essent difícil de tractar a causa de la manca de biomarcadors clars de resposta o resistència a les teràpies actuals i les seves complexes interaccions amb el sistema immunitari. Comprendre els mecanismes moleculars subjacents a la progressió del melanoma i la resposta a la immunoteràpia és fonamental per al desenvolupament d'estratègies terapèutiques eficaces.

En aquest estudi, hem investigat el paper de p38α, una molècula de senyalització clau, en el desenvolupament i la progressió del melanoma, i el seu impacte al microambient tumoral (MAT) i la resposta a la immunoteràpia. Aquest estudi aporta nous coneixements sobre la doble funció de p38α en el desenvolupament i la progressió del melanoma *Braf*^{V600E} induït per UVB. Utilitzant models de ratolí, els nostres resultats suggereixen que p38α pot actuar com a supressor tumoral en la transformació de melanòcits induïda per l'activació de l'oncogen *Braf*^{V600E} i la irradiació UVB, però pot facilitar el creixement i la progressió del tumor de melanoma. L'anàlisi de les cèl·lules immunitàries que infiltren el tumor demostra que p38α contribueix a la progressió del melanoma regulant la immunitat antitumoral, perjudicant les respostes immunitàries citotòxiques i modulant el reclutament i l'activitat de les cèl·lules mieloides immunosupressores. Les nostres resultats revelen perfils d'expressió gènica diferencials entre tumors amb i sense expressió de p38α, particularment en processos relacionats amb la immunitat. Les cèl·lules tumorals regulen l'expressió d'una sèrie de molècules inflamatòries a través de p38α que poden potencialment impactar a la resposta immune antitumoral i al MAT. A més, mostrem que l'absència de p38α a les cèl·lules tumorals condueix a una resposta més favorable al bloqueig de PD-1, cosa que suggereix que dirigir-se p38α podria millorar l'eficàcia de la immunoteràpia en pacients amb melanoma. Una firma gènica associada a p38α identificada en aquest estudi es correlaciona amb una bona resposta a la immunoteràpia en pacients amb melanoma, destacant el potencial translacional de les nostres troballes.

En conclusió, el nostre estudi proporciona informació valuosa sobre el paper de p38α en el desenvolupament del melanoma, la progressió i la resposta a la immunoteràpia. Dirigir-se a p38α pot representar un enfocament terapèutic prometedor per potenciar la resposta immunitària antitumoral i millorar els resultats dels pacients amb melanoma.

INTRODUCTION

1. Skin cancer.

1.1. Classification and epidemiology.

Skin cancer is the most common human malignancy and its global incidence is increasing at an alarming rate, with approximately 2-3 million documented cases of skin cancer worldwide each year[1]. In a general classification, skin cancer is divided into two main types: melanoma, which originates from melanocytes, and non-melanoma skin cancers, which originate from epidermal-derived cells[2]. The most common forms of non-melanoma skin cancer are basal cell carcinoma (BCC) and squamous cell carcinoma (SCC). While BCC arises from basal cells that line the bottom of the epidermis and is the most common form of skin cancer, representing around 80% of diagnosed skin cancers, SCC starts in the squamous cells that line the top of the epidermis and accounts for about 20% of skin cancers[3,4]. Both BCC and SCC have a good prognosis, especially when detected in the early stages[5].

Melanoma, on the other hand, results from abnormal proliferation of melanocytes, specialized cells in the basal layer of the skin that produce melanin, the pigment that gives color to our hair and skin. Although melanomas represent around 1% of all skin cancers, it is responsible for about 80% of all skin cancer-related deaths[4,6]. In fact, 324,635 new cases of melanoma and 57,043 deaths were registered worldwide in 2020, making melanoma the 17th most commonly diagnosed cancer worldwide[7]. Unlike other solid malignancies, melanoma affects a higher proportion of younger patients and its incidence continues to increase with age[4,8]. In particular, up to the age of 55, the incidence of melanoma is almost twice as high in women as in men. Thereafter, this pattern shifts with a higher prevalence in men[9,10].

In terms of prognosis, early diagnosis of melanoma can lead to a complete cure with surgical resection[11], and more than 99% of early diagnosed patients are successfully treated in this manner [12]. However, metastatic malignant melanoma exhibits significant resistance to existing therapies and has a very poor prognosis, with a 5-year survival rate of 35.1%[12]. Therefore, there is an urgent need to develop new treatment strategies.

1.2. Risk factors.

The development of skin cancer, particularly melanoma, is influenced by the interaction between genetic and environmental factors.

1.2.1. Environmental factors: ultraviolet (UV) radiation.

The main environmental risk factor for the development of melanoma is ultraviolet (UV) radiation. Two types of UV radiation are the primary contributors to carcinogenic skin damage: UVA (320 nm to 400 nm) and UVB (280 nm to 320 nm). Although UVA radiation is the most abundant waveband in sunlight, accounting for 95% of solar UV radiation, UVB radiation is considered the primary carcinogen associated with melanoma development[13,14]. The mechanisms by which UV radiation induces the malignant transformation of melanocytes include DNA damage, accumulation of reactive oxygen species (ROS), oxidative stress, and inflammatory responses.

UVB penetrates into the epidermis and causes direct DNA damage mainly by inducing the formation of cyclobutene pyrimidine dimers (CPDs) and pyrimidine-pyrimidone (6-4) photoproducts (6-4PPs). When not efficiently repaired by the cells through the nucleotide excision repair (NER) pathway, it leads to the accumulation of the characteristic C>T mutations associated with UV radiation[14,15]. The persistence of these lesions increases the probability of errors during DNA replication, resulting in mutations in key genes associated with cell cycle regulation and tumor suppression. The accumulation of such mutations contributes to the oncogenic transformation of melanocytes, leading to the development of melanoma[14,16]. In contrast, UVA radiation penetrates deeper into the skin and causes indirect DNA damage by producing ROS, which are chemically reactive molecules containing oxygen, leading to oxidative stress. This condition can cause cellular damage, including lipid peroxidation, DNA fragmentation, apoptosis and cell death, thus contributing to melanoma development[17].

Exposure to UV radiation also triggers inflammatory responses in the skin, characterized by the infiltration of immune cells such as macrophages and neutrophils. In general, these cells play a role in the body's defense mechanism. However, under certain conditions they can also contribute to tissue damage and promote tumor progression[14].

Epidemiological studies show that intense levels of intermittent sun exposure, especially during childhood, are associated with a higher risk of melanoma development[18–22]. Moreover, exposure to UVA from artificial light sources, especially frequent use of tanning beds, has also been associated with an increased risk of melanoma[23,24].

1.2.2. Genetic factors.

Pigmentation has an undeniably important impact on the susceptibility of the skin to malignant changes. The melanocortin 1 receptor (MC1R) is a cell surface receptor of melanocytes that induces melanin production (via recruitment of the microphthalmia-associated transcription factor (MITF) signaling cascade) when activated by its ligand, α-melanocyte-stimulating hormone (α-MSH)[25]. Specifically, in response to UV, keratinocytes secrete α-MSH, which binds to MC1R and stimulates melanin production by melanocytes. This melanin is rarely stored in melanocytes but is transferred to surrounding epithelial cells such as keratinocytes, resulting in the tanning response to protect our skin from the damaging effects of UV radiation and thus prevent skin cancer[26]. Polymorphisms of the *MC1R* gene are responsible for the different skin color phenotypes observed in humans. Variants such as red hair, fair skin and light eyes are characterized by a low pigmentation and therefore have a higher sensitivity to UV exposure and, consequently, an increased risk of developing melanoma[25,27].

Other risk factors, such as the number and type of congenital and acquired nevi and family history are also important in the development of melanoma. Approximately 25% of melanoma cases develop on pre-existing nevi[28], with the risk of melanoma influenced not only by the total number of nevi, but also by the size and type of the existing nevi[29]. Family history can increase the risk of melanoma, with some cases showing hereditary patterns, such as the familial atypical multiple mole-melanoma syndrome (FAMMM syndrome) and its variant, the melanoma-astrocytoma syndrome (MAS). Germline mutations in genes such as cyclin-dependent kinase inhibitor 2A (*CDKN2A*) and cyclin-dependent kinase 4 (*CDK4*) are common in these melanoma-prone families[30].

2. Melanoma.

2.1. Classification.

Melanoma, the deadliest form of skin cancer, arises from melanocytes, specialized cells that originate from neural crest progenitors and migrate during embryonic development to various tissues throughout the body, including the skin, eyes and meninges. In the skin, melanocytes are primarily found in the basal layer of the epidermis and in hair follicles[26]. Based on the primary site of origin, melanoma can be classified as cutaneous (skin), mucosal (mucous membrane) and uveal (eye) melanoma[31]. Among these, cutaneous melanoma is by far the most common subtype[31], and can be further subdivided into four main clinical subtypes: superficial spreading, nodular, lentigo maligna and acral lentiginous (Table 1).

Table 1 | Cutaneous melanoma subtypes. Table showing the different subtypes of cutaneous melanoma, their incidence and their main characteristics in the Caucasian population[10,32].

Cutaneous melanoma subtype	Incidence	Main characteristics
Superficial spreading	70%	It usually presents as a flat, slowly growing lesion, but it can invade the skin vertically. It is associated to intermittent sun exposure.
Nodular	20%	It develops as a nodule, which may be pigmented or amelanotic, with a rapid growth and high rate of metastasis. It is associated to intermittent sun exposure.
Lentigo maligna	4-15%	It starts as a flat, brown lesion in the surface of the skin that may evolve for decades before starting to invade deeper in the skin. It is associated with long-term sun exposure, thus typically occurring in face and neck of older individuals.
Acral lentiginous	1-2%	It is often found on the palms, soles or under the nails. It is uncommon in Caucasian populations, but is the most common type among Asian, Hispanic and African individuals. It is not strongly associated with UV exposure.

2.2. Melanoma tumor progression and staging.

The Clark's level is a staging system that describes the level of penetration of melanoma into the skin layers. It consists of five levels, each representing a different depth of invasion[33] (Table 2).

Table 2 | Clark's levels. Table showing the main characteristics of the different levels of the Clark's classification [33].

Level of invasion	Description
Level I	Lesions involving only the epidermis (*in situ* melanoma); not an invasive lesion.
Level II	Invasion of the papillary dermis.
Level III	Invasion to the junction of the papillary and reticular dermis.
Level IV	Invasion into the reticular dermis.
Level V	Invasion through the reticular dermis into the subcutaneous tissue.

Based on the Clark's model, the development and progression of melanoma involves a gradual transformation from benign melanocytic nevi to metastatic melanoma driven by genetic and/or epigenetic alterations[34,35].

Melanocytic nevi are benign proliferations of melanocytes that are unlikely to progress to melanoma[35]. It is known that *BRAF* is mutated in up to 80% of benign nevi, resulting in limited melanocyte proliferation due to the occurrence of senescence-like cell cycle arrest, which is known as oncogene-induced senescence (OIS)[36,37]. These nevi remain dormant for decades, suggesting that *BRAF* mutation alone may not be sufficient to potentiate melanoma

tumorigenesis. Therefore, additional genetic events are required to bypass the OIS and acquire a tumorigenic phenotype[38]. The synergistic effect of acquiring mutations in tumor suppressor genes such as *CDKN2A* or *PTEN* may promote melanoma initiation and transformation. Once the tumor cells reach the radial growth phase, the deregulation of other cell differentiation and metabolic pathways, as well as the loss of E-cadherin and the upregulation of N-cadherin are essential for tumor cell invasiveness and metastasis[34] (Figure 1).

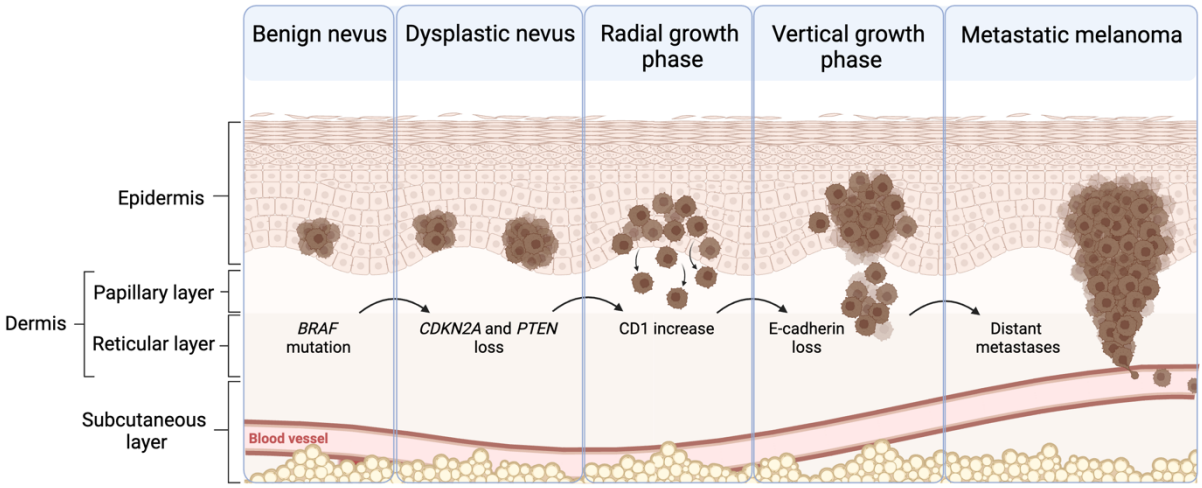


Figure 1 | Melanoma tumor progression. Representative scheme showing the different stages of melanoma initiation and transformation from a benign melanocytic nevus to a metastatic melanoma.

It is important to note that melanomas associated with chronic sun exposure usually do not arise from pre-existing nevi, but from melanoma *in situ* or dysplastic lesions, and carry a different set of mutations[38].

The American Joint Committee on Cancer (AJCC) no longer considers Clark's level, as it has been found to be less prognostic and more subjective than other alternatives. The revised AJCC system now relies on tumor, node, metastasis (TNM) scores and other prognostic factors to determine melanoma staging[39]. However, despite its exclusion from the AJCC system for clinical purposes, Clark's classification remains a valuable model for understanding the transformation of melanoma.

2.3. Main alterations in melanoma.

Melanoma has been found to have one of the highest somatic mutational burdens of all human tumors. The most common somatic mutations in melanoma affect genes involved in key cellular processes, including proliferation (*BRAF*, *NRAS* and *NF1*), growth and metabolism (*PTEN, AKT3* and *KIT*), resistance to apoptosis (*TP53*), cell cycle control (*CDKN2A*), replicative lifespan (*TERT*) or melanocyte proliferation and survival (*MITF*)[40,41] (Table 3).

In addition to *KIT* mutations, amplification of other receptor tyrosine kinases (RTKs) such as *MET*, *PDGFRA* or *VEGFR2* have been reported to be involved in melanoma progression[42]. Furthermore, mutations in *GNAQ* and *GNA11*, which encode to G-protein alpha subunits involved in the transmission of signals between G-protein coupled receptors (GPCRs) and downstream effectors, are the most common in uveal melanoma[43]. All of these genomic alterations result in the constitutive activation of two major signaling pathways in melanoma: the mitogen-activated protein kinase (MAPK) pathway, specifically the RAS/RAF/MEK/ERK cascade, and the phosphoinositol 3-kinase (PI3K)/AKT pathway[40,41].

Table 3 | Predominant genetic alterations in human cutaneous melanoma. Table showing the main genes altered in cutaneous melanoma (CM), the biological pathway involved, the alteration frequency (data from The Cancer Genome Atlas (TCGA) database), the specific type of alteration and their respective function.

Biological pathway	Gene	Frequency in CM (%)	Type of alteration	Function
MAPK pathway	*BRAF*	~50%	Mutation	Oncogene
	NRAS	~30%	Mutation	Oncogene
	NF1	~15%	Mutation	Tumor suppressor
	KIT	~10%	Mutation, amplification	Oncogene
PI3K/AKT pathway	*PTEN*	~20%	Deletion, mutation	Tumor suppressor
	AKT3	~20%	Amplification	Oncogene
Cell cycle	*CDKN2A*	~45%	Deletion, mutation	Tumor suppressor
	TP53	~25%	Mutation	Tumor suppressor
Transcription factor	*MITF*	~15%	Amplification	Melanocyte survival
Telomerase pathway	*TERT*	~85%	Promoter mutations, amplification	Replicative lifespan

2.3.1. MAPK pathway alterations.

The MAPK signaling pathway is hyperactivated in over 90% of melanomas and plays a critical role in melanoma development[41]. This pathway is involved in the transduction of signals from RTKs to downstream effectors, resulting in the regulation of several cellular processes, including cell proliferation, differentiation, motility, and survival[44].

The RAS/RAF/MEK/ERK signaling is driven by the binding of growth factors to RTKs, which induces the receptor dimerization. This stimulates the intrinsic tyrosine-kinase activity of the receptor and the subsequent activation of RAS, a family of small G-proteins (HRAS, KRAS and NRAS) that, when bound to GTP, initiate the signaling cascade by activating MAPK kinase kinases (MAP3Ks; ARAF, BRAF and CRAF). RAF proteins dimerize and phosphorylate MAPK kinases (MAP2Ks; MEK1/2), which in turn phosphorylate MAPKs

(ERK1/2). Finally, activated ERK1/2 phosphorylate nuclear transcription factors involved in the regulation of cell differentiation, proliferation and survival[44] (Figure 2).

The most commonly mutated component of this pathway is *BRAF*, which is mutated in approximately 50% of cutaneous melanomas (TCGA database). The most common *BRAF* mutation detected in melanoma, accounting for approximately 90% of all mutations, occurs at position T1796A in exon 15, resulting in a valine to glutamic acid substitution at position 600 (V600E). Although $BRAF^{V600E}$ is the most common mutation, 5-6% of mutations are valine to lysine substitution (V600K) and less than 5% are valine to aspartic acid (V600D) or valine to arginine (V600R) substitutions[45]. These mutations alter the catalytic domain of the BRAF protein, where the substitution of the hydrophobic valine for a polar, hydrophilic amino acid results in a constitutively active conformation with kinase activity 500-fold higher than the wild-type BRAF[46]. This results in the hyperactivation of ERK1/2, leading to aberrant regulation of cell proliferation and survival of melanoma cells[45].

NRAS is the second most commonly mutated gene in cutaneous melanoma and is mutated in approximately 30% of the cases (TCGA database). The majority of *NRAS* mutations are missense mutations in codons 12, 13 or 61, with the most common mutation being a glutamine (Q) to arginine (R), lysine (K), or leucine (L) substitution at position 61, which accounts for 80% of all *NRAS* mutations in melanoma. Mutations in these codons lead to the prolongation of the active GTP-bound form of NRAS, resulting in aberrant NRAS signaling through both MAPK and PI3K/AKT pathways. Importantly, *NRAS* and *BRAF* mutations are considered mutually exclusive, but co-mutations can rarely occur[47].

The *NF1* gene, which is the third most frequently mutated gene in melanoma, occurring in approximately 15% of the cases (TCGA database), encodes a protein called neurofibromin 1, which acts as a tumor suppressor, primarily by inhibiting the activity of RAS proteins. NF1 accelerates the conversion of RAS from its active GTP-bound form to its inactive GDP-bound conformation, thereby inhibiting downstream RAS signaling. Mutations in the *NF1* gene often result in a loss-of-function, which in turn leads to the hyperactivation of the NRAS protein increasing signaling through the MAPK and PI3K/AKT pathways, which are critical for cell proliferation and survival[48].

Furthermore, somatic activating mutations and amplifications in the *KIT* receptor tyrosine kinase gene, which cause receptor dimerization, autophosphorylation of tyrosine residues and

the activation of the downstream oncogenic pathways[49], have been found in 10% of cutaneous melanomas (TCGA database).

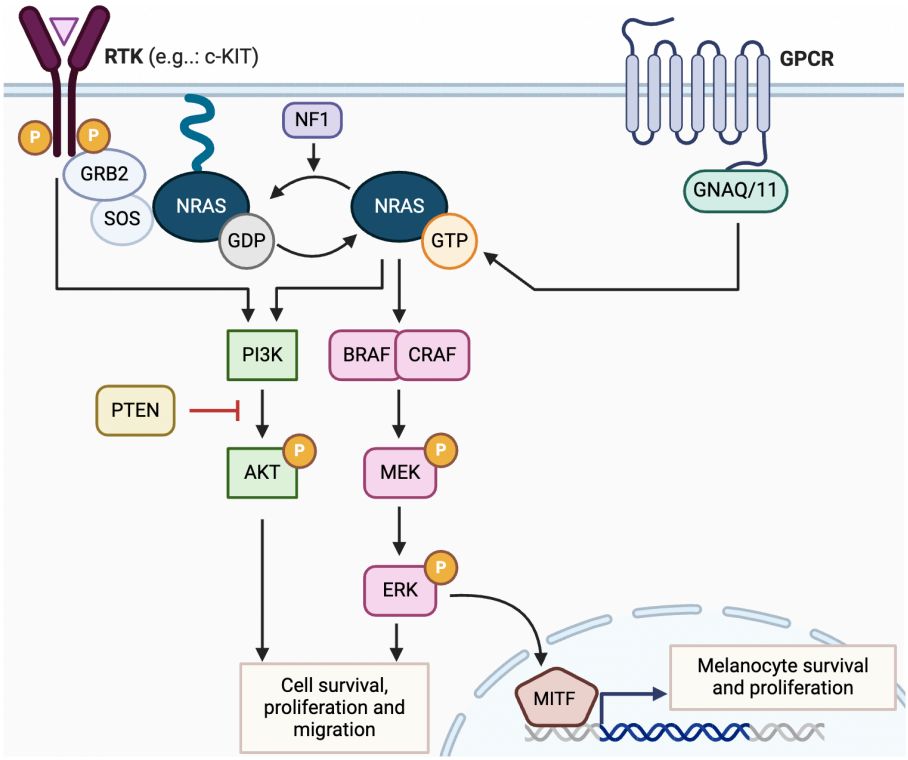


Figure 2 | MAPK and PI3K/AKT pathways. Schematic representation of the two major altered signaling pathways in melanoma: the mitogen-activated protein kinase (MAPK) and the phosphatidylinositol 3-kinase (PI3K)/AKT pathways. Mutations in *NRAS*, *BRAF*, *NF1* and *KIT* result in constitutive MAPK pathway activation. The PI3K/AKT cascade is activated by oncogenic *NRAS*, *KIT* alterations and loss of *PTEN*. Furthermore, mutations in *GNAQ* and *GNA11*, commonly found in uveal melanomas, also lead to the hyperactivation of MAPK and PI3K/AKT pathways. Amplification of the melanocyte-specific transcription factor *MITF* also promote melanoma survival. The aberrant activation of these pathways leads to uncontrolled proliferation, survival and migration of tumor cells.

2.3.2. PI3K/AKT pathway alterations.

The second most frequently activated pathway in melanoma is the PI3K/AKT pathway, and its activation is driven by a number of different factors, including ligand binding to RTKs and GPCRs, and by active GTP-bound RAS proteins. These signals activate the catalytic activity of PI3K, which then activates AKT, resulting in the regulation of essential processes such as cell proliferation and survival. The phosphatase and tensin homolog (PTEN) regulates the activation of the PI3K/AKT pathway by antagonizing the PI3K activity [50] (Figure 2).

The dysregulated activation of the PI3K/AKT pathway in melanoma is in some cases the result of *AKT3* amplification or *PTEN* loss[50]. *PTEN* is a tumor suppressor gene, and missense mutations and chromosomal deletions in this gene are found in approximately 20% of cutaneous melanomas (TCGA database). This loss of *PTEN* results in the constitutive activation of AKT and thus the hyperactivation of this oncogenic pathway[50].

2.3.3. Other pathways alterations.

Alterations in *BRAF*, *NRAS*, *NF1* and *KIT* genes are considered drivers of melanoma development. However, other genes are also involved in melanoma pathogenesis. For instance, amplification of the melanocyte-specific transcription factor *MITF* gene is found in approximately 15% of melanoma samples (TCGA database). MITF is a transcription factor that can regulate multiple biological processes in melanocytes, including differentiation, proliferation, migration, and senescence. In addition, MITF expression and transcriptional activity are regulated by ERK1/2 and p38 activation, among others[51].

Mutations in the telomerase reverse transcriptase (*TERT*) promoter lead to increased *TERT* expression, thus conferring a proliferative advantage to melanoma cells. *TERT* promoter mutations, together with heterozygous alterations in the *CDKN2A* gene, have been frequently detected in *in situ* melanoma[52]. Mutations in the *CDKN2A* gene, which encodes two proteins $p16^{Ink4a}$ and $p14^{Arf}$ through distinct translational programs, lead to uncontrolled cell cycle progression by impairing the function of downstream RB1 and p53, respectively. Bi-allelic inactivation of *CDKN2A* is rarely observed in precursor lesions but serves as a subsequent step in the development of the invasive melanoma phenotype[53].

2.4. Treatment of melanoma.

The majority of newly diagnosed melanoma patients with early-stage disease (more than 99% of patients) can be successfully treated with surgical removal of the tumor[12]. However, some patients may relapse with disseminated disease. Furthermore, approximately 15% of melanoma cases are diagnosed at an advanced stage and are unresectable or have already metastasized[12]. Until a decade ago, the chemotherapeutic agent dacarbazine and interleukin-2 (IL-2) were the only FDA-approved treatment options for these patients, showing very low response rates. However, melanoma treatment has been revolutionized since 2011 with the approval of several therapeutic agents including RAF and MEK inhibitors and immune checkpoint inhibitors[54]. While the existing therapies have significantly changed the standard of care for patients with advanced melanoma, the limited response rates and the emergence of resistance to treatments impede further advances in therapeutic outcomes. Consequently, there is an unmet need to better understand the molecular mechanisms that drive melanoma pathogenesis, which might lead to the development and implementation of more effective therapies for the treatment of advanced melanoma.

2.4.1. Targeted therapy.

As stated above, most of melanomas exhibit hyperactivation of the RAS/RAF/MEK/ERK signaling pathway[41]. Therefore, several therapies targeting components of this pathway have been developed. Approximately 50% of melanomas harbor mutations in the *BRAF* gene, with the most common mutation being $BRAF^{V600E}$. In this regard, the specific BRAF inhibitors vemurafenib and dabrafenib were approved in 2011 and 2013, respectively, for the treatment of metastatic and unresectable *BRAF* mutant melanomas, showing an improved survival when compared to the previously used chemotherapeutic agent dacarbazine[55,56]. However, while these drugs are highly effective in approximately half of patients with *BRAF*-mutated melanomas, most patients develop resistance within a relatively short period of time[55–57].

Some of the mechanisms by which melanoma cells evade BRAF inhibitor therapies have been described, revealing that the majority of resistances involve the reactivation of the MAPK pathway. Upstream of BRAF, pathway reactivation can be driven by overexpression or activating mutations of *NRAS* or loss of *NF1*, leading to MEK activation in a BRAF-independent manner[58,59]. In the presence of activated NRAS, inhibition of BRAF induces the binding of wild-type BRAF to CRAF, resulting in hyperactivation of CRAF and consequently increased MEK and ERK signaling, leading to paradoxical reactivation of the RAS/RAF/MEK/ERK signaling[60]. Furthermore, the constitutive activation of several RTKs such as platelet-derived growth factor receptor β (PDGFRβ), epidermal growth factor receptor (EGFR) or insulin-like growth factor 1 receptor (IGF1R) has also been found to drive resistance by the activation of the MAPK but also the PI3K/AKT signaling pathways[59,61,62]. At the level of RAF kinases, the overexpression of *CRAF*, the amplification of the *BRAF* gene and the presence of truncated forms of BRAF due to alternative splicing also result in constitutive ERK activation[63–65]. Downstream of the BRAF protein, the overexpression or mutation of *MEK* or its activators, such as MLKs or COT/TPL2/MAP3K8, also reactivate the MAPK pathway[66–68].

On the other hand, hyperactivation of the PI3K/AKT signaling pathway has also been identified as a key factor contributing to the development of resistance to BRAF inhibitors in melanoma. One of the most commonly described mechanisms underlying this resistance is the loss of *PTEN*, leading to uncontrolled activation of this pathway and promoting cell survival and proliferation despite the presence of BRAF inhibitors[69]. Moreover, high expression of MITF has also been associated with acquired resistance to BRAF inhibitors, which upregulate

MITF expression particularly in the early stages of patient treatment, allowing melanoma cells to enter a drug tolerance phase in the early steps of BRAF inhibitor treatment[70] (Figure 3).

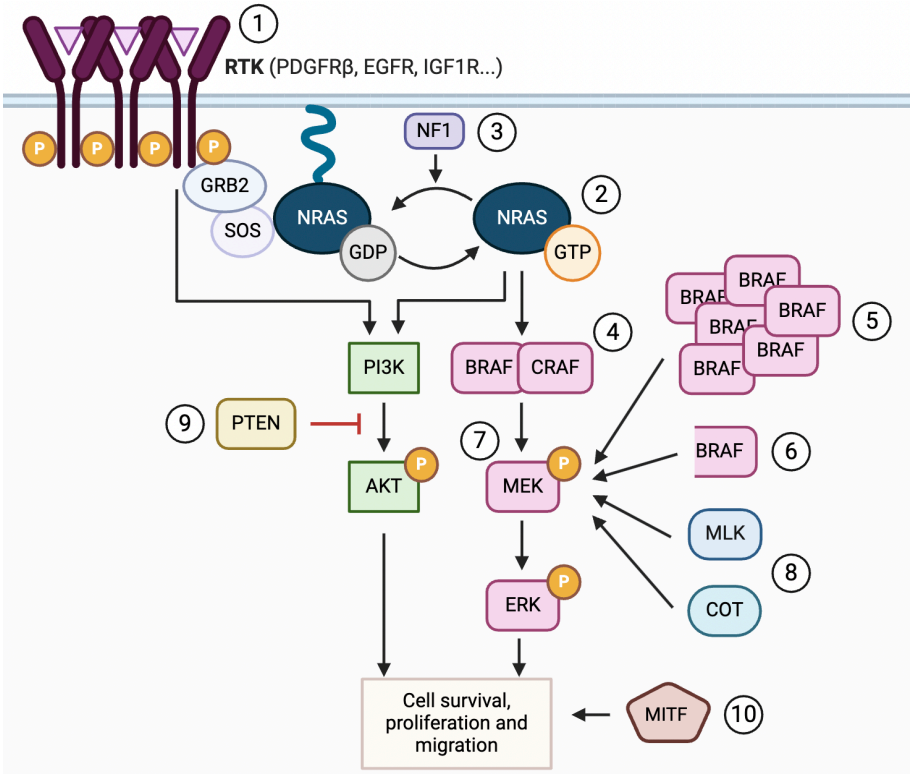


Figure 3 | The most common resistance mechanisms to BRAF inhibition. Representative scheme of the described mechanisms of resistance to BRAF inhibitors: (1) Upregulation of RTKs. (2) Overexpression/activating mutations of *NRAS*. (3) Loss of *NF1*. (4) *CRAF* overexpression. (5) *BRAF* amplification. (6) *BRAF* alternative splicing. (7) *MEK* overexpression or mutation. (8) *COT*/*TPL2*/*MAP3K8* and *MLK* overexpression or mutations. (9) Loss of *PTEN*. (10) *MITF* overexpression.

To overcome BRAF inhibitor resistance, co-administration of BRAF and MEK inhibitors was proposed to avoid the reactivation of the RAS/RAF/MEK/ERK signaling, showing a great success in *BRAF* mutant patients[71,72]. Indeed, the use of BRAF inhibitors, such as vemurafenib, dabrafenib and encorafenib, in combination with MEK inhibitors, like trametinib, binimetinib and cobimetinib, is the standard of care for patients with advanced melanoma that harbor *BRAF* mutations[52]. However, these therapeutic approaches provide a clinical benefit only to patients with *BRAF*-mutated melanomas and the duration of response is still limited, with patients developing acquired resistance after a short period of time in the same genes that support single-agent resistance[73].

The second most frequently mutated gene in melanoma is *NRAS*. Despite the significant role of *NRAS* mutations in melanoma, the development of effective targeted therapies has been largely unsuccessful. First, the development of direct inhibitors of NRAS has been challenging due to the lack of druggable pockets on the RAS protein[74]. Therefore, other strategies have

been attempted to target *NRAS*-mutant melanomas. Farnesyl transferase inhibitors, which prevent the post-translational modification of RAS and its translocation to the cell membrane, have been investigated as a potential treatment strategy. However, clinical trials with these inhibitors have been disappointing due to severe off-target effects and lack of efficacy due to alternative prenylation by geranylgeranyl transferase type 1, which also allows NRAS translocation to the membrane[74,75]. MEK inhibitors, particularly binimetinib, have shown some activity against *NRAS*-mutant melanoma. However, MEK inhibition alone is not sufficient to provide durable responses and the rapid acquisition of resistance hinders successful long-term treatment[72]. To improve the therapeutic efficacy of MEK inhibition, many drug combinations are currently being evaluated, with dual therapies with MEK and pan-RAF inhibitors such as belvarafenib being of particular interest, given the critical dependence of BRAF-CRAF dimerization to mediate NRAS signaling through MAPK pathway[74,76].

Targeting the receptor tyrosine kinase c-KIT, which is frequently mutated especially in acral and mucosal melanomas, is also a potential treatment. Indeed, the use of the specific RTK inhibitors imatinib and nilotinib has shown efficacy in the treatment of *KIT*-mutant, but not *KIT*-amplified, melanomas[77,78].

2.4.2. Immune response in melanoma and immunotherapy.

2.4.2.1. Anti-tumor immune response and immune evasion mechanisms.

The human immune system can distinguish between self and non-self through major histocompatibility complex (MHC) class I molecules, which are involved in the presentation of epitopes derived from proteins that have been expressed and subsequently degraded by the cell and can be either self or non-self. When non-self-epitopes are presented on MHC-I molecules, the immune system is signaled to neutralize these cells. Cancer cells, while essentially self-cells, are highly mutagenic, and the epitopes presented by MHC-I molecules on their surface can be recognized as abnormal by immune cells indicating that these cells require neutralization[79].

Melanoma, in particular, has the highest mutation rate of all cancers[40], thus producing a broad spectrum of highly immunogenic tumor antigens that are recognized by the immune system. These tumor antigens can be divided into tumor-associated antigens (TAA), which are primarily found on tumor cells but are also expressed on normal cells[80], and tumor-specific antigens (TSA) or neoantigens, which are expressed exclusively on tumor cells[81]. In

melanoma, TAAs also include a subset of antigens specific to melanoma cells, including tyrosinase, PMEL/gp100, MART1/Melan-A or tyrosinase-related protein (TRP) 1 and 2, known as melanoma differentiation antigens (MDA)[82–84]. All of these proteins, TAAs, TSAs, and MDAs, are presented on MHC-I molecules on the surface of melanoma cells, which can alert the immune system to the diseased state of the cells. The antigens presented on the MHC-I proteins are recognized by T cell receptors (TCR) found on $CD8^+$ cytotoxic T lymphocytes (CTLs), which can eliminate the detected tumor cells. On the other hand, antigen-presenting cells (APCs), such as macrophages and dendritic cells (DCs), can internalize antigens derived from extracellular proteins and present them via MHC class II molecules to activate $CD4^+$ T helper (Th) cells in the draining lymph nodes (dLNs), which then activate the specific immune response against a particular tumor antigen. Once immune cells have been primed to recognize tumor cells, lymphocytes infiltrate the tumor and stroma and begin to recognize and eliminate these abnormal cells and are now referred as tumor-infiltrating lymphocytes (TILs) (Figure 4). These TILs include $CD4^+$ and $CD8^+$ T cells, B cells, natural killer (NK) and natural killer-T (NK-T) cells, with $CD8^+$ T cells being the most common subtype in melanoma and associated with a better prognosis[79]. In contrast, other immune cells such as M2 macrophages, regulatory T cells (Treg), and myeloid-derived suppressor cells (MDSCs), can infiltrate the tumor and act immunosuppressive, leading to tumor progression[79,85,86].

Despite the initial recognition and elimination of tumor cells by the immune system, tumor cells that are not eliminated develop mechanisms to evade the immune detection and elimination through a process known as tumor immunoediting[85]. Specifically, melanoma cells downregulate the expression of MHC-I, as well as TAAs and MDAs, thereby inhibiting the recognition and elimination of tumor cells by CTLs[87,88]. Furthermore, melanomas also secrete immune inhibitory molecules such as transforming growth factor-beta (TGF-β), prostaglandin E_2 (PGE_2), and immunosuppressive cytokines[85,89,90]. The absence of chemoattractants or their receptors on the infiltrating T cells and the secretion of suppressor factors not only by tumor cells but also by neighboring cells or suppressor immune cells in the tumor microenvironment (TME) also influence tumor immune evasion[85].

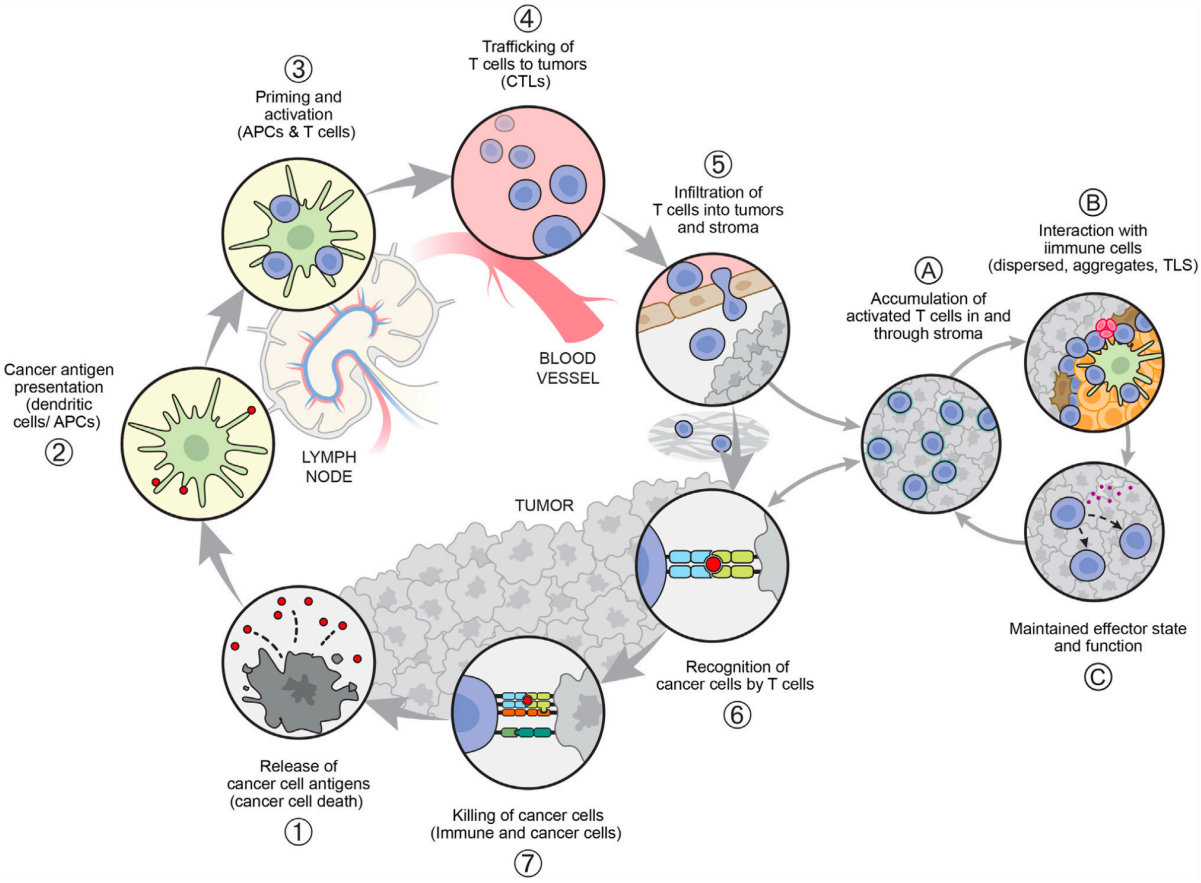


Figure 4 | The cancer-immunity cycle. Schematic representation of the anti-tumor immune response. Released tumor-derived antigens are processed by antigen-presenting cells (APCs), which activate $CD4^+$ T cells to recognize and eliminate tumor cells. Activated T cells migrate and infiltrate into the tumor and stroma, where they detect and kill cancer cells. This anti-tumor response leads to the accumulation of activated T cells in the tumor microenvironment (TME) which interact with other immune cells to effectively eliminate tumor cells. However, within the TME, inhibitory immune cells and stroma, and loss of T cell function can occur, halting the cancer-immunity cycle. TLS, tertiary lymph node structure. *Mellman I. et al. 2023*[86].

Melanoma cells can also evade immune detection by manipulating immune checkpoints, which are regulatory programs that normally ensure an appropriate immune response. However, cancer cells can exploit these mechanisms to avoid detection and elimination by the immune system. Cytotoxic T-lymphocyte-associated protein 4 (CTLA-4) was the first immune checkpoint molecule to be identified. CTLA-4 is a protein receptor that, when expressed on the surface of T cells after antigen activation, can bind to the ligands CD80 and CD86 on APCs with a higher affinity than the co-stimulatory molecule CD28, which also binds to these ligands. The binding of CTLA-4 to CD80/CD86 inhibits the co-stimulatory signal that is necessary for T cell activation, leading to an immunosuppressive effect[91]. Programmed cell death protein 1 (PD-1) was the second immune checkpoint to be discovered. Similar to CTLA-4, PD-1 acts as a negative regulator of T cell activity. When PD-1 on T cells binds to its ligands, PD-L1 or PD-L2, on APCs, it results in inhibition of T cell activity[92].

PD-L1 and PD-L2 have been found to be overexpressed in melanoma, allowing them to evade immune detection and elimination by inhibiting T cell activity[93] (Figure 5).

Other immune checkpoints include lymphocyte activation gene-3 (LAG-3), T cell immunoglobulin and mucin-domain containing-3 (TIM-3), V-domain immunoglobulin suppressor of T cell activation (VISTA) and T cell immunoreceptor with immunoglobulin and ITIM domains (TIGIT). In particular, after chronic antigen stimulation, as occurs in cancer, $CD8^+$ T cells overexpress these co-inhibitory receptors and acquire an exhausted phenotype characterized by loss of cytotoxic activity, reduced cytokine production and reduced proliferative capacity[85,94].

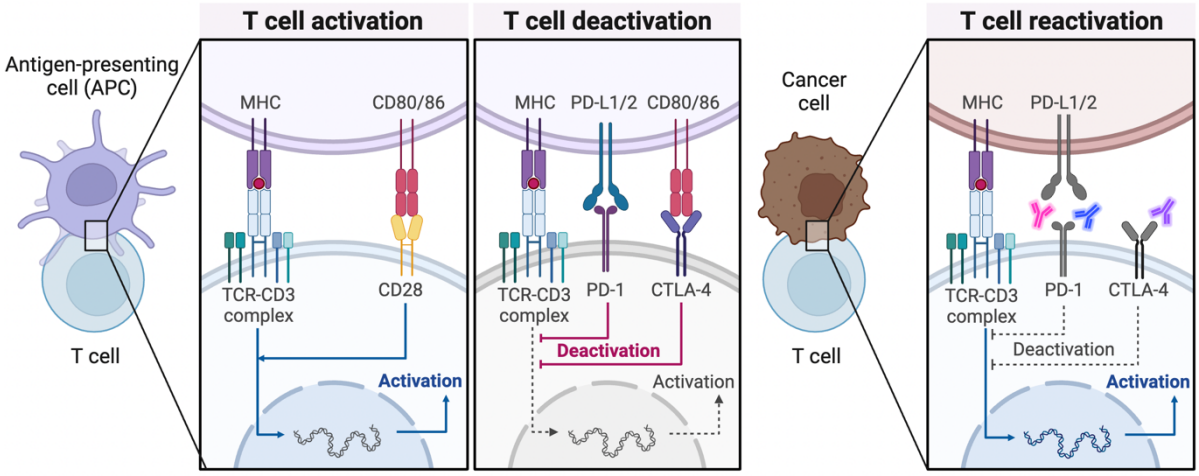


Figure 5 | Immune checkpoint blockade. Representative scheme showing the functionality of immune checkpoints in normal immune response and in tumors, and the use of antibodies against immune checkpoint molecules to reactivate the anti-tumor immune response. Co-stimulatory signals are required for T cell activation by antigen presenting cells (APCs). Binding of CD28 on T cells to CD80 or CD86 expressed on APCs induces activation of T cell function. Activated T cells express immune checkpoint molecules such as CTLA-4 and PD-1, which, when bound to their ligands CD80/86 and PD-L1/2 on APCs, respectively, induce T cell deactivation to ensure an appropriate immune response. However, immune checkpoint molecules such as PD-L1 are often overexpressed on tumor cells, allowing cancer cells to evade immune elimination. In addition, chronic stimulation of antigen-activated T cells induces overexpression of these immune checkpoint molecules, resulting in an exhausted phenotype characterized by loss of T cell activity. For this reason, some cancers, including melanoma, are amenable to treatment with immunotherapy based on antibodies against these immune checkpoint molecules.

2.4.2.2. Immune-based therapies.

To reactivate the immune system and stimulate the anti-tumor immune response, novel therapeutic immune strategies have been developed, including immune checkpoint inhibitors, cancer vaccines and adoptive cell therapies.

2.4.2.2.1. *Immune checkpoint inhibitors (ICIs).*

One of the first immune-based therapies developed for metastatic melanoma, which was approved for use in 1998, was the treatment with the pro-proliferative cytokine IL-2, which promotes the expansion of melanoma-specific T cells. However, only a small percentage of patients responded to IL-2 treatment, which was associated with a high toxicity[11,95].

The most effective treatments for metastatic melanoma to date are the immune checkpoint inhibitors (ICIs). These therapies have revolutionized the management of advanced melanoma, offering the potential for durable tumor regression and long-term cancer control in a significant proportion of patients. The first immune checkpoint inhibitor approved for clinical use was the CTLA-4 blocking antibody ipilimumab in 2011[96]. In 2014, the anti-PD-1 antibodies pembrolizumab and nivolumab were approved for the treatment of advanced and unresectable melanoma, showing an extended survival compared to ipilimumab or chemotherapy[97–99]. Treatment with these antibodies effectively blocks binding to their respective ligands and the corresponding inhibitory signals that cause T cell dysfunction, allowing the re-stimulation of the immune response against the tumor (Figure 5). The subsequent combination of CTLA-4 and PD-1 antibodies demonstrated greater long-term efficacy than either agent alone in metastatic melanoma[100]. However, toxicity was higher and other regimens and/or doses are being investigated[101].

Despite the success of ICIs targeting CTLA-4 and PD-1, not all patients respond to these treatments. This has led to the exploration of additional immune checkpoint molecules to broaden the therapeutic landscape and overcome resistance to current therapies, including LAG-3, TIM-3 and TIGIT. For example, LAG-3 shares a structural similarity with the CD4 receptor and is overexpressed on Treg cells, contributing to their immunosuppressive activity, and on antigen-stimulated T cells, including exhausted T cells. LAG-3 has a higher affinity than CD4 for binding to MHC-II, which has been suggested to affect $CD4^+$ T cell function by inducing cell cycle arrest[102]. However, there is evidence showing that competitive inhibition of CD4 is not a major mechanism of LAG-3-mediated inhibition. In fact, LAG-3 is expressed at higher levels on $CD8^+$ T cells compared to $CD4^+$ T cells and plays an important role in inhibiting their activation, which is independent of CD4. Studies have shown that LAG-3 can regulate the accumulation and effector function of $CD8^+$ T cells in both self-tolerance and tumor-tolerance systems[103]. In March of 2022, the combination of the anti-LAG-3 monoclonal antibody relatlimab with the anti-PD-1 antibody nivolumab was approved for the treatment of

untreated advanced melanoma. This combination demonstrated similar progression-free survival results to the anti-CTLA-4 + anti-PD-1 combination[104].

TIM-3 is another negative regulator of T cell activation, and its interaction with ligands such as galectin-9 can induce T cell apoptosis, contributing to immune evasion by tumors. It is also involved in T cell exhaustion, making combination therapy with PD-1 blocking antibodies an attractive option to enhance the efficacy of anti-PD-1 therapy[105]. Moreover, TIGIT is an inhibitory receptor also expressed by antigen-activated T cells, Tregs and NK cells. Preclinical data showed that TIGIT was upregulated in tumor-antigen-specific $CD8^+$ T cells and $CD8^+$ TILs from patients with melanoma and that these TIGIT-expressing $CD8^+$ T cells also co-expressed PD-1. Indeed, dual blockade of PD-1 and TIGIT, but not single TIGIT blockade, enhanced the proliferation and function of tumor antigen-specific $CD8^+$ T cells and $CD8^+$ TILs of melanoma patients[106,107]. However, the combination of anti-PD-1 with anti-TIGIT antibodies should be further explored for the treatment of patients with advanced melanoma.

Although ICIs have significantly advanced cancer treatment, durable responses remain elusive for most patients, mainly due to the limited understanding of the interaction of the immune system with the tumor and the lack of clear biomarkers of response or resistance to immunotherapy. The reasons for both initial and subsequent resistance to ICIs are not fully understood and include several factors: inadequate infiltration of cytotoxic T cells into the tumor, impaired formation of T memory cells, the presence of immunosuppressive cytokines and immunosuppressive cells within the TME, T cell dysfunction due to upregulation of other co-inhibitory molecules, alterations in interferon-gamma (IFNγ) signaling resulting from mutations in JAK1/2, and impaired presentation of tumor antigens and loss of neoantigens[108,109]. Understanding these mechanisms is critical for developing strategies to overcome resistance and improve the efficacy of ICIs.

2.4.2.2.2. Cancer vaccines.

The discovery of TAAs opened the door for the development of therapeutic cancer vaccines that, unlike prophylactic vaccines that are administered to healthy people to prevent disease, these are administered to patients in the late stages of cancer to try to sensitize the immune system to cancer antigens. Initial vaccination approaches were based on the administration of patient-derived tumor cells together with an adjuvant or virus to activate polyclonal immune responses against TAAs. For example, administration of autologous tumor cells infected with Newcastle disease virus or the combination of vaccine approaches with immune checkpoint

blockade agents showed efficacy in preclinical studies of melanoma and laid the groundwork for the development of more sophisticated vaccine approaches[110,111]. The advent of next-generation sequencing (NGS) technologies has been pivotal in the development of personalized neoantigen-based vaccines. NGS allows for the detailed analysis of the genomic DNA from tumors, identifying unique mutations (neoantigens) that can be targeted by the immune system. Clinical trials using peptide and RNA vaccines designed to target these neoantigens have shown promising results in the treatment of melanoma[112,113]. However, the ability of cancer cells to adapt and evade the immune system and the high mutational burden of melanoma tumors make it difficult to predict which neoantigens will elicit strong anti-tumor responses and to develop effective cancer vaccines. Furthermore, the development of personalized cancer vaccines is also time-consuming and costly, further hindering their widespread clinical use. Despite these efforts, no melanoma vaccines have been approved for clinical use[105].

2.4.2.2.3. Adoptive cell therapy (ACT).

Adoptive cell therapy (ACT) with tumor-infiltrating lymphocytes (TILs) is a form of personalized cancer immunotherapy that uses a patient's own immune cells to fight cancer. TILs collected from the patient's tumor are identified, expanded and stimulated *ex vivo*, and then infused back into the patient to target and eliminate cancer cells. Lymphodepletion followed by non-myeloablative chemotherapy or total body irradiation is usually required before T cell transfer to the patient, which is performed in combination with high doses of IL-2 to increase the survival of the transferred T cells. This approach enhances innate immunity, reduces the competition for homeostatic cytokines and decreases the number of immunosuppressive myeloid cells and Treg cells. However, because the potential targets selected are TAAs, which are present in both healthy and malignant tissues, this therapy leads to autoimmune toxicity, preventing wider use of ACT. To overcome this autoimmune toxicity, genetically engineered T cells expressing chimeric antigen receptors (CARs) or highly active T cell receptors (TCRs) have been developed to target specific antigens expressed on cancer cells[114]. For example, genetically modified T cells expressing TCRs against NY-ESO-1 or expanded $CD8^+$ T cell clones targeting the melanoma-associated antigens gp100 and MART1/Melan-A have demonstrated high efficacy and low toxicity in the treatment of melanoma[115,116]. Despite promising clinical outcomes, however, the extensive effort, cost and time required generating individual TIL cultures limit the use of ACT to only a selected number of specialized institutions. Additionally, the efficacy of ACT is compromised by the

variability in myeloid and lymphocytic infiltration within tumors, as well as the heterogeneous mutational and neoantigen burden. These factors contribute to tumor evasion of immune recognition and elimination by T cells. The unpredictable nature of TIL infiltration after transfer and the potential downregulation of tumor-specific antigens further limits the therapeutic potential of ACT[114].

3. Mitogen-activated protein kinase (MAPK) pathways.

3.1. Classification.

MAPK signaling pathways are critical signaling cascades in cells that mediate responses to various extracellular stimuli, leading to a wide range of cellular behaviors including proliferation, survival, differentiation, development, inflammation and apoptosis. They are generally divided into four major distinct subgroups: extracellular signal-regulated kinase (ERK), p38 MAPK, stress-activated protein kinase/c-Jun NH2-terminal kinase (SAPK/JNK), and ERK5/big MAP kinase 1 (BMK1) pathways. These pathways are highly conserved among eukaryotes and are characterized by a three-tiered kinase cascade involving MAP3Ks, MAP2Ks, and MAPKs. Each cascade is initiated by specific extracellular stimuli that lead to the activation of protein kinases downstream of cell surface receptors and/or small GTPases, which subsequently activate MAP3Ks. Activated MAP3Ks directly phosphorylate and activate MAP2Ks, which in turn activate MAPKs through dual phosphorylation of threonine and tyrosine at conserved tripeptide threonine-x-tyrosine (TXY) motifs within their activation loops. Activated MAPKs phosphorylate a variety of substrates, including other kinases and transcription factors, leading to changes in protein function and gene expression that mediate the cellular response to the initial stimulus. MAPKs typically contain docking motifs that facilitate high-affinity protein-protein interactions. These interactions ensure that MAPKs are activated by the correct upstream MAP2K and that they phosphorylate specific downstream targets[117].

Each member of this family can be activated in response to different stimuli, and they also have specific intracellular activators and targets. The ERK cascade is generally activated by mitogens, growth factors and GPCR agonists, resulting in the regulation of cell proliferation, survival and differentiation. On the other hand, the SAPK/JNK and p38 kinase pathways are not only activated by these stimuli, but also respond to stress and inflammatory cytokines, exerting both protective and pro-apoptotic effects depending on the context memory[117,118]. Similar to the ERK pathway, the ERK5/BMK1 pathway can be activated by mitogens, growth

factors, and GPCR agonists, but it also responds to stress stimuli. ERK5 plays roles in cell proliferation and survival similar to ERK1/2 but is distinguished by a unique C-terminal domain that regulates its activation, subcellular localization, and nuclear shuttling[119] (Figure 6).

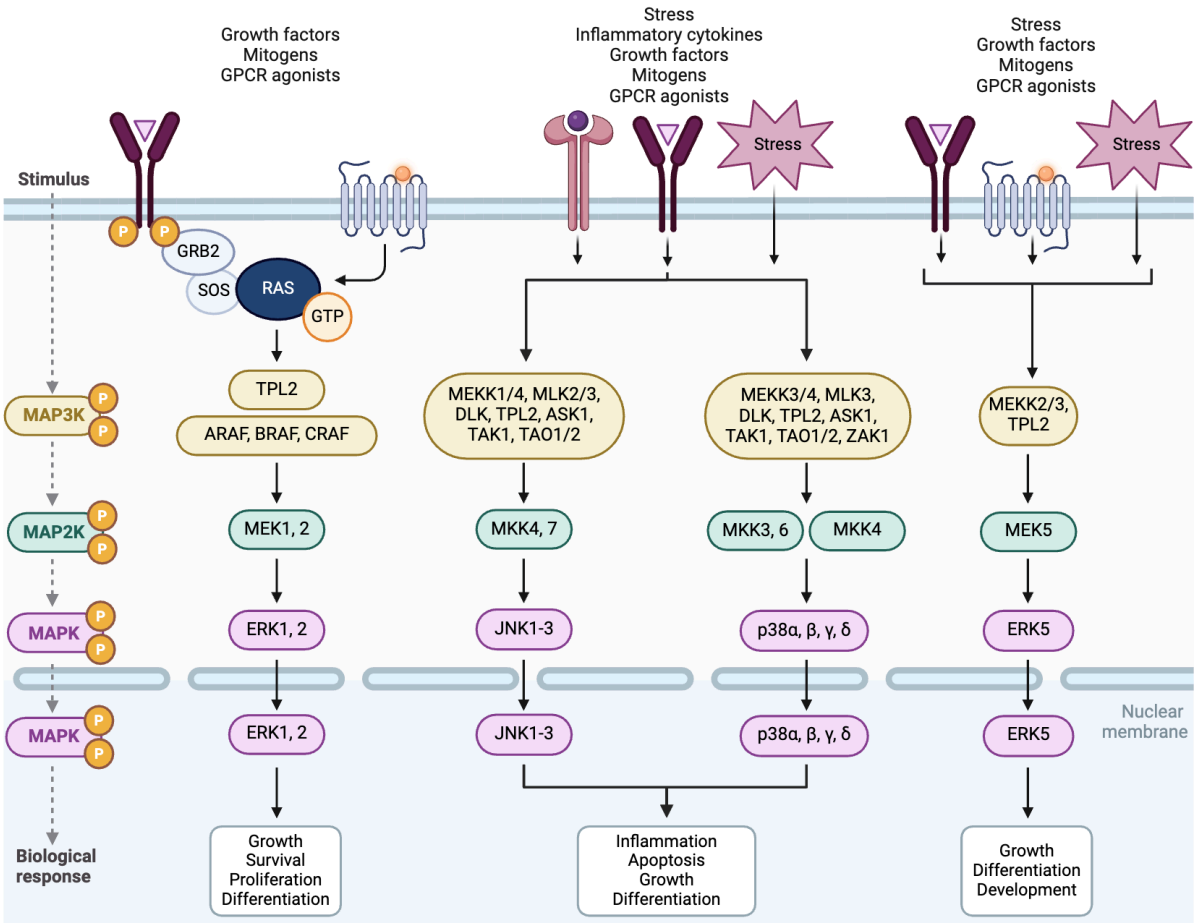


Figure 6 | MAPK signaling pathways. Schematic representation of the four major subgroups of MAPK signaling pathways: ERK, p38 MAPK, SAPK/JNK, and ERK5/BMK1. MAPKs are central to cellular signaling and mediate responses to a variety of extracellular stimuli. These responses encompass a wide range of cellular processes, including proliferation, differentiation, survival, inflammation and apoptosis. They are activated through a kinase cascade involving MAP3Ks, MAP2Ks, and MAPKs. Activation of these pathways involves the sequential phosphorylation and activation of these kinases, culminating in the activation of MAPK, which then phosphorylates various substrates including other kinases and transcription factors to execute cellular responses.

3.2. p38 MAPK pathway.

3.2.1. The p38 MAPK family.

The first member of the p38 MAPK family was identified by four independent studies: as a 38-kDa protein that was rapidly tyrosine phosphorylated in response to lipopolysaccharide (LPS) stimulation[120]; as a target of pyridinyl imidazole derivatives that inhibit the biosynthesis of some inflammatory cytokines such as interleukin-1 (IL-1) and tumor necrosis factor (TNF) in LPS-stimulated human monocytes[121]; as a MAPK-activated protein kinase 2 (MAPKAPK2/MK2) activator in response to arsenite, heat shock or osmotic stress[122]; and as

a protein kinase which was activated in response to IL-1[123]. This new identified protein kinase showed high sequence homology to the *Saccharomyces cerevisiae* HOG1, a kinase involved in the regulation of the osmotic response[124].

Up to date, four members of the p38 MAPK family have been identified: p38α, p38β, p38γ (ERK6, SAPK3), and p38δ (SAPK4), which are encoded by *MAPK14*, *MAPK11*, *MAPK12*, and *MAPK13* genes, respectively[121,125–127]. Despite p38 kinases share more than 60% of th amino acid sequence, these isoforms differ significantly in tissue expression, upstream activators and downstream effectors, and sensitivity to chemical inhibitors[124]. Of these, p38α and p38β isoforms are expressed in most cell types and can be targeted by a class of pyridinyl imidazole drugs such as the widely used SB203580, whereas p38γ and p38δ have more tissue-specific expression patterns and cannot be inhibited by these types of drugs[128,129]. Furthermore, p38α is the only isoform whose genetic disruption causes embryonic lethality due to its key function in placental morphogenesis[130,131], whereas p38β, p38γ or p38δ deficiency in mice has no effect on embryonic viability[132,133]. While p38β can perform some of the functions of p38α, particularly in the absence of p38α, the inability of p38β to fully compensate for the loss of p38α in certain developmental and physiological contexts and the higher expression of p38α in most cell types, highlight the non-redundant and specific functions of p38α[124]. It is important to note that all the isoforms except the p38δ are expressed in melanoma[134].

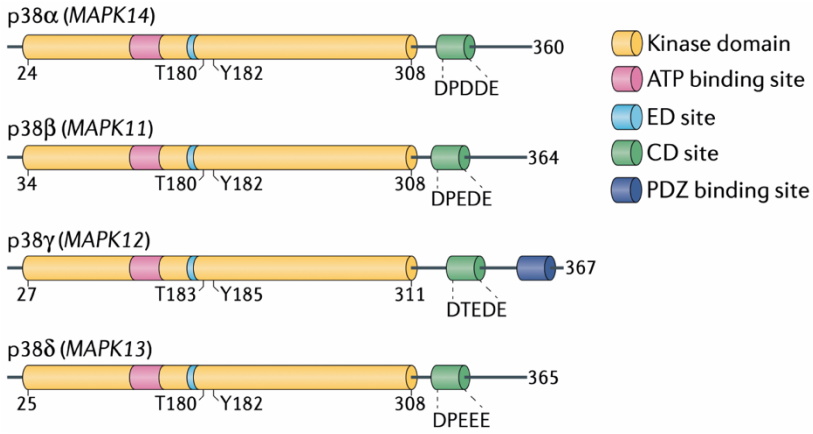


Figure 7 | p38 MAPK family. Schematic representation of the structure of the four human p38 kinases. Gene names (in parentheses), amino acid numbers and the different domains are indicated. The p38 MAPK family members share a highly conserved kinase domain that is central to their catalytic activity. The CD and ED domains play significant roles in substrate and regulator interactions, contributing to the specificity of signaling. The unique carboxy-terminal region of p38γ allows it to interact with PDZ domain-containing proteins, potentially affecting various signaling pathways. Adapted from *Canovas et al. 2021*[124].

The four members share 90% of the amino acid sequence of the kinase domain, which is responsible for their catalytic activity. The domain contains a dual phosphorylation motif

consisting of threonine-glycine-tyrosine (TGY) within the activation loop. The phosphorylation of threonine (T) and tyrosine (Y) residues is crucial for kinase activation, resulting in a conformational change that activates the kinase domain. This process involves the transfer of a phosphate group from ATP, which is bound to the ATP binding site, to specific substrate proteins[124,128]. The common docking (CD) domain is a conserved region located outside the catalytic region of p38 MAPKs. This region is characterized by negatively charged residues that facilitate high-affinity interactions with positively charged docking motifs of substrates and regulators[135]. The ERK docking (ED) site contributes to substrate docking and specificity, particularly for interactions with MAPKAPK2/MK2 and MK3[136,137]. Additionally, p38γ has a carboxy-terminal region that binds to PDZ domain-containing proteins. These proteins often act as scaffolds for signaling pathways. Interactions with p38γ may affect their localization and function[138,139] (Figure 7).

3.2.2. Pathway activation and signal transduction.

The p38 MAPK pathway is activated by external stress such as oxidative stress, UV irradiation, inflammatory cytokines, osmotic shock and growth factors, leading to the activation of a high number of protein kinases and transcription factors involved in the regulation of numerous cellular processes, including cytokine production, apoptosis, migration, proliferation and differentiation[140].

Like other MAPK signaling pathways, p38 kinases are activated by dual phosphorylation by a MAP2K, which in turn is activated by a MAP3K. Several MAP3Ks have been reported to contribute to the activation of p38 kinases, including apoptosis signal-regulating kinase 1 (ASK1), dual-leucine zipper-bearing kinase 1 (DLK1), MAPK/ERK kinase kinase 3 (MEKK3) and MEKK4, mixed-lineage kinase 3 (MLK3), TGF-β-activated kinase 1 (TAK1), thousand-and-one amino acid 1 (TAO1) and TAO2, tumor progression loci 2 (TPL2), and leucine zipper and sterile-α-motif kinase 1 (ZAK1)[128]. Upstream of the cascade, the regulation of MAP3Ks activation involves phosphorylation by STE20 family kinases, binding to small GTPases of the Rho family such as Cdc42 and Rac1, and ubiquitylation by TRAF ubiquitin ligases[124,141]. Different MAP3Ks are activated by different signals, allowing the pathway to integrate a wide range of stimuli, provide versatility in response and integrate p38 MAPK activation with other signaling pathways. Once activated, MAP3Ks phosphorylate the MAP2Ks[124]. Although the dual phosphorylation sites are conserved among p38 members, selective activation by different MAP2Ks has been observed depending on the cell type and stimulus context. The two major upstream MAP2Ks that activate p38 are MKK3, which

preferentially activates p38α, p38γ and p38δ but not p38β, and MKK6, which can phosphorylate all four members[142,143]. Moreover, MKK4, an upstream kinase of JNK, has been reported to phosphorylate p38α and p38δ in certain cell types[144]. This phosphorylation cascade is known as the canonical activation pathway[124] (Figure 8).

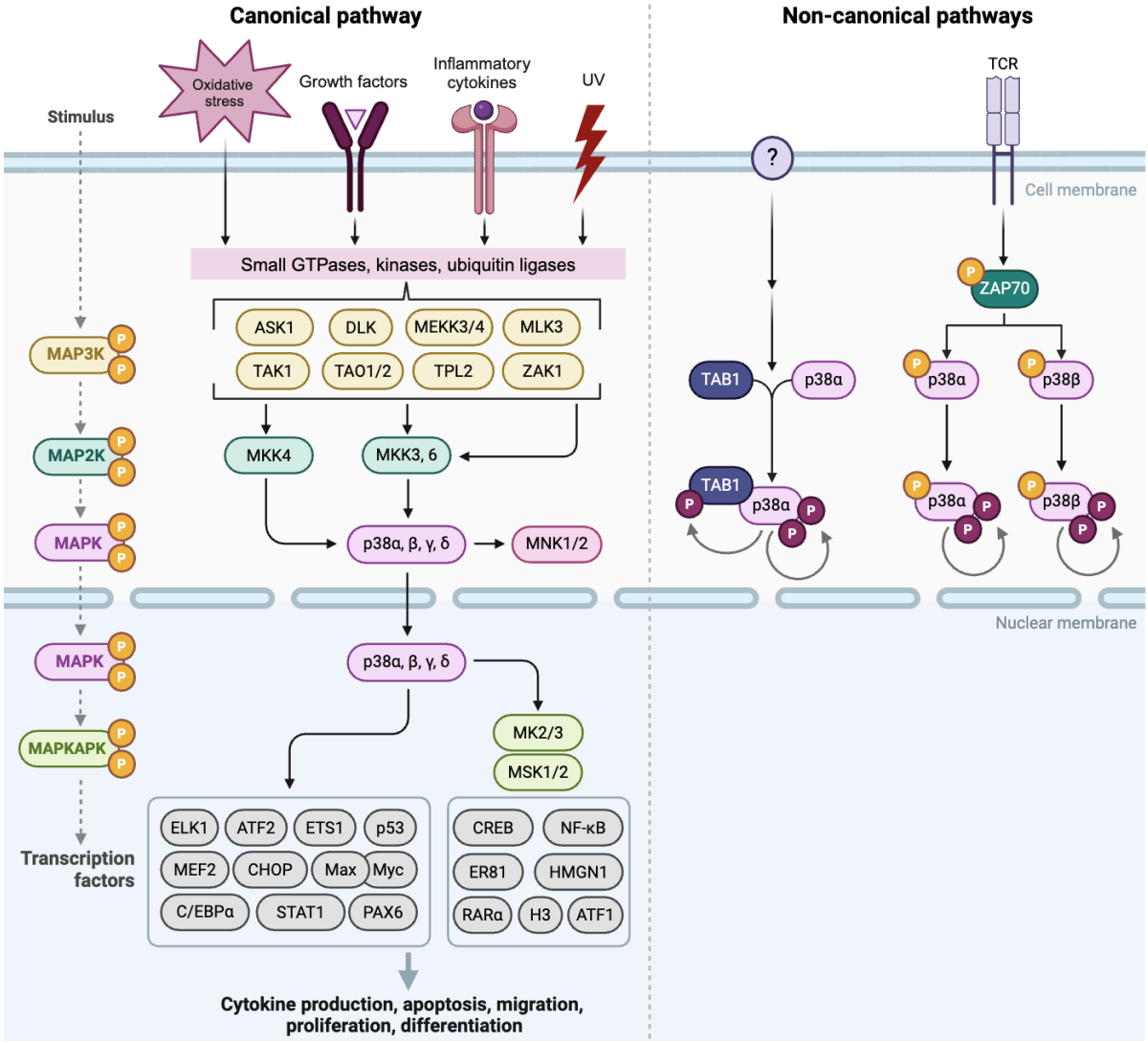


Figure 8 | Canonical and non-canonical p38 MAPK activation pathways. The canonical pathway is activated in response to various stimuli, including stress signals such as oxidative stress and ultraviolet (UV) radiation, growth factors, and inflammatory cytokines, which lead to activation of MAP3Ks through phosphorylation by kinases, binding to small GTPases, and ubiquitylation. Activated MAP3Ks phosphorylate and activate MAP2Ks, which in turn phosphorylate p38 kinases, which activate specific substrates, including other kinases and transcription factors, to regulate numerous cellular processes. Non-canonical pathways include the autophosphorylation of p38α by binding to transforming growth factor-β-activated kinase 1-binding protein 1 (TAB1) triggered by unknown stimuli, or the phosphorylation of both p38α and p38β by ZAP70 following T cell receptor (TCR) activation.

In addition to the activation by upstream MAP2Ks, p38α can also be activated by two non-canonical pathways. One of the MAP2K-independent mechanisms involves binding to TGF-β-activated kinase 1 (TAK1)-binding protein 1 (TAB1), which induces p38α autophosphorylation at T^{180} and Y^{182}, resulting in full activation of the protein[145]. This

mechanism has been implicated in ischemic myocardial injury, T cell senescence, skin inflammation, GPCR agonist-induced endothelial inflammation and triiodothyronine-mediated browning of white adipose tissue, but the signals responsible for the activation of this pathway are not well defined[124]. Furthermore, TAB1 can also induce p38α activation through the canonical pathway by binding to TAK1[146]. The other non-canonical mechanism of p38 activation is mediated by zeta-chain associated protein kinase 70kDa (ZAP70) exclusively in T cells after TCR stimulation, leading to the phosphorylation of p38α and p38β at Y^{323} by ZAP70, which subsequently leads to autophosphorylation of both p38α and p38β preferentially at the T^{180} residue[147]. The monophosphorylated p38α show some kinase activity but altered substrate specificity *in vitro*[148] (Figure 8).

Several mechanisms regulate p38 activation to ensure proper cell homeostasis, as p38 hyperactivation can be detrimental to the cell. Dephosphorylation appears to play an important role in the downregulation of p38α activity. To inactivate the catalytic kinase activity of p38α, there are several phosphatases that target the threonine and tyrosine residues in the activation loop. These include serine/threonine phosphatases such as protein phosphatase 2A (PP2A) and PP2C, and dual-specificity phosphatases of the DUSP/MKP family, which dephosphorylate both threonine and tyrosine residues[124,128]. Interestingly, p38α can induce the expression of some phosphatases such as DUSP1 and create a negative feedback loop[149]. Other regulatory feedback loops include the downregulation of MKK6 expression, the phosphorylation of TAB1 thus affecting both the non-canonical and TAK1-mediated canonical activation, and the phosphorylation of ZAP70 preventing its association with the TCR[124,128].

There are other mechanisms for regulating p38α activity that do not involve dephosphorylation of activation loop residues. Post-translational modifications, including phosphorylation of other residues, acetylation, methylation and proline isomerization, can modulate p38α activity by either facilitating or impairing the interaction with upstream and downstream effectors. Furthermore, p38α signaling can be modulated by scaffold proteins that bind multiple components of the pathway and localize them to a specific area of the cell for site-specific signaling. Moreover, post-translational modifications of MAP3Ks and MAP2Ks also contribute to the regulation of the pathway[124,128].

3.2.3. Downstream substrates of p38α.

As mentioned above, MAPKs possess docking (D) domains, such as CD and ED motifs, to interact with specific upstream MAP2Ks, scaffold proteins, phosphatases and downstream

substrates, allowing for the ordered and sequential regulation of the p38 MAPK pathway and the correct response to a specific stimulus[150].

The use of chemical inhibitors and downregulation of several components of the pathway has led to the identification of many proteins that are potentially phosphorylated by p38 MAPKs. Substrates of p38α are involved in diverse cellular processes, including transcription and chromatin remodeling, protein degradation and localization, mRNA stability, cell cycle, metabolism, endocytosis, apoptosis, cytoskeletal dynamics, and cell migration[128]. In addition, some of the substrates of p38α are also protein kinases that can in turn phosphorylate other proteins, thereby expanding the processes regulated by this pathway. Among the most relevant are MK2 and MK3[122,151], which play an important role in the post-transcriptional regulation of gene expression. Furthermore, MSK1 and MSK2, which are also activated by ERK1/2 in response to mitogens, control gene expression by phosphorylating transcription factors such as cyclic AMP-responsive element-binding protein (CREB), nuclear factor-kappa-B (NFκB) and signal transducer and activator of transcription (STAT) or nucleosome components such as histone H3. Moreover, MNK1 and MNK2 can phosphorylate the initiation factor eIF4E, thereby regulating protein synthesis[124,128].

In addition to protein kinases, p38α activates several transcription factors involved in diverse cellular functions such as apoptosis, inflammation, angiogenesis or proliferation, including cyclic AMP-dependent transcription factor 1 (ATF1)[152] and ATF2[153], p53[154], growth arrest and DNA damage inducible gene 153 (GADD153, or CHOP)[155], CCAAT/enhancer binding protein alpha (C/EBPα)[156], myocyte enhance factor 2 (MEF2)[157], HMG-box transcription factor 1 (HBP1)[158], retinoic acid receptor α (RARα)[159], protein C-ets-1 (ETS)[160], ETS-related protein 81 (ER81)[161], ETS domain-containing protein (ELK1)[162], STAT1[163], activator protein 1 (AP-1)[162,164], paired box protein 6 (PAX6)[165] and MITF[166], among others.

3.2.4. p38α in cancer.

The p38 MAPK signaling pathway is involved in processes important for normal cell function, such as the response to environmental stimuli, and the regulation of gene expression, cell growth, DNA repair, and apoptosis, which are often deregulated in many diseases, including cancer. In this context, both tumor suppressor and pro-tumorigenic functions have been attributed to the activation of this pathway and in particular to p38α[124].

3.2.4.1. Role of the p38 MAPK pathway in the response to stress stimuli.

p38α has been described as a regulator of the cell cycle, specifically the G_1/S and G_2/M checkpoints, acting as a tumor suppressor. UV radiation alters cellular function through several mechanisms, including DNA damage, ROS accumulation, and inflammatory responses. In response to oxidative stress and UV radiation, p38 is activated and phosphorylates transcription factors involved in cell cycle arrest, DNA repair and apoptosis[167]. For example, in response to UV, p38-mediated activation of the transcription factor p53 induces the expression of genes such as $p21^{Waf1}$, which promote cell cycle arrest in G_1 phase, allowing time for DNA repair before cell division, thereby reducing the DNA mutation rate[168]. In addition, p38 can induce G_2/M cell cycle arrest through MK2-mediated phosphorylation of Cdc25B and Cdc25C. This phosphorylation increases the affinity for 14-3-3δ binding, leading to the inactivation of Cdc25B and Cdc25C and preventing the cell from entering the mitotic phase[169]. Furthermore, the p38-dependent activation of p53 promotes the transcription of 14-3-3δ, which binds to phosphorylated Cdc25B and Cdc25C, and GADD45A, which binds to the Cdk1/cyclin B complex, thereby inducing cell cycle arrest at the G_2/M transition and further preventing the propagation of damaged DNA[168,170] (Figure 9).

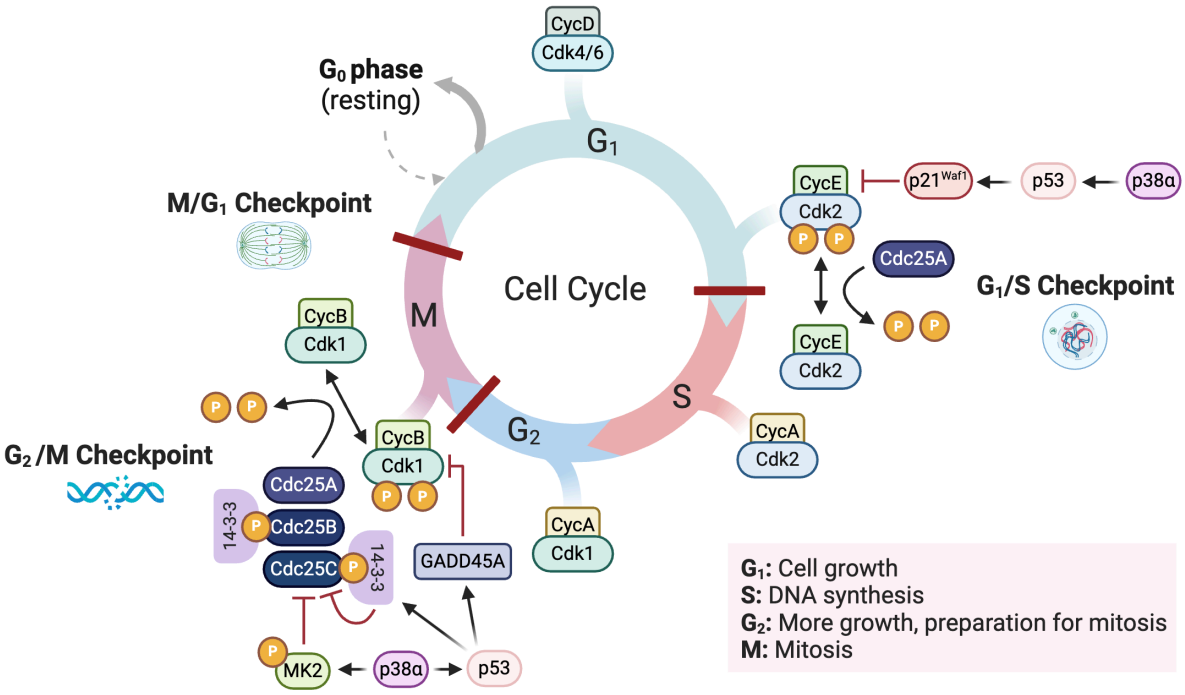


Figure 9 | p38α induced cell cycle arrest in response to stress stimuli. In response to stress, p38 can induce cell cycle arrest at the G_1 and G_2/M phases, preventing the spread of damaged DNA. Specifically, p38 activates p53, leading to the expression of genes such as $p21^{Waf1}$, which induces cell cycle arrest in G_1. In addition, the p53 effector genes 14-3-3δ and GADD45A contribute to G_2/M cell cycle arrest. Furthermore, p38 induces G_2/M cell cycle arrest through MK2-mediated phosphorylation of Cdc25B and Cdc25C, inhibiting their activity and preventing the cell from entering mitosis.

However, most of the irreparably DNA-damaged cells induced by UV irradiation are eliminated by apoptosis. UV-induced apoptosis is thought to be a protective mechanism that ensures the removal of irreversibly damaged and potentially cancerous cells[168]. On the one hand, p38 contributes to UV-induced apoptosis by mediating the release of mitochondrial cytochrome *c* into the cytosol, a critical step in the intrinsic apoptotic pathway. This release leads to the activation of effector caspases, such as caspase-3 and caspase-9, which execute the apoptotic program. In addition, p38 can also phosphorylate and activate proteins of the B-cell lymphoma 2 (Bcl-2) family. These include both anti-apoptotic proteins (Bcl-2, Bcl-xL and myeloid leukemia 1 (Mcl-1)) and pro-apoptotic proteins (Bcl-2 associated X protein (Bax) and Bim). These proteins are essential for regulating mitochondrial integrity and function, which is a central control point for the apoptotic process[168,171]. On the other hand, p38 also mediates UV-induced apoptosis in a p53-dependent manner. Activated p53 can transactivate genes involved in apoptosis, such as Bax, and inhibit the expression of anti-apoptotic genes, such as Bcl-2, thereby promoting apoptosis in response to UV-induced DNA damage[168].

In the skin, p38 has been suggested to play an important role in protecting the skin from UV damage by promoting the tanning response, which is an important protective mechanism against UV-mediated DNA damage. This process involves the increased production of melanin in melanocytes, which is subsequently transferred to keratinocytes to reduce the risk of DNA damage that can lead to skin cancer. In melanocytes, in response to UV, p38 phosphorylates and activates upstream stimulatory factor 1 (USF-1), which induces the expression of *Tyrosinase*, an essential enzyme for the production of melanin[172]. Furthermore, USF-1 also induces the expression of pro-opiomelanocortin (*POMC*) and *MC1R*, which encode a precursor of α-MSH and its receptor, respectively, which are crucial for the pigmentation process[173]. At the same time, binding of α-MSH to its receptor MC1R on melanocytes induces the activation of p38, which regulates melanogenic and proliferative responses[174]. On the other hand, p38 phosphorylates CREB in response to UV, which induces *MITF* expression required for melanocyte survival, proliferation, and activation of melanogenic enzymes such as tyrosinase, TRP-1 and L-dopachrome tautomerase (DCT)[175].

Additionally, p38 plays an important role in the UV-induced inflammatory response, particularly in the skin, leading to the expression of COX-2, which plays an important role in tumorigenesis, and the production of pro-inflammatory cytokines such as TNF, IL-6, IL-8 and IL-1[168,176].

3.2.4.2. Role of the p38 MAPK pathway in the inflammatory cytokine response.

The p38 MAPK pathway plays an important role in mediating responses to inflammatory cytokines and regulating their expression. Inflammatory cytokines such as TNF, IL-6, and IL-1β are key activators of p38α, regulating the production of inflammatory mediators in different cell types[124]. At the same time, p38α signaling regulates the production of these pro-inflammatory cytokines, which modulate growth and survival and therefore show remarkable pro-tumorigenic capacities, through the activation of transcription factors, such as NFκB, or at the posttranscriptional level, by regulating the stability or the translation of the corresponding mRNAs, which is mostly mediated by the downstream kinase MK2[124,177]. In addition, cancer cells also rely on p38α for the production of cytokines and chemokines that recruit pro-tumorigenic myeloid cells into the tumor niche[178].

Apart from the regulation of cytokine production, p38α can also modulate the expression of cytokine receptors. For example, p38α can phosphorylate the IFNα/β receptor IFNAR1, leading to ubiquitin-dependent degradation of the receptor, which has been associated with metastatic disease and poor prognosis in several cancers including colorectal cancer and melanoma[179,180].

3.2.4.3. Role of the p38 MAPK pathway in oncogene-induced senescence.

Oncogene-induced senescence (OIS) is a critical tumor suppressor mechanism that arrests the proliferation of cells harboring oncogenic mutations, thereby acting as a barrier to cancer development. Several studies have shown that the p38 MAPK pathway plays a key role in this process by mediating cell cycle arrest induced by oncogenic *ras* or its downstream effector *raf-1*[181–184]. These studies have shown that activation of p38 by oncogenic *Ha-rasV12*, which is an activated *ras* allele, or active *raf-1*, leads to a state of permanent cell cycle arrest or senescence through the stimulation of its protein kinase activity by the upstream kinases MKK3 and MKK6[181–184]. Conversely, inhibition of p38 activity can prevent the induction of senescence, highlighting the essential role of this pathway in OIS[181]. In addition, the p38 MAPK pathway acts downstream of the RAS/RAF/MEK/ERK cascade to mediate *ras*-induced OIS[181,182].

Regarding the molecular mechanisms linking the ERK and p38 MAPK pathways in the induction of OIS, several mechanisms have been proposed. On the one hand, activation of the RAS/RAF/MEK/ERK cascade by oncogenic *ras* can lead to the accumulation of ROS, which in turn may activate p38 and induce OIS[185,186]. On the other hand, hyperproliferative signals

from activated ERK can cause DNA damage due to DNA hyper-replication, activating p38 and leading to senescence-like cell cycle arrest[185,187,188]. It has been shown that oncogenic *ras*-induced ROS cause activation of DNA damage responses[189,190]. Therefore, the involvement of ROS and DNA damage in the sequential activation of the ERK and p38 MAPK pathways may not be mutually exclusive.

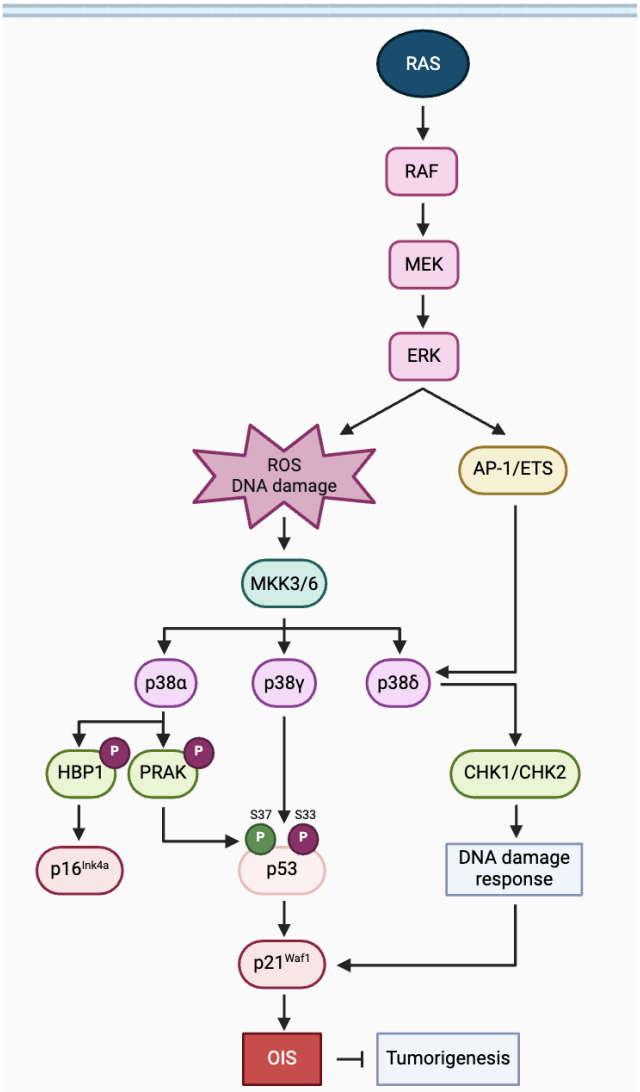


Figure 10 | Oncogenic *ras*-induced senescence is mediated by sequential activation of the RAS/RAF/MEK/ERK and p38 pathways. The p38 MAPK pathway, specifically involving p38α, p38γ, and p38δ, plays a crucial role in oncogene-induced senescence (OIS). In response to oncogenic *ras*, ERK activates the transcription factors AP-1 and ETS, inducing the expression of p38δ, which contributes to OIS by regulating CHK1 and CHK2. p38α mediates OIS by phosphorylating of HBP1, which induces $p16^{Ink4a}$ expression, and by activating PRAK, which phosphorylates p53 at serine 37. p38γ phosphorylates p53 at serine 33, which leads to $p21^{Waf1}$ expression and, together with $p16^{Ink4a}$, promotes OIS.

Among the p38 MAPK members, only p38α, p38γ, and p38δ mediate OIS through different mechanisms. The expression of p38δ is stimulated by the transcription factors AP-1 and ETS, which in turn are activated by ERK in response to oncogenic *ras*. Furthermore, p38δ mediates OIS by regulating the activity of checkpoint kinase 1 (CHK1) and CHK2, two DNA damage

checkpoint kinases involved in *ras*-induced DNA damage responses[191]. In addition, p38α can mediate OIS by phosphorylating HBP1, which induces $p16^{Ink4a}$ expression[192,193], or by activating the p38-regulated/activated protein kinase (PRAK), which in turn activates p53 through phosphorylation at serine 37[194]. Moreover, p38γ also phosphorylates p53, but at serine 33. Activated p53 induces the expression of $p21^{Waf1}$, which together with $p16^{Ink4a}$ contributes to OIS[192]. The requirement of p38 for OIS suggests that the p38 MAPK pathway may have a tumor suppressor function in addition to its previous roles in inflammatory and stress responses.

3.2.4.4. Role of the p38 MAPK pathway in tumor growth and progression.

Despite the p38 MAPK signaling pathway is best known for its tumor suppressor functions due to its involvement in cell cycle arrest and apoptosis, there is evidence suggesting that it may also have oncogenic potential under certain conditions, particularly in the context of metastasis and the regulation of the immune response within the tumor microenvironment[195]. In general, experimental evidence suggests that, during tumor initiation, p38 MAPK acts primarily as a tumor suppressor, maintaining cell homeostasis and ultimately inducing cell death. However, more advanced tumors may benefit from increased activation of the pathway, by inducing cell survival and proliferation, and promoting the production of extracellular factors that support tumor progression[124,196].

Moreover, p38α may promote metastasis of different types of cancer, including melanoma, by targeting several proteins involved in the regulation of epithelial-mesenchymal transition (EMT), cell migration and vascularization. In particular, matrix metalloproteinases (MMPs), especially MMP-2 and MMP-9, play a key role in promoting tumor cell infiltration and migration by degrading components of the extracellular matrix[197]. The expression of these MMPs has been suggested to be regulated by p38 MAPK through the activation of several transcription factors such as NF-κB and AP-1 in various cancers, including melanoma[198–202]. It has also been shown that NF-κB induces the overexpression of MMP-2 and MMP-9 through the activation of osteopontin (OPN/SPP1), another protein of the tumor microenvironment, thus playing a fundamental role in the development and progression of melanoma[203,204].

Furthermore, p38 MAPK also plays a role in the regulation of angiogenesis. For example, p38 MAPK is involved in both the production and the downstream signaling of the vascular endothelial growth factor (VEGF), leading to the secretion of angiogenic factors to promote the formation of new blood vessels[205,206]. In melanoma, p38 induces the degradation of plasma

membrane Ca^{2+} pump isoform 4b (PMCA4b), a metastasis suppressor that contributes to the invasive activity of *BRAF*-mutant melanoma cells[207].

Pro-tumorigenic roles of p38 MAPK signaling have also been reported in immune cells such as macrophages and DCs, where p38α signaling promotes inflammation associated with tumorigenesis in mouse models[208–210].

3.2.5. p38α as a therapeutic target.

The discovery of p38α as a regulator of inflammation and immune response has led to the development of chemical inhibitors for various inflammatory diseases. To date, several selective inhibitors of p38 MAPK have been synthesized, including SB203580[211], doramapimod (BIRB-796)[212], talmapimod (SCIO-469)[213], neflamapimod (VX-745)[214], losmapimod (GW856553X)[215], PH-797804[216] and LY2228820[217]. However, the translation of p38α inhibitors into the clinic has been challenging due to the non-specific effects of some inhibitors, the use of models that do not accurately recapitulate the actual disease environment, and the complexity of the functions regulated by p38α. As a result, no compounds have yet been approved[124].

The p38 MAPK signaling pathway has a broad regulatory impact on cellular functions, and its prolonged inhibition in chronic conditions such as autoimmune or neurodegenerative diseases may lead to adverse effects and reduced efficacy due to adaptation. However, in the context of cancer, acute application of p38α inhibitors, particularly in combination with other drugs, may provide more favorable responses[124]. Several *in vivo* studies have shown that p38 inhibitors can suppress tumor progression. However, inhibition of p38α may promote tumor initiation in other tissues exposed to oncogenic stimuli[196]. Given that p38 MAPK also regulates the response to chemotherapeutic agents and contributes to the development of resistance[196], an increasingly relevant approach is based on the synergistic effect observed when classical anticancer drugs are combined with p38 inhibitors. Inhibiting p38 MAPK can decrease the expression of stemness factors, impair the survival of circulating tumor cells, and overcome chemoresistance. This suggests that combining p38 inhibitors with chemotherapy could allow for lower doses of toxic chemotherapy drugs to be used, potentially reducing side effects and improving treatment outcomes[218]. In addition, p38 MAPK inhibitors have been reported to synergize with cisplatin in breast cancer[219], reduce resistance to the multi-kinase inhibitor sorafenib in hepatocarcinoma[220], restore sensitivity to fibroblast growth factor receptor (FGFR) inhibitors in non-small cell lung cancer[221], and enhance the cytotoxic effects of other

chemotherapeutic agents in various cancer types[124]. These findings suggest that targeting p38 MAPK may enhance the effects of chemotherapy and may be a promising approach to cancer treatment.

Given the role of the p38 MAPK pathway in the response and production of inflammatory cytokines with pro-tumorigenic effects[177,178], and in modulating the immunosuppressive function of several immune cells such as macrophages, DCs, and Treg cells[208–210,222], therapeutic inhibition of p38 MAPK may benefit patients receiving immunotherapies. Indeed, pharmacological inhibition of p38 in tumor-reactive T cells *ex vivo* enhanced their anti-tumor functions *in vivo* in melanoma and in acute lymphoblastic leukemia mouse models, and also improved the functionalities of human tumor-reactive and genetically engineered T cells, suggesting the use of p38 inhibitors to improve the therapeutic efficacy of ACT[223]. Another study showed that the addition of the p38 inhibitor doramapimod increased T cell proliferation and function, and conferred resistance to TGF-β-induced functional suppression of T cells, resulting in enhanced T cell generation for ACT[224]. Moreover, blocking both the p38 MAPK signaling and PD-1 enhanced the proliferation of senescent $CD8^+$ T effector memory cells *in vitro*, suggesting a potential benefit of this combination in cancer patients[225]. Indeed, p38 inhibition enhanced the efficacy of the treatment with PD-L1 and CTLA-4 blocking antibodies in mouse models[226]. In addition, p38 inhibition in DCs has been shown to enhance the priming of tumor-specific effector T cells[227] and to improve the efficacy of the treatment with a monoclonal antibody against CD137 in glioblastoma cells *in vitro*[228]. Taken together, these studies suggest a potential clinical benefit for the use of p38 inhibitors to improve the efficacy of immunotherapies.

Targeting downstream kinases of the p38 MAPK pathway, such as MK2, represents a promising strategy to improve the efficacy of cancer treatments while limiting the broad and sometimes adverse effects associated with direct p38 inhibition. For example, inhibition of MK2 has been shown to inhibit pro-inflammatory cytokine production without serious adverse effects[229] and to induce regression of p53-deficient tumors *in vivo* after treatment of mice with cisplatin and doxorubicin[230], supporting its further clinical use.

Nearly all clinical trials to date have failed, and the development of compounds that induce p38 degradation[231] and the potential to target p38 in a tissue-specific manner[232] have been considered to improve efficacy and reduce the adverse effects of systemic administration. Furthermore, inhibition of the nuclear translocation of p38α, and thus its functions in the

nucleus, has been shown to reduce cancer cell proliferation and inflammation in mouse models[233].

Therefore, efforts should be focused on gaining a better understanding of how p38 contributes to cancer development and progression at both the cellular and organismal level, in order to develop better compounds that specifically target other components or products of this MAPK pathway to improve treatment efficacy, overcome the limitations associated with conventional inhibitors, and open the possibility of combining p38 inhibitors with other therapeutic strategies to enhance their efficacy.

HYPOTHESIS AND OBJECTIVES

Melanoma, one of the most aggressive forms of skin cancer, has been extensively used as a model tumor for understanding immunity to cancer and for the development of immunotherapy. Although immune-based therapies have dramatically changed the treatment of many types of cancers, including melanoma, their effectiveness is limited to a small fraction of patients, primarily due to the lack of clear biomarkers for the response or resistance to immunotherapy. Therefore, understanding the interactions between melanoma tumor cells and the immune system, and the evolving changes that lead to tumor immune evasion, is critical for the development and implementation of more effective cancer treatments. In this context, not much is known about how oncogenic pathways influence the immune infiltrate, which could have a significant impact on therapies.

Although RAS pathway activation is a central event in melanoma, MAPK stress pathways also play an important role in several processes related to the melanoma development and progression, including the signaling of several cytokines that modulate and activate the immune system. Previous results from our group showed that spontaneous mouse tumors and human samples harbor genetic alterations in these pathways, including alterations in *MAPK14*, the gene encoding p38α. Despite the well-established contribution of p38α in response to UV in the existing literature, its role in UV-induced melanoma development remains unexplored. Furthermore, the involvement of p38α in melanoma progression, including potential modulation of the immune system and tumor microenvironment, is also unknown.

In line with this, the overall aim of this thesis is to understand the role of p38α in melanoma development and progression in cooperation with $BRAF^{V600E}$ oncogene and UV irradiation, and its contribution to the modulation of the intratumoral immune response. To further elucidate how p38α may be involved in melanoma pathogenesis and potentially lead to the identification of new biomarkers and the development of new immune-based therapeutic strategies, the following objectives have been outlined.

Objectives:

1. **To determine the status of p38α in human cutaneous melanoma.**

2. **To define the status and functionality of p38α in *BRAF* mutated human melanoma cells.**
   2.1 To study the consequences of p38α downregulation and inhibition in *BRAF* mutated melanoma cells.

3. **To establish the significance of p38α in melanoma development and progression using UV-induced *Braf*^{V600E} mouse melanoma models.**
   3.1 To generate UV-inducible *Tyr::CreER*^{T2}; *Braf*$^{CA/CA}$; *p38α*$^{F/F}$ melanoma mouse model.
   3.2 To evaluate the role of p38α in melanoma development and progression in response to UVB.
   3.3 To establish the contributions of p38α in modulating the intratumoral immune response.
   3.4 To study the role of p38α in regulating of the expression of critical inflammatory molecules that modulate the anti-tumoral immune response.
   3.5 To investigate the role of p38α in the response to immunotherapy in syngeneic mouse models.

4. **To correlate our results with human data and evaluate the contribution of p38α in the immunotherapy response to determine response biomarkers.**

RESULTS

p38α is altered in human cutaneous melanoma and is associated to a poor survival of patients.

Initially, we leveraged previous work from our group where we analyzed the whole-exome sequencing data from tumors from three different melanoma mouse models (UVB-induced Tyr::*CreER*^{T2};*Braf*$^{CA/CA}$;*Lkb1*$^{F/F}$ (McGrail K. *et al.*, 2024)[234], *Sleeping beauty*; Tyr::*CreER*^{T2};*Braf*$^{CA/CA}$ (Mann MB. *et al.*, 2015)[235] and a chronic UV irradiation Tyr::*CreER*^{T2};*Braf*$^{CA/CA}$ (Viros A. *et al,* 2014)[236]), and compared this analysis with the human melanoma data from The Cancer Genome Atlas (TCGA Firehose Legacy) database (n = 479 tumors/470 patients) (Figure 11).

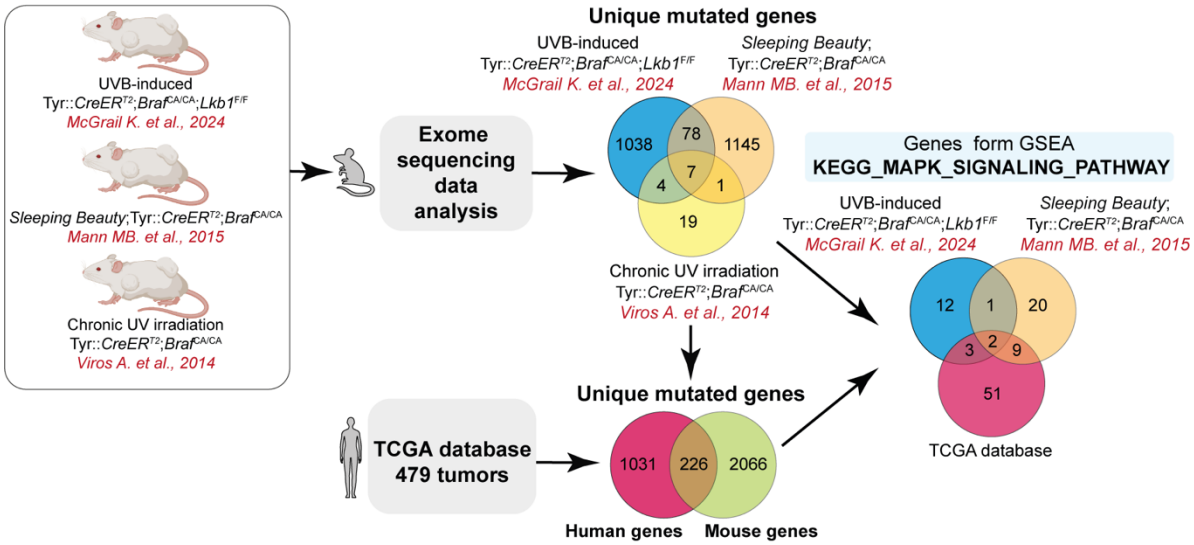


Figure 11 | Common altered genes in mouse and human melanoma. Whole-exome sequencing data form three different melanoma mouse models including UVB-induced Tyr::*CreER*^{T2}; *Braf*$^{CA/CA}$; *Lkb1*$^{F/F}$ (n = 8 tumors), *Sleeping beauty*; Tyr::*CreER*^{T2}; *Braf*$^{CA/CA}$ (n = 77 tumors), and chronic UV irradiation Tyr::*CreER*^{T2}; *Braf*$^{CA/CA}$ (n = 77 tumors) were analyzed, and unique mutated mouse genes (n = 2292) were compared with the mutated genes found in the human Skin Cutaneous Melanoma dataset (TCGA, Firehose Legacy, n = 479 samples/470 patients) (n = 1257). These common altered genes in both mouse and human melanomas (n = 226) underwent to a GSEA analysis, that revealed the involvement of some of these common genes in MAPK signaling pathways (n = 98).

The analysis of the UVB-induced Tyr::*CreER*^{T2}; *Braf*$^{CA/CA}$; *Lkb1*$^{F/F}$ (our model) and the *Sleeping beauty*; Tyr::*CreER*^{T2}; *Braf*$^{CA/CA}$ revealed a total of 1127 and 1231 unique mutated genes (VAF 10%) respectively, whereas Viros *et al.*, study published only 31 of the identified mutated genes[236]. TCGA human data analyses showed that human melanoma harbored similar number of unique mutated genes (1257 (VAF 10%) out of approximately 20.000 genes). Despite the low number of genes published by Viros *et al.*, 35% of these genes were also altered in our UVB-induced melanoma model. The study from Mann *et al.* (*sleeping beauty*) was designed to identify tumor suppressor genes (loss of function) that would cooperate with BRAF activation (*Braf*^{V600E}). Eighty-five of those genes were also found altered in our

UVB-induced melanoma model. Among all used mouse models, we identified 2292 unique mutated genes, out of which, 226 genes were also altered human melanoma tumors indicating the robustness of these spontaneous melanoma models recapitulating the genetic alterations in the human disease. Further functional and pathway enrichment analysis (Gene Set Enrichment Analysis, GSEA) revealed that 98 of these 226 commonly altered genes were associated to the MAPK signaling pathways (Figure 11).

MAPK signaling pathways are subdivided into four main different pathways: extracellular signal-regulated kinase (ERK), p38 MAPK, stress-activated protein kinase/c-Jun NH2-terminal kinase (SAPK/JNK) and ERK5/big MAP kinase 1 (BMK1) signaling pathways[117]. In melanoma, the most commonly mutated genes are *BRAF* and *NRAS*, which are involved in the ERK pathway. However, the analysis of the commonly altered genes associated to the MAPK signaling pathways in human and mouse melanomas revealed that a number of these genes were components of the SAPK/JNK and p38 MAPK stress pathways[237]. Detailed analysis of genetic alterations in the components of the SAPK/JNK and p38 MAPK pathways in the Skin Cutaneous Melanoma dataset (TCGA, Firehose Legacy) identified *MAPK14* as the most frequently altered gene (25% of the patients) (Figure 12).

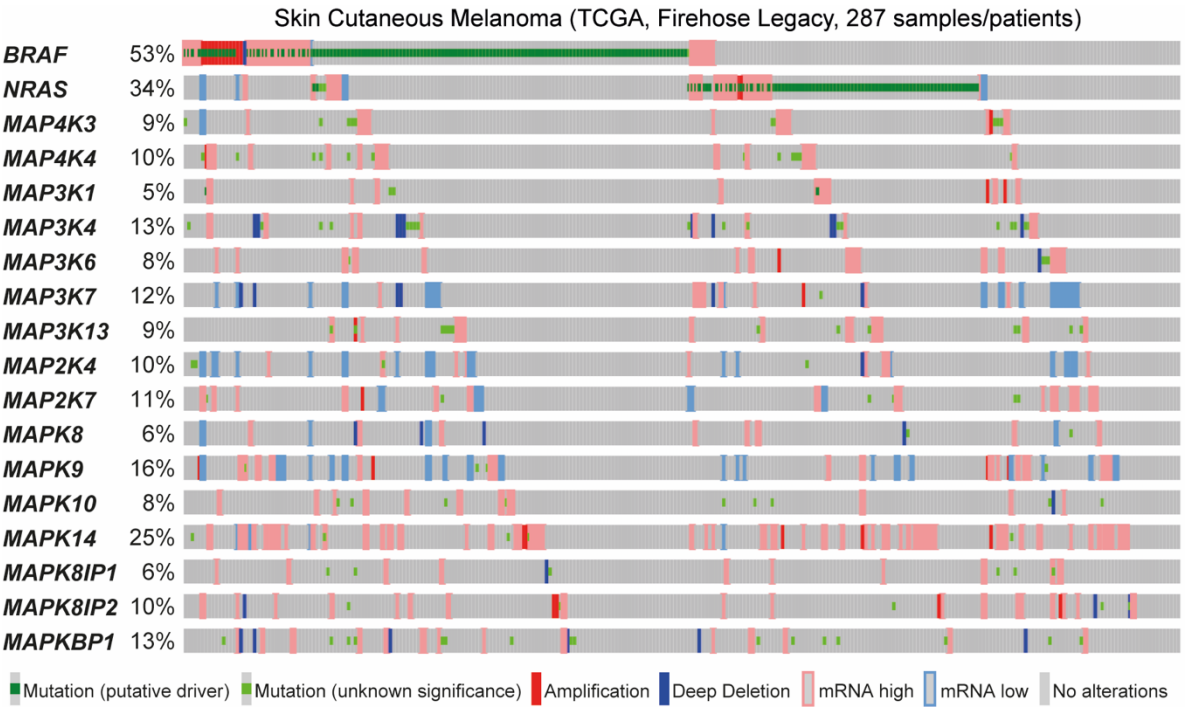


Figure 12 | Genetic alterations in SAPK/JNK and p38 MAPK pathway components in human skin cutaneous melanoma (TCGA database). Human data from the Skin Cutaneous Melanoma dataset (TCGA, Firehose Legacy, n = 287 samples/patients) showing the percentage of genetic alterations found in cutaneous melanoma for the following genes: *BRAF*, *NRAS*, *MAP4K3*, *MAP4K4*, *MAP3K1*, *MAP3K4*, *MAP3K6*, *MAP3K7*, *MAP3K13*, *MAP2K4*, *MAP2K7*, *MAPK8*, *MAPK9*, *MAPK10*, *MAPK14*, *MAP8IP1*, *MAPK8IP2* and *MAPKBP1*.

Further analysis of *MAPK14* genetic alterations (mutation, structural variant, amplification or deletion) among 10,967 tumor samples (10,953 patients) across 32 different tumor types (TCGA database), identified skin cutaneous melanomas as the tumor type more frequently altered in this gene (Figure 13A). The percentage of samples harboring mutations in *MAPK14* was relatively low; however, it appeared to be transcriptionally upregulated and/or amplified in 25% of the skin cutaneous melanomas during tumor progression (from Clark stage II to stage IV) (Figure 13B). These alterations were more frequent in *NRAS*- than in *BRAF*-mutated melanomas, mostly at early stages (Clark stage II and III, 50-54% vs. 20-22%, of tumors, respectively) (Figure 13C).

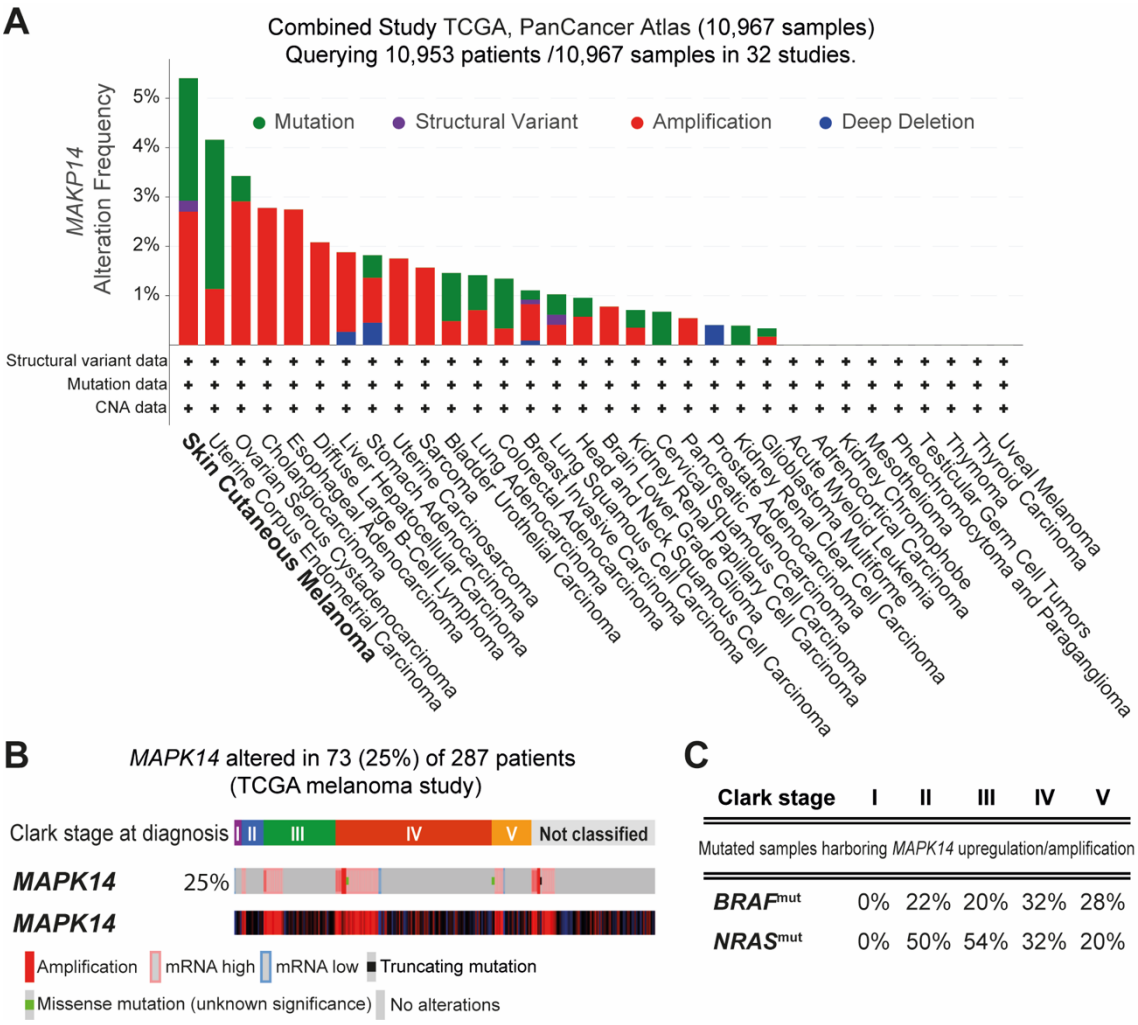


Figure 13 | *MAPK14* alterations in cutaneous melanoma. (**A**) Human data from TCGA database (PanCancer Atlas, n = 10967 samples/10953 patients) showing *MAPK14* alteration frequency in 32 studies from different cancer types. (**B**) Human data from the Skin Cutaneous Melanoma dataset (TCGA, Firehose Legacy, n = 287 samples/patients) showing *MAPK14* alterations in cutaneous melanoma. Samples are sorted by Clark level at diagnosis (I-V). (**C**) Table showing the percentage of *BRAF* or *NRAS* mutated samples harboring either mRNA upregulation or amplification of *MAPK14*.

Importantly, patients harboring alterations in *MAPK14* were associated to a poor survival independently to any other genetic alteration/s (Figure 14A); however, this condition did not

impact on melanoma recurrence (Figure 14B). Furthermore, the presence of alterations in *MAPK14* decreased the survival of patients harboring mutations in either *BRAF* (Figure 14C) or *NRAS* (Figure 14D) genes.

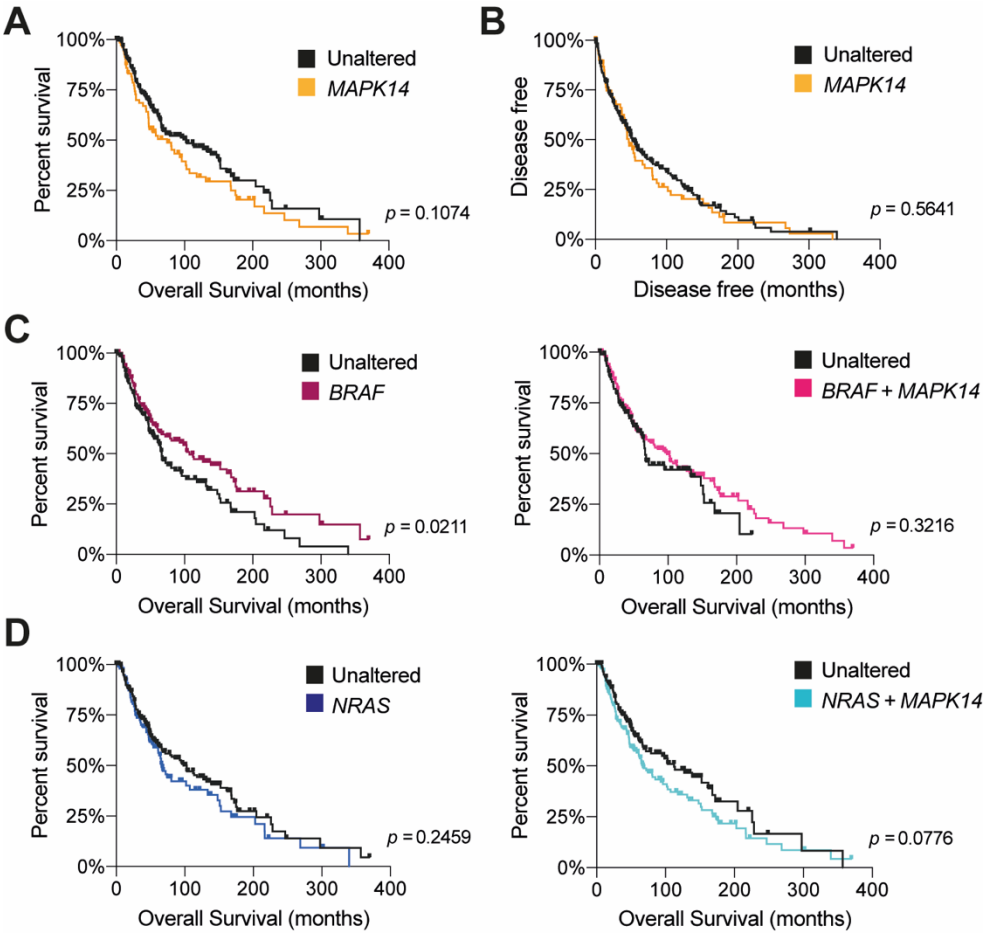


Figure 14 | Alterations in *MAPK14* are associated with a poor survival of cutaneous melanoma patients. Kaplan-Meier graphs from human data from Skin Cutaneous Melanoma (TCGA, Firehose Legacy, n = 287 patients) dataset showing (**A**) the percent survival and (**B**) disease free survival of patients with alterations in *MAPK14*, (**C**) the percent survival of patients with alterations in *BRAF* and in *BRAF* together with *MAPK14*, and (**D**) the percent survival of patients with alterations in *NRAS* and in *NRAS* together with *MAPK14*.

To determine the correlation between p38α protein amounts and the observed mRNA upregulation and amplification, we first examined the data available in The Human Protein Atlas database. We observed that the amount of p38α protein was increased in human melanoma samples when compared with the expression in normal melanocytes. In agreement with the mRNA expression data (TCGA), the expression of p38α was heterogeneous among melanoma samples, and 20% of the samples presented a moderate increased expression of p38α (Figure 15A). To validate these data, we evaluated by immunofluorescence the p38α expression in 8 additional human melanoma samples. Again, the expression of p38α among different tumor samples was heterogeneous ranging from low to medium H-Score values (Figure 15B).

We also analyzed p38α expression in normal skin and *in situ* melanoma. Consistent with the previous data, p38α expression was absent in normal melanocytes. Interestingly, in melanoma *in situ* samples, tumor cells at the advance front of the tumor (starting to cross the basal membrane of the epidermis to the dermis), increased the expression of p38α when compared to melanoma cells that were still confined to the epidermis or melanocytes (Figure 15C).

Altogether, these data suggest that upregulation of p38α expression may contribute to melanoma development and progression.

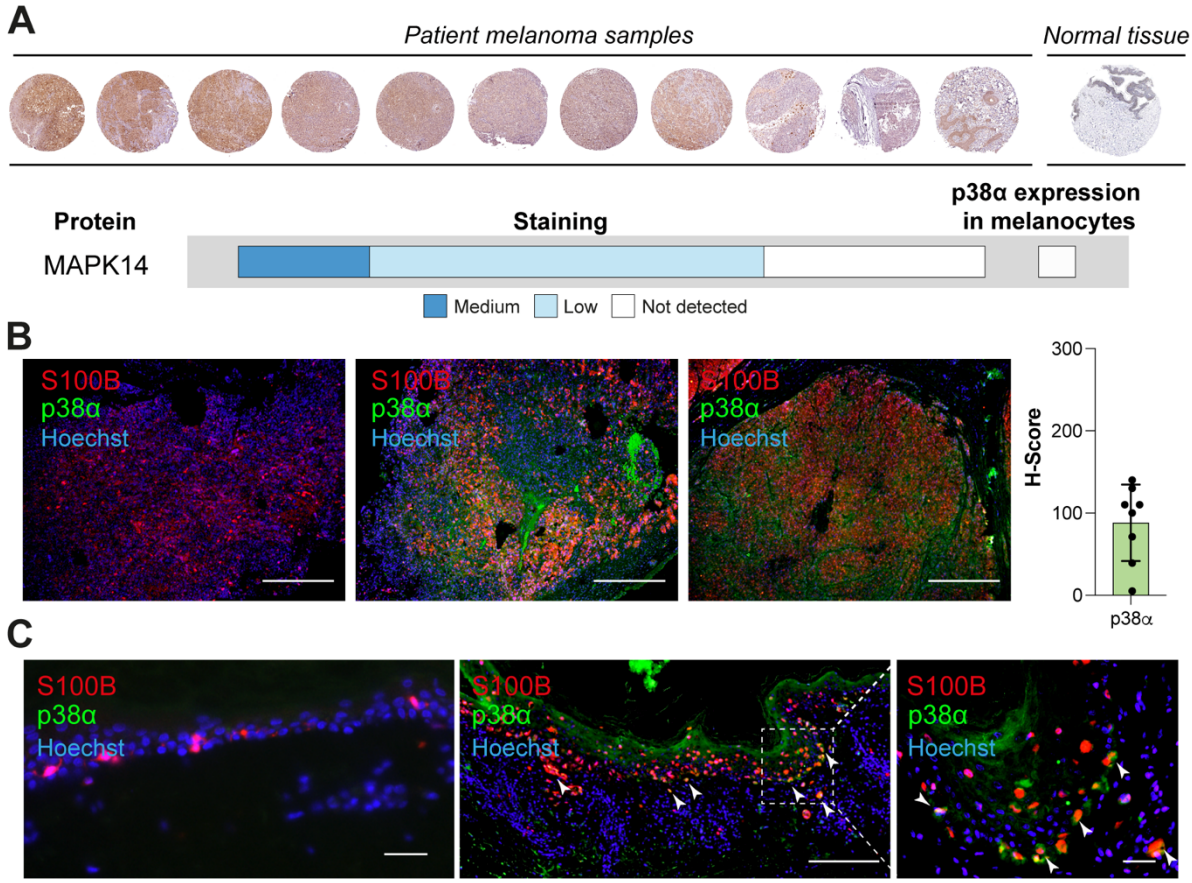


Figure 15 | Expression of p38α in human cutaneous melanoma samples. (**A**) p38α expression in human melanoma and normal skin samples from the Protein Atlas database. (**B**) Representative images of immunohistochemistry showing the expression of p38α (green) and the melanocyte marker S100B (red) in human melanoma tumors. Hoechst (blue) was used for nuclei visualization. Scale bars represent 100 µm. Graph showing the quantification (H-Score) of p38α expression. Data are represented as means ± SD (n = 8). (**C**) Representative images of immunohistochemistry showing the expression of p38α (green) and the melanocyte marker S100B (red) in normal skin (left) and *in situ* melanoma (right). Hoechst (blue) was used for nuclei visualization. Scale bars represent 50 µm (right), 100 µm (left), 50 µm (zoom-in).

p38α is involved in melanocyte survival, proliferation and stress response.

It is well known that the p38 MAPK pathway is involved in the regulation of essential cellular processes, including proliferation, stress response and apoptosis[128]. To validate the role/s of p38α in melanoma cell lines, we transduced *NRAS*- and *BRAF*-mutated melanoma cells with an inducible shRNA construct targeting p38α (Supplementary Figure 1).

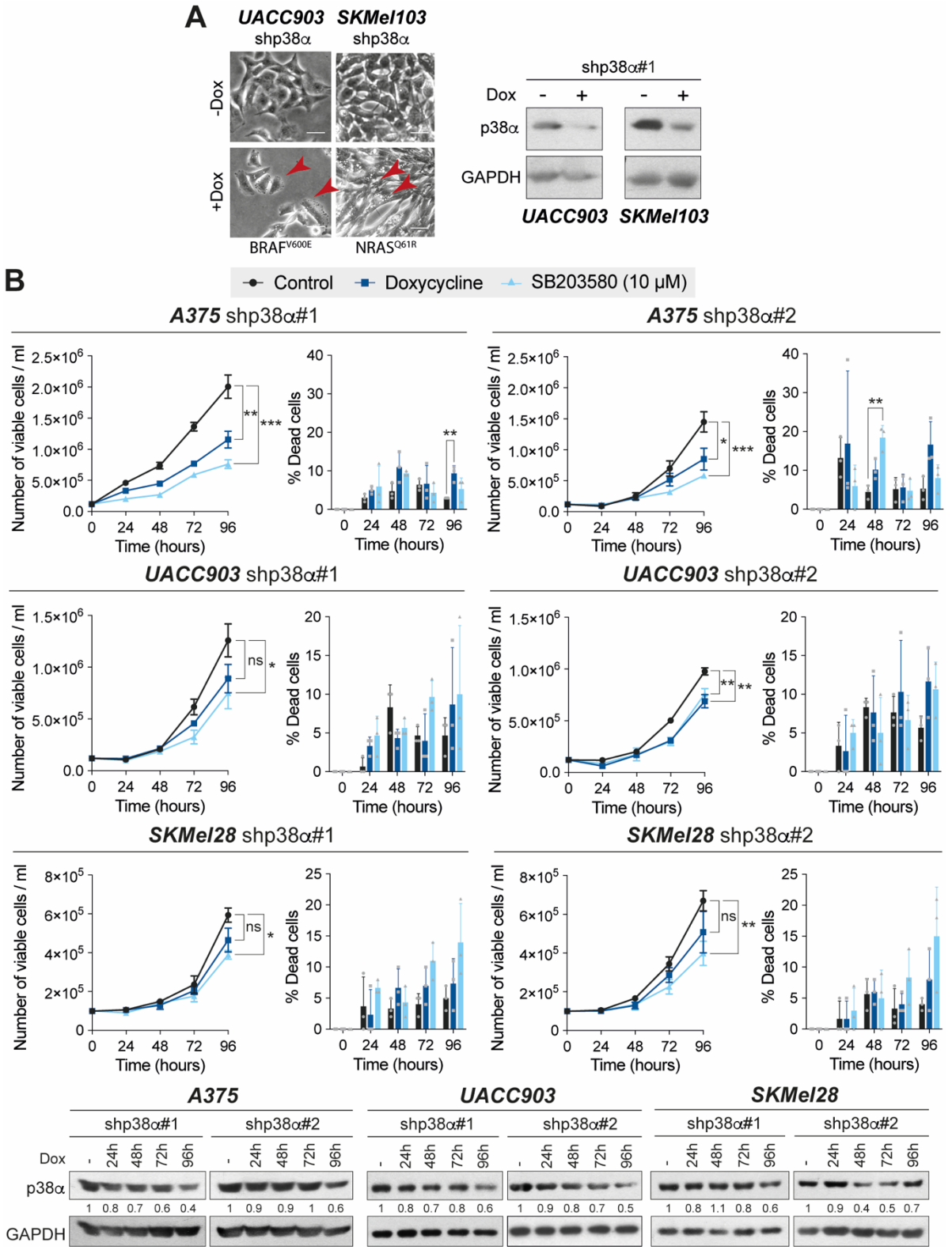


Figure 16 | p38α regulates proliferation and survival of melanoma cells. (**A**) Representative images showing the phenotypic changes associated to the downregulation of p38α in *UACC903* and *SKMel103* cell lines. Western blot showing the amounts of p38α 96h after expression of *shRNA* for *p38α* induced by doxycycline (Dox +) (2 μg/ml). Arrows point to vacuole formation. Scale bars represent 50 μm. (**B**) Graphs showing proliferation curves of *A375*, *UACC903* and *SKMel28* cell lines upon induction of *shRNA* for *p38α* or treatment with the p38 inhibitor SB203580 (10 μM). Percentage of dead cells determined by trypan blue staining in each case is shown on the right to the proliferation curves. Data are represented as means ± SD of triplicates. Representative western blots showing the downregulation of p38α upon *shRNA* expression are shown below. GAPDH was used as loading control. The numbers indicate the fold change with respect to the control (Dox -). Statistical significance was determined using unpaired *t*-test; (ns) non-significant, (*) $p \leq 0.05$, (**) $p \leq 0.01$, (***) $p \leq 0.001$.

The specific knockdown of p38α resulted in an increased vacuole formation associated with cell death in both *UACC903* ($BRAF^{V600E}$) and *SKMel103* ($NRAS^{Q61R}$) cell lines 96 hours after *shRNA* induction (Figure 16A). Proliferation and viability assays of $BRAF^{V600E}$-mutant melanoma cells (*A375*, *UACC903* and *SKMel28*) either treated with a p38 inhibitor (SB203580) or after the induction of two different *shRNA* constructs targeting *p38α,* revealed a significant decreased in proliferation in response to both, the treatment with the p38 inhibitor SB203580 or p38α depletion. In response to the p38 inhibitor, the extent of this reduction was cell line-dependent, ranging from 20% to 60% reduction in proliferation compared to the control cells, where *A375* cells appeared to be the more sensitive cell line (Figure 16B). The knockdown of p38α also resulted in a cell line-dependent reduction in the proliferation rate (ranging between 20% and 40%). Again, *A375* cells showed the most significant reduction in proliferation after the induction of the different assayed *shRNAs (#1 and #2)*. On the other hand, *UACC903* only showed a significant reduction after the induction of the *shRNA#2*, while knockdown of p38α did not result in a significant decrease in *SKMel28* proliferation (Figure 16B). Although we detected a slight increase of dead cells in all cell lines after the treatment with SB203580 or the knockdown of p38α, especially evident at later time points, in *A375* cells this observation did not correlate with the decreased in cell proliferation (Figure 16B).

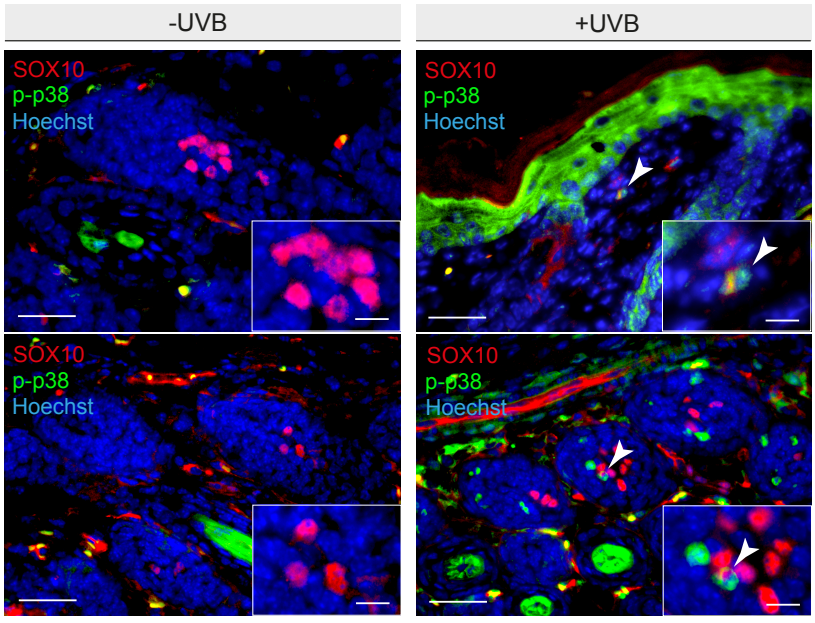


Figure 17 | Activation of p38 in melanocytes of the skin in response to UV irradiation. Representative images of immunohistochemistry showing the activation of p38 (nuclear staining of p-p38 in green) and the melanocyte marker SOX10 (red) in mouse skin 4 h after UVB irradiation. Hoechst (blue) was used for nuclei visualization in all immunohistochemistry. Scale bars represent 50 μm and 10 μm (zoom-in).

The main environmental risk factor is ultraviolet radiation (UVR), which may influence melanoma risk through multiple mechanisms[14,238]. In addition to its recognized role in the regulation of cell proliferation and survival, the p38 MAPK pathway is also involved in the

response to UV irradiation[167]. In this regard, we wanted to corroborate the participation of p38 in the UV radiation-mediated response in cutaneous melanocytes. To that end, we subjected 3-days old mice to a single physiological dose of 6.24 kJ/m^2 of UVB radiation and checked p38 phosphorylation in the skin after 4 hours. As expected, in response to UVB irradiation p38 became phosphorylated in different cell types including keratinocytes and dermal and intra hair-follicle melanocytes (Figure 17), supporting the implication of p38 in UV-induced melanomagenesis.

Altogether, these data warrant the role of p38 in the melanocyte stress response to UV irradiation and confirm the previously described contributions of this molecule to melanoma cell proliferation and survival.

Absence of *p38α* expression in melanocytes is associated with a delay in melanoma development, a higher tumor multiplicity and reduced tumor size in a UVB-induced *Braf*^{V600E} melanoma mouse model.

The *BRAF* oncogene is the most commonly mutated gene in melanoma, leading to hyperactivation of the downstream RAS/RAF/MEK/ERK pathway[46]. However, *BRAF* mutations result in cell cycle arrest and/or oncogene-induced senescence (OIS)[37]. Therefore, additional genetic events are necessary to bypass the OIS and acquire a tumorigenic phenotype[38]. UV radiation is the major environmental risk factor associated with the development of melanoma[14], and several studies have demonstrated that UVR cooperate with the *BRAF*^{V600E} mutation to promote melanoma development[234,236,239]. The p38 MAPK pathway is activated in response to environmental stress, such as UVR, resulting in cell cycle arrest, DNA repair and apoptosis[167]. Furthermore, the p38 MAPK pathway mediates cell cycle arrest and/or OIS downstream of the RAS/RAF/MEK/ERK cascade[181,182]. Additionally, the p38 MAPK pathway plays a role in cytokine signaling and regulates the expression of particular cytokines and chemokines that are essential for the anti-tumor immune response[124,177,178]. Due to the numerous functions attributed to the p38 MAPK pathway, particularly p38α, including the response to UVR, cytokine signaling and the regulation of cell proliferation and survival, and the above results, we aimed to investigate the role of p38α *in vivo* in cooperation with *BRAF*^{V600E} oncogene and UVB irradiation in melanoma development and progression *in vivo*.

To that end, we crossed the Tyr::*CreER*^{T2};*Braf*$^{CA/CA}$ strain with the *p38α*$^{lox/lox}$ mouse to generate a conditional inducible melanoma mouse model, where the administration of 4-hydroxytamoxifen (4-OHTx) induced the expression of *Braf*^{V600E} and the concomitant

targeted loss of p38α, exclusively in the melanocytes. Subsequently, by successive backcrossing of the resulting offspring, we generated an extensive set of mice with different allelic combinations for *Braf*^{CA} and *p38α*^{lox} alleles. All resulting offspring were included in our investigation, regardless of the allelic combinations for *Braf* and p38α. This approach aims to investigate the influence of the genetic dose of p38α in a *Braf*^{V600E} mutational background on melanoma development and progression. In addition, to investigate the effect of the UVB in melanoma development within the different resulting genotypes, we designed two study subgroups: a spontaneous melanoma model activated by topical administration of 4-OHTx at postnatal days 2.5 and 3.5, and a UVB-induced melanoma model, where 4-OHTx was administered in the same manner but coupled with a single physiological dose of UVB irradiation (6.24 kJ/m^2) at postnatal day 3.5[240] (Figure 18A). These specific time points were chosen in accordance with epidemiological data suggesting that cutaneous melanoma may arise as a consequence of intense, intermittent exposure of the skin to UV radiation, particularly in children, rather than from the cumulative lifetime exposure that is associated with other forms of skin cancer[19–22,241].

It is known that the expression of mutated BRAF^{V600E} alone is insufficient for the generation of melanoma tumors since it promotes cell cycle arrest and/or OIS[37]. Consistent with previous research[242,243], the expression of a single allele of *Braf*^{V600E} did not lead to melanoma tumor development and the activation of the second allele of *Braf*^{V600E} promoted the melanoma development in three aged mice (Figure 18B). Interestingly, although the deletion of p38α alone had no effect in melanoma development, the loss of one or both alleles of p38α cooperated with mutated *Braf*^{V600E} in melanomagenesis, resulting in a 20% increase in tumor incidence in a p38α genetic dose-dependent manner (Figure 18B).

UV radiation constitutes the main environmental insult associated to melanoma development and progression[14]. Thus, we incorporated to the model a physiological neonate UVB irradiation dose. As expected[234], concomitant *Braf*^{V600E} activation and UVB irradiation induced melanoma development in 85% of the mice (Figure 18C). The loss of both alleles of p38α, but not haploinsufficiency, delayed the development and/or progression of UVB-induced *Braf*^{V600E} melanomas. However, we did not observe significant differences in tumor onset promoted by the loss of one or two alleles of p38α when both *Braf*^{V600E} mutated alleles were active (Figure 18C).

Interestingly, the depletion of p38α (one or both alleles) correlated with an increased tumor multiplicity (Figure 18D). Furthermore, tumors lacking p38α appeared to be significantly

smaller than tumors expressing this protein (Figure 18E and 18F), suggesting a potential role of p38α in tumor growth biology.

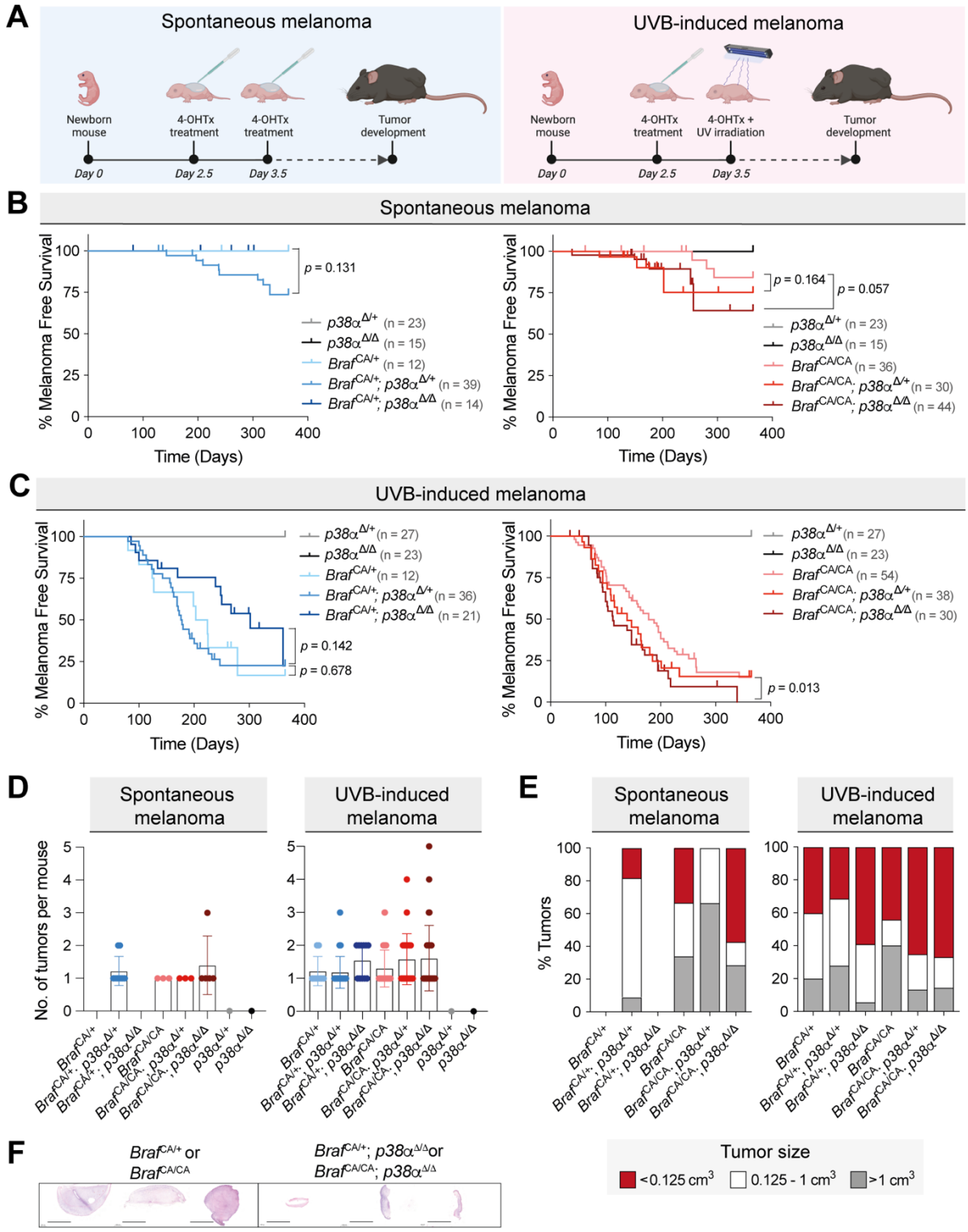


Figure 18 | p38α plays an important role in the regulation of *Braf*^{V600E}-mutated melanoma development and progression. (**A**) Scheme showing the followed treatment steps for spontaneous and UVB-induced melanoma mouse models. (**B,C**) Kaplan-Meier graphs showing the percentage of melanoma free survival in (**B**) spontaneous and (**C**) UVB-induced melanoma models. (**D**) Graphs showing tumor multiplicity in spontaneous and UVB-induced melanoma models. Data are represented as means ± SD. (**E**) Graphs showing percentage of tumors with the different sizes indicated in the figure legend in spontaneous and UVB-induced melanoma models. (**F**) Representative images showing the differences in tumor sizes. Scale bars represent 50 mm.

Altogether, these findings indicate that p38α may have a dual effect on melanoma pathogenesis. On the one hand, in melanocytes it could confer protection against melanoma development restricting the number of developed tumors, particularly in response to UVB radiation, but on the other hand, it also plays a pro-tumoral role in melanoma cells allowing the timely full size tumor growth.

Smaller size of *B;p38α* tumors correlates with a decreased proliferation of melanoma cells.

Noting that UVB-induced melanoma tumors from *Tyr::CreER*^{T2};*Braf*$^{CA/CA}$;*p38α*$^{\Delta/\Delta}$ mice (hereafter referred as *B;p38α*) presented some difficulties to develop and grow to full size when compared to tumors derived from *Tyr::CreER*^{T2};*Braf*$^{CA/CA}$ mice (*B* mouse model), we decided to further characterize these tumors by immunohistochemistry.

First, we examined the expression of p38α in the resulting melanoma tumors to validate the functionality of our model. Staining of tumor samples using p38α antibody demonstrated the absence of p38α in *B;p38α* melanomas but not in tumors generated in *B* mouse model (Figure 19A). Furthermore, according to p-ERK1/2 staining both *B* and *B;p38α* melanomas exhibited similar levels of ERK1/2 activation (Figure 19B), confirming *Braf*^{V600E} expression and the p38α-independent activation of the RAS pathway.

Since we had previously observed that p38 inhibition or downregulation hampered melanoma cell proliferation and survival, we decided to investigate whether the reduced size of *B;p38α* tumors, could be attributed to an increased apoptosis or decreased proliferation of tumor cells lacking p38α expression. We observed a significant reduction of Ki67-expressing cells in *B;p38α* tumors (10%) when compared to *B* melanomas (Figure 19C), suggesting a reduced tumor cell proliferation. Moreover, both *B* and *B;p38α* tumors showed similar expression of the apoptotic marker cleaved caspase-3 (Figure 19D).

Therefore, these data suggest that the smaller size of *B;p38α* tumors may be partially attributed to a reduced proliferation of melanoma cells, but the existence of other contributing mechanisms should be considered.

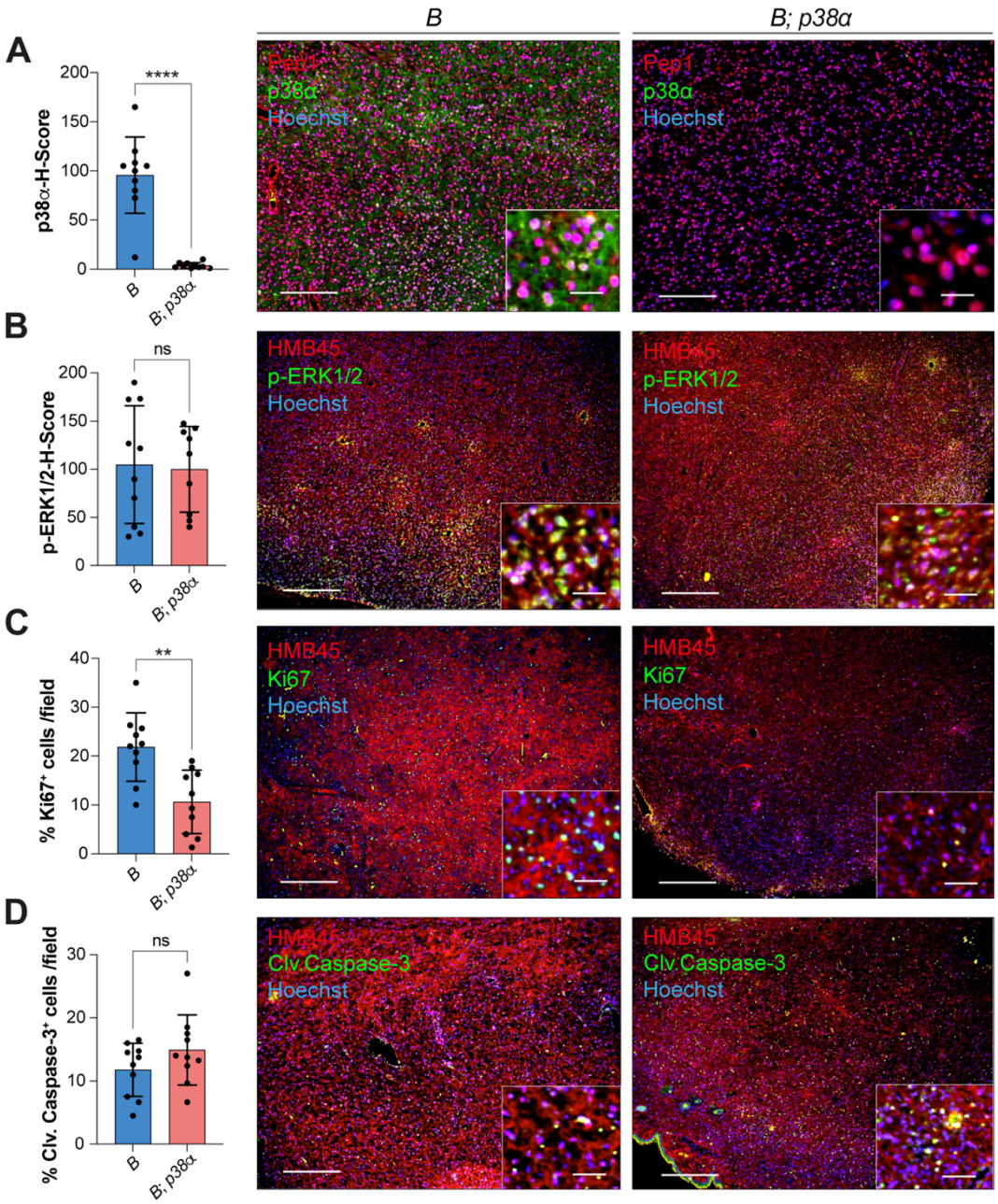


Figure 19 | Characterization of mouse melanoma tumors by immunohistochemistry showed a decreased expression of the proliferation marker ki67 in tumors lacking *p38α* expression. Representative images of immunohistochemistry showing expression of (**A**) the melanocyte marker Pep1 (red) and p38α (green), (**B**) the melanoma marker HMB45 (red) and the activation of ERK1/2 (p-ERK1/2) (green), (**C**) HMB45 (red) and ki67 (green), and (**D**) HMB45 (red) and cleaved caspase-3 (green) in *B* and *B;p38α* tumors. Graphs with the corresponding quantification (H-Score) or the percentage of the corresponding positive cells per field are shown. Hoechst (blue) was used for nuclei visualization in all immunohistochemistry. Scale bars represent 100 µm and 50 µm (zoom-in). Data are represented as means ± SD (n = 10 for each group). Statistical significance was determined using unpaired *t*-test; (ns) non-significant, (*) $p \leq 0.05$, (**) $p \leq 0.01$, (****) $p \leq 0.0001$.

Absence of *p38α* in tumor cells results in increased and prolonged cytotoxic immune response in *Braf*^{V600E} mouse melanoma tumors.

It is well established that the p38 MAPK signaling pathway is a critical mediator of the inflammatory response, playing a role in both the response to inflammatory cytokines and the regulation of cytokine and chemokine production, which are essential for the immune

response[124,177,178]. Given the delay in tumor development, the diminished tumor size in *B;p38α* mice and the role of p38α in mediating cytokine signaling and production, p38α inactivation in melanoma cells could potentially alter the cytokine profile within the tumor microenvironment (TME), thereby affecting the recruitment and activation of immune cells and consequently the anti-tumor response. Therefore, we decided to investigate the potential role of p38α in the modulation of the intratumoral immune response by immunophenotyping *B* and *B;p38α* tumors. To characterize all immune cells irrespectively of their anatomical position within the tumor, we decided to use whole spontaneous tumors for immunophenotyping (13 tumors per genotype). After whole tumor disaggregation, tumoral cells were selected *in vitro* to generate different tumor cell lines for further studies, and intratumoral CD45$^+$ cells were analyzed by flow cytometry to phenotype the immune cells present in the TME (Figure 20).

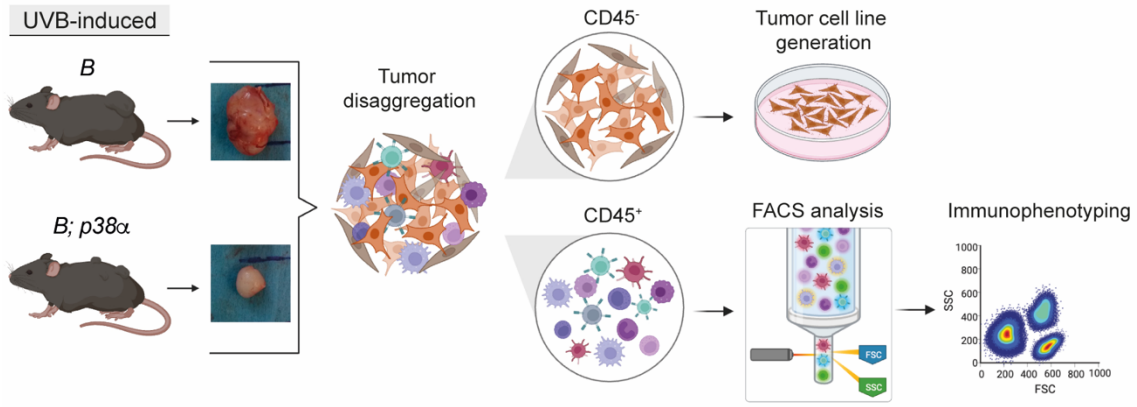


Figure 20 | Scheme showing the procedure for processing mouse melanoma tumors to generate tumor cell lines and to immunophenotype the intratumoral immune cell populations by flow cytometry. Tumors from *B* and *B;p38α* mice were collected and disaggregated. Tumoral cells were selected *in vitro* for tumor cell line generation. On the other hand, the phenotype of the intratumoral immune cells (CD45$^+$) was analyzed by flow cytometry.

We initially hypothesized that the reduced size of *B;p38α* tumors may be due to a possible differential anti-tumoral immune response. Both *B* and *B;p38α* tumors showed similar amounts of total infiltrating immune cells (CD45$^+$) (Figure 21A) and total T cells (CD3$^+$) (Figure 21B). We therefore wondered whether the phenotype and the functional status of these T cells may be influence by the lack of *p38α* in melanoma cells.

Within the immune response against tumors, CD4$^+$ T cells function as helpers, contributing to durable and effective cellular immune responses[244]. On the other hand, CD8$^+$ T cells are the primary effector cells in the anti-tumor response, exerting a cytotoxic effect that is crucial for the elimination of tumor cells[245]. In this matter, we did not observe any difference in the total number of CD4$^+$ and CD8$^+$ T cells (Figure 21C). However, although CD4$^+$ T cells were the

predominant subtype in both tumors, some *B;p38α* tumors tended to have a higher ratio of $CD8^+/CD4^+$ T cells (Figure 21C).

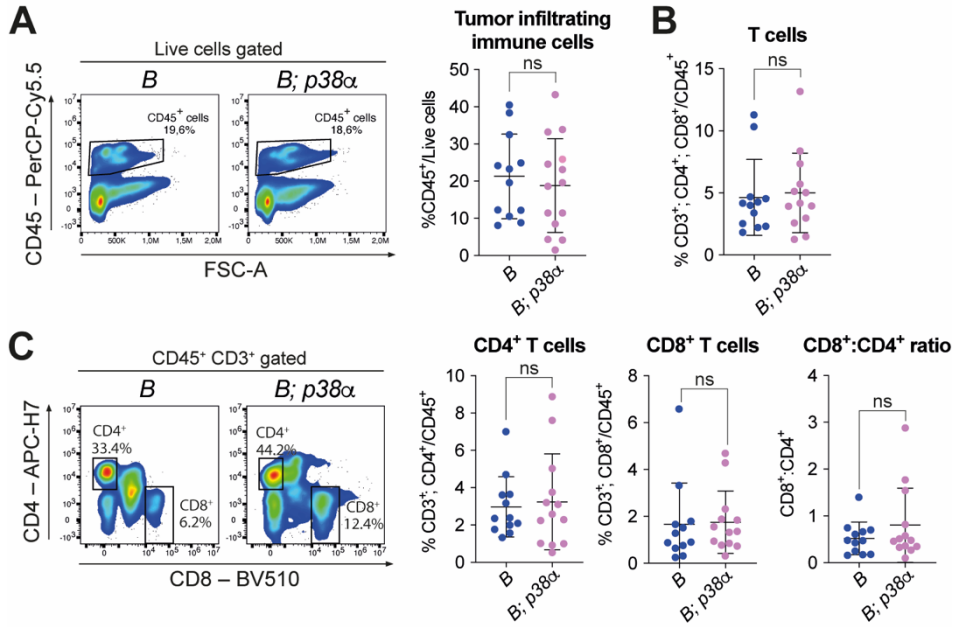


Figure 21 | Absence of *p38α* expression in melanoma cells has no impact in the recruitment of total immune cells and total T cells to the tumor. (**A**) Representative density plot and graph showing the percentage of tumor infiltrating immune cells ($CD45^+$). (**B**) Graph showing the percentage of T cells. (**C**) Representative density plot and graphs showing the percentage of $CD4^+$ and $CD8^+$ T cells. Graph showing the $CD8^+$:$CD4^+$ ratio. Data are represented as means ± SD of biologically independent tumor samples (n = 12 (*B*) and n = 13 (*B;p38α*)). Statistical significance was determined using unpaired *t*-test; (ns) non-significant.

According to their state of differentiation, $CD4^+$ and $CD8^+$ T cells can be categorized into naïve T cells, effector T cells, and subsets of memory cells, each with unique characteristics and functions in the immune response[246]. Naïve T cells are primed by antigen presenting cells (APCs) in the draining lymph nodes, where they are activated and expanded. Subsequently, they differentiate into T effector (TE) cells, which are responsible for the immediate anti-tumor defense through the production of effector cytokines and granzyme/perforin-mediated cytotoxicity. However, these TE cells have a short lifespan and limited capacity for self-renewal, so the surviving T cells differentiate into T effector memory (EM) cells, which have a higher long-term survival and confer immunity against previously encountered antigens[94,247,248].

As expected, since we are analyzing the intratumoral immune populations, we observed similar low amounts of infiltrating $CD4^+$ and $CD8^+$ naïve T cells ($CD44^-CD62L^+$) in both *B* and *B;p38α* melanomas (Figure 22A and 22B). Moreover, there were not significant differences in the amount of $CD4^+$ TE/EM cells ($CD44^+CD62L^-$) between both tumor types (Figure 22A). However, although not significant, *B;p38α* tumors tended to have an increased

number of CD8$^+$ TE/EM cells (Figure 22B) compared to *B* tumors, suggesting a possible stronger cytotoxic effector response in *B;p38α* melanoma tumors when compared to *B* tumors.

During a prolonged and chronic immune response, such as that occurring in cancer, tumor-antigen reactive T memory/central memory (TM/CM) cells are generated. These TM/CM cells are less differentiated, exhibit a higher anti-tumor activity compared to TE/EM cells and have the capability of durably persisting and functioning in the tumor[247,249]. Interestingly, tumors lacking p38α presented significant increased numbers of both, CD4$^+$ and CD8$^+$ TM/CM cells (CD44$^+$CD62L$^+$) (Figure 22A and 22B), suggesting that there was an enhanced anti-tumor immune response during the development and/or progression of *B;p38α* compared to *B* tumors.

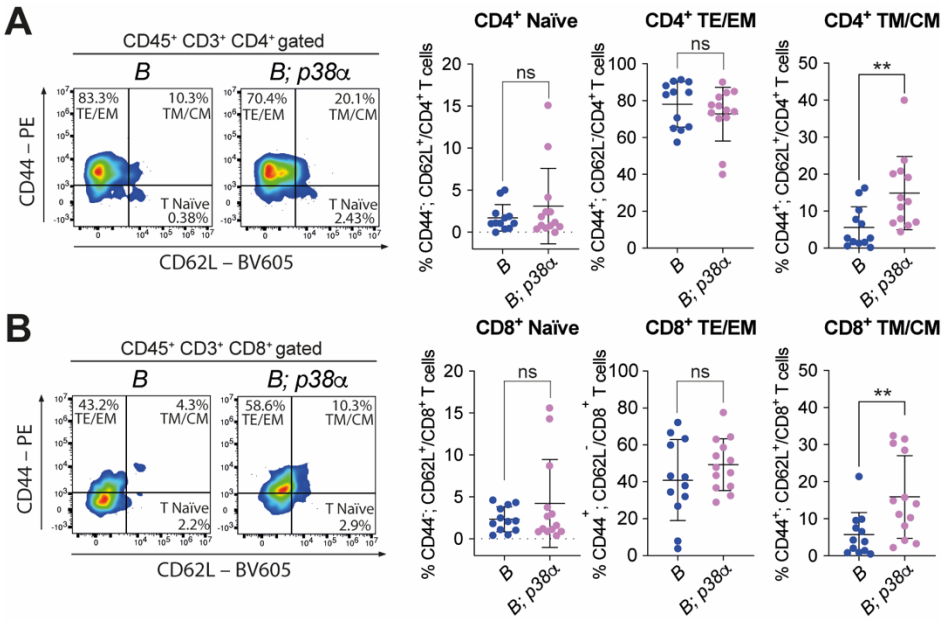


Figure 22 | Absence of *p38α* expression in melanoma cells enhances the generation of tumor-antigen reactive T memory cells. (**A**) Representative density plot and graphs showing the percentage of CD4$^+$ T naïve, TE/EM and TM/CM cells. (**B**) Representative density plot and graphs showing the percentage of CD8$^+$ T naïve, TE/EM and TM/CM cells. T effector/Effector Memory (TE/EM); T Memory/Central Memory (TM/CM). Data are represented as means ± SD of biologically independent tumor samples (n = 12 (*B*) and n = 13 (*B;p38α*)). Statistical significance was determined using unpaired *t*-test; (ns) non-significant, (**) $p \leq 0.01$.

However, a prolonged and unresolved anti-tumor immune response causes TE/EM cells to become exhausted and express high levels of inhibitory receptors on their surface, including PD-1 and TIM-3. This state of T cell exhaustion impairs the proliferative and cytotoxic capacity of effector T cells, thus producing less effector cytokines and losing the ability to eliminate tumor cells[94].

We observed that both *B* and *B;p38α* tumors showed similar amounts of exhausted CD4$^+$ TE/EM expressing either PD-1, TIM-3 or both PD-1 and TIM-3 exhaustion markers

(Figure 23A). However, CD8$^+$ TE/EM cells in *B;p38α* tumors exhibited a more exhausted phenotype, primarily due to a higher expression of PD-1 (Figure 23B), suggesting an increased but unresolved cytotoxic response in these tumors compared to *B* melanomas.

Furthermore, no correlation was observed between the amount of CD4$^+$ TE/EM and the exhaustion of these cells in either *B* or *B;p38α* tumors (Figure 23C). Interestingly, the increased exhausted phenotype of CD8$^+$ TE/EM was homogeneously observed in all *B;p38α* tumors, in contrast to the heterogeneous correlation observed in *B* melanomas (Figure 23D), highlighting once again that p38α may play a crucial role in the modulation of the anti-tumor cytotoxic response.

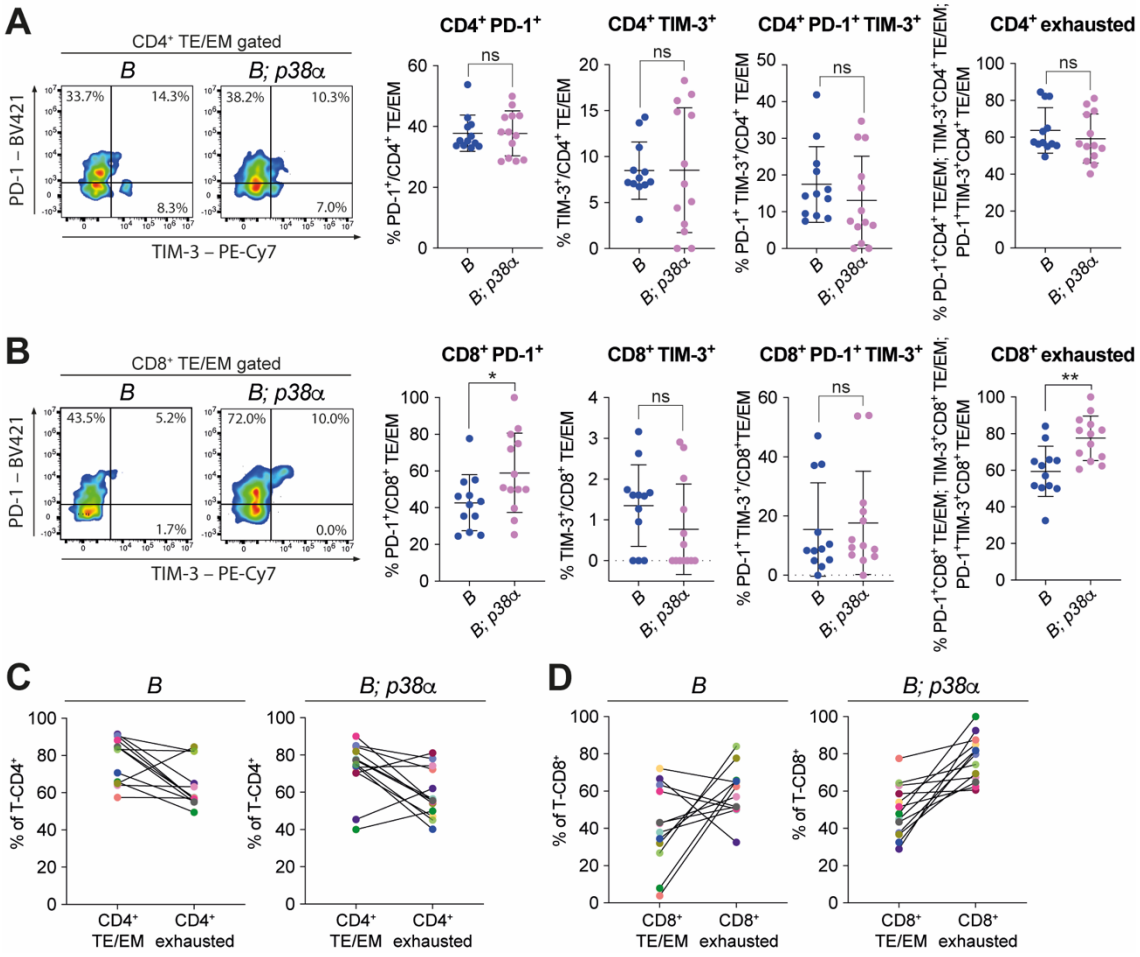


Figure 23 | Lack of *p38α* in tumor cells leads to an increased induction of exhaustion in cytotoxic T cells. (**A**) Representative density plot and graphs showing the percentage of CD4$^+$ TE/EM cells expressing PD-1 and TIM-3 exhaustion markers. Graph showing the percentage of total CD4$^+$ exhausted TE/EM cells. (**B**) Representative density plot and graphs showing the percentage of CD8$^+$ TE/EM cells expressing PD-1 and TIM-3 exhaustion markers. Graph showing the percentage of total CD8$^+$ exhausted TE/EM cells. (**C**) Graphs showing the correlation between CD4$^+$ TE/EM and CD4$^+$ exhausted TE/EM cells in *B* and *B;p38α* tumors. (**D**) Graphs showing the correlation between CD8$^+$ TE/EM and CD8$^+$ exhausted TE/EM cells in *B* and *B;p38α* tumors. T effector/effector memory (TE/EM). Data are represented as means ± SD of biologically independent tumor samples (n = 12 (*B*) and n = 13 (*B;p38α*)). Statistical significance was determined using unpaired *t*-test; (ns) non-significant, (*) $p \leq 0.05$, (**) $p \leq 0.01$.

Among the subtypes of immune cells with regulatory roles, it has been widely demonstrated that Treg cells have an immunosuppressive and pro-tumoral function by inhibiting the activity of TE/EM[250]. Accordingly, we analyzed the frequency of Tregs in our tumors. The results showed that both tumor types (*B* and *B;p38α*) harbored similar amounts of $CD4^+$ and $CD8^+$ Tregs ($FoxP3^+$; $CD25^+$) (Figure 24).

Taken together, these findings indicate that the absence of p38α in melanoma cells facilitates an enhanced and more prolonged cytotoxic immune response against the tumor but has no effect on the recruitment and/or differentiation of Tregs.

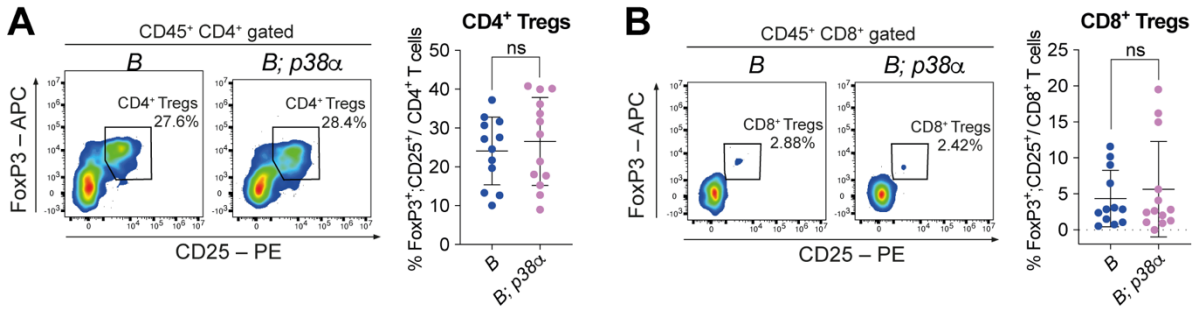


Figure 24 | Treg infiltration into the tumor is not modulated by *p38α* expression in melanoma cells. Representative density plots and graphs showing the percentage of (**A**) $CD4^+$ and (**B**) $CD8^+$ regulatory T cells (Tregs). Data are represented as means ± SD of biologically independent tumor samples (n = 12 (*B*) and n = 13 (*B;p38α*)). Statistical significance was determined using unpaired *t*-test; (ns) non-significant.

Tumors lacking *p38α* exhibit an enhanced activity and recruitment of NK and NK-T cells.

In addition to the adaptive immune response, the innate immune response also plays an important role in tumor immunity. As innate immune cells, NK cells can eliminate tumor cells without prior sensitization[251]. Our results revealed that the lack of *p38α* did not have a major effect in the amount of tumor infiltrating NK cells (Figure 25A). However, NK cells from *B;p38α* tumors showed an increased expression of CD62L (Figure 25B), a lymphoid tissue homing receptor, concomitant with a significant decreased expression of the exhaustion marker PD-1 (Figure 25C), which has been associated with an enhanced anti-tumor activity and a reduced exhaustion of these cells[251–253]. Moreover, both tumor types (*B* and *B;p38α*) showed similar amounts of NK cells expressing CD44, a receptor associated with increased cytotoxic activity of NK cells[254] (Figure 25D).

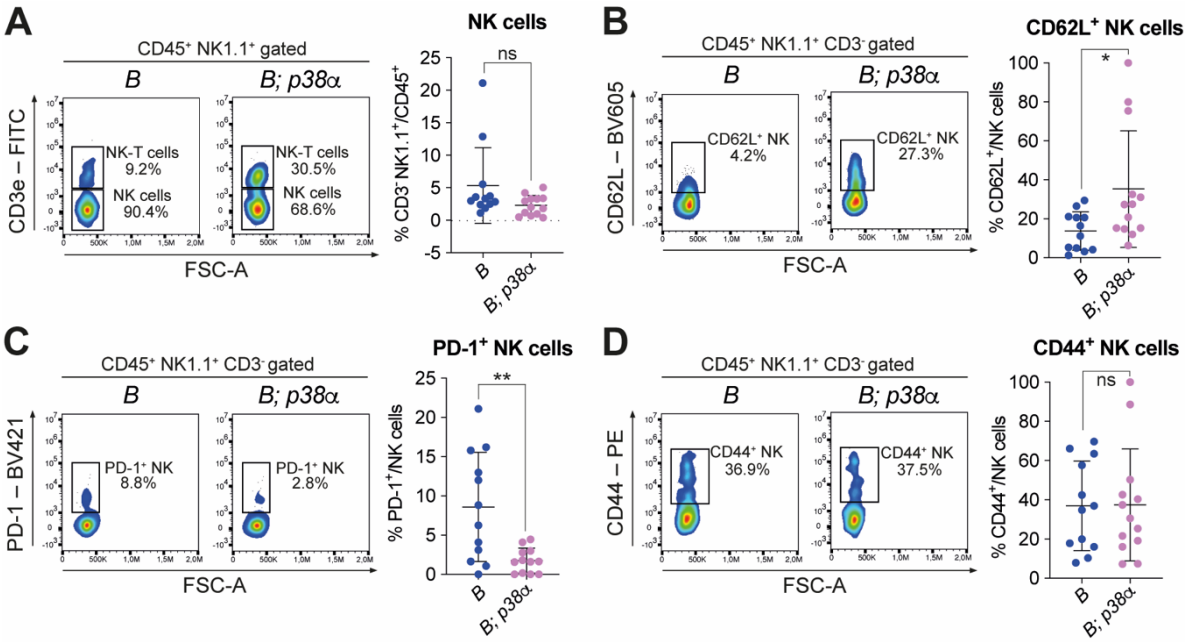


Figure 25 | NK cells show a higher activated and less exhausted phenotype in *B;p38α* tumors. (**A**) Representative density plot and graph showing the percentage of natural killer (NK) cells. Representative density plots and graphs showing the percentage of NK cells expressing (**B**) CD62L, (**C**) PD-1, and (**D**) CD44. Data are represented as means ± SD of biologically independent tumor samples (n = 12 (*B*) and n = 13 (*B;p38α*)). Statistical significance was determined using unpaired *t*-test; (ns) non-significant, (*) $p \leq 0.05$, (**) $p \leq 0.01$.

NK-T cells are a subpopulation of T cells that express T cell receptors (TCR) and also share surface markers with NK cells, thus combining features of both the innate and the adaptive immunity[255]. In addition to the above data, we also observed that tumors lacking *p38α* (*B;p38α*) were infiltrated with a significant higher number of NK-T cells compared to *B* melanomas (Figure 26A). Furthermore, as in the case of NK cells, the number of NK-T-CD62L$^+$ cells from *B;p38α* melanomas was significantly increased in comparison with this type of cells identified in *B* melanomas. This feature in NK-T cells, has also been associated with the recruitment of these cells to the tumor and with a higher anti-tumor activity[256] (Figure 26B), which also correlates with the tendency towards a less exhausted phenotype (PD-1$^+$) of NK-T cells in *B;p38α* melanomas, albeit not significant (Figure 26C).

Altogether, these data suggest that lack of p38α in tumor cells may enhance the recruitment and anti-tumor cytotoxic activity of the innate immune NK and NK-T cells.

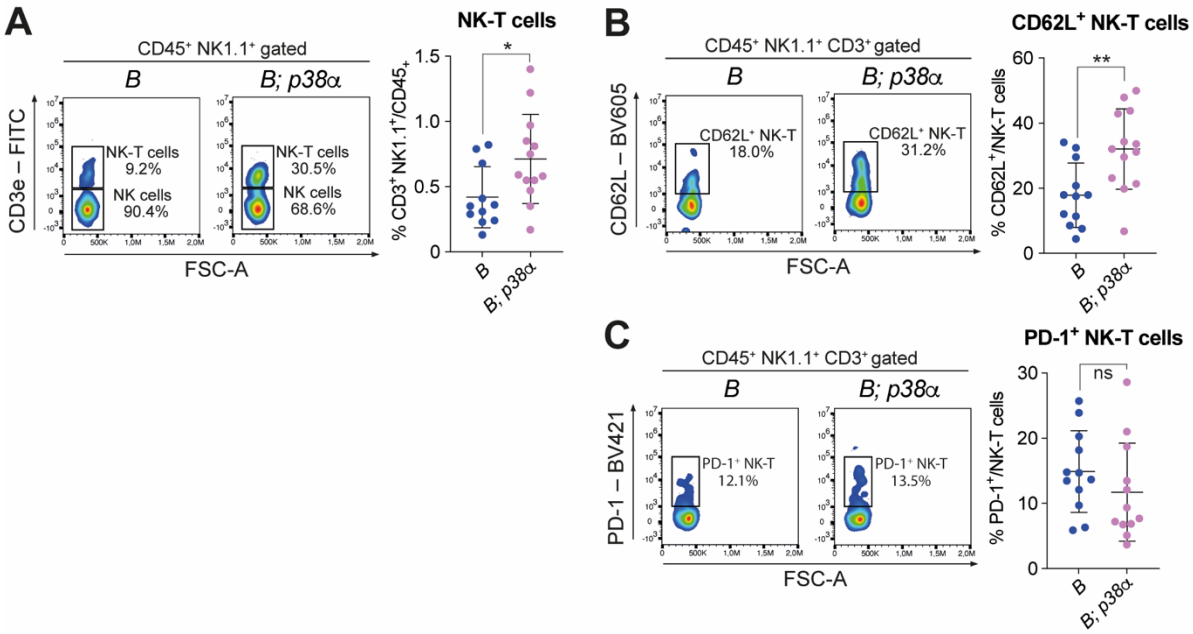


Figure 26 | *B;p38α* tumors show a higher recruitment of NK-T cells. (**A**) Representative density plot and graph showing the percentage of natural killer T (NK-T) cells. Representative density plots and graphs showing the percentage of NK-T cells expressing (**B**) CD62L, and (**C**) PD-1. Data are represented as means ± SD of biologically independent tumor samples (n = 12 (*B*) and n = 13 (*B;p38α*)). Statistical significance was determined using unpaired *t*-test; (ns) non-significant, (*) $p \leq 0.05$, (**) $p \leq 0.01$.

Lack of *p38α* in tumor cells favors the accumulation of polymorphonuclear over monocytic MDSCs and decreases the recruitment of macrophages and activated DCs.

Myeloid cells are a diverse group of innate immune cells that contribute significantly to the anti-tumor response by shaping the TME and modulating immune cell differentiation and activation. Among the most important myeloid cells in the TME are dendritic cells (DCs), macrophages and myeloid-derived suppressor cells (MDSCs)[257]. In relation to this, we did not observe any difference in the total number of myeloid cells ($CD11b^+$) between *B* and *B;p38α* melanomas (Figure 27A). Therefore, we decided to analyze the specific subtypes of myeloid cells.

MDSCs are immature myeloid cells with potent immunosuppressive activity, playing an important role in tumor progression by inhibiting the activity of cytotoxic T cells and NK cells. There are two subtypes of MDSCs differentiated by their phenotype and their mode of suppression. Monocytic MDSCs (M-MDSCs) are phenotypically similar to monocytes and mediate immune suppression mainly through nitric oxide (NO), arginase 1 (ARG1), immunosuppressive cytokines, and the expression of immune regulatory molecules such as PD-L1. On the other hand, polymorphonuclear MDSCs (PMN-MDSCs), which are morphologically similar to neutrophils, preferentially use reactive oxygen species (ROS), ARG1, peroxynitrite, and prostaglandin E_2 (PGE_2) to suppress antigen-specific $CD8^+$ T cells.

Furthermore, M-MDSCs have a higher immunosuppressive activity than PMN-MDSCs, and the number of M-MDSCs, but not of PMN-MDSCs, directly correlated with suppression of *in vitro* T cell activation[257–259]. Interestingly, although the number of total MDSCs was similar in both tumor types (*B* and *B;p38α*), the analysis of these populations revealed a switch between the MDSC subtypes (PMN-MDSCs and M-MDSCs) in respect to the tumor genotype. While the analysis of the infiltrates from *B* tumors showed mostly and significantly higher amounts of M-MDSCs ($CD11b^+Ly6G^-Ly6C^{high}$), *B;p38α* melanomas were infiltrated by mainly by PMN-MDSCs ($CD11b^+Ly6G^+Ly6C^{low}$), which have less immunosuppressive activity and were the predominant subtype in these tumors (*B;p38α*) (Figure 27B).

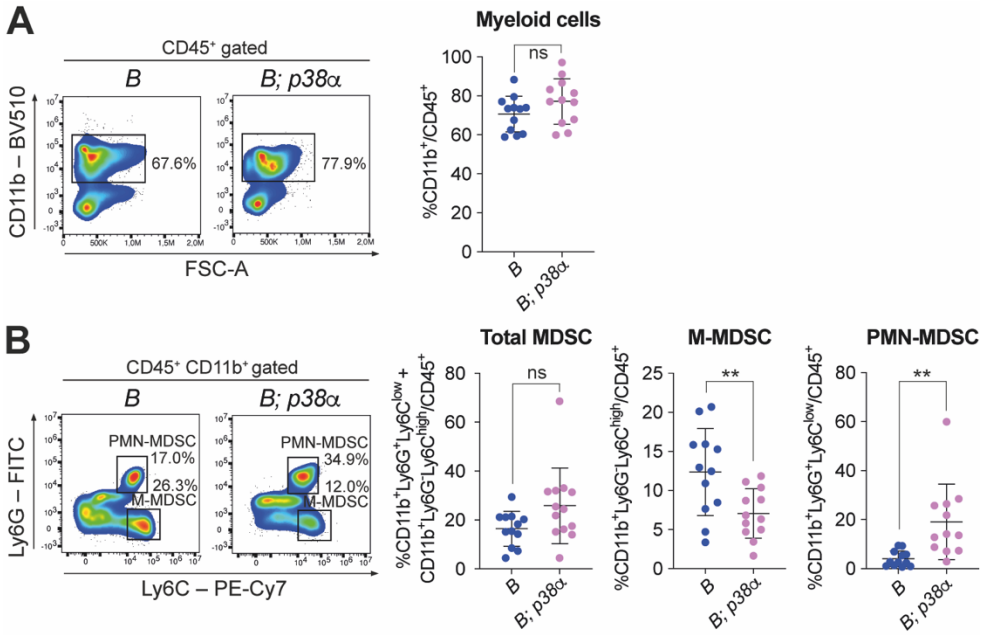


Figure 27 | Lack of *p38α* in tumor cells favors the accumulation of PMN-MDSCs over M-MDSCs. (**A**) Representative density plots and graphs showing the percentage of total myeloid cells. (**B**) Representative density plots and graphs showing the percentage of total myeloid-derived suppressor cells (MDSC), monocytic MDSCs (M-MDSC) and polymorphonuclear MDSCs (PMN-MDSC). Data are represented as means ± SD of biologically independent tumor samples (n = 12 (*B*) and n = 13 (*B;p38α*)). Statistical significance was determined using unpaired *t*-test; (ns) non-significant, (**) $p \leq 0.01$.

As of the macrophages, they can promote tumor progression by producing growth factors and cytokines that shape the TME. Macrophages are often classified into M1 and M2 profiles, with the M2-like phenotype being the most prevalent in growing tumors, promoting tumor cell growth and invasion, enhancing tumor angiogenesis, and blunting anti-tumor T cell functions[260]. Melanomas lacking the expression of *p38α* in tumor cells showed a significant decrease in macrophage infiltration ($Ly6G^-CD11b^+F4/80^+$) (Figure 28A). In addition, infiltrating macrophages in *B;p38α* tumors tended to show a reduced polarization towards an M2-like phenotype ($Ly6C^-CD206^+Ly6G^-CD11b^+F4/80^+$) (Figure 28B).

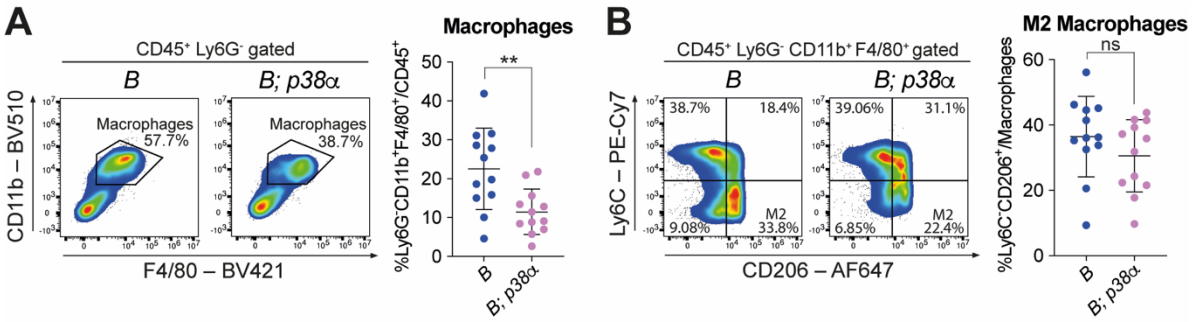


Figure 28 | Absence of *p38α* in tumor cells produces a decrease in macrophages. (**A**) Representative density plot and graph showing the percentage of total macrophages. (**B**) Representative density plot and graph showing the percentage of M2-like macrophages. Data are represented as means ± SD of biologically independent tumor samples (n = 12 (*B*) and n = 13 (*B;p38α*)). Statistical significance was determined using unpaired *t*-test; (ns) non-significant, (**) $p \leq 0.01$.

DCs are not abundant at tumor sites but are central for the initiation of antigen-specific immunity and tolerance due to their ability to process and present tumor-associated antigens via major histocompatibility (MHC) molecules to activate naïve T cells[261]. Tumors lacking p38α expression showed less infiltrating DCs ($CD11b^+CD11c^+$), although the difference was not statistically significant (Figure 29A). Additionally, these infiltrating DCs in *B;p38α* tumors showed a decreased expression of the major histocompatibility complex class II (MHC-II) (Figure 29B), thus limiting their function of presenting antigens to other immune cells.

Overall, these data suggest that p38α may influence the composition and function of myeloid cells within the TME by modulating the balance between M-MDSCs and PMN-MDSCs, the recruitment of macrophages and their polarization to an M2 phenotype, and the recruitment and activation of DCs.

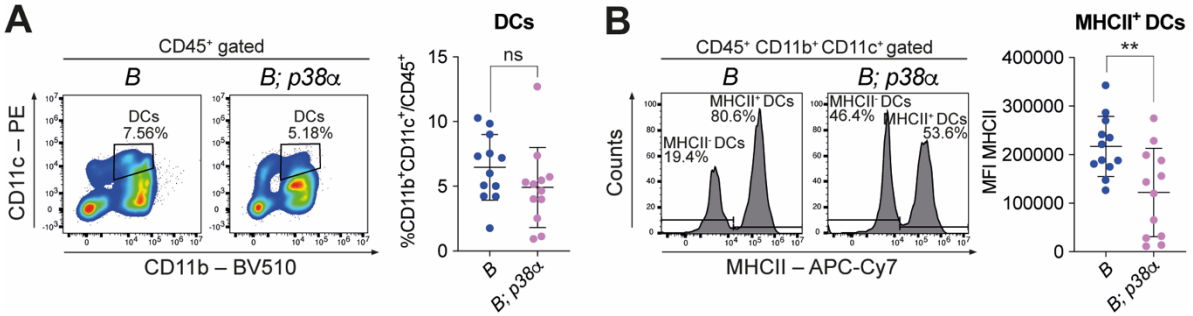


Figure 29 | DCs of *B;p38α* tumors showed a less activated phenotype. (**A**) Representative density plot and graph showing the percentage of total dendritic cells (DCs). (**B**) Representative histogram and graph showing the mean fluorescence intensity (MFI) of the major histocompatibility complex class II (MHC-II) in DCs. Data are represented as means ± SD of biologically independent tumor samples (n = 12 (*B*) and n = 13 (*B;p38α*)). Statistical significance was determined using unpaired *t*-test; (ns) non-significant, (**) $p \leq 0.01$.

Gene expression analysis confirmed the role of p38α in the modulation of the tumor microenvironment and the anti-tumor immune response by tumor cells.

The data indicated that p38α may contribute to melanoma progression by regulating the anti-tumor immunity, impairing the cytotoxic immune response and modulating the recruitment and the activity of immunosuppressive myeloid cells. It is well known that cytokines and chemokines are essential for the modulation of the immune response, including the recruitment and activation of different immune cell populations that have distinct effects on tumor progression and therapeutic outcomes[262]. Indeed, p38α is known to be involved in regulating the production of pro-inflammatory cytokines and chemokines [124,177,178]. To validate our data and to further investigate the mechanisms involved in the distinct immune responses observed in *B* and *B;p38α* tumors, we performed a gene expression profile analysis to characterize the molecular features and the active biological processes of these tumors.

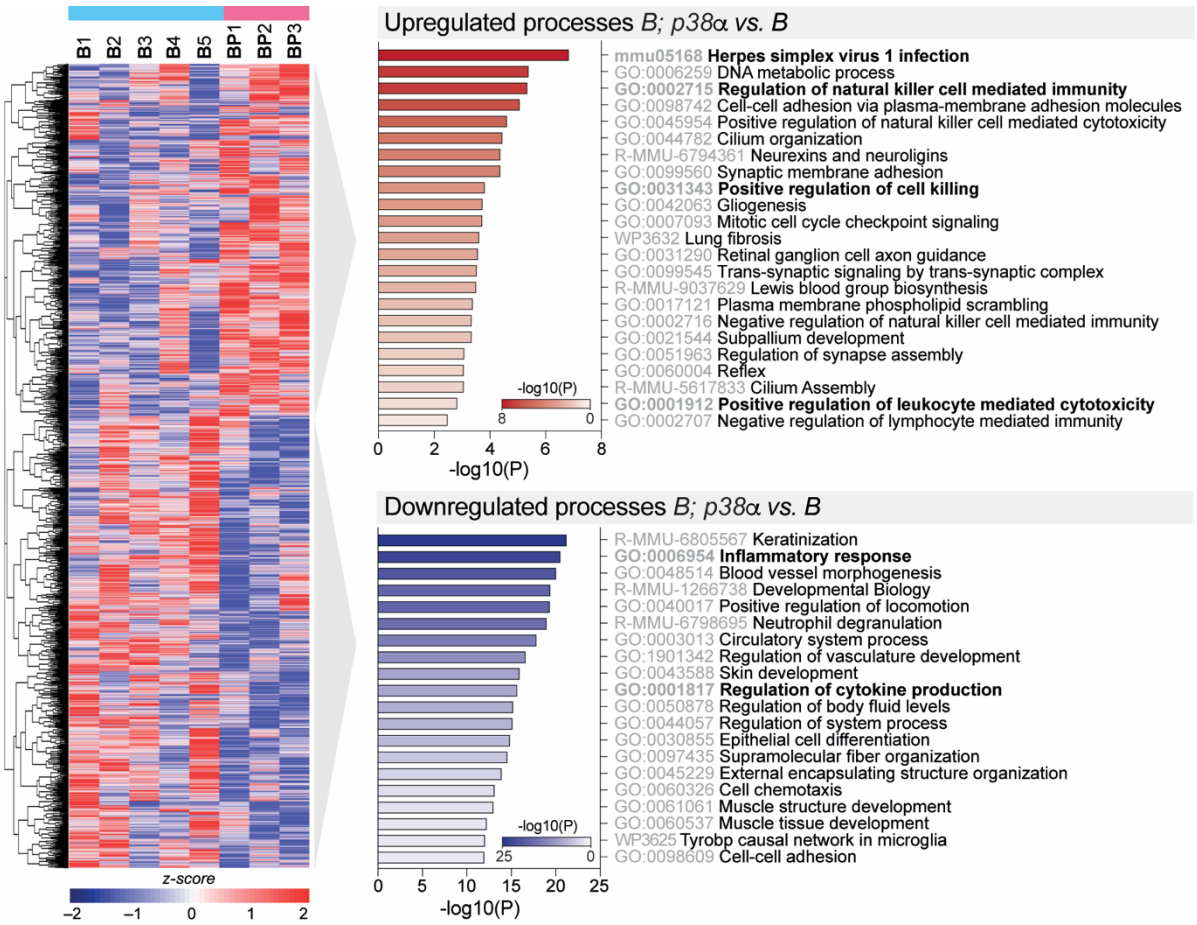


Figure 30 | Differentially regulated processes in *B;p38α* compared to *B* tumors. Heatmap showing the differentially upregulated ($log_2FC \geq 0.265$, n = 2214 genes) and downregulated ($log_2FC \leq -0.265$, n = 3000 genes) genes in *B;p38α* vs. *B* tumors (left) and the regulated processes obtained from the analysis of the differentially regulated genes using *Metascape* (right).

Metascape analysis of the top upregulated genes in *B;p38α* vs. *B* tumors ($log_2FC \geq 0.265$, n = 2214 genes) (Supplementary Table 1) showed that these genes were associated with immune-related processes including "*herpes simplex virus 1 infection*", "*regulation of natural killer cell mediated immunity*", "*positive regulation of cell killing*" and "*positive regulation of leukocyte mediated cytotoxicity*" (Figure 20). On the other hand, the top downregulated genes in the absence of p38α ($log_2FC \leq 0.265$, n = 3000 genes) (Supplementary Table 2) were also found to be involved in processes related to the immune response, such as "*inflammatory response*" and "*regulation of cytokine production*" (Figure 30).

Further analysis of upregulated processes ("*herpes simplex virus 1 infection*", "*positive regulation of lymphocyte mediated immunity*" and "*regulation of natural killer cell mediated immunity*") revealed that the upregulated genes in *B;p38α* vs. *B* tumors were mainly cytokines (e.g., *Il1b, Il12b, Ifng, Ifna1* and *Ifna6)* and immune receptors (mostly Killer cell lectin-like receptors (*Klr*), or genes involved in apoptosis (e.g., *Apaf1*, *Casp3* and *Fasl*), antigen presentation and T cell activity regulation and exhaustion (e.g., *H2*-MHC Class-I molecules, *H60a*, *Harvcr2*, *Lag3*) (Figure 31).

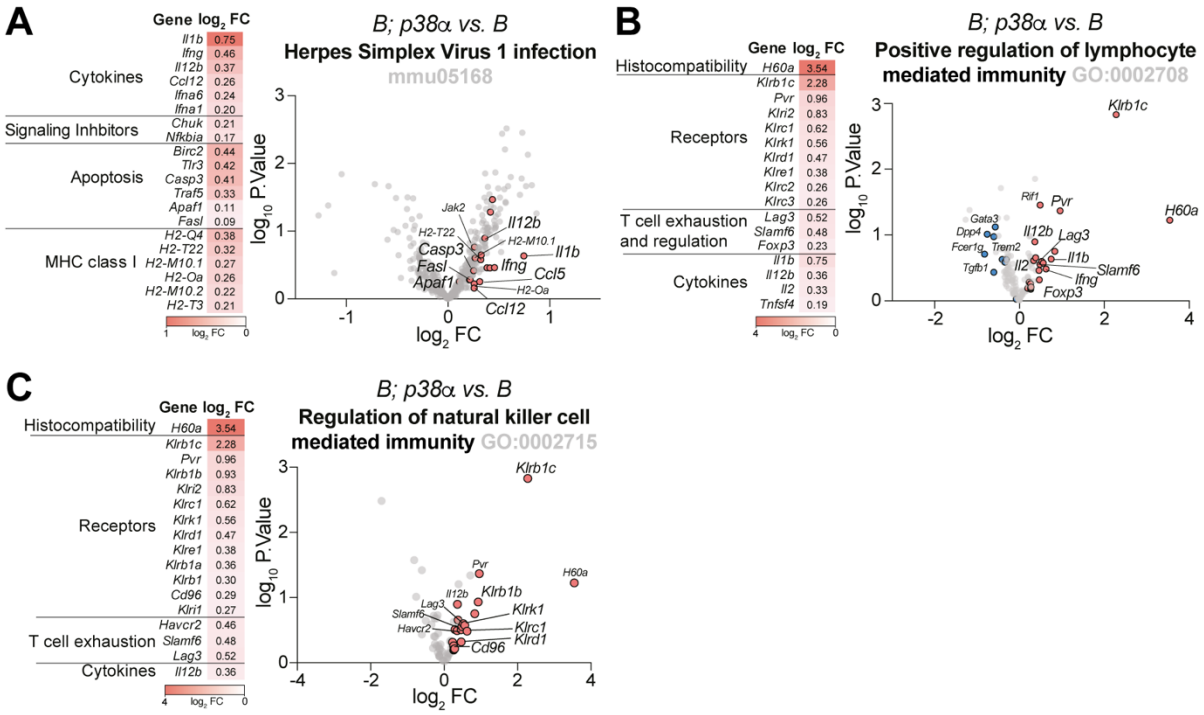


Figure 31 | Upregulated immune-related processes in *B;p38α* vs. *B* tumors. (A) Volcano plot showing the differentially regulated genes in *B;p38α* vs. *B* tumors of the herpes simplex virus 1 infection (mmu05168) process. **(B)** Volcano plot showing the differentially regulated genes in *B;p38α* vs. *B* tumors of the positive regulation of lymphocyte mediated immunity (GO:0002708) process. **(C)** Volcano plot showing the differentially regulated genes in *B;p38α* vs. *B* tumors of the regulation of natural killer cell mediated immunity (GO:0002715) process. List of relevant upregulated genes, the corresponding log_2FC and the processes involved are shown in the left of the corresponding volcano plot.

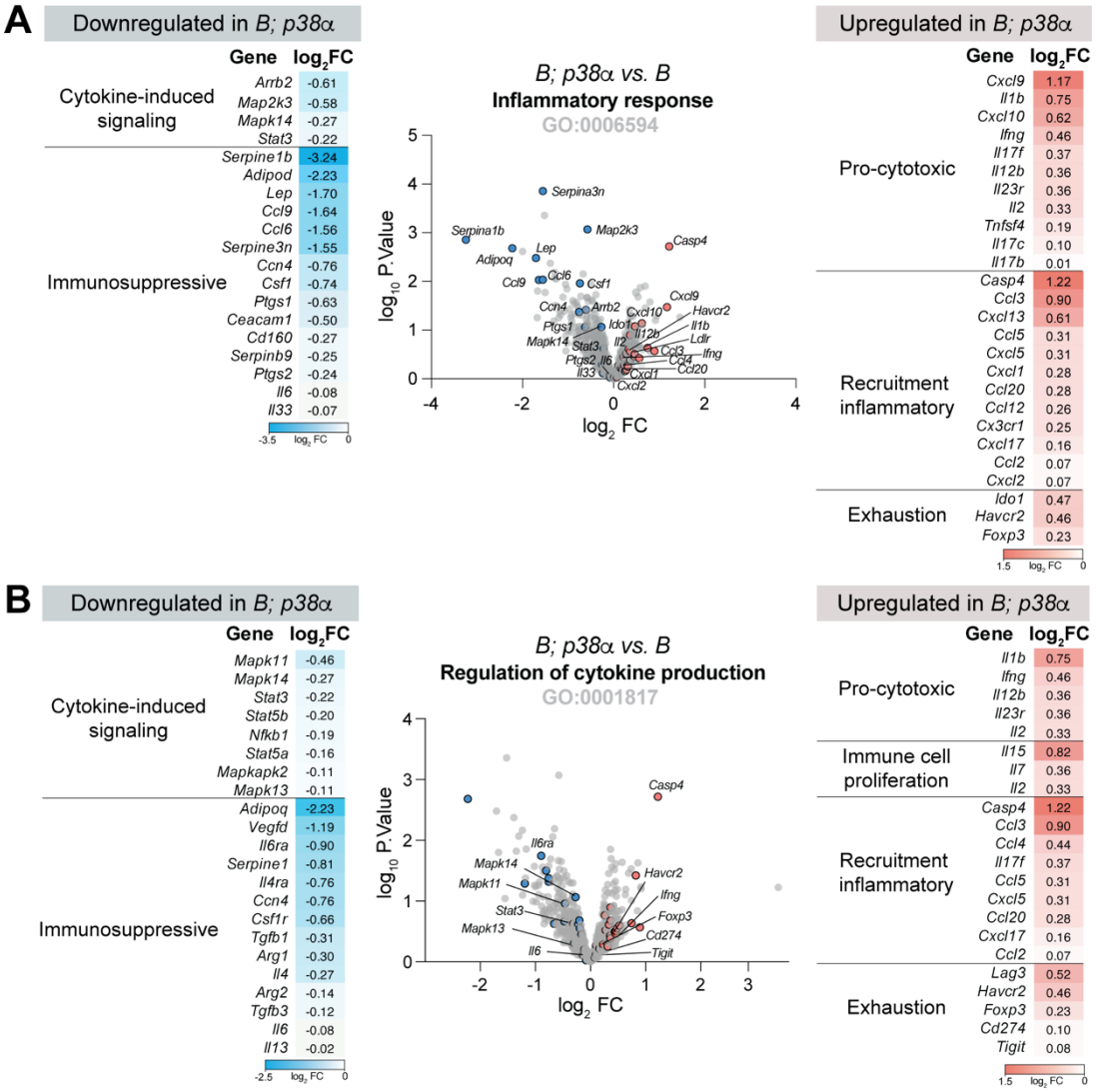


Figure 32 | Differentially regulated immune-related genes in *B;p38α* vs. *B* tumors. (A) Volcano plot showing the differentially regulated genes in *B;p38α* vs. *B* tumors of the regulation of cytokine production (GO:0001817) process. **(B)** Volcano plot showing the differentially regulated genes in *B;p38α* vs. *B* tumors of the inflammatory response (GO:0006954) process. List of relevant downregulated (left) and upregulated (right) genes, the corresponding log_2FC and the processes involved are shown for each graph.

Although the "*inflammatory response*" and "*regulation of cytokine production*" processes appeared to be downregulated, a deeper analysis of the differentially expressed genes associated to these terms revealed that the lack of p38α resulted in a significant downregulation of genes involved in cytokine-induced signaling, including *p38α* (*Mapk14*), *p38β* (*Mapk11*) and *p38δ* (*Mapk13*), *p38α* downstream effectors and *Stat* family members (e.g., *Stat3*, *Stat5a* and *Stat5b*). Moreover, downregulated genes also include a number of molecules involved in immunosuppression (e.g., *Il6*, *Csf1*, *Arg1*, *Lep*, *Tgfb1*…). Conversely, the upregulated genes within this GO-terms were mostly associated with the activation of the immune response, including genes contributing to cytotoxicity (e.g., *Ifng, Il1b*, *Il12b*…), immune cell proliferation (e.g., *Il2*), recruitment of inflammatory cells (e.g., *Cxcl9*, *Cxcl10*,

Ccl20…), and immune cell exhaustion (e.g., *Havcr2*, *Cd274*, *Tigit* …), supporting the role of *p38α* in restricting the antitumoral immune response. (Figure 32).

The gene expression data is circumscribed at the tumor recolection endpoint. Thus, this data is reflecting the gene expression status at the time of collection according to the functional status of the different cell populations, and in the case of *B;p38α* tumors, the lack of *p38α* in tumor cells. Therefore, the recapitulation of the whole immune response history according to the status of these molecules would be highly complex. However, it would be very informative to discern between the contribution/s of immune tumor-infiltrating cells and tumor/stroma to this expression profile at this endpoint. To determine the contribution of the tumor/stroma or the tumor-infiltrating immune cells to the differential expression of immune-related genes, we used magnetic beads to separate and enrich the $CD45^-$ (tumor/stroma) and $CD45^+$ (immune cells) populations and performed a microarray analysis to investigate the transcriptional regulation of genes involved in immune processes (Figure 33A).

Analysis of the data revealed that immune-related genes were differentially regulated in both $CD45^-$ and $CD45^+$ populations of *B;p38α* vs. *B* tumors, suggesting that lack of *p38α* not only modify the tumor cell transcriptional regulation, but also the transcriptional reprograming of the tumor microenvironment. The tumor/stroma cells ($CD45^–$) of *B;p38α* tumors compared to *B* tumors showed a decreased expression of several chemokines, including *Ccl5*, *Ccl6*, *Ccl9*, *Ccl12*, *Ccl22, Xcl1* and *Cxcl16*, chemokine and cytokine receptors such as *Ccr2*, *Ccr3*, *Ccr6*, *Cxcr4*, *Cxcr5, Xcr1* and *Csf1r* (mostly associated to the atraction of immune cell populations, including myeloid cells), immune checkpoint molecules (*Ctla4*, *Vsir* (*VISTA*) and *Pdcd1lg2* (*PD-L2*)), pro-inflammatory cytokines (*Tnf, Il1a*, and *Il1b)* and molecules associated with invasion and metastasis, including *Mmp9*, *Ifi202b*, *Spp1*, *Serpina1b* and *Serpina3n*. However, these cell ($CD45^–$) populations of *B;p38α* tumors showed increased amounts of *Ackr1*, *Cxcl9* and *Cxcl10* mRNA expression when compared to *B* melanomas, which have been associated with an IFNγ signature and higher T cell infiltration[263,264], yet molecules associated with immunosuppression such as *Cd276* (*B7-H3*), *Lif*, *Lag3* or *Slamf7* appeared to be also upregulated in *B;p38α* vs. *B* stroma/tumor cells (Figure 33B).

In respect to the tumor-infiltrating immune cells ($CD45^+$), *B;p38α* compared to *B* tumors showed a decreased mRNA expression of several cytokines and chemokines, including *Il13*, *Il25*, *Ifna1*, *Ccl22*, *Cxcl16*, several receptors such as *Ifngr1*, *Il23r, Ccr6* and *Ccr7*, and immune checkpoint molecules such as *Btla* and *Pdcd1lg2* (*PD-L2*). Consistent with the previous

observation related to the increased number of exhausted T cells in *B;p38α* compared to *B* tumors, tumor-infiltrating immune cells of melanomas lacking *p38α* expression showed increased expression of the exhaustion markers *Pdcd1* (*PD-1*) and *Havcr2* (*TIM-3*), as well as, other immune checkpoint molecules such as *Cd274* (*PD-L1*) and *Slamf7*. Interestingly, infiltrated immune cells (CD45$^+$) of *B;p38α* melanomas compared to *B* tumors showed an increased expression of several cytokines and chemokines, as well as molecules with anti-tumor functions, such as *Il12a*, *Il17f*, *Ifna4*, *Casp4*, *Cxcl10*, *Cxcl1*, *Cxcl2*, *Cxcl5* and *Ccl4*. However, the expression of genes with immunosuppressive functions, such as *Il1b*, *Il6* and *Csf1*, was also increased (Figure 33B).

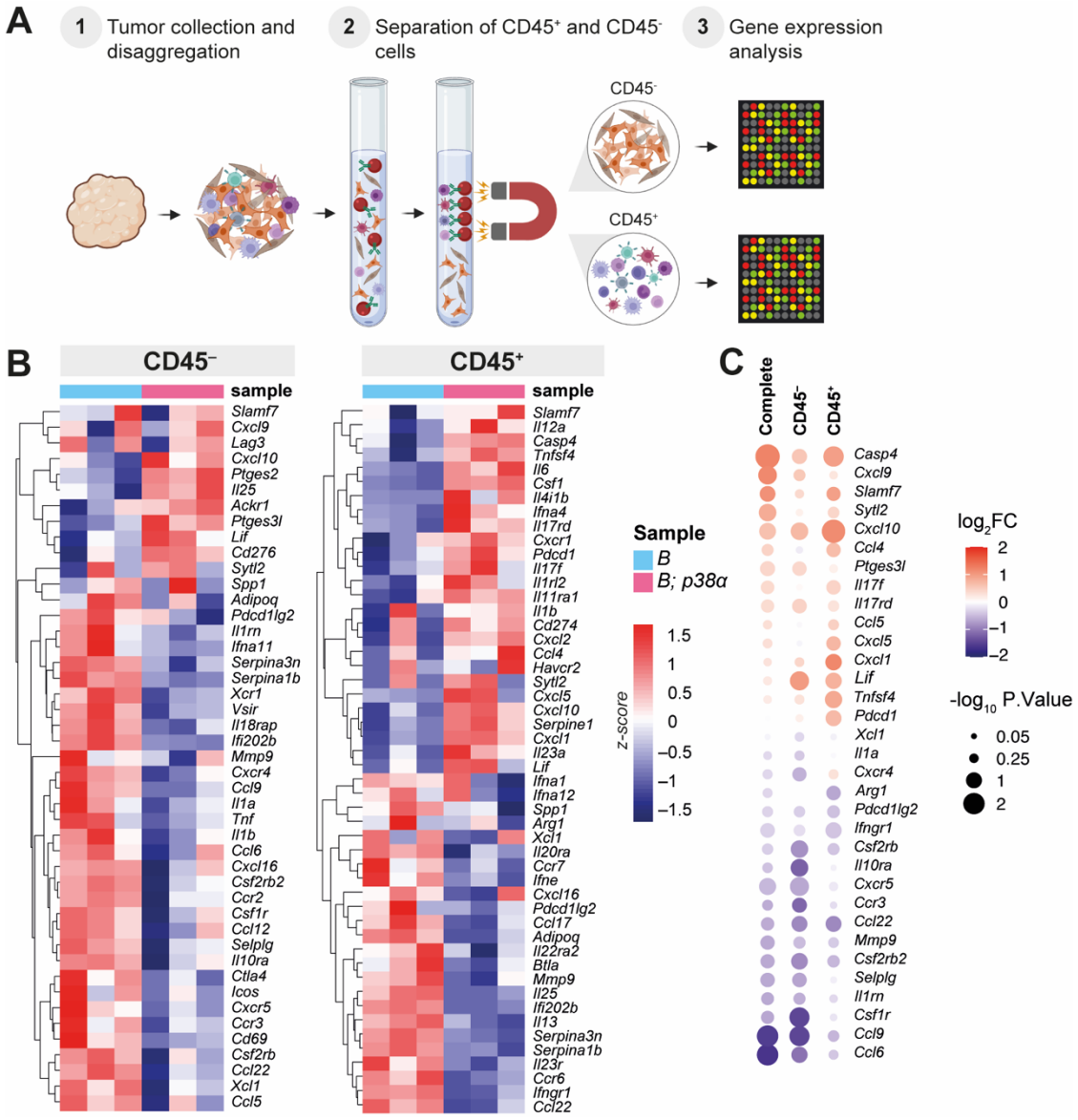


Figure 33 | Differentially regulated immune-related genes in CD45$^-$ and CD45$^+$ populations from *B;p38α* compared to *B* tumors. (A) Schematic representation of the CD45$^-$ and CD45$^+$ separation process from mouse melanoma tumors using magnetic beads to perform the gene expression analysis of the separated populations. **(B)** Heatmap showing the differentially regulated immune-related genes in CD45$^-$ (left) and CD45$^+$ (right) populations from *B;p38α* vs. *B* tumors. **(C)** Dotplot showing the log_2FC (color) and -log_{10} P.Value (dot size) of relevant differentially regulated immune-related genes in complete, CD45$^-$ and CD45$^+$ samples from *B* and *B;p38α*.

When comparing these results with those observed in whole tumor, we detected the absence of some important molecules related to the observed response (*Il2* or *Ifng*). Disaggreation of tumors will cause the loss of a number of regulatory mechanisms induced by ligands or cell-cell interactions. Isolated cells most likely retain features asociated to their functional phenotype but not related to local physiological regulations. Thus, to identify molecules strongly linked to the the loss of *p38α* and the functional phenotype of cells, we selected molecules that where regulated in the same direction in the analysis of the whole tumors and the $CD45^-$ and $CD45^+$ tumor cell populations. Overall, we observed that the $CD45^-$ population showed a higher contribution to the downregulation of immune-related genes that were downregulated in *B;p38α* vs. *B* complete tumors, while the $CD45^+$ population showed a higher contribution to the upregulated genes (Figure 33C).

Stroma/tumor cells from *B;p38α* compared to same type of cells from *B* tumors showed a decrease expression of immunosuppressive molecules (*Csf* receptors, *Il10r*, *Ccl22*, *Mmp9, Xcl1*) and overexpression of relevant molecules related to the anti-tumor response and T cell or NK cell attraction and activation such as, *Casp4*, *Sytl2*, *Ccl4*, *Ccl5*, *Cxcl1*, *Cxcl9 Cxcl10* and *Tnfsf4* (OX40-L). Since tumors were not complete resolved, stroma/tumor cells (*B;p38α* vs. *B*) also overexpressed immune checkpoint molecules (*Slamf7* and *Pdcd1* (*PD-1*)) and immunosuppressive molecules such as *Lif* (Figure 33C). In line with these data, tumor immune-infiltrated cells (*B;p38α* vs. *B*) had downregulated the same immunosuppressive molecules, particularly *Ccl22*, *Arg1* and *Pdcd1lg2* (*PD-L2*), and contributed to the tumor microenvironment upregulating, principally, *Casp4*, *Cxcl1*, *Cxcl5*, *Cxcl10* and *Tnfsf4*. Immunoregulation of these immune cell population was also inferred by the increased expression of *Pdcd1* (*PD-1*) and the expression of *Lif* (Figure 33C).

Altogether, these data suggest that, in melanoma cells, p38α regulates the expression of immune-related genes, modulating the anti-tumor immune response. This, in turn, results in the modulation of the tumor microenvironment, including the gene expression profile of tumor-infiltrating immune cells, where the loss of p38α in tumor cells appears to promote the gene expression programs toward a more active and less suppressed immune response.

p38α mediates the expression of cytokines and chemokines that are critical for the modulation of the anti-tumor immune response.

The above transcriptional regulation analysis supported the role of *p38α* restricting the anti-tumor immune response, where cytokines such as IFNγ are clearly involved. To

functionally validate the role of *p38α* regulating cytokine production in tumor cells, we performed a mouse cytokine array analyzing the secretion 111 different cytokines in *B;p38α* (*VHMM203*) or *B* (*VHMM109*) tumor-derived cells (as tumor models) (Figure 34A,B) at basal level or after IFNγ treatment for 24 hours.

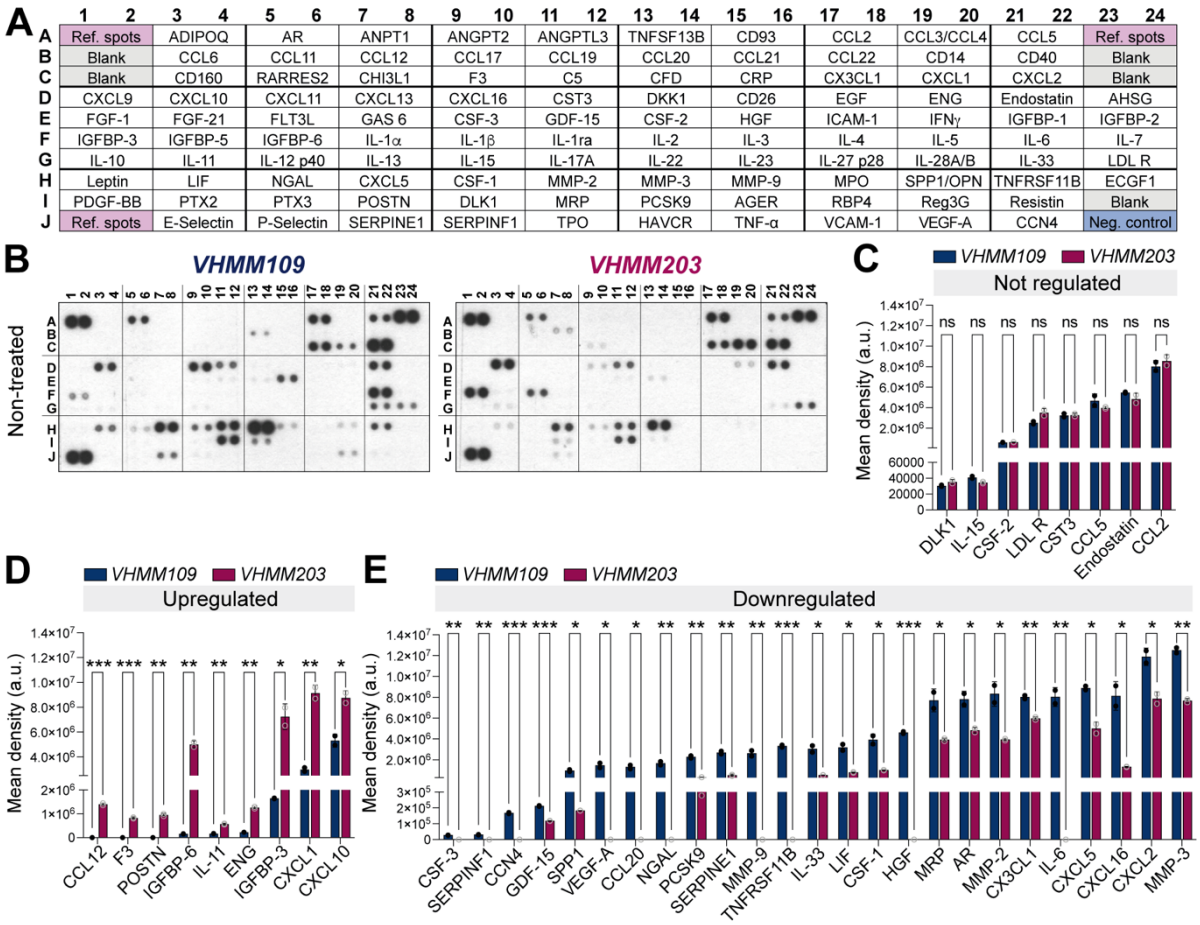


Figure 34 | p38α regulates the expression of cytokines crucial for the modulation of the anti-tumor immune response. (**A**) Schematic representation of the spot positions of the indicated cytokines/chemokines in duplicate on the membranes with the respective internal controls, adapted from the manufacturer's information. (**B**) Representative images of membranes from the cytokine array. (**C**) Graph showing the quantification of not differentially regulated cytokines in *VHMM203* vs. *VHMM109* cells. (**D**) Graph showing the quantification of upregulated cytokines in *VHMM203* vs. *VHMM109* cells. (**E**) Graph showing the quantification of downregulated cytokines in *VHMM203* vs. *VHMM109* cells. Mean pixel density of the corresponding dots was determined using ImageJ software. Statistical significance was assessed by multiple unpaired *t*-test; (ns) non-significant, (*) $p \leq 0.05$, (**) $p \leq 0.01$, (***) $p \leq 0.001$.

Initial analysis of the cytokine array using the basal secretome of *B* and *B;p38α* tumor-model cells, revealed the detection of 42 out of the 111 cytokines present in the array. Thirty-four of those cytokines were differentially regulated between *B* and *B;p38α* cells, including some of the aforementioned cytokines regulated at transcriptional level. *VHMM109* and *VHMM203* cells secreted similar amounts of DLK1, IL-15, CSF-2, LDL R, CST3, CCL5, endostatin and CCL2. Protein expression of CCL12, F3, POSTN, IL-11, ENG, CXCL1 and CXCL10 were increased in *VHMM203* compared to *VHMM109* (Figure 34D), while CXCL9 protein

expression was not detected at basal levels in any of the cell lines (Figure 34B). Moreover, *VHMM203* cells showed increased protein expression of IGFBP-3 and IGFBP-6 compared to *VHMM109* cell line (Figure 34D), which have been associated with anti-tumoral functions[265–267]. In contrast, *VHMM203* cells secreted fewer amounts of SERPINF1, CCN4, GDF-15, CCL20, NGAL, PCSK9, TNFRSF11B, IL-33, MRP, AR, CX3CL1, CXCL2 and CXCL5 compared to *VHMM109* cells (Figure 34E). Furthermore, the protein expression of CSF-3, SPP1, VEGF-A, SERPINE1, MMP-9, LIF, CSF-1, HGF, MMP-2, IL-6, CXCL16 and MMP-3, associated with invasion, metastasis and immunosuppression[197,268–280], were also decreased in *VHMM203* cells compared to *VHMM109* cells (Figure 34E).

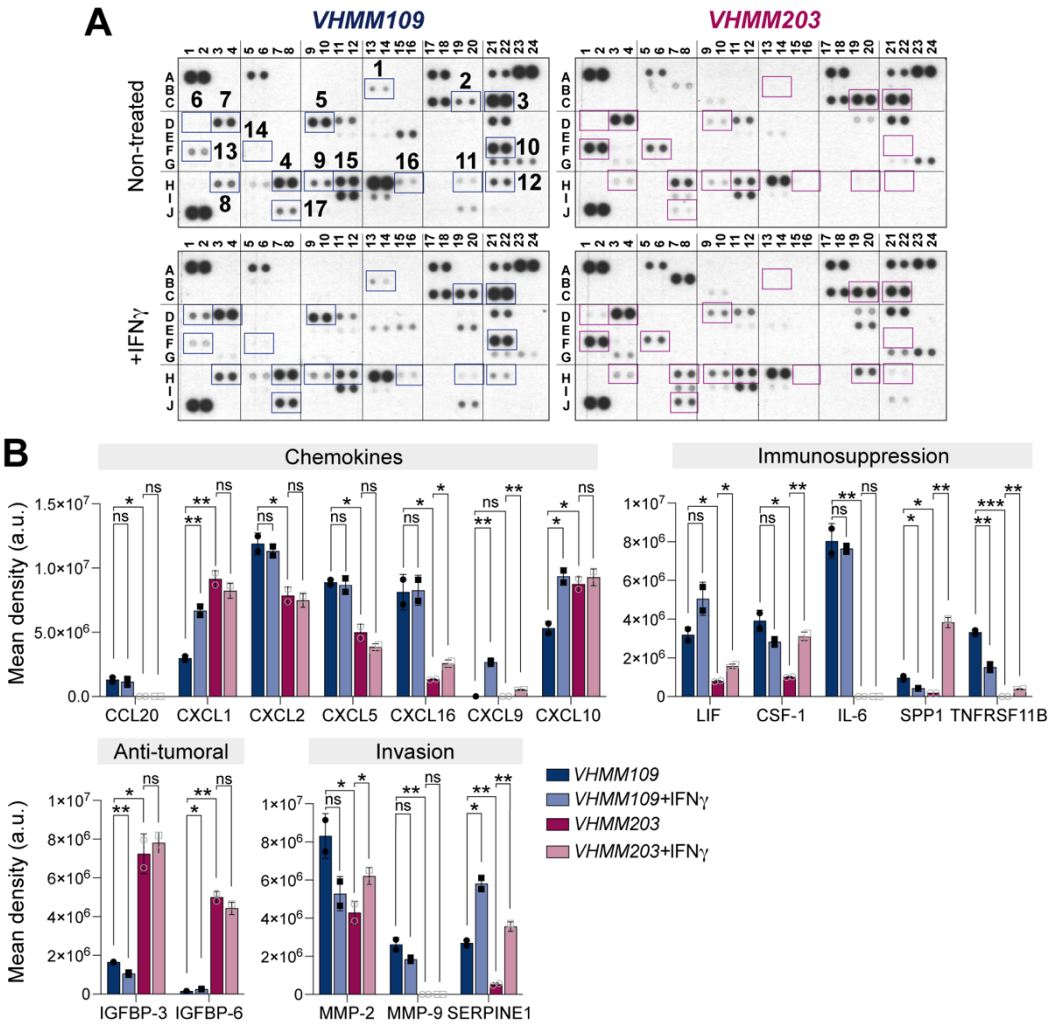


Figure 35 | p38α regulates the expression of cytokines crucial for the modulation of the anti-tumor immune response. (**A**) Representative images of membranes from the cytokine array are shown. The following cytokines are highlighted in the membranes: (1) CCL20, (2) CXCL1, (3) CXCL2, (4) CXCL5, (5) CXCL16, (6) CXCL9, (7) CXCL10, (8) LIF, (9) CSF-1, (10) IL-6, (11) SPP1, (12) TNFRSF11B, (13) IGFBP-3, (14) IGFBP-6, (15) MMP-2, (16) MMP-9, (17) SERPINE1. (**B**) Graphs showing the corresponding quantification of the dots by pixel density determination using ImageJ software. Statistical significance was assessed by multiple unpaired *t*-test; (ns) non-significant, (*) $p \leq 0.05$, (**) $p \leq 0.01$, (***) $p \leq 0.001$.

In response to IFNγ, the regulation of the protein expression among the cytokines analyzed was a highly variable. We focused on the regulation of cytokines that showed differential expression at the basal level and that were also relevant according to the previous results.

IFNγ treatment did not significantly modify the basal expression of CCL20, CXCL2, CXCL5, MMP-9 and IL-6 in any of the two models. However, treatment of *VHMM109* cells with IFNγ increased the protein expression of CXCL1, CXCL10 and IGFBP-6, and decreased the protein amounts of IGFBP-3. Furthermore, some cytokines such as CSF-1, SPP1, TNFRSF11B and MMP.2 showed opposite responses to IFNγ treatment in the two cell lines, whereas the protein amounts of CXCL9, LIF and SERPINE1 increased in response to IFNγ in both cell lines. In addition to the differential regulation in the production of these cytokines in response to IFNγ, the resulting absolute amount in response to the treatment of some of the immunosuppressive cytokines was also different. In this matter, in addition to the lack of expression of IL-6 and MMP-9, *VHMM203* cells produced a significant lower amounts of SERPINE1, CXCL16, LIF and TNFRSF11B (Figure 35).

The above data suggested that the absence of p38α in tumor cells may lead to differential expression of cytokines and chemokines involved in immune cell recruitment and regulation, thus resulting in a less immunosuppressive TME that allows the successful tumor recognition and elimination by immune cells. Based on these findings and considering the role of the p38 MAPK pathway in cytokine response and production[124,177,178], we wanted to validate the contribution of p38α in regulating the expression of relevant cytokines for the anti-tumor immune response. To this end, we analyzed the expression of relevant inflammatory molecules by RT-qPCR in response to the p38 inhibitor SB203580 and/or after the treatment with IFNγ, a key cytotoxic cytokine, in five different *B* tumor-derived cell lines. Additionally, we used four cell lines derived from *B;p38α* tumors to validate the genetic expression of these cytokines in the absence of p38α expression at basal levels and after IFNγ stimulation.

It is known that p38β can compensate some of the functions of p38α, particularly in its absence[124]. To ensure that the absence of p38α was not compensated by the upregulation of other p38 MAPK members and considering that p38δ is not expressed in melanoma[134], we first validated the protein expression of p38α, p38β, and p38γ in the tumor-derived cell lines. We found that cell lines lacking p38α expression also did not express p38β or p38γ (Figure 36A).

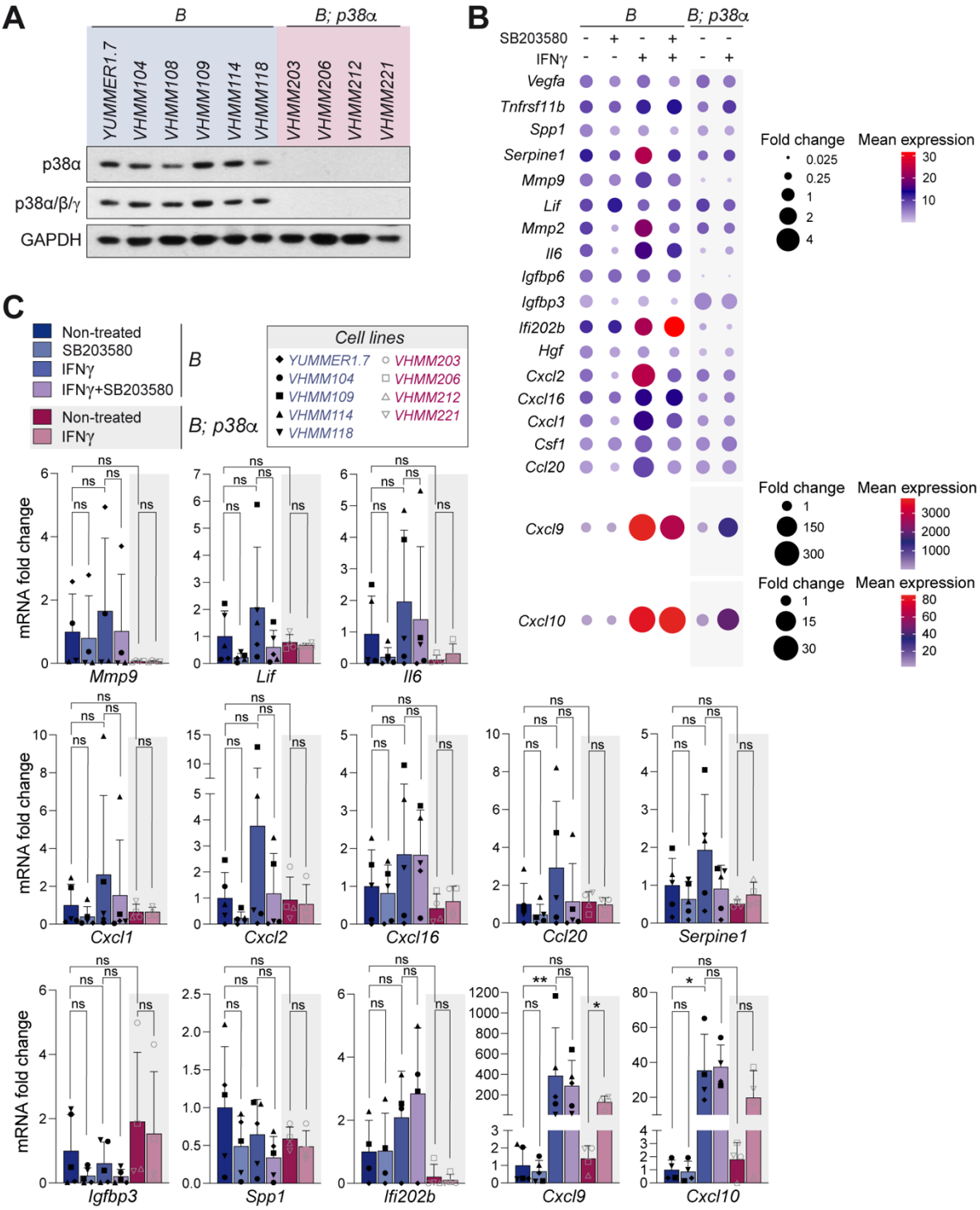


Figure 36 | p38α regulates the expression of cytokines crucial for the modulation of the anti-tumor immune response. (**A**) Western blot showing p38α and p38α/β/γ protein expression in *B* and *B;p38α* tumor-derived cell lines. GAPDH was used as loading control. (**B**) Dotplot showing the fold change (dot size) and mRNA mean expression (color scale bar) of the indicated cytokines in *B* and *B;p38α* cell lines after 24 hours treatment with IFNγ (50 ng/ml) and/or the p38 inhibitor SB203580 (10 μM). (**C**) Graphs showing the mRNA fold change of the indicated cytokines in *B* and *B;p38α* cell lines after 24 hours treatment with IFNγ (50 ng/ml) and/or the p38 inhibitor SB203580 (10 μM). Statistical significance was assessed by Mann-Whitney *t*-test; (ns) non-significant, (*) $p \leq 0.05$, (**) $p \leq 0.01$.

In response to SB203580 (p38 inhibitor), *B* cell lines downregulated the mRNA expression of several inflammatory molecules including *Spp1*, *Serpine1*, *Lif*, *Il6*, *Igfbp3*, *Cxcl2*, *Cxcl1* and *Ccl20*, although not significantly due to cell line variability. Furthermore, upon IFNγ

treatment, the expression of most of the cytokines and chemokines analyzed, including *Mmp9*, *Lif*, *Il6*, *Cxcl1*, *Cxcl2*, *Cxcl16*, *Ccl20*, *Serpine1*, *Igfbp3*, *Spp1*, *Ifi202b*, *Cxcl9* and *Cxcl10*, was increased. However, the expression of *Spp1* and *Igfbp3* decreased and no differences were observed in the expression of *Mmp2*, *Igfbp6*, *Hgf*, *Vegfa* and *Tnfrsf11b* in response to IFNγ treatment (Figure 36B,C and Supplementary Figure 4). The inhibition of p38 reduced the induction of the expression of *Serpine1*, *Mmp9*, *Lif*, *Il6*, *Cxcl2*, *Cxcl1*, *Csf1*, and *Ccl20* in response to IFNγ (Figure 36B,C and Supplementary Figure 4), suggesting a regulatory role of the p38 MAPK in the expression of these inflammatory molecules upon IFNγ treatment. In agreement with this, *B;p38α* cell lines showed a reduced expression of *Spp1*, *Serpine1*, *Mmp9*, *Lif*, *Il6*, *Ifi202b*, and *Cxcl16* at basal level compared to the expression of *B* cell lines (Figure 36B,C). The observed reduction in the expression of *Igfbp6* at basal levels in *B;p38α* compared to *B* cell lines was due to the high contribution of two *B* cell lines, whereas no expression was detected in the other three *B* cell lines and in neither of the *B;p38α* cell lines (Figure 36B and Supplementary Figure 4). Furthermore, molecules associated with anti-tumoral functions such as *Igfbp3*, *Cxcl9* and *Cxcl10*[263,265], showed an increased expression at basal level in *B;p38α* compared to *B* cell lines. Overall, the expression of the inflammatory molecules analyzed did not increase or showed a lower increase in response to IFNγ in *B;p38α* cell lines compared to the response observed in *B* cells (Figure 36B,C), again highlighting the role of p38α in modulating cytokine expression in response to IFNγ.

Altogether, these results indicate that tumor cells regulate the expression of a number of inflammatory molecules through p38α. Consequently, the lack of p38α leads to a distinct cytokine expression profile that will impact in the anti-tumor immune response and the TME.

p38α expression by tumor cells determines the response to PD-1 immune checkpoint blockade.

The consistent data suggesting that p38α may regulate the production of relevant cytokines and chemokines critical for the anti-tumor immunity, resulting in an immunosuppressed TME and an impaired cytotoxic immune response, prompted us to investigate its relevance in the context of immunotherapy. Moreover, we had previously observed that tumors lacking p38α expression exhibited a higher proportion of exhausted $CD8^+$ T cells, primarily due to a higher PD-1 expression, but a subpopulation also co-expressed TIM-3, suggesting that blockade of these immune checkpoint molecules might enhance the anti-tumor response in p38α-deficient tumors. Therefore, to evaluate the potential therapeutic impact of the TME modulation by p38α, we used syngeneic mouse models to investigate the response to PD-1 and/or TIM-3

blockade in the presence or absence of p38α expression in melanoma cells. We subcutaneously inoculated *YUMMER1.7* (*Braf*$^{CA/WT}$; *Pten*$^{-/-}$; *Cdkn2a*$^{-/-}$) and *VHMM212* (*Braf*$^{CA/CA}$; *p38α*$^{-/-}$) cell lines in C57BL/6JRj mice and when tumor size reached 50-100 mm^3, mice were treated with 200 µg of either isotype (rat IgG2a, κ) for the control group, αPD-1, αTIM-3 or the combination of both antibodies via intraperitoneal injection. Mice were dosed twice a week for a total of five doses and were euthanized one week after the end of the treatment. The intratumoral immune cell populations of the remaining tumors were analyzed by flow cytometry.

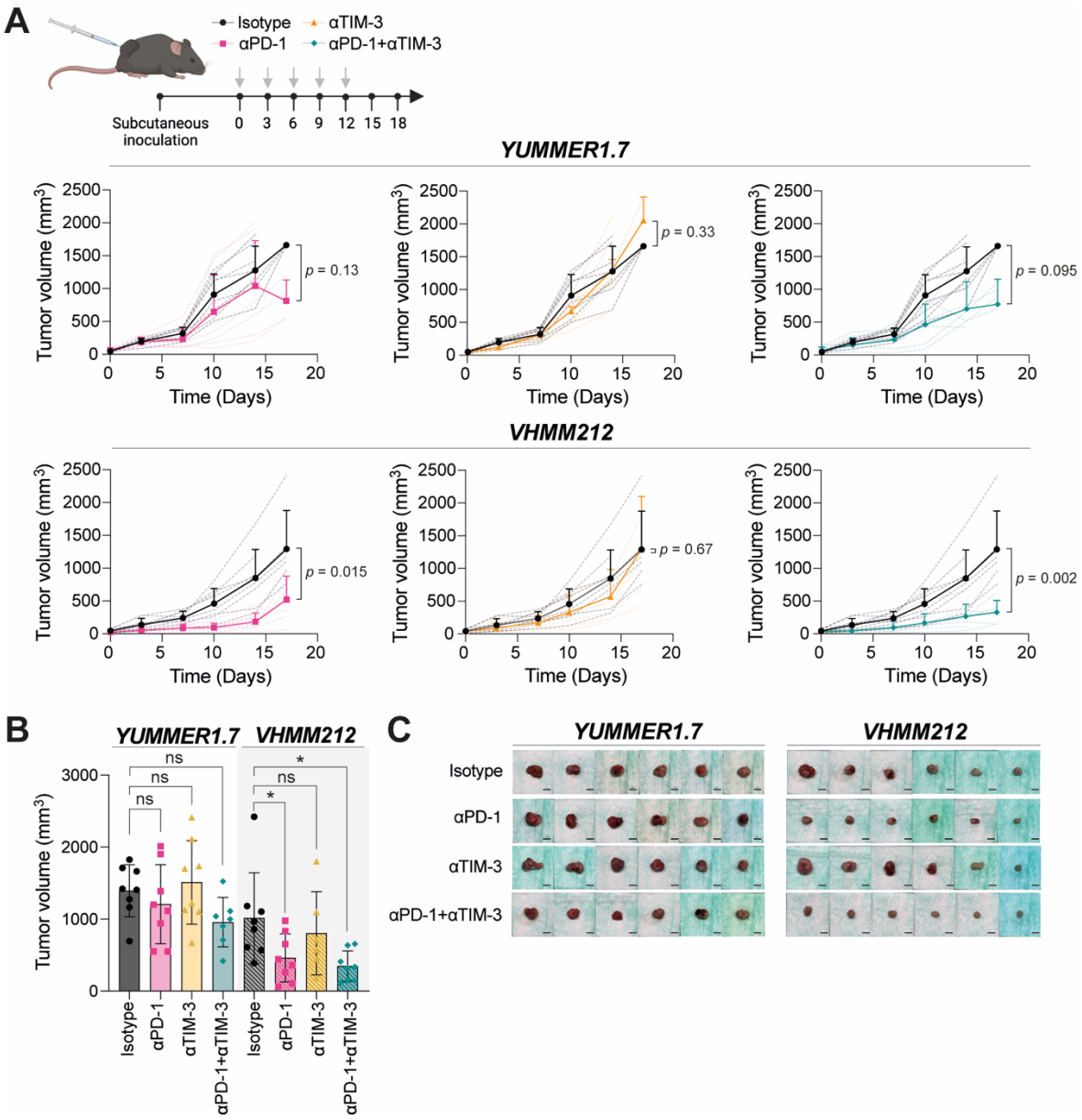


Figure 37 | p38α expression by tumor cells determine the response to αPD-1 *in vivo*. (**A**) Graphs showing *in vivo* tumor growth of *YUMMER1.7* and *VHMM212* cell lines treated with isotype (rat IgG2a, κ), αPD-1, αTIM-3, or the combination αPD-1+αTIM-3. Dashed lines represent individual tumors. Scheme representing the experimental procedure is shown. (**B**) Graph showing *YUMMER1.7* and *VHMM212* tumor volumes at endpoint of the study. Statistical significance was assessed by unpaired *t*-test; (ns) non-significant, (*) $p \leq 0.05$. (**C**) Representative images of *YUMMER1.7* and *VHMM212* tumors treated with αPD-1, αTIM-3, or the combination. Bars represent 1 cm.

Treatment with αPD-1 antibody or with the combination of αPD-1+αTIM-3 antibodies significantly reduced tumor growth only in *VHMM212* tumors which lack p38α expression. However, single treatment with the αTIM-3 antibody did not reduce tumor growth in either *YUMMER1.7* or *VHMM212* tumors (Figure 37), suggesting that the primary mechanism driving the reduction in tumor growth with the combination of αPD-1+αTIM-3 antibodies was the blockade of PD-1.

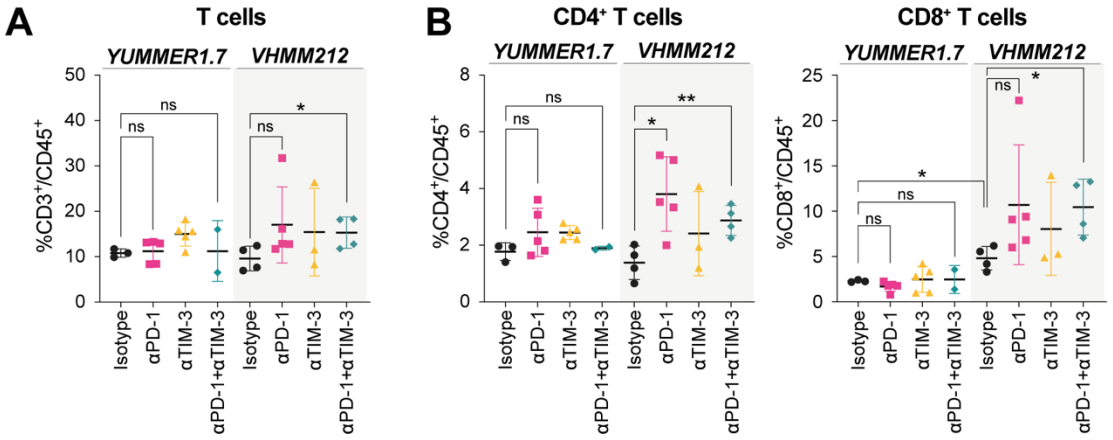


Figure 38 | The increased response to PD-1 or PD-1+TIM-3 blockade in *VHMM212* syngeneic tumors was associated with an increased T cell infiltration. (**A**) Graph showing the percentage of T cells in *YUMMER1.7* and *VHMM212* syngeneic tumors treated with isotype (rat IgG2a, κ), αPD-1, αTIM-3, or the combination αPD-1+αTIM-3. (**B**) Graphs showing the percentage of $CD4^+$ and $CD8^+$ T cells in *YUMMER1.7* and *VHMM212* syngeneic tumors treated with isotype (rat IgG2a, κ), αPD-1, αTIM-3, or the combination αPD-1+αTIM-3. Statistical significance was assessed by unpaired *t*-test; (ns) non-significant, (*) $p \leq 0.05$, (**) $p \leq 0.01$.

The increased response of *VHMM212* tumors to the treatment with αPD-1 or αPD-1+αTIM-3 was associated with an increased recruitment of T cells (Figure 38A), including both $CD4^+$ and $CD8^+$ T cells (Figure 38B). Notably, the recruitment of cytotoxic $CD8^+$ T cells was significantly increased in the isotype-treated control group in *VHMM212* tumors compared to control *YUMMER1.7* tumors (Figure 38B). This enhanced recruitment of T cells, particularly the significant increase in cytotoxic $CD8^+$ T cells, further supports the notion that the absence of p38α in tumor cells contributes to a more favorable environment for T cell-mediated anti-tumor activity.

Altogether, these results suggest that the absence of p38α makes the tumors more susceptible to PD-1 blockade, highlighting the critical role of p38α in modulating the immune response within the TME and suggesting a potential therapeutic strategy of inhibiting p38α to enhance the anti-tumor immune response of PD-1 blocking antibodies.

Absence of *p38α* expression in tumor cells recapitulates a good prognosis signature to immune checkpoint blockade in humans.

To evaluate the similarity of our model to the human response to immunotherapy, we compared the gene expression data from *B;p38α* vs. *B* tumors with published signatures of response to the treatment with immune checkpoint inhibitors (ICIs) in melanoma. We interrogated five gene signatures associated with good prognosis (good response to αPD-1 in αCTLA-4-resistant or αCTLA-4-naïve patients[281], upregulated genes in responders to αPD-1 or αPD-1+αCTLA treatments[282], good response to αPD-1 in αCTLA-4-resistant melanoma patients[283] and an IFNγ signature of good response to αPD-1 treatment[284]) and seven gene signatures associated with bad prognosis (tumor immune dysfunction and exclusion (TIDE) signature associated with bad response to αPD-1 or αCTLA treatments[285], upregulated genes in non-responders to αPD-1 or αPD-1+αCTLA treatments[282], innate αPD-1 resistance signature[286], T cell-induced CSF1 signature associated with resistance to αPD-1 treatment[270], bad response to αPD-1 in αCTLA-4-resistant or αCTLA-4-naïve patients[281] and upregulated genes associated with resistance to αPD-1 therapy[287]) to immune checkpoint blockade in human melanoma patients.

We found that genes associated with a good response to immunotherapy were mostly upregulated in *B;p38α* vs. *B* tumors, whereas genes associated with bad response to the treatment with ICIs were downregulated in tumors lacking p38α expression (Figure 39). Specifically, 54,7% (111 of 203 genes) of unique genes included in all good prognosis signatures were upregulated in *B;p38α* vs. *B* tumors (Supplementary table 3), whereas 69,3% (264 of 381 genes) of the genes associated with bad prognosis were downregulated in *B;p38α* vs. *B* mouse melanomas (Supplementary table 4). Therefore, the lack of p38α in melanoma cells recapitulates a good response gene signature to the treatment with ICIs in melanoma patients.

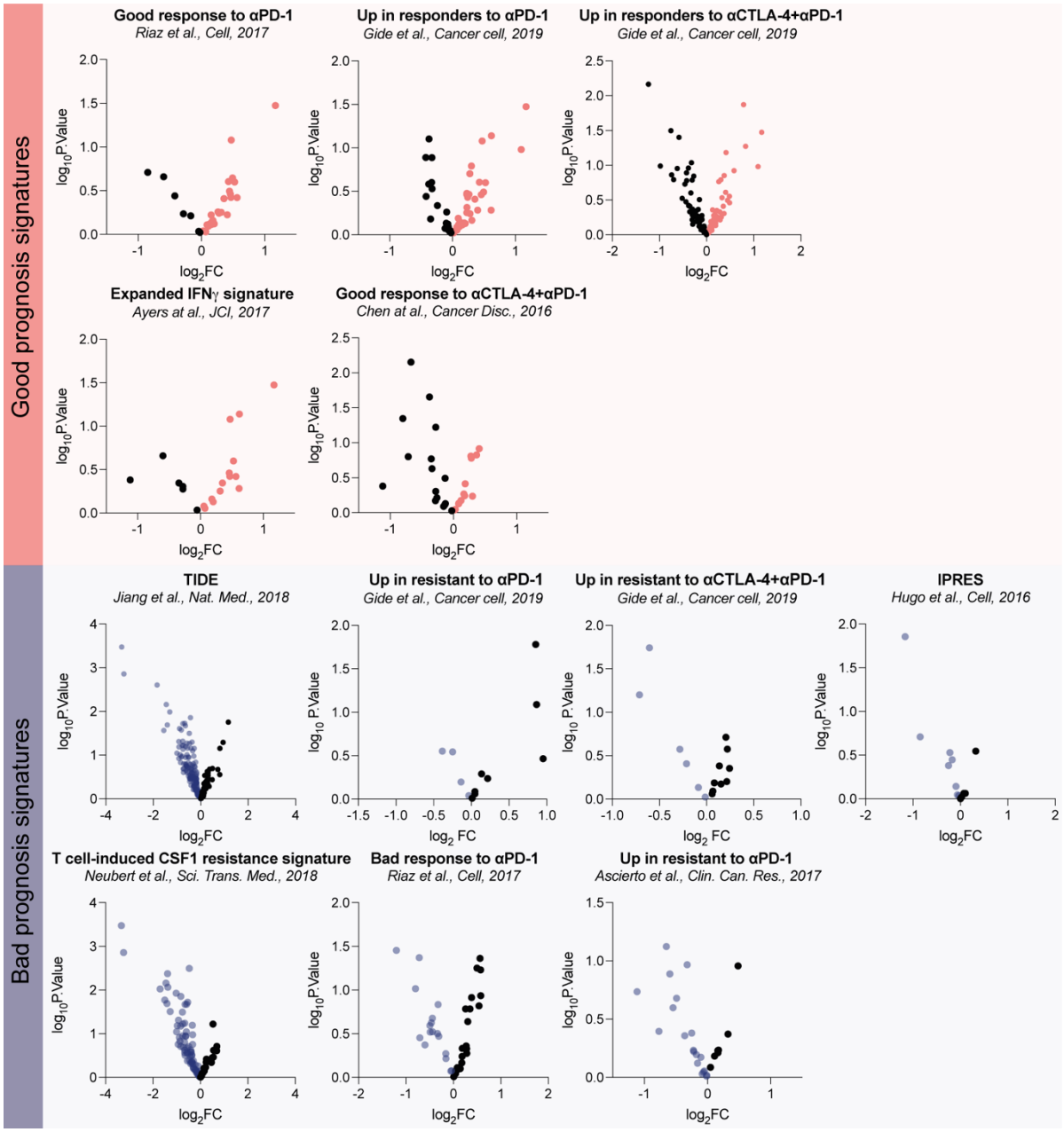


Figure 39 | Absence of p38α in tumor cells recapitulate a good prognosis signature to immune checkpoint blockade in humans. Volcano plots showing the differential transcriptional regulation in *B;p38α* vs. *B* tumors of genes previously associated with good (red) and bad (blue) prognosis in the indicated signatures in patients treated with immune checkpoint inhibitors (ICIs). Upregulated genes in *B;p38α* vs. *B* of good prognosis signatures are highlighted in red. Downregulated genes in *B;p38α* vs. *B* of bad prognosis signatures are highlighted in blue. TIDE: Tumor Immune Dysfunction and Exclusion; IPRES: Innate αPD-1 Resistance.

To generate a p38α-associated gene signature of good response to the treatment with ICIs, we selected the top upregulated genes ($log_2FC > 0.5$) among all good prognosis signatures in *B;p38α* vs. *B* tumors. A nine-gene signature of good response associated with the absence of p38α expression in melanoma cells was identified, consisting of *Cxcl9*, *Slamf7*, *Sytl2*, *Adam28*, *Cxcl10*, *Cxcl13*, *Fmo3*, *Cxcr6* and *Lag3*, which could potentially predict the outcome of melanoma patients to the treatment with ICIs (Figure 40A,B).

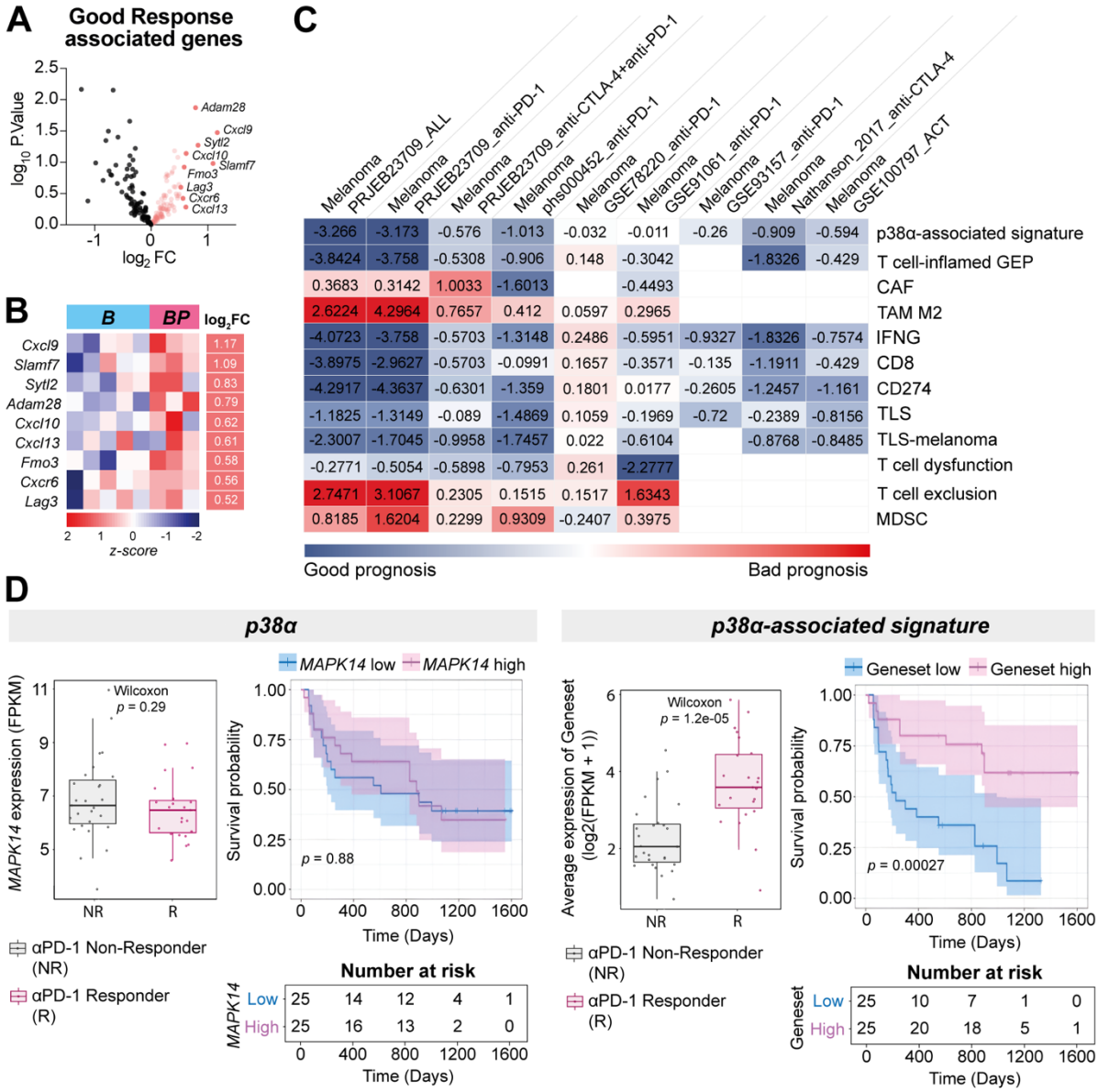


Figure 40 | A p38α-associated nine-gene signature can predict the response to PD-1 blockade. (**A**) Volcano plot showing the upregulated genes (red) in *B;p38α* vs. *B* tumors associated with a good prognosis to the treatment with immune checkpoint inhibitors (ICIs). Top upregulated genes ($log_2FC > 0.5$) are highlighted. (**B**) Heatmap showing the top upregulated genes ($log_2FC > 0.5$) associated with a good prognosis to the treatment with ICIs (p38α-associated gene signature). BP: *B;p38α*. (**C**) Survival matrix from the Tumor Immunotherapy Gene Expression Resource (TIGER) database showing the predictive good (blue) or bad (red) response of different gene signatures, including the p38α-associated gene signature, in different melanoma studies of response to the treatment with ICIs or adoptive cell therapy (ACT). CAF: cancer-associated fibroblasts; GEP: gene expression profile; TAM: tumor-associated macrophages, IFNG: interferon gamma; TLS: tertiary lymphoid structure; MDSC: myeloid-derived suppressor cells. (**D**) Graphs generated in the TIGER database showing the gene expression of *MAPK14* or the p38α-associated gene signature in non-responders (NR) (n = 27) and responders (R) (n = 23) to αPD-1 treatment (study: PRJEB23709 from *Gide et al. 2019*[282]). Associated survival graphs of patients having low or high expression of *MAPK14* or the p38α-associated gene signature are shown.

To validate the predictive power of our p38α-associated nine-gene signature to the response to the treatment with ICIs, we used the Tumor Immunotherapy Gene Expression Resource (TIGER) database (www.tiger.canceromics.org), which is a web portal that integrates bulk and single-cell gene expression data related to cancer immunotherapy[288], to analyze the

expression of the signature in melanoma tumor samples and correlate it with immunotherapy outcomes by comparing the expression levels of the signature in responders versus non-responders. Notably, the p38α-associated gene signature predicted a good response to immunotherapy in all melanoma studies analyzed in the TIGER database with similar predictive power to established signatures of response to immunotherapy (Figure 40C), validating the robustness of our nine-gene signature.

In addition, we evaluated the predictive power of p38α and of our p38α-associated signature for the response to αPD-1 treatment in the *Gide et al. 2019* patient cohort[282] in the TIGER database. The responder (R) cohort was defined as complete response (CR) or partial response (PR), and the non-responder (NR) cohort was defined as stable disease (SD) or progressive disease (PD). While p38α expression did not predict the response to αPD-1, responders to αPD-1 treatment had significantly higher expression of the p38α-associated signature, with patients with high expression of the nine-gene signature having approximately 50% higher probability of survival (Figure 40D).

Overall, these data support the critical role of p38α in controlling the expression of genes that define the response to the treatment with ICIs in melanoma patients and validate the robustness of our model in the response to immunotherapy, suggesting p38α as a potential therapeutic target to improve the response to the treatment with PD-1 blocking antibodies in melanoma.

DISCUSSION

Melanoma is a highly aggressive form of skin cancer with increasing incidence rates worldwide[1]. The treatment of melanoma has been revolutionized in recent years with the approval of targeted therapies and immunotherapy, which have shown promising results in improving patient outcomes[54,96,98–100,104,289]. Despite these advances, challenges such as primary or acquired resistance to current therapies and disease progression persist, highlighting the need for further research and development of more effective strategies to treat melanoma[54]. Immunotherapy, particularly ICIs, has become the first-line treatment for advanced melanoma. However, response rates are still limited to a subset of patients mainly due to the development of immune evasion strategies by melanoma cells, including the expression of molecules that limit the functionality of tumor-reactive T cells or the recruitment of immunosuppressive immune cells[108,109,290]. Despite the growing knowledge of the interaction between the immune system and the tumor, the mechanisms underlying immune evasion by cancer cells are not fully understood due to the high complexity of the anti-tumor immune response, which is the major obstacle to optimizing the efficacy of immunotherapy in cancer patients. Therefore, a better understanding of both tumor cell intrinsic and extrinsic mechanisms used to evade the detection and elimination by immune cells is an unmet need to develop more effective therapeutic approaches and to identify patients with greater potential to respond to immunotherapy.

The RAS/RAF/MEK/ERK signaling pathway has long been recognized as a central player in melanoma oncogenesis, with mutations in key oncogenes such as *BRAF* and *NRAS* driving hyperactivation of this pathway[41]. However, emerging evidence suggests that additional signaling cascades, such as the stress-responsive SAPK/JNK and p38 MAPK pathways, also contribute significantly to melanoma biology[207,291–294]. Indeed, analysis of whole-exome sequencing data from three different mouse melanoma models and human skin cutaneous melanoma data from the TCGA database revealed commonly mutated genes that were involved in these stress MAPK pathways. Despite their important roles in proliferation, survival and signaling of cytokines that modulate the immune system[117], their precise role in melanoma pathogenesis remains unclear. Here we showed that melanoma was the most prevalent tumor type showing alterations in the *MAPK14* gene. Mutations in this gene were not commonly observed in melanoma or other tumors. However, 25% of the skin cutaneous melanoma samples from the TCGA database showed transcriptional upregulation and/or amplification of this gene. These observations support a previously postulated idea suggesting that, despite its tumor suppressor role in normal epithelial cells, inactivating mutations of *p38α* are not frequently identified in tumors because it acts as a non-oncogene addiction factor in

malignant cells[124,196]. Indeed, upregulation and/or amplification of *MAPK14* was associated with poor survival of melanoma patients, independently of other genetic alterations. These alterations decreased the survival of melanoma patients harboring mutations in either *BRAF* or *NRAS* genes, suggesting a potential contribution of p38α to melanoma pathogenesis.

The development and progression of a tumor involves alterations in the regulation of signaling pathways that normally maintain tissue homeostasis[295]. Although mutations in key protein kinases are the main drivers causing uncontrolled proliferation of melanoma cells[41], tumor development also involves interactions between tumor cells and the surrounding microenvironment[295]. The p38 MAPK signaling pathway is involved in processes important for normal cell function, such as the response to environmental stimuli, cytokine signaling, and the regulation of gene expression, cell growth, and apoptosis[124]. Therefore, cancer cells may benefit from the versatility of this signaling pathway to contribute to primary tumor growth but also facilitate the dissemination of tumor cells[196]. Further analysis of the human melanoma samples from the TCGA dataset showed that alterations in the *p38α* gene appeared to occur during the invasive phase (from Clark stage II to stage IV), when melanoma cells cross the basement membrane of the skin, thus getting in contact with the underlying microenvironment. Consequently, these melanoma cells are compelled to confront the detection and elimination by immune cells. Immunohistochemical analysis of *in situ* melanoma samples showed that while p38α expression was absent in normal melanocytes, melanoma cells that were beginning to cross the basal layer of the skin had higher p38α expression than melanoma cells that remained confined to the epidermis, further supporting the idea that p38α expression may confer an advantage to melanoma progression.

The p38α signaling pathway has been classically considered a tumor suppressor, inducing apoptosis, differentiation, and cell cycle arrest and/or OIS in response to oncogenic stimuli[167,168,182,184,296]. Although it seems that p38α may act as a tumor suppressor during early stages of tumorigenesis, recent reports have also shown pro-tumorigenic functions for p38α, promoting cell growth and survival and facilitating metastasis[124,196,205–207,294,297,298]. Given that the role of p38α in tumorigenesis seems to be cell and context dependent, in this work we have addressed the function of p38α in the particular context of melanoma cells. Consistent with previous research showing a crucial role of p38α in regulating cell proliferation and migration of A375 melanoma cells[294], we showed that downregulation of *p38α* or pharmacologic inhibition of p38 with SB203580 decreased the proliferation rate of *BRAF*-mutated melanoma cells, providing additional support for the pro-tumoral role of p38α in melanoma cells.

However, given the number of stimuli that can activate the p38α signaling pathway in the tumor microenvironment and the plethora of functions regulated by this pathway, investigating the systemic effects of p38α signaling by tumor cells may be particularly necessary for understanding its role in melanoma progression.

In melanoma, mutations in the *BRAF* oncogene are observed in approximately 50% of the tumor samples[46]. It is well established that *BRAF* mutations result in cell cycle arrest and/or OIS[37]. Previous studies have described the role of p38α in tumor initiation in cooperation with *ras* or *raf-1* as driving oncogenes. These studies have demonstrated that activation of p38α leads to permanent cell cycle arrest and/or OIS and indicate a link between the RAS/RAF/MEK/ERK and the p38 MAPK signaling pathways, suggesting that p38α may act as a tumor suppressor, preventing oncogene-driven tumor initiation[181–184]. In this work, we characterized the role of p38α in melanoma development and progression in a $Braf^{V600E}$ mutational background. Our findings align with previous studies[242,243], which have demonstrated that the expression of $Braf^{V600E}$ alone does not promote melanoma tumor development. Notably, we found that *p38α* deletion cooperates with mutated $Braf^{V600E}$ in the generation of spontaneous melanoma tumors. This observation is consistent with previous studies that have demonstrated the potential role of p38α as a tumor suppressor in oncogene-driven tumor development[181–184,296]. Therefore, we speculate that p38α may prevent melanoma initiation by promoting cell cycle arrest and/or OIS through a negative feedback mechanism for $BRAF^{V600E}$ proliferative signaling.

The main environmental risk factor for the development of melanoma is UV radiation[14]. It is well established that p38α is activated in response to UV radiation, promoting cell cycle arrest, DNA repair and apoptosis[167], but also the expression of pro-carcinogenic molecules such as COX-2, TNF, IL-6, IL-8 and IL-1[168,176]. Two previous studies have characterized the role of p38α in UV-induced non-melanoma skin carcinogenesis with controversial results. In these studies, a hairless mouse model of chronic UV-induced skin carcinogenesis with a dominant-negative inactive p38α was used. In one of the studies, p38α dominant-negative mice showed a reduced epidermal apoptosis after acute UVB exposure, but not after chronic UVB exposure. However, these mice also showed a reduced number and growth of UVB-induced skin tumors, which they attributed to a reduced number of proliferative cells[299]. In the other study, chronic solar UV irradiation of p38α dominant-negative mice also resulted in fewer and smaller tumors[300], suggesting a pro-tumoral function of p38α in the development and progression of non-melanoma skin carcinogenesis induced by UV radiation. However, the role of p38α in

UV-induced melanoma development and progression has not been previously addressed. Therefore, we incorporated to our *Braf*^{V600E} mouse melanoma model a single physiological neonate dose of UVB irradiation. While *Braf*^{V600E} oncogene activation together with UVB irradiation promoted melanoma development with high penetrance, as previously reported by our group[234], we observed that loss of p38α resulted in a delay in the development and/or progression of UVB-induced *Braf*^{V600E}-mutant melanomas. Nevertheless, these differences were not observed when both *Braf*^{V600E} mutated alleles were active. This may be attributed to the high penetrance in melanoma tumor formation that is already induced by both active alleles of *Braf*^{V600E} in cooperation with UVB irradiation. Importantly, depletion of p38α resulted in increased tumor multiplicity but reduced tumor size of these UVB-induced *Braf*^{V600E}-mutant melanomas. The smaller size of tumors lacking p38α expression correlated with a significant reduction of Ki67-expressing cells in these tumors. The Ki67 protein is expressed at its highest levels in cycling cells, indicating proliferation of cells expressing this protein[301]. This lower percentage of proliferating cells observed in *B;p38α* tumors is in line with the reduced proliferation rate observed in *BRAF*-mutant human melanoma cells after p38α inhibition, which would support previous studies suggesting that p38α plays an important role in promoting melanoma cell proliferation both *in vitro* and *in vivo*[294,302].

Collectively, our results suggest a dual role of p38α in melanoma tumorigenesis. On the one hand, p38α may act as a tumor suppressor in the malignant transformation of melanocytes. This phenomenon may be attributed to the normal cellular response wherein p38α is activated after oncogene activation or UV damage, leading to cell cycle arrest or apoptosis[128]. The lack of p38α in melanocytes may prevent the progression of stress-damaged cells after *Braf*^{V600E} oncogene activation and UVB irradiation, allowing their survival and ultimately resulting in a higher number of tumors per mouse. On the other hand, p38α may also facilitate cancer cell proliferation in both established melanoma cell lines and in mouse melanoma tumors, for example through mechanisms involving proliferation, gene expression regulation and the interaction with the surrounding microenvironment. In line with this idea, some reports have provided evidence for a dual role of p38α in several cancer types, including breast, lung and colon cancer[196,296,303]. For example, in a colitis-associated colorectal cancer mouse model, p38α expression suppressed colitis-associated tumor initiation but was required for the proliferation and survival of colon cancer cells[296]. Another study found that p38α controls the renewal of lung stem and progenitor cells, and that inactivation of p38α leads to increased proliferation and less differentiated lung cells, promoting increased *Kras*^{G12V}-induced tumorigenesis[303]. Therefore, our model provides additional evidence for the dual function of

p38α in tumor initiation and progression. We suggest that p38α may act as a tumor suppressor in the malignant transformation of melanocytes induced by *Braf*^{V600E} oncogene activation and UVB irradiation. However, it may also have a pro-tumoral role in melanoma tumor growth and progression.

While low Ki67 expression in *B;p38α* tumors may partially explain the reduced size of these tumors, other factors, such as the interaction of the tumor with the surrounding tumor microenvironment, also play a critical role in tumor progression[295]. A key strength of our model system is that, in contrast to syngeneic melanoma models (such as B16), it allows the study of melanoma progression under conditions of natural interactions between tumor and host cells over time. This has allowed us to study the intratumoral immune populations in spontaneously arising melanoma tumors that develop and progress over months, thereby recapitulating the anti-tumor immune response more closely to what occurs in humans. Immunophenotyping of UVB-induced *Braf*^{V600E}-mutated mouse melanoma tumors showed that p38α expression by melanoma cells orchestrate the anti-tumor immune response, regulating the recruitment and activity of immune cells, including cytotoxic T cells and immunosuppressive myeloid cells (Figure 41). It is important to note that the tumors analyzed are already immunoedited, meaning that clones that have developed mechanisms to evade the immune system have been selected. The immunoediting process is a complex and dynamic interaction between the immune system and the tumor cells. It involves multiple phases, including elimination, equilibrium, and escape or immune evasion. During these phases, the immune system detects and eliminates highly immunogenic melanoma clones, while the tumor cells adapt and evolve to evade detection and elimination[85]. Consequently, the observed immunophenotype only reflects the response in the remaining tumors that have evade the immune system. However, it provides valuable insights into the anti-tumor immune response that has previously occurred in the remaining tumors.

The presence of T cells within the TME is a crucial indicator of a pre-existing anti-tumor immune response. Nevertheless, the activity and functionality of these cells to combat the tumor is frequently impaired. The inhibitory properties of PD-1 receptor binding on activated T cells are well established in physiological and pathological contexts[94]. However, PD-1 expression on antigen-specific CD8$^+$ T cells has also been shown to reflect the functional capacity and anti-tumor reactivity of these T cells in melanoma[304–307]. In contrast to previous studies on breast, colon and melanoma syngeneic tumors, where CD8$^+$ T cells co-expressing both PD-1 and TIM-3 were the most abundant[308], in our melanoma spontaneous model the

most prevalent population of $CD8^+$ TE/EM cells expressing exhaustion markers was the PD-1 single-positive. Additionally, they also found that these PD-1^+TIM-3^+ $CD8^+$ T cells had the most exhausted phenotype, while $CD8^+$ T cells only expressing PD-1 contained the highest frequency of IFNγ-producing cells, even higher than the PD-1^-TIM-3^- population, suggesting a functional effector activity of these cells[308]. Interestingly, tumors lacking p38α expression showed a higher proportion of these PD-1^+ $CD8^+$ TE/EM cells, which would reflect a higher cytotoxic immune response against these tumors that has not yet been resolved. The presence of PD-1-expressing $CD8^+$ T cells at the tumor site has been associated with increased therapeutic responses to anti-PD-1 therapy[309]. Both cells with high anti-tumor functionality and cells capable of sustaining a durable response are required for effective T cell-mediated immunity. In this line, *B;p38α* tumors showed higher amounts of both $CD4^+$ and $CD8^+$ TM/CM cells. A high ratio of TM/CM cells to TE/EM cells in the blood has been shown to be a positive predictor of response to anti-PD-1 therapy and survival in patients with advanced melanoma and non-small cell lung cancer[310], which may be attributed to the ability of these T memory cells to rapidly respond to reactivation signals and mount a strong anti-tumor response[247,249]. Taken together, these data suggest that the absence of p38α expression in melanoma cells may facilitate a more effective T cell-mediated immune response, thereby offering novel avenues for the development of immunotherapeutic strategies.

Although the primary focus of current immunotherapies has been on T cells, there is a growing appreciation of the potential of NK and NK-T cells because of their distinct mechanism for recognizing cancer cells without prior sensitization[85]. Nevertheless, their utilization in clinical settings is constrained by the same limitations observed for T cells[311]. Despite the fact that infiltrating NK cells are usually poor in melanoma tumors, the presence of NK cells in melanoma TME has been associated with tumor regression, response to anti-PD-1 immunotherapy, and better overall survival[312,313]. In this regard, a higher number of infiltrating NK-T cells and fewer exhausted NK cells were observed in *B;p38α* tumors. This may enhance the anti-tumor immune response independently of tumor-antigen recognition. This is of particular significance in the context of tumors lacking p38α expression, as we also observed a reduced number of activated DCs expressing MHC-II in these tumors. The presentation of tumor-derived antigens by DCs is a crucial aspect of the anti-tumor immune response, particularly at the initial stages[261]. As mentioned above, the tumors analyzed have already undergone the immune recognition and elimination of highly immunogenic melanoma cells. Consequently, when analyzing these tumors at an advanced stage where this response has already occurred, the activation of these cells may not be necessary. On the other hand, the

remaining tumor cells may have developed mechanisms to evade the immune detection, being the downregulation of the expression of MHC-I and tumor antigens one of the most frequent mechanisms observed in melanoma cells[87,88]. In fact, we have observed that some of the tumor-derived cell lines from *B;p38α* melanomas have lost MHC-I expression (data not shown).

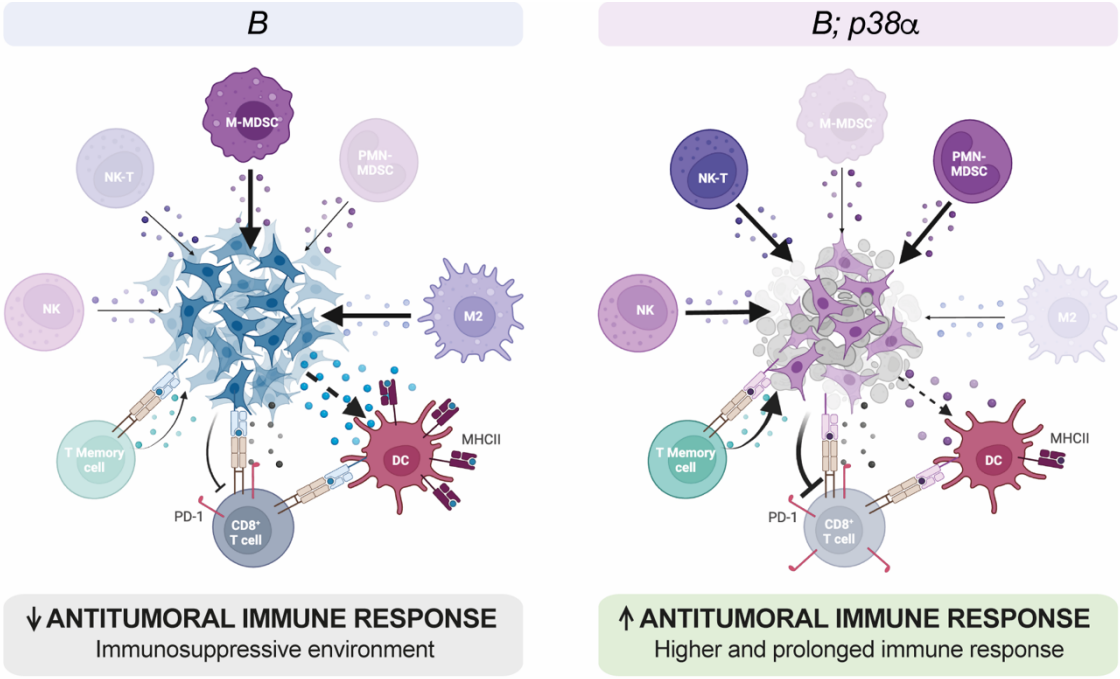


Figure 41 | Summary scheme highlighting the resulting immunophenotypes in *B* and *B;p38α* tumors. Absence of p38α in tumor cells modulates the immune profile of the tumor, which results in a higher and more cytotoxic immune response against the tumor, which is reflected with a higher T memory/central memory (TM/CM) cells and a higher exhaustion of $CD8^+$ T effector/effector memory (TE/EM) cells. Furthermore, *B; p38α* tumors showed a higher recruitment and activation of natural killer (NK) and NK-T cells. As the myeloid cells are known to promote tumor progression, the decrease in the number of macrophages, M2-type macrophages as well as the switch from monocytic (M)- to polymorphonuclear (PMN)-myeloid derived suppressor cells (MDSCs) confers a less immunosuppressive environment to these tumors. Moreover, *B; p38α* tumors exhibited less activated dendritic cells (DCs).

Most of the studies have been focused on T cell populations as mainly mediators of anti-tumor immune responses. Nevertheless, myeloid cells represent a major component of the TME and play a pivotal role in tumor progression, primarily through the exertion of immunosuppressive functions. The potential role of M2-like macrophages and MDSCs as biomarkers of patient outcomes and response to immunotherapy remains a topic of active investigation. Both M2-like macrophages and MDSCs are known to play critical roles in maintaining an immunosuppressive TME[260], which can hinder the effectiveness of immunotherapies. In melanoma, the accumulation of M2-like macrophages is associated with poor patient outcomes, including reduced overall survival, an increased risk of metastasis and increased resistance to immunotherapy[314–316]. Among the two subtypes of MDSCs, M-MDSCs have

been suggested to have a higher immunosuppressive activity than PMN-MDSCs, and the number of M-MDSCs, but not of PMN-MDSCs, directly correlated with suppression of *in vitro* T cell activation[257–259]. A correlation has been observed between high levels of MDSCs and a poor prognosis for patients with melanoma treated with ICIs[317]. Specifically, lower levels of M-MDSCs have been associated with a more favorable clinical response to immunotherapy in melanoma patients[318]. The analysis of the myeloid compartment of *B;p38α* tumors revealed a significant decrease in the frequency of macrophages, as well as a trend towards less M2-like polarization, together with a shift from M-MDSC to a less immunosuppressive PMN-MDSC subtype, compared to *B* melanomas. Our results indicate that p38α signaling may be involved in the recruitment and differentiation of immunosuppressive immune cell populations, which may contribute to an impaired anti-tumor immune response.

The infiltration of immune cells into the TME is indeed a crucial factor in cancer prognosis. Cytokines and chemokines play a pivotal role in orchestrating immune cell trafficking, activation and function within the TME, influencing the anti-tumor immune response and ultimately the outcome of cancer treatment[319]. Given the pivotal role of p38α signaling in the regulation of cytokine and chemokine production[124,177,178], it was hypothesized that p38α expression in tumor cells might modulate the recruitment and functional activity of immune cell populations through the expression of specific cytokines and chemokines. It is important to note that the gene expression data is limited to the time of tumor collection, which makes it challenging to recapitulate the complete immune response history based on the expression of these molecules. Furthermore, discrepancies were observed in the differential regulation of certain immune-related genes in the analysis of enriched $CD45^-$ (tumor/stroma) and $CD45^+$ (immune cells) populations compared to whole tumors, which may be attributed to the disruption of complex cell-cell interactions and local regulatory mechanisms that occur during tumor disaggregation. Consequently, we focused on the molecules that were regulated in the same direction in the analysis of the whole tumors and the $CD45^-$ and $CD45^+$ tumor cell populations. Notwithstanding these limitations, the gene expression profile of mouse melanoma tumors revealed that tumor cell-intrinsic p38α expression regulates the expression of pro-inflammatory cytokines and chemokines, as well as immunosuppressive factors, thereby contributing to immune evasion and immunotherapy resistance.

Although the functions of cytokines and chemokines in cancer are context-dependent, meaning their roles can vary depending on the specific type of cancer, the individual patient's

immune response, and the TME[319], the differential expression of many of them correlated with the immunophenotype observed in the tumors. Several chemokines have previously been associated with the recruitment of T cells into the tumor site in melanoma, including CCL2, CCL3, CCL4, CCL5, CXCL9, and CXCL10[320]. In particular, CXCL9 and CXCL10 are potent chemoattractants for tumor-reactive effector $CD8^+$ T cells expressing CXCR3[263], and are associated with an increased functional activity of these cells and an effective response to ICIs[321–324]. Our results revealed that p38α-deficient tumors exhibited elevated expression of *Ccl2*, *Ccl3*, *Ccl4*, *Ccl5*, *Cxcl9*, and *Cxcl10*. Although this result was not correlated with an increased T cell infiltration, it is possible that these chemokines, particularly *Cxcl9* and *Cxcl10*, are contributing to the enhanced activity of these cells. In addition, the upregulation of these molecules may occur at early stages of tumor development and contribute to T cell recruitment, as we have also observed an increased number of $CD3^+$ cell populations in UVB-irradiated skins of p38α-deficient mice (data not shown). OX40-L (TNFSF4) is a co-stimulatory molecule expressed on activated APCs and its interaction with OX40 on T cells has been demonstrated to promote T cell survival, proliferation, effector functions and memory generation[325,326]. The upregulation of *Tnfsf4* in tumors lacking p38α expression, particularly in immune-infiltrated cells, further supports that T cell activation and effector responses may be enhanced, and correlates with the increased accumulation of T memory cells observed in *B;p38α* tumors. The pyroptosis-associated gene *Casp4* was also found to be upregulated in tumors lacking p38α expression. This molecule has been demonstrated to be critical for the induction of pyroptosis in cancer cells in response to granzyme B secreted by $CD8^+$ T effector cells[327]. Furthermore, it has been associated with an increased anti-tumor immune response and an effective response to anti-PD-1 therapy in melanoma[328]. Additionally, the increased expression of *Sytl2* in tumor-infiltrating cells of *B;p38α* tumors, which is required for granule exocytosis in cytotoxic T cells[329], further supports the increased functional activity of T cells in these tumors. Despite the upregulation of many genes indicating an active immune response, molecules associated with T cell exhaustion, including *Slamf7*, *Lag3*, *Havcr2* (*TIM-3*), *Pdcd1* (*PD-1*), *Cd274* (*PD-L1*) and *Tigit*, were also upregulated in p38α-deficient tumors, particularly in tumor-infiltrating cells. These results are consistent with the observation of increased exhaustion of $CD8^+$ T cells in tumors lacking p38α expression and indicate a T cell-mediated anti-tumor immune response that has not yet been resolved.

LIF is a member of the IL-6 cytokine family that has been reported to promote the development and progression of several tumor types and is commonly associated with poor

prognosis. Furthermore, it has been suggested to drive the polarization of immunosuppressive macrophages in human tumors[274] and to prevent $CD8^+$ T cell infiltration through the regulation of CXCL9 expression in TAMs[330]. However, it has also been reported to have tumor suppressive functions in melanoma through the regulation of TGF-β-mediated cell cycle arrest and cell death[331]. Our results showed that both tumor/stroma and immune cells from *B;p38α* tumors expressed higher amounts of *Lif*. These results did not correlate with a decreased *Cxcl9* expression, which was actually increased, or a decreased $CD8^+$ T cell infiltration. Therefore, in order to better understand its effects, LIF expression in melanoma tumors needs to be further characterized. However, this piece of data could be related to the spatio-temporal functional status of the immune system, i.e., the time at which the tumors are analyzed.

Neutrophils and PMN-MDSCs are recruited primarily by CXCL1, CXCL5, CXCL6, CXCL8 and CXCL12, whereas CCL2, CCL3, and CCL4 are critical for the recruitment of M-MDSCs[332]. Although *B;p38α* tumors expressed higher amounts of *Cxcl1* and *Cxcl5*, which correlate with the increased infiltration of PMN-MDSCs, we also observed upregulation of *Ccl3* and *Ccl4* in these tumors. These chemokines are associated with the recruitment of M-MDSCs[332] but have also been previously associated with the recruitment of $CD8^+$ T cells in melanoma[320], highlighting the complexity of recapitulating the full immune response with the expression of these molecules. We detected decreased expression of *Arg1* in tumors lacking p38α expression, particularly in the tumor-infiltrating immune cells, which as been linked to the immunosuppressive activity of MDSCs[258]. We speculated that reduced *Arg1* expression in immune-infiltrated cells may correlate with the less immunosuppressive phenotype attributed PMN-MDSCs[257–259]. CXCL16 has been proposed to have a dual role in regulating the anti-tumor immune response. In glioblastoma, CXCL16 has been demonstrated to facilitate the initial recruitment of T cells to the tumor site, yet it exerts immunosuppressive functions once infiltrated into the tumor[333]. Additionally, CXCL16 expression has been associated with higher M2-like macrophage infiltration in thyroid cancer[279] and its neutralization increased the efficacy of ICIs in triple-negative breast cancer[334]. Moreover, the chemokines CCL2, CXCL5 and CXCL12, but also CSF-1 and VEGFs act as recruiting and differentiating factors for M2-like macrophages[335–337]. The downregulation of *Csf1, Vegfd* and *Cxcl16*, but also of *Tgfb1*, which encodes to the cytokine TGF-β1 produced by TAMs and has immunosuppressive functions[335], correlate with the decreased amounts of macrophages and M2-like polarization observed in *B;p38α* tumors. One of the most downregulated genes in both tumor/stroma and infiltrated immune cell populations from *B;p38α* was *Ifi202b*, which is an interferon-inducible gene that has been previously associated with immunosuppression.

A recent study reported that the expression of *Ifi202b* by breast cancer cells induced the secretion of pro-inflammatory cytokines such as IL-1β, IL-6 and TNF-α from macrophages, thereby contributing to their immunosuppressive activity. Indeed, tumors lacking *Ifi202b* expression showed a reduced tumor growth that correlated with the increased recruitment and cytotoxic activity of $CD8^+$ T cells[338]. In immune cells, *Ifi202b* has been reported to modulate the differentiation of monocyte into macrophages[339] and to promote the suppressive capacity of $CD8^+$ Tregs in lupus[340]. The observed downregulation of these molecules, together with the reduced infiltration of immunosuppressive myeloid cells in tumors lacking p38α expression, provides evidence that p38α plays a role in establishing an immunosuppressive TME.

In addition to molecules involved in the modulation of the immune response, other molecules with a critical role in melanoma progression due to their roles in angiogenesis and metastasis were also found to be downregulated in tumors lacking p38α. Matrix metalloproteinases (MMPs), particularly MMP-2 and MMP-9, play a pivotal role in facilitating melanoma cell infiltration and migration by degrading components of the extracellular matrix[197,203,341]. In fact, the regulation of MMPs expression by the p38 MAPK pathway has been previously reported[199,202]. Moreover, SPP1/OPN has been demonstrated to induce the overexpression of MMP-9[203], and has also been shown to promote metastasis[342] and immunosuppression[268]. Consistent with this, the expression of both *Mmp9* and *Spp1* was decreased in *B;p38α* tumors, suggesting that tumor cell-intrinsic p38α expression may contribute to melanoma progression, metastasis and immunosuppression by regulating the expression of these molecules.

The differential regulation of some of the aforementioned inflammatory molecules was also confirmed in tumor-derived cell lines (*B* and *B;p38α*). The cytokine array analysis identified differential secretion profiles between *B* and *B;p38α* cells, highlighting the significant upregulation of chemokines such as CXCL1 and CXCL10, which are involved in the recruitment of neutrophils/PMN-MDSCs[332] and T cells[263], respectively. Importantly, the increased amounts of CXCL10 in the secretome of tumor cells lacking p38α expression correlated with the absence of MMP-9 expression in these cells, as MMP-9 has been shown to produce the cleavage and degradation of CXCL9 and CXCL10[343], contributing to tumor progression and migration. Additionally, the lower amounts of immunosuppressive factors such as CXCL16, CSF-1, IL-6 and SPP1 observed in *B;p38α* tumor-derived cells further supports the notion that p38α expression by tumor cells confers an immunosuppressive TME. In contrast to the transcriptional data from tumors, LIF secretion was downregulated in tumor cells lacking p38α expression. This may be due to the complexity of the TME, where cell-cell

interactions and the presence of other soluble factors and other cell types may contribute to the upregulation of LIF in the tumor, having different effects on different cell types. In fact, as stated above, it has been previously reported that TGF-β-induced LIF expression is required for the cell cycle arrest and apoptosis effects induced by TGF-β in melanoma cells[331]. Therefore, the expression of LIF may have different effects depending on the context. Nevertheless, the fact that p38α-deficient tumor cells express lower amounts of LIF may have a positive effect on the functional activity of immune cells.

Evaluation of the transcriptional regulation of these molecules in response to p38 inhibition (SB203580) and IFNγ stimulation in tumor-derived cell lines (*B* and *B;p38α*) confirmed the regulation of the expression of the inflammatory molecules discussed through p38α and the inability of these cells to increase the expression of immunosuppressive cytokines in response to IFNγ. It is important to point out the almost complete absence of transcriptional expression of *Mmp9*, *Il6* and *Ifi202b* in p38α-deficient tumor cells, which are inflammatory molecules that have been demonstrated to facilitate tumor progression and immune evasion[197,280,338,343]. Overall, these data indicate that tumor cells regulate the expression of certain inflammatory molecules through p38α. The expression of these molecules is essential for the recruitment and functional activity of both anti-tumoral and immunosuppressive immune cells, suggesting a potential therapeutic strategy of inhibiting p38α to enhance the anti-tumor immune response.

Immune checkpoint inhibitors targeting PD-1 and CTLA-4 have revolutionized melanoma therapy by triggering anti-tumor immune responses. However, resistance to ICIs remains a significant clinical challenge, requiring the identification of predictive biomarkers and combination strategies to improve treatment efficacy. The p38 MAPK pathway has been demonstrated to regulate the response to chemotherapeutic agents and contribute to the development of resistance[196]. Consequently, the use of p38 inhibitors has been demonstrated to exhibit a synergistic effect when combined with chemotherapy and the use of other inhibitors in several cancers, including breast cancer, hepatocarcinoma and non-small cell lung cancer [219–221]. However, the extent to which the expression of p38α by tumor cells contributes to the response to ICIs has not yet been investigated. We found that the expression of p38α in melanoma cells determines the response to immune checkpoint blockade, particularly to PD-1 blockade. Absence of p38α expression in melanoma cells resulted in improved efficacy of treatment with αPD-1 or the combination of αPD-1+αTIM-3 antibodies, which was correlated with the increased recruitment of both $CD4^+$ and $CD8^+$ T cells. Interestingly, the combination of both antibodies resulted in decreased tumor growth in both tumor models independently of

p38α expression. Indeed, targeting both PD-1 and TIM-3 has previously been reported to be more effective in controlling tumor growth[308]. These results suggest a potential therapeutic strategy of inhibiting p38α to enhance the anti-tumor immune response of PD-1 blocking antibodies. Further experiments using p38 inhibitors in combination with αPD-1 or αPD-1+αTIM-3 antibodies are needed to validate the efficacy of this therapeutic strategy for the treatment of melanoma.

One of the main concerns regarding the use of p38 inhibitors pertains to their potential impact on the immune system. Nevertheless, several studies have indicated that p38 inhibition may enhance the cytotoxic capacity of T cells and improve the functionality of other immune cells. For example, *ex vivo* inhibition of p38 in tumor-reactive T cells has been demonstrated to enhance their anti-tumor functions *in vivo* in melanoma[223]. Additionally, p38 inhibition has been shown to increase T cell proliferation, function, and generation for ACT[224]. Moreover, p38 inhibition has been demonstrated to enhance the priming of tumor-specific effector T cells by DCs[227,228] and to increase the efficacy of ICIs *in vitro*[225] and *in vivo*[226]. Consequently, the concurrent use of p38 inhibitors with immunotherapy may prove advantageous, as it may enhance the efficacy of immunotherapy treatments by affecting both tumor cells and immune cells.

The development of gene signatures to predict immunotherapy response in melanoma and other cancers has been a significant area of research. However, the use of these signatures in clinical settings has been challenging due to the large number of genes they contain. Currently, the markers of response to ICIs in melanoma are the presence of T cell infiltration into the tumor, the expression of immune checkpoint molecules such as PD-L1, the IFNγ signature, and the mutational load or predicted neoantigen load[85]. Nevertheless, only a small fraction of patients respond to immunotherapy due to the lack of clear biomarkers that can predict response or resistance to the treatment with ICIs[108]. We compared transcriptomic data of published signatures of response to the treatment with ICIs in melanoma[270,281–287] with the gene expression data from our mouse tumors. Our findings indicate that p38α expression is associated to resistance to ICIs in melanoma patients. Furthermore, the robustness of our model in predicting responses to immunotherapy was validated. These results are consistent with the observation that tumors lacking p38α expression respond more effectively to anti-PD-1 treatment.

Further increasing the translational relevance of our work, the analysis of our data together with the transcriptome analysis of human melanoma studies of good response to ICIs[281–284]

identified a gene signature associated with the lack of p38α expression in melanoma cells which could potentially predict the immunotherapy response in melanoma. The high expression of the p38α-associated gene signature correlates with favorable treatment outcomes, particularly to PD-1 blockade. The predictive power of the p38α-associated gene signature was validated in different public datasets of melanoma patients treated with ICIs in the TIGER database, demonstrating a similar predictive power to established signatures of response to immunotherapy. This underscores the potential clinical utility of the signature in predicting the response to anti-PD-1 treatment and guiding therapeutic decisions. These findings highlight the potential clinical utility of targeting p38α in combination with ICIs, particularly with PD-1 blocking antibodies, to enhance patient responses to immunotherapy. Nevertheless, further studies are necessary to confirm the prognostic value of the p38α-associated gene signature and to investigate its potential as a predictive biomarker in clinical practice.

In conclusion, our study provides novel insights into the dual role of p38α in UVB-induced *Braf*^{V600E} melanoma development and progression. Our results suggest that p38α may act as a tumor suppressor in melanocyte transformation but may facilitate melanoma tumor growth and progression. In addition, our data provide further insight into the role of tumor cell-intrinsic p38α expression in shaping the tumor immune microenvironment. Given its multiple roles in promoting tumor growth and immune evasion, our study adds p38α as a promising target for enhancing the efficacy of existing immunotherapies, particularly PD-1 blockade. Moreover, our findings suggest that alterations in p38α expression may serve as predictive biomarkers of patient response to immunotherapy. This may facilitate the development of more personalized treatment strategies and improve clinical outcomes.

CONCLUSIONS

1. p38α is upregulated and/or amplified in human cutaneous melanomas, which is associated to a poor survival of the patients independently to other genetic alterations.

2. p38α plays a dual role in melanoma tumorigenesis. p38α may act as a tumor suppressor in melanocyte transformation in response to *Braf*^{V600E} oncogene activation and UVB irradiation, but may promote melanoma tumor growth and progression.

3. p38α contributes to melanoma progression by regulating the anti-tumor immunity, impairing the cytotoxic immune response, and modulating the recruitment and activity of immunosuppressive myeloid cells.

4. p38α is involved in the regulation of the production of pro-inflammatory cytokines and chemokines, which are essential for the modulation of the immune response and the recruitment of different immune cell populations.

5. p38α expression by melanoma cells determine the response to αPD-1 treatment *in vivo*, suggesting p38α as a potential therapeutic target to improve the response to ICIs in melanoma.

6. A nine-gene signature associated with the absence of p38α in tumor cells (*Cxcl9*, *Slamf7*, *Sytl2*, *Adam28*, *Cxcl10*, *Cxcl13*, *Fmo3*, *Cxcr6* and *Lag3*) can predict a good response to immunotherapy in melanoma patients.

MATERIALS AND METHODS

Cell culture and treatments.

Human melanoma cell lines *A375* (CRL-1619) and *SKMel28* (HTB-72) were purchased from the American Type Culture Collection (ATCC, Manassas, VA, USA). *UACC903* (CVCL_4052) cells were a gift from J. Trent (Tgen, Phoenix, AZ, USA). *SKMel103* cell line was obtained from M. Soengas (CNIO, Madrid, Spain). *YUMMER1.7-H2B-GFP5* mouse melanoma cell line was purchased from Sigma-Aldrich (St Louis, MO, USA).

A375 and *SKMel103* cell lines were cultured in Dulbecco's Modified Eagle Media (DMEM) (Biowest). *UACC903* cell line were cultured in Roswell Park Memorial Institute (RPMI) media (Biowest). *SKMel28* cell line was cultured in Eagle's Minimum Essential Media (EMEM) (ATCC). In all these cell lines, media was supplemented with 10% fetal bovine serum (FBS) (Gibco), 2 mM L-glutamine (Gibco), 100 u/ml penicillin, 100 µg/ml streptomycin (Gibco), 5 µg/ml Plasmocin (Invivogen, Toulouse, France). *YUMMER1.7-H2B-GFP5* cells were cultured in DMEM-F12 (Biowest) supplemented with 10% FBS, 2 mM L-glutamine, 100 u/ml penicillin, 100 µg/ml streptomycin and 1x MEM Non-Essential Amino Acids (NEAA) (Gibco).

The p38 inhibitor SB203580 (used at 10 µM) was purchased from Selleckchem (Houston, TX, USA). Mouse recombinant IFNγ (used at 50 ng/ml) was obtained from R&D Systems (Minneapolis, MN, USA). For IFNγ treatment, mouse cells were cultured in DMEM without FBS for 24 hours.

Immunohistochemistry.

Immunostaining was performed on sections from formalin-fixed, paraffin-embedded tumor samples according to the manufacturer's antibody protocol. All patient-derived samples were obtained upon the informed consent of the patients and the Vall d'Hebron Hospital Ethical and Clinical Research Committee approval. First, tumors were fixed in 4% formaldehyde (Sigma) for 24 hours. Then, samples were embedded in paraffin blocks and 4 µm sections were obtained using a microtome. Before the staining process, sections were incubated at 56ºC overnight followed by a deparaffinization and rehydration steps consisting in two incubations with xylol 100% for 10 minutes, and a chain of 5-minute washes with 100%, 96% and 75% ethanol. Subsequently, slides were placed in Milli-Q water for 10 minutes. For antigen retrieval, samples were incubated with target retrieval solution pH 6.0 or pH 9.0 according to manufacturer's antibody recommendations (Dako, Agilent, Santa Clara, CA, USA) at 100ºC for 20 minutes. Once cooled, samples were permeabilized by incubating with Tris-buffered

saline (TBS) containing 0.2% Triton X-100 (Sigma) for 5 minutes at room temperature. Next, samples were blocked for 1 hour at room temperature with TBS containing 1% bovine serum albumin (BSA) (PanReac AppliChem, Barcelona, Spain) and 10% goat serum. Forthwith, slides were incubated at 4ºC overnight with the primary antibody (Table 4) diluted in TBS, 1% BSA. Next day, samples were washed twice with TBS, 0.025% Triton X-100, and incubated with the corresponding secondary antibodies linked to a fluorophore. Staining with Hoechst solution (1:10000, Sigma-Aldrich) was used for nuclei visualization. Finally, slides were subjected to three more washes with TBS, 0.025% Triton X-100, and were immediately mounted using Vectashield mounting media (Vector Laboratories Inc., Burlingame, CA, USA). Images were acquired using the fluorescence FSX100 inverted microscope (Olympus, Tokyo, Japan).

Table 4 | List of antibodies used for immunohistochemistry. Information of all the antibodies, including the reference, manufacturer, source and dilution. NIH: National Institute of Health.

Antibody	Reference	Manufacturer	Source	Dilution
Primary antibodies				
Cleaved caspase-3 (Asp175) (5A1E)	#9664	Cell Signaling	Rabbit	1:500
ki67 (SP6)	ab16667	Abcam	Rabbit	1:100
Melanoma Marker (HMB45)	sc-59305	SCBT	Mouse	1:50
p-ERK1/2 (Thr202/Tyr204) (D13.14.4E)	#4370	Cell Signaling	Rabbit	1:300
p-p38 (Thr180/Tyr182) (D3F9)	#4511	Cell Signaling	Rabbit	1:25
p38 alpha (F-9)	sc-271120	SCBT	Mouse	1:25
PEP1 (TYRP1)	From Dr. Vincent J. Hearing (NIH)		Rabbit	1:1000
S100B (16HCLC)	#710363	Invitrogen	Rabbit	1:50
SOX10 (A-2)	sc-365692	SCBT	Mouse	1:25
Secondary antibodies				
Anti-Rabbit IgG (H+L) Alexa Fluor 488	A11070	Invitrogen	Goat	1:200
Anti-Rabbit IgG (H+L) Alexa Fluor 594	A11012	Invitrogen	Goat	1:200
Anti-Mouse IgG (H+L) Alexa Fluor 488	A11001	Invitrogen	Goat	1:200
Anti-Mouse IgG (H+L) Alexa Fluor 594	A11005	Invitrogen	Goat	1:200

Lentiviral infection for p38α knockdown.

TRIPZ lentiviral doxycycline-inducible plasmids with two different shRNA sequences for human *MAPK14* gene (shp38α#1: TCTTCCAGTCAACAGCTCG (CloneID: V2THS_113220), shp38α#2: TTCATATGTTTAAGTAACC (CloneID: V2THS_113215)) were purchased from Horizon Discovery (Cambridge, UK). For lentivirus production, HEK293-T cells were seeded at 80% of confluency in 100 mm plates (Sarstedt, Barcelona, Spain) with 8 ml of DMEM containing 10% FBS, 2 mM L-glutamine, 100 u/ml penicillin,

100 μg/ml streptomycin, 5 μg/ml Plasmocin. Before transfection, media was replaced with DMEM supplemented with 10% heat inactivated (HI)-FBS and chloroquine (Sigma) at 15 μM final concentration. HEK293-T cells were then transfected with 20 μg of the plasmid of interest, 15 μg of pPAX2 and 5 μg of pMD2.G in 150 mM sodium chloride (NaCl) using polyethyleneimine (PEI). After 16 h, media was replaced with fresh medium containing 2% HI-FBS and 5 mM sodium butyrate (Sigma-Aldrich). Virus-containing media was harvested after 24 h and replaced with fresh media. The collected media was centrifuged at 1000 rpm for 5 minutes, filtered through a 0.2 μm filter (Sarstedt) and used for infection of the target cells with polybrene (SCBT) at 8 μg/ml final concentration. This procedure was repeated after 24 hours. Induction with doxycycline (2 μg/ml) (Sigma-Aldrich) allow the expression of the shRNA and detection of infected cells by red fluorescent protein (RFP) signal.

Cell proliferation and viability assay.

A known number of *A375*, *UACC903* and *SKMel28* cells were seeded in 6-well plates (Sarstedt) and data were collected in triplicate at 24, 48, 72 and 96 h after treatment with SB203580 (10 μM) or downregulation of p38α upon shRNA expression with doxycycline (2 μg/ml). For every time point, cells were trypsinized and counted using a Neubauer chamber. The viability was determined using trypan blue stain solution 0.4% (Gibco).

Immunoblotting.

For protein extraction, cells were first washed twice with cooled phosphate buffered saline (PBS) (Biowest) followed by the addition of NP-40 lysis buffer (150 mM NaCl, 50 mM Tris, 1 mM EDTA and 1% NP-40) containing protease and phosphatase inhibitor cocktails (Millipore). Cells were then scrapped, collected into a tube, and incubated on ice for 20 minutes to ensure an appropriate cell lysis. Following this, samples were centrifuged at 4ºC and 15000 rpm for 30 minutes, and supernatant was collected and transferred into a new tube. Protein concentration was assessed using the Pierce BCA Protein Assay Kit (Thermo Fisher) and an equal amount of protein (30-50 μg) was used for sample preparation. For protein denaturation, Laemmli sample buffer 1X (62.5 mM Tris-HCl, 25% glycerol, 2% SDS, 0.01% Bromophenol Blue and 5% β-mercaptoethanol) was added and the mixture was then incubated at 95ºC for 5 minutes. Next, samples were loaded into 10% SDS-PAGE and proteins were transferred at a voltage of 400mA for 90 minutes to a Polyvinylidene Difluoride (PVDF) membrane (Millipore). Beforehand, the PVDF membrane was activated for one minute with methanol (Sigma). To prevent non-specific binding, the membrane was incubated with a

solution of 5% non-fat dry milk (SCBT) dissolved in Tris-buffered saline containing 0.1% Tween 20% (Sigma) (TBS-T) for one hour at room temperature. Subsequently, membranes underwent three washes with TBS-T and were incubated with the corresponding primary antibody (Table 5) at 4ºC overnight with shaking. Next day, membranes were subjected to an additional three washes with TBS-T followed by the incubation with the horseradish peroxidase (HRP)-conjugated secondary antibody (Table 5) for 1 hour at room temperature. After a final set of three washes in TBS-T, protein detection was performed by chemiluminescence method using ECL (GE Healthcare).

Table 5 | List of antibodies used for western blot (WB). Information of all the antibodies, including the reference, manufacturer, source and dilution.

Antibody	Reference	Manufacturer	Source	Dilution
Primary antibodies				
GAPDH	60004-1	Proteintech	Mouse	1:10000
p38	#9212	Cell Signaling	Rabbit	1:1000
p38 alpha (L53F8)	#9228	Cell Signaling	Mouse	1:1000
Secondary antibodies				
Rabbit IgG HRP-linked	NA934	GE Healthcare	Donkey	1:10000
Mouse IgG HRP-linked	NA931	GE Healthcare	Sheep	1:10000

Mouse model and UVB irradiation.

Braf$^{CA/CA}$ strain has been previously described[344]. Original Tyr::*CreER*^{T2} mice were from Lynda Chin (Dana Farber, Boston, USA). Tyr::*CreER*^{T2}; *Braf*$^{CA/CA}$ mice were obtained and described by our lab as previously reported[345]. *p38α*$^{lox/lox}$ mice were provided by Angel R. Nebreda (Institute for Research in Biomedicine, IRB, Barcelona, Spain). We crossed the Tyr::*CreER*^{T2}; *Braf*$^{CA/CA}$ strain with *p38α*$^{lox/lox}$ mice and generated their mendelian offspring in a mixed genetic background (FVB-C57BL/6J). All the resulting genotypes were used for the study independently of allelic combinations for *Braf*^{CA} and *p38α*^{lox} alleles. Both genders were used in all the experiments.

To induce *Braf*^{V600E} expression and *p38α* deletion in melanocytes, neonatal mice were topically treated with 200 µl of a 5 mg/ml solution of 4-hydroxitamoxifen (4-OHTx) in acetone (Sigma-Aldrich) at post-natal days 2.5 and 3.5. Moreover, mice were irradiated at post-natal day 3.5 with a single dose of 6.24 kJ/m^2 of UVB radiation using a bank of six Phillips TL 40/12 UV lamps. For the irradiation, neonatal mice were placed in separate wells of a 6-well plate with the lid removed, which was positioned 20 cm beneath the bank of sunlamps. The details about the spectral power distribution and UV monitoring regimens have

been described in a previous study[240]. Exposed mice exhibited skin reddening and sporadic superficial desquamation. Notably, there was no observed neonatal mortality associated with UV exposure. Data for time to tumor development was analyzed by Kaplan-Meier survival analysis. Animal experiments were designed and performed in accordance with protocols and regulations approved by the Institutional Animal Care and Use Committee of Vall d'Hebron Research Institute (VHIR, Barcelona, Spain) and the Biomedical Research Park of Barcelona (PRBB, Barcelona, Spain).

Mouse genotyping.

Genomic DNA was isolated from the ear tissue fragment obtained during mouse identification. Ear tissue was lysed in 100 µl of STE buffer (50 mM Tris-HCl [pH 8.0], 100 mM NaCl, 10 mM EDTA and 0,1% SDS) at 56ºC and 1200 rpm in a ThermoMixer (Eppendorf) for 1 hour. Then, samples were centrifuged at 15000 rpm for 15 minutes and the supernatant was collected and transferred into a new tube. An equal volume of isopropanol was added to the supernatant and mixed by inversion until the cloud of DNA was observed. Samples were then centrifuged at 15000 rpm for 10 minutes and the supernatant was discarded. DNA pellet was washed with 100 µl of 70% ethanol, vortexed and centrifuged at 15000 rpm for 5 minutes. Supernatant was discarded and the pellet was airdried for 10 minutes. Then, the pellet was resuspended in 50 µl of DNase-free water and incubated at 65ºC to ensure an appropriate resuspension. One microliter (~100 ng) of genomic DNA were used for PCR. Primers used for genotyping are shown in Table 6. PCR conditions and product sizes are indicated in Table 7. PCR products were resolved by agarose gel electrophoresis and visualized in a Gel Doc XR+ System (Bio-Rad, Hercules, CA, USA).

Table 6 | Primer sequences used for mouse genotyping.

Targeted allele	Primer name	Sequence
Tyr::CreER^{T2}	MB182F	CAATGGTAGGCTCACTCTGGGAGATGATA
	MB182R	AACACACACTGGCAGGACTGGCTAGG
	MB183F	CAGGGTGTTATAAGCAATCCC
	MB183R	CCTGGAAAATGCTTCTGTCCG
Braf	FWD A1	TGAGTATTTTTGTGGCAACTGC
	REV B1	CTCTGCTGGGAAAGCGGC
p38α	Flox-X	CTACAGAATGCACCTCGGATG
	Flox-Y	AGAAGGCTGGATTTGCACAAG

Table 7 | PCR conditions and product sizes.

Tyr::CreER^{T2} **PCR protocol**		***Braf*** **PCR protocol**		***p38α*** **PCR protocol**	
92ºC – 2 min		92ºC – 2 min		94ºC – 5 min	
92ºC – 30 s 58º – 45 s 72ºC – 45 s	x30 cycles	92ºC – 30 s 60º – 30 s 72ºC – 45 s	x34 cycles	94ºC – 30 s 60º – 30 s 72ºC – 30 s	x35 cycles
72ºC – 5 min 4ºC – ∞		72ºC – 3 min 4ºC – ∞		72ºC – 3 min 4ºC – ∞	
Allele	**Product size**	**Allele**	**Product size**	**Allele**	**Product size**
GABRA (control)	300 bp	WT	187 bp	WT	121 bp
Tyr-CreER^{T2}	400 bp	Targeted	307 bp	Floxed	188 bp

Mouse melanoma cell lines generation.

To generate mouse melanoma cell lines, a section of approximately 10-20 mm^2 was excised from each tumor and placed in a 60 mm plate (Sarstedt) containing 1 ml of DMEM supplemented with 20% FBS, 2 mM L-glutamine, 100 u/ml penicillin, 100 µg/ml streptomycin, 5 µg/ml Plasmocin, insulin 5 µg/ml (Sigma), and 5 µg/ml Human Recombinant EGF (Peprotech, Rocky Hill, NJ, USA). The tumor sample was then mechanically disrupted into small pieces using a scalpel and additional 2 ml of complete media were added to the plate. Once established (approximately 4-8 weeks), tumor cell lines were maintained in DMEM containing 10% FBS, 2 mM L-glutamine, 100 u/ml penicillin, 100 µg/ml streptomycin, 5 µg/ml Plasmocin. *VHMM104*, *VHIMM108*, *VHMM109*, *VHMM114*, *VHMM118* cell lines were generated from *Tyr::CreER^{T2}, Braf$^{CA/CA}$* (*B*) tumors and *VHMM203*, *VHMM206*, *VHMM212*, *VHMM221* derived from *Tyr::CreER^{T2}, Braf$^{CA/CA}$; p38α$^{Δ/Δ}$* (*B;p38α*) melanomas. p38α expression was validated by immunoblot using protein lysate from the tumor-derived cell lines.

Immunophenotyping.

Spontaneous melanoma tumors from *Tyr::CreER^{T2}, Braf$^{CA/CA}$* and *Tyr::CreER^{T2}, Braf$^{CA/CA}$; p38α$^{Δ/Δ}$* mice were used for the phenotyping of the intratumoral immune cell populations. One week after tumor detection, mice were sacrificed, and tumors were collected and processed. Briefly, tumors were first mechanically disrupted into small pieces following an enzymatic digestion using 1 mg/ml of collagenase type-IA (Sigma-Aldrich) and 2.5 µg/ml of DNase I (Sigma-Aldrich) for 45 minutes at 37ºC in DMEM supplemented with 20% FBS, 2 mM

L-glutamine, 100 u/ml penicillin, 100 µg/ml streptomycin, 5 µg/ml Plasmocin, insulin 5 µg/ml, and 5 µg/ml Human Recombinant EGF.

Table 8 | List of antibodies used for flow cytometry. Information of all the antibodies, including the fluorochrome, clone, reference, manufacturer and dilution.

Antibody	Fluorochrome	Clone	Reference	Manufacturer	Dilution
CD3e	FITC	145-2C11	561827	BD Biosciences	1:50
CD4	APC-H7	GK1.5	560246	BD Biosciences	1:500
CD8a	BV510	53-6.7	563068	BD Biosciences	1:200
CD11b	BV510	M1/70	562950	BD Biosciences	1:1000
CD11c	PE	HL3	561044	BD Biosciences	1:50
CD25	PE	PC61.5	12-0251-81	eBioscience	1:50
CD44	PE	IM7	561860	BD Biosciences	1:1000
CD45	PerCP-Cy5.5	30-F11	561869	BD Biosciences	1:1000
CD45	FITC	30-F11	103107	BioLegend	1:100
CD62L	BV605	MEL-14	563252	BD Biosciences	1:50
CD86	BV605	GL1	563055	BD Biosciences	1:100
CD206	AF647	C068C2	141711	BioLegend	1:100
F4/80	BV421	T45-2342	565411	BD Biosciences	1:100
FoxP3	APC	FJK-16s	17-5773-80	eBioscience	1:100
I-A/I-E (MHC-II)	APC-Cy7	M5/114.15.2	107627	BioLegend	1:500
Ly6C	PE-Cy7	AL-21	560593	BD Biosciences	1:1000
Ly6G	FITC	1A8	561105	BD Biosciences	1:100
NK1.1	APC	PK136	561117	BD Biosciences	1:100
PD-1	BV421	29F.1A12	135217	BioLegend	1:200
TIM-3	PE-Cy7	RMT3-23	25-5870-80	eBioscience	1:200

Single-cell suspensions were passed through a 70 µm nylon mesh cell strainer (Corning), and centrifugated at 1500 rpm for 5 minutes at room temperature. Cells were washed twice with PBS, counted, and then resuspended in PBS in the order of 10^6 cells/50 µl. Next, cells were stained with Fixable Viability Stain 700 (564997, BD Biosciences, San Jose, CA, USA) for 15 minutes at 4ºC for cell viability determination. Non-specific unions were then blocked incubating with the anti-mouse CD16/32 antibody (553141, BD Biosciences San Jose, CA, USA) for 10 min at room temperature. The phenotyping of the different intratumoral immune cell populations was performed using the corresponding cocktail of anti-mouse antibodies listed in Table 8, prepared in PBS buffer containing 1% BSA and 0.05% sodium azide (Sigma-Aldrich). Following cell-surface staining, cells were fixed and permeabilized using the FOXP3/Transcription Factor Staining Buffer Set (eBioscience, San Diego, CA, USA) for the FoxP3 staining or the Fixation/Permeabilization Solution Kit (BD Biosciences, San Jose,

CA, USA) for the CD206 antibody, according to the manufacturer's indications, following an incubation with the corresponding antibodies. The acquisition of the data was performed using a CytoFLEX flow cytometer (Beckman Coulter, Brea, CA, USA) coupled to CytExpert Software (version 1.2.11, Beckman Coulter, Brea, CA, USA). The selection and quantification of clusters representing the populations of interest was performed using FlowJo™ Software (version 10.6.2, Becton Dickinson, Ashland, OR, USA) (Table 9 and Supplementary Figures 2 and 3).

Table 9 | Defined markers for immune cell populations. The gating strategy followed for the phenotype determination of the intratumoral immune cell populations was (1) FSC vs SSC debris exclusion; (2) FSC-H vs FSC-A for doublets exclusion; (3) Dead cell exclusion with Fixable Viability Stain 700; (4) Selection of $CD45^+$ cells. Further population definition was performed by clustering methods described in this table. Natural Killer (NK); Natural Killer T (NK-T), T effector/effector memory (TE/EM); T memory/central memory (TM/CM); Polymorphonuclear (PMN) and monocytic (M) myeloid derived suppressor cells (MDSC); Dendritic cells (DCs).

	Cell type	Markers
T cells	$CD4^+$ T cells	$CD45^+CD3^+CD4^+CD8^-$
	$CD8^+$ T cells	$CD45^+CD3^+CD4^-CD8^+$
	Naïve T cells	$CD45^+CD3^+CD4^+/CD8^+CD44^-CD62L^{+/high}$
	TE/EM	$CD45^+CD3^+CD4^+/CD8^+CD44^{+/high}CD62L^-$
	TM/CM	$CD45^+CD3^+CD4^+/CD8^+CD44^+CD62L^{+/high}$
	Exhausted T cells	$CD45^+CD3^+CD4^+/CD8^+CD44^{+/high}CD62L^-Tim3^+/PD\text{-}1^+$
	T regulatory cells	$CD45^+CD3^+CD4^+/CD8^+CD25^+FoxP3^+$
NK cells	NK	$CD45^+CD3^-NK1.1^+$
	NK-T	$CD45^+CD3^+NK1.1^+$
Myeloid cells	PMN-MDSC	$CD45^+CD11b^+Ly6G^+Ly6C^{low}$
	M-MDSC	$CD45^+CD11b^+Ly6G^-Ly6C^{high}$
	Neutrophils	$CD45^+CD11b^+Ly6G^{high}$
	Macrophages	$CD45^+Ly6G^-CD11b^+F4/80^+$
	M2 macrophages	$CD45^+Ly6G^-CD11b^+F4/80^+Ly6C^-CD206^+$
	DCs	$CD45^+CD11b^+CD11c^+$
	DCs activation state	Expression of IA/IE (MHC-II) and CD86 in the $CD45^+CD11b^+CD11c^+$ population

Gene expression analysis.

For complete tumors, frozen samples of mouse melanoma tumors were first cryoground to obtain tumor powder. On the other hand, $CD45^+$ and $CD45^-$ cells were separated from single cell suspensions of fresh mouse tumor samples using the MagniSort Mouse CD45 Positive Selection Kit (Invitrogen) following the manufacturer's protocol. Samples were then lysed in TRIsure (Bioline Ltd, UK) and RNA was purified using a Direct-Zol RNA kit (Zymo Research, Irvine, CA, USA) according to the manufacturer's recommendations. RNA quantity

and quality were assessed using a 2100 Bioanalyzer (Agilent). Only high-quality samples with RNA Integrity Number (RIN) ≤ 9 were selected for the analysis. Gene expression analysis was performed using a *Clariom S Mouse Array* (Affymetrix, Santa Clara, CA, USA). The open-source software R Studio was used to process the raw data collected from the array. The first step in the analysis was to convert the intensity values into gene expression values. This was done using the Robust Multiarray Average (RMA) method through the *BioConductor* package *oligo*. The process included background correction, logarithmic transformation, quantile normalization and probe normalization. The *limma* package was then used to identify differentially expressed genes. A moderated *t*-test based on the empirical *Bayes* method was applied for each comparison. The resulting top tables contained genes ranked from most to least differentially expressed genes according to the log_2FC value. *Metascape* (metascape.org)[346] was used for functional analysis of the differentially expressed genes obtained. In addition, *Morpheus* (software.broadinstitute.org/morpheus) and the *pheatmap* package in R Studio were used to generate heatmaps for data visualization.

Quantitative Reverse Transcription Polymerase Chain Reaction (RT-qPCR).

YUMMER1.7-H2B-GFP, *VHMM104*, *VHMM109*, *VHMM114*, *VHMM118*, *VHMM203*, *VHMM206*, *VHMM212*, *VHMM221* cells were seeded in 60 mm plates at 70% confluence, incubated overnight and then subjected to 2 h of serum starvation prior to the treatment with mouse recombinant IFNγ (50 ng/ml) and SB203580 (10 mM) in serum-free media for another 24 h. RNA was isolated using a Direct-Zol RNA kit (Zymo Research, Irvine, CA, USA) according to the manufacturer's protocol. One hundred micrograms of RNA per sample was used to generate cDNA using the SuperScript III First-Strand Synthesis System SuperMix for RT-PCR (Invitrogen). Quantitative PCR analysis was performed using the SYBR Green PCR Master Mix Kit (Applied Biosystems Inc., Foster City, CA, USA) and the QuantStudio™ 5 Real-Time PCR System (Applied Biosystems Inc.). The primers used are shown in Table 10. The measurements were calculated employing the ΔΔCt method using Design and Analysis 2.6.0 Software (Applied Biosystems, Inc.). We applied geNorm algorithms to select vimentin (Vim) and 14-3-3 protein zeta/delta (Ywhaz) as the most stable reference transcripts. The geometric means of the expression values for both housekeeping genes were used to normalize the expression and to calculate the normalized SD of all transcripts analyzed. Relative expression levels were calculated after normalization. Data were represented as mean ± SD of

replicates from independent cell lines. The *ggplot2* package in R Studio was used to generate the dotplot for data visualization.

Table 10 | Primer sequences used for qRT-PCR.

Gene	Forward (5'– 3')	Reverse (5'– 3')
Ccl20	GCTATCATCTTTCACACGAAG	TCTTGACTCTTAGGCTGAGG
Csf1	CTTCAGCCACTAGCGAGCAA	CCATGTCGAAGAAGGGCA
Cxcl1	CCGAAGTCATAGCCACACTC	GGGGACACCTTTTAGCATCT
Cxcl2	CATCCAAAAGATACTGAACAAAGGC	TTCTCTTTGGTTCTTCCGTTGAG
Cxcl9	TTCGAGGAACCCTAGTGAT	GGCAAACTGTTTGAGGTCTT
Cxcl10	TCAAGGGATCCCTCTCGC	CTCGCAGGGATGATTTCA
Cxcl16	CCAGATACCGCAGGGTACTT	GGACTGCAACTGGACCTGATA
Hgf	TCGGATAGGAGCACAAGGA	GCCGGGCTGAAAGAATCAAAG
Igfbp3	GAGACAGAATACGGTCCCTG	CAGTTTGGGATGTGGACG
Igfbp6	GCCGTCGGAGGAGACTACAA	GAGCAGCAGAGGTCCGTG
Il6	GCAAGAGACTTCCATCCAGT	GGAGTGGTATCCTCTGTGAAG
Lif	GCCCAACAACGATGGTGT	CCTGATTTATATACTGGAGCCGTGG
Mmp2	TGCCCCCATGAAGCCTTGT	GTTGTAGGAGGTGCCCTGGAAG
Mmp9	CAGCGCCAGCCGACTTTT	GCGGTACAAGTATGCCTCTGC
Serpine1	CAACTACACTGAGTTCACCACCC	CTCAAAGGGTGCAGCGAT
Spp1	TCGTCCCTACAGTCGATGT	GCATCAGGATACTGTTCATCAG
Stat3	AAAGTACTGTAGGCCCGAGAGC	CTGCAGGTCGTTGGTGTCA
Tnfrsf11b	TGGTGCTCCTGGACATCATT	TGTCACACAGGAGCTGATGACC
Vegfa	TGAAGTGATCAAGTTCATGG	CTATCTCGTCGGGGTACTC
Vim	TGTTCCTACCCCCAATGT	TCAGTGTAGCCCAAGATG
Ywhaz	CCTGCTCTCTTGCAAAAAC	GTATCCGATGTCCACAATG

Cytokines array.

In a 6-well plate, 0.8 x 10^6 *VHMM109* (*Braf*$^{CA/CA}$) and *VHMM203* (*Braf*$^{CA/CA}$; *p38α*$^{\Delta/\Delta}$) cells were seeded, incubated overnight, and treated the next day. Cells were subjected to serum starvation for 2 hours and then treated with 50 ng/ml of mouse recombinant IFNγ in serum-free DMEM. After 24 h, media was collected, centrifuged at 1500 rpm for 5 minutes at 4ºC, and 500 µl of media were used to perform the Proteome Profiler Mouse XL Cytokine Array (R&D Systems) according to manufacturer's protocol. Quantification of the dots was performed by pixel density determination using ImageJ software.

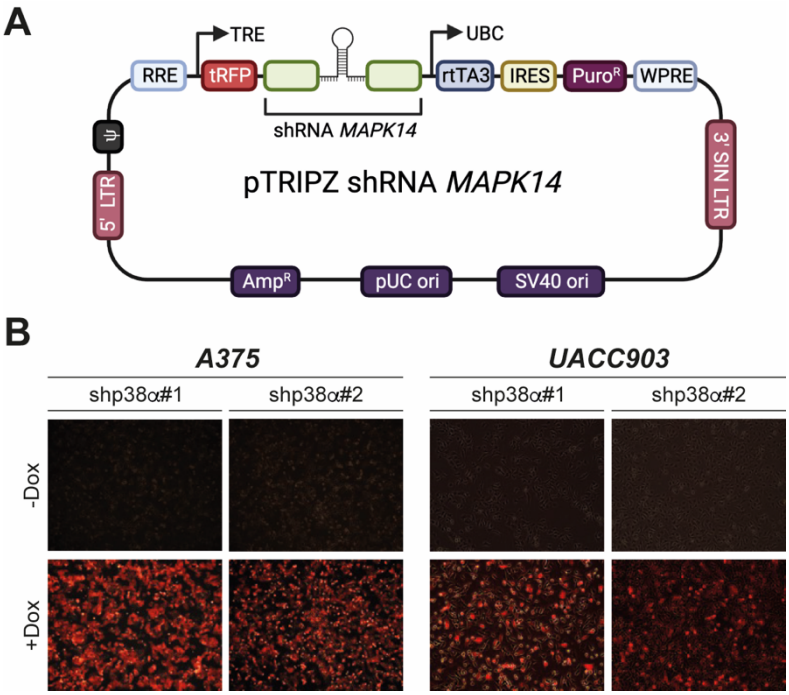
In vivo immunotherapy.

For syngeneic mouse models, 1.5 x 10^6 *YUMMER1.7-H2B-GFP* and *VHMM212* cells were subcutaneously inoculated in 100 µl of PBS on each flank of 8 weeks-old C57BL/6JRj males (Janvier Labs, Le Genest-Saint-Isle, France). Mice were weighed and tumors were measured with a digital Vernier caliper twice a week. Tumor volume was calculated as $D \times d^2/2$, where D was the major diameter and d was the minor diameter. Mice were randomized into different treatment groups (n = 8 per group) when tumors reached a volume of 50-100 mm^3. A dose of 200 µg of either rat IgG2a, κ isotype (BE008, BioXCell), rat anti-mouse PD-1 blocking antibody (αPD-1, BP0146, BioXCell), rat anti-mouse TIM-3 blocking antibody (αTIM-3, BP0115, BioXCell), or the combination of both αPD-1 + αTIM-3, was administered intraperitoneally twice a week for a total of 5 doses. At the end of the experiment, representative tumor pictures were taken and tumor samples were collected for further analysis. Results are presented as mean ± SD of tumor volume.

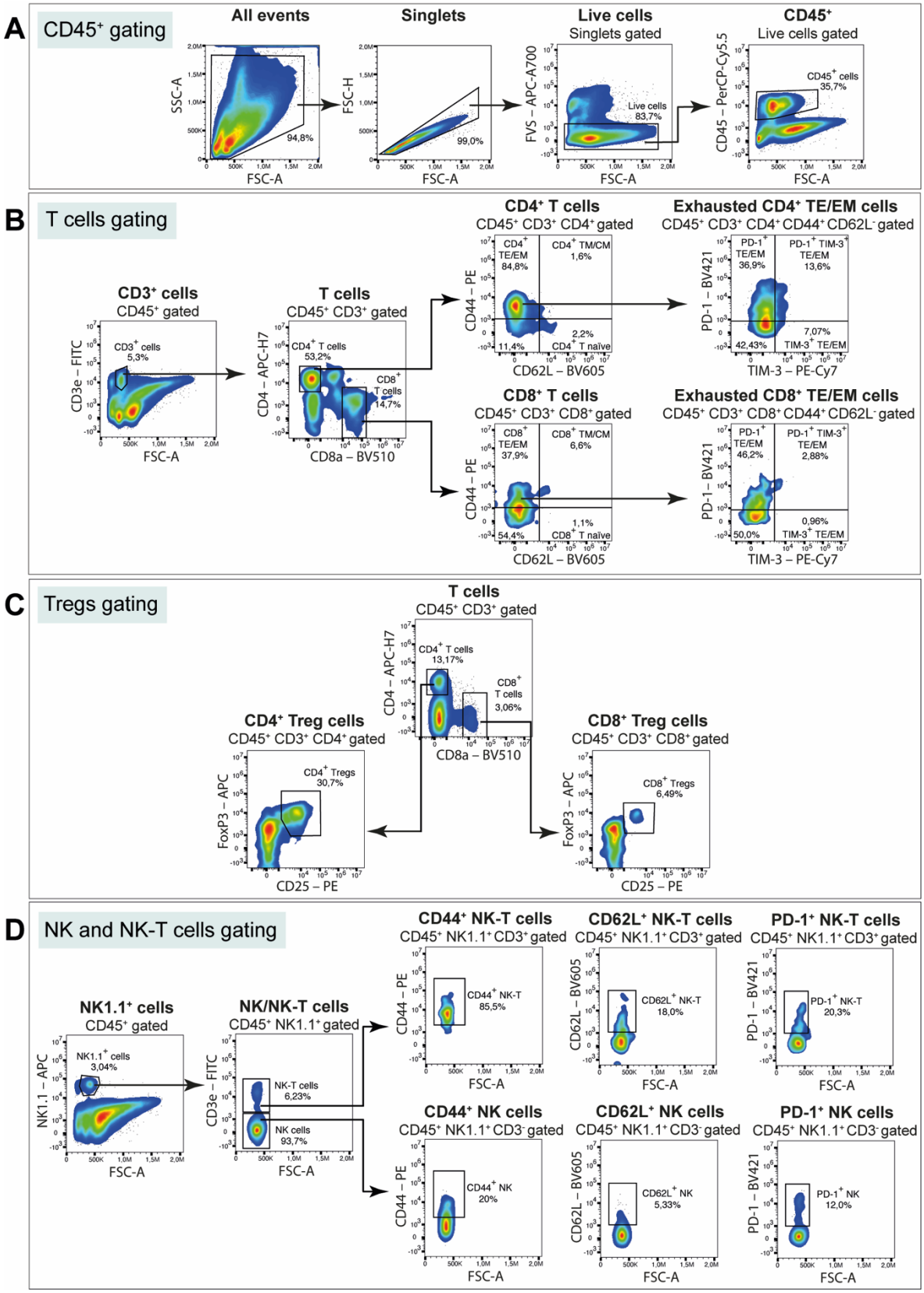
Statistical analysis.

Statistical analyses were performed in GraphPad Prism 9.0 (GraphPad Software Inc.). To compare differences between two groups, we calculated p value (p) using Student's t-test (paired or unpaired) for parametric variables and Mann–Whitney test for non-parametric variables. Survival curves comparison was performed using Kaplan-Meier test. (*) $p \leq 0.05$; (**) $p \leq 0.01$; (***) $p \leq 0.001$; (****) $p \leq 0.0001$. The schemes and explanatory figures were generated using BioRender (www.biorender.com).

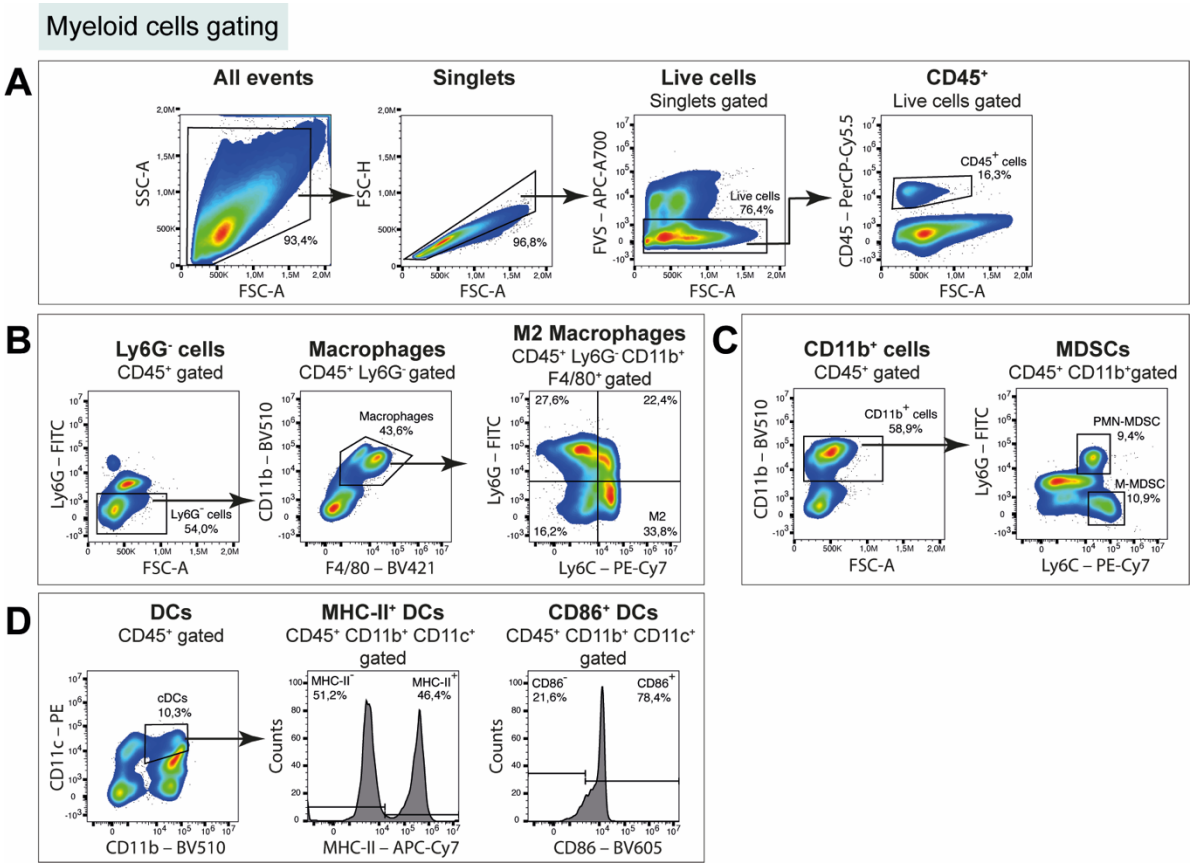
SUPPLEMENTARY INFORMATION



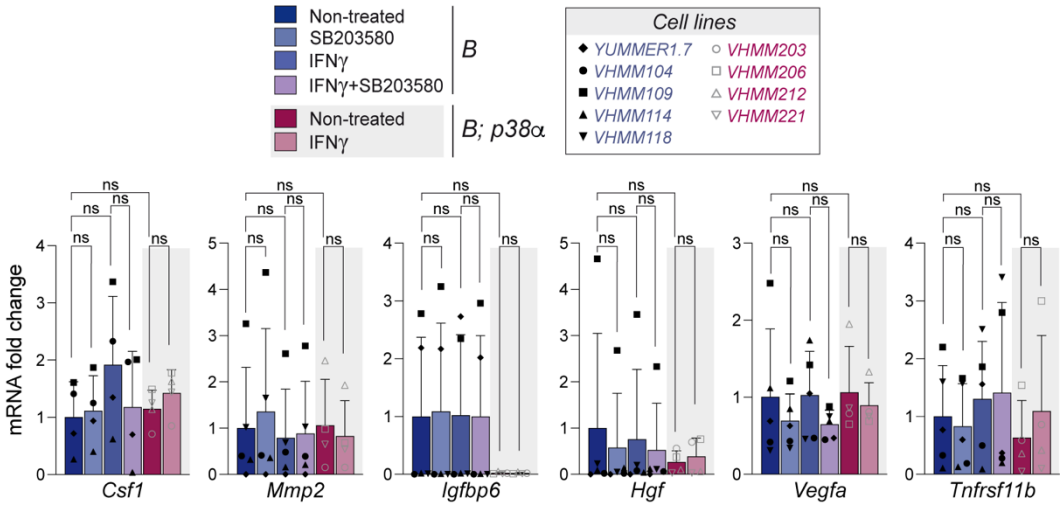
Supplementary Figure 1 | Generation of human melanoma cells expressing inducible shRNA targeting p38α. (A) Lentiviral vector map containing the inducible shRNA for p38α (*MAPK14*). **(B)** Representative images of uninduced (-Dox) and induced with doxycycline (+Dox) (2 µg/ml) infected *A375* and *UACC903* cells.



Supplementary Figure 2 | Flow cytometry gating strategy of the indicated immune cell subsets. (**A**) $CD45^+$ cell population from total tumor cells disaggregation. (**B**) $CD4^+$ and $CD8^+$ T cells (T Effector/Effector Memory (TE/EM), T Memory/Central Memory (TM/CM), and T naïve) and exhausted $CD4^+$ and $CD8^+$ TE/EM subsets expressing PD-1 and TIM-3. (**C**) $CD4^+$ and $CD8^+$ regulatory T (Treg) cells. (**D**) Natural killer (NK) and natural killer T (NK-T) cells and the subpopulations expressing CD44, CD62L and PD-1.



Supplementary Figure 3 | Flow cytometry gating strategy of myeloid cell subpopulations. (**A**) CD45$^+$ cell population from total tumor cells disaggregation. (**B**) Macrophages and M2 type macrophages. (**C**) Polymorphonuclear (PMN) and monocytic (M) myeloid derived suppressor cells (MDSCs). (**D**) Dendritic cells (DCs) and the expression of the activation markers major histocompatibility complex II (MHC-II) and CD86.



Supplementary Figure 4 | Cytokine mRNA expression in *B* and *B; p38α* cell lines. Graphs showing the mRNA fold change of the indicated cytokines in *B* and *B;p38α* cell lines after 24 hours treatment with IFNγ (50 ng/ml) and/or the p38 inhibitor SB203580 (10 μM). Statistical significance was assessed by Mann-Whitney *t*-test; (ns) non-significant.

Supplementary Table 1 (1/3) | Upregulated genes in *B; p38α* vs. *B* tumors ($log_2FC \geq 0.265$) (n = 2214).

Upregulated genes in *B; p38α* vs. *B*									
Aadacl2fm2	Alk	B3galt5	Carf	Cenpp	Crabp2	Dgkh	Ephb6	Filip1l	Gpbp1l1
Abca16	Alkal2	B4galnt2	Carmil2	Cep112	Crebl2	Dhtkd1	Erbin	Fjx1	Gpc4
Abca5	Alms1	Bag4	Casc1	Cep126	Crebrf	Dhx32	Ercc6l2	Fkbp3	Gpcpd1
Abca6	Ambp	Baiap2l1	Casc4	Cep152	Crispld1	Dhx36	Erich2	Fkbp7	Gpm6b
Abca8a	Amelx	Banf2	Cask	Cep164	Crp	Dip2c	Erich3	Fktn	Gpn1
Abca8b	Amph	Bard1	Casp12	Cep192	Crppa	Dixdc1	Ermard	Flrt3	Gpr142
Abcb11	Amt	Bbip1	Casp3	Cep250	Crtac1	Dkc1	Esp24	Fmn1	Gpr143
Abcb7	Amy1	Bbof1	Casp4	Cep290	Crybb1	Dld	Esp3	Fmnl2	Gpr15
Abhd17b	Amy2b	Bbs10	Casq2	Cep295	Crym	Dlg3	Esp34	Fmo3	Gpr155
Abhd2	Anapc4	Bbs12	Catspere2	Cep44	Cryzl1	Dlgap1	Esp36	Fnbp4	Gpr156
Abhd3	Angptl3	BC049715	Cbll1	Cep57	Csmd2	Dmac2l	Etd	Fndc10	Gpr161
Abtb1	Ankdd1b	BC051142	Cbr4	Cep78	Csn1s2b	Dmbt1	Etfbkmt	Fndc9	Gpr17
Acbd4	Ankib1	BC052040	Cbx7	Cep83	Csn3	Dmd	Etfrf1	Fos	Gpr173
Acbd5	Ankra2	BC106179	Cby1	Cep85l	Csnk1g3	Dmxl2	Etnk1	Fosb	Gpr19
Acer3	Ankrd1	Bcap29	Cc2d2a	Cerkl	Csnka2ip	Dnaaf4	Etv1	Foxd1	Gpr26
Acot1	Ankrd13b	Bcar3	Ccdc13	Cetn2	Cspg4	Dnah7a	Etv4	Foxf2	Gpr31b
Acp1	Ankrd28	Bche	Ccdc141	Cetn4	Cspg5	Dnajc16	EU599041	Foxj1	Gpr37l1
Acp6	Ankrd6	Bckdhb	Ccdc144b	Cfap126	Cst12	Dnajc17	Evi5	Foxp2	Gpr52
Acr	Ankrd9	Bcl2a1a	Ccdc149	Cfap20	Cst6	Dnal1	Exoc4	Fpr-rs4	Gpr65
Acsbg2	Anks1b	Bcl2a1b	Ccdc152	Cfap45	Cstad	Dner	Exosc8	Frg2f1	Gpr82
Acsbg3	Ano3	Bcl2a1d	Ccdc178	Cfap69	Cstdc1	Dnmt1	Extl1	Frg2f12	Gpr88
Acsl4	Ano4	Bcl2l11	Ccdc18	Cfap77	Ctc1	Dnmt3b	Eya1	Frg2f2	Gramd1c
Actr6	Ano5	Bcl2l12	Ccdc180	Cfhr1	Ctla4	Dnmt3l	F2rl1	Frg2f3	Grb14
Acvr2b	Ano7	Bcl2l15	Ccdc184	Cfl2	Ctnnd1	Dnttip2	Fabp7	Frg2f4	Gria3
Adam20	Anp32e	Bclaf1	Ccdc34	Chd6	Ctrc	Doc2b	Fam120c	Frmd4a	Grid2ip
Adam22	Apbb1	Bdkrb1	Ccdc39	Chd9	Cts3	Dock11	Fam135a	Frmd6	Grik1
Adam28	Apc2	Bend6	Ccdc59	Chek1	Cttnbp2	Dock3	Fam13a	Frzb	Grik2
Adam3	Apobec1	Best3	Ccdc62	Chgb	Ctu1	Dock7	Fam151b	Fscb	Grik3
Adam32	Apod	Bfsp1	Ccdc68	Chic1	Cubn	Dok6	Fam167a	Fscn2	Grik4
Adamdec1	Apoh	Bhlhe40	Ccdc74a	Chil1	Cul4b	Donson	Fam169b	Fsd1l	Grin2b
Adamts17	Apol11b	Bicd1	Ccdc78	Chl1	Cul5	Dph5	Fam171b	Fstl4	Grk3
Adamts19	Apol7e	Birc2	Ccdc81	Chmp4c	Cwc22	Dpp6	Fam177a2	Fstl5	Grtp1
Adamts8	Appl2	Blm	Ccl20	Chrm5	Cwc27	Dpy19l3	Fam180a	Fundc2	Gsap
Adamtsl1	Aqp12	Bmi1	Ccl3	Cilp2	Cwf19l2	Dpyd	Fam183b	Fut10	Gsdme
Adamtsl2	Aqp8	Bmp15	Ccl4	Cip2a	Cxcl1	Drc3	Fam184a	Fut4	Gstcd
Adamtsl3	Arap2	Bmp5	Ccl5	Cirbp	Cxcl10	Drd1	Fam184b	Fv1	Gstk1
Adarb1	Arfgef3	Bmper	Ccnd1	Ckap2	Cxcl13	Dscaml1	Fam204a	Fxyd6	Gstt2
Add2	Arhgap18	Bmpr1b	Ccnd3	Ckap5	Cxcl14	Dscc1	Fam214a	Fyttd1	Gsx2
Adgb	Arhgap22	Bnc2	Ccnl1	Cks2	Cxcl5	Dsn1	Fam216b	Fzd2	Gtpbp10
Adgra1	Arhgap36	Bnip1	Ccser2	Clasp2	Cxcl9	Dtna	Fam217a	G2e3	Gtpbp8
Adgrb3	Arhgap5	Bphl	Cct6b	Clca3a2	Cxcr6	Dtwd2	Fam227a	Gab1	Guf1
Adgrl3	Arhgef26	Bpifb9a	Cd109	Clca4a	Cxxc4	Dus4l	Fam228b	Gabra3	Gulp1
Adk	Arhgef28	Bpifc	Cd177	Clcn1	Cyhr1	Dusp15	Fam229b	Gabrb2	Gypa
Adm2	Arhgef39	Braf	Cd200	Clcn2	Cyld	Dync1li2	Fam3b	Gabre	Gzmb
Adnp	Arhgef9	Brca2	Cd27	Clcn3	Cyp2c37	Dynlt1a	Fam3c	Gabrg3	Gzmc
Adnp2	Arid3b	Bricd5	Cd46	Cldn1	Cyp2d22	Dynlt1b	Fam57b	Gal3st3	Gzmf
Adra2c	Arl15	Brinp1	Cd5	Cldn34c2	Cyp2d37-ps	Dynlt1c	Fam76b	Galnt12	Gzmm
Aff3	Arl4a	Brinp2	Cd52	Clec1a	Cyp2g1	Dynlt1f	Fam81a	Galnt18	H1f7
Afmid	Arl5a	Bsph2	Cd69	Clec2e	Cyp2j6	Dynlt3	Fam83b	Ganc	H2-M10.1
Agbl1	Arl6	Btbd35f5	Cd72	Clec7a	Cyp2j9	Dytn	Fam98b	Gapdhs	H2-Q4
Agbl2	Arl6ip6	Btbd35f6	Cd8b1	Clec9a	Cyp2u1	Dzank1	Fan1	Garem1	H2-T22
Agbl3	Armc10	Btbd8	Cd9	Clgn	Cyp39a1	Dzip1	Fancb	Garnl3	H2al3
Agbl5	Armc3	Btf3l4	Cd96	Clk4	Cyp3a11	Ebf2	Fancd2	Gas2	H2ap
Agmo	Armc4	Btnl6	Cdan1	Clmp	Cyp3a13	Echdc3	Fancd2os	Gbp10	H60a
Agrn	Armh4	Bub1	Cdc14a	Cmbl	Cyp3a57	Ect2l	Far2	Gca	H60c
Agrp	Arnt2	Bub1b	Cdc14b	Cmc1	Cyp46a1	Eda	Faxc	Gcfc2	Hal
Agtr1b	Arntl2	Bves	Cdc20b	Cmss1	Cyp4f15	Eda2r	Fbxl2	Gcg	Hamp
Agtr2	Art3	Bzw2	Cdc37l1	Cnga4	Cyp4f18	Efcab11	Fbxl21	Gdap1	Has1
Agxt	Art4	C130073F10Rik	Cdc42bpa	Cngb1	Dbh	Efcab5	Fbxl3	Gemin8	Haus2
Ahcyl1	As3mt	C1ql1	Cdc42bpg	Cnksr2	Dbndd1	Efcab7	Fbxl4	Gfod1	Havcr2
AI182371	Asah1	C1rl	Cdc6	Cnksr3	Dbp	Efcab8	Fbxo10	Ggh	Hbq1a
AI429214	Asf1a	C7	Cdh10	Cnn1	Dbpht2	Efhb	Fbxo16	Gins1	Hbq1b
AI504432	Aspa	Cacna2d4	Cdh19	Cnot10	Dclk2	Efna5	Fbxo3	Gja10	Hccs
AI506816	Asrgl1	Cacng2	Cdh20	Cnot6	Dclre1a	Efnb3	Fbxo7	Gjc3	Hcn4
AI987944	Asxl3	Cacng5	Cdh23	Cntn6	Dcp1b	Egfl6	Fbxw14	Gjd2	Hcrt
Aim2	Atad1	Cadm2	Cdh6	Col10a1	Ddah1	Ehbp1	Fbxw26	Gjd3	Hdac8
Aimp1	Atad5	Cage1	Cdhr4	Col20a1	Ddb2	Eid3	Fbxw9	Gk	Hddc2
Ajap1	Atf2	Calm5	Cdk14	Col26a1	Ddi1	Eif2s3x	Fcnb	Gk5	Hdx
Akap11	Atf7ip	Caln1	Cdk15	Col4a3	Ddias	Eif5a2	Fcrl1	Gkn3	Hectd2
Akap12	Atl1	Calr4	Cdk19	Col4a5	Ddx10	Elac1	Fcsk	Glcci1	Hells
Akap14	Atm	Camk1g	Cdk5rap2	Col6a5	Ddx43	Elk3	Fdxr	Gldc	Helq
Akap5	Atp10b	Camk2b	Cdk6	Col9a2	Ddx52	Elovl2	Fgd4	Gldn	Henmt1
Akap6	Atp6ap1l	Camk4	Cdk8	Colgalt2	Defa41	Elovl4	Fgf1	Gli3	Herc1
Akap8	Atp6v0e2	Camkmt	Cdkl5	Commd3	Defb34	Elp4	Fgf13	Glis3	Hesx1
Akip1	Atp6v1g2	Capn6	Cdkn2b	Coq7	Defb43	Eml6	Fgf17	Glmn	Hexb
Akr1c12	Atp8a1	Capn7	Cdkn3	Cox6b2	Defb47	Enc1	Fgf2	Gltpd2	Hexdc
Akr1c20	Atp8b1	Caps2	Cdr1	Cpa4	Defb6	Enpp4	Fgf21	Glyat	Hgh1
Akt3	Atpaf1	Capza3	Cdyl	Cpd	Dennd2a	Enpp5	Fgf23	Glycam1	Hhat
Aldh1a3	Atr	Car12	Cecr2	Cphx1	Dennd3	Epb41l5	Fgf6	Gnaz	Hhip
Aldh1a7	Aurkc	Car14	Cela1	Cplane1	Dennd5b	Epc2	Fgl1	Gng4	Hibch
Aldh1l2	AY761185	Car6	Celf5	Cplx2	Depdc1a	Epdr1	Fhdc1	Gnpda2	Hint2
Alg11	B3galt1	Card11	Cenph	Cplx3	Depdc7	Epha7	Fhl1	Gp1ba	Hivep2
Alg6	B3galt2	Card14	Cenpn	Cpsf6	Dgke	Ephb2	Filip1	Gp2	Hmg20a

Supplementary Table 1 (2/3) | Upregulated genes in *B; p38α* vs. *B* tumors ($log_2FC \geq 0.265$) (n = 2214).

Upregulated genes in *B; p38α* vs. *B*									
Hmga2	Irgm1	Klrc1	Lypd2	Mmp15	Nek5	Pak3	Pih1d2	Prokr1	Rbm34
Hnf4aos	Irgm2	Klrd1	Lypd6	Mmp16	Nek8	Palb2	Pik3c2g	Prorp	Rbm44
Hnrnpd	Irs4	Klre1	Lypd8	Mmp20	Nell1	Pam	Pik3ip1	Pros1	Rbm46
Hnrnpdl	Isg15	Klrh1	Lyrm4	Mmp25	Nemf	Panx2	Pip	Prpf39	Rbmx
Homer1	Itfg1	Klri1	Lyrm7	Mnat1	Nemp2	Parn	Pip4p2	Prph2	Rbp3
Homer2	Itga1	Klri2	Lyzl6	Mnd1	Neto2	Parp4	Pithd1	Prps1l3	Rcbtb1
Homez	Itga2	Klrk1	Macrod2	Mns1	Neurod4	Parp8	Pkd1l1	Prps2	Rccd1
Hoxa10	Itga8	Kng2	Mael	Mnt	Neurog1	Pate2	Pkdrej	Prr33	Rchy1
Hoxa7	Itgax	Knl1	Maff	Moap1	Neurog3	Patj	Pkhd1	Prrg1	Rcvrn
Hoxc11	Itgb3bp	Krt19	Magea3	Mocs2	Nexn	Pax5	Pkib	Prrg4	Rdh10
Hoxd3os1	Itgb4	Krtap13	Magea5	Morc4	Nf1	Paxbp1	Pkp2	Prss1	Rdh14
Hpn	Itgb8	Krtap20-2	Mageb18	Morf4l1-ps1	Nfe2l3	Pbdc1	Pla2g12a	Prss3	Recql
Hpse2	Itih2	Ktn1	Mageh1	Mospd4	Nfia	Pbx3	Pla2g3	Prss33	Reep1
Hrg	Itm2a	L2hgdh	Magi3	Mpl	Nhs	Pbx4	Plaat1	Prss37	Reep6
Hs3st5	Ivd	L3mbtl3	Magohb	Mplkip	Nipal1	Pbxip1	Plac9a	Prss45	Rev3l
Hscb	Ivns1abp	Lag3	Mal	Mpp5	Nipsnap1	Pcbd1	Plcb4	Prss51	Rfesd
Hsd17b7	Izumo2	Lair1	Mamstr	Mpv17l	Nkain2	Pcdh10	Pld1	Prxl2a	Rfpl4b
Hsf2	Jakmip2	Larp1b	Manba	Mr1	Nkapl	Pcdh15	Plekha4	Psd2	Rftn2
Hspa2	Jam2	Lat	Manbal	Mre11a	Nlgn1	Pcdh17	Plekha5	Psg17	Rfx3
Htr2b	Jchain	Lax1	Manea	Mrgpra2b	Nlgn3	Pcdh7	Plekha6	Psg18	Rgcc
Hunk	Jkamp	Lca5	Mansc4	Mrgpra9	Nlrc5	Pcdh9	Plekhb1	Psg22	Rgs1
Hus1	Jmjd1c	Lce1k	Map2k4	Mrgprb4	Nlrp10	Pcdhb11	Plekhh1	Psip1	Rgs9
Idi1	Jmy	Lce1l	Map2k6	Mro	Nme4	Pcdhb12	Plod2	Psmc3ip	Rhbdl3
Ido1	Josd2	Lce3b	Map3k1	Mroh7	Nme5	Pcdhb13	Plp1	Psmc6	Rhox13
Ier3	Jrkl	Lcor	Map3k13	Mrpl1	Nmi	Pcdhb14	Plpp4	Psme4	Rhox3g
Iffo1	Kank4	Lcorl	Map3k19	Mrpl46	Nnt	Pcdhb15	Plppr1	Psmg3	Ribc1
Ifi208	Kansl1l	Ldc1	Map3k7	Mrps35	Nobox	Pcdhb18	Plppr3	Pspc1	Rictor
Ifi209	Kat2b	Ldhb	Map3k9	Ms4a19	Nol4	Pcdhb19	Plscr1	Psrc1	Rida
Ifi213	Kat6b	Ldlr	Map6d1	Ms4a4b	Nol7	Pcdhb20	Plscr4	Pstk	Rif1
Ifit1	Katnal1	Ldlrad3	Map9	Msh3	Nostrin	Pcdhb21	Plxdc1	Ptbp2	Riiad1
Ifit1bl1	Kbtbd13	Lef1	Mapk10	Msh4	Nox4	Pcdhb3	Plxna3	Ptcd3	Rimklb
Ifit2	Kbtbd7	Lekr1	Mapk8ip2	Msi2	Npas3	Pcdhb6	Pmaip1	Ptch1	Rims3
Ifit3	Kcna2	Lelp1	Mapre3	Msl2	Nphp1	Pcdhb7	Pms1	Ptges3l	Ripor2
Ifit3b	Kcna3	Leng8	Marc2	Msmo1	Nppa	Pcdhb8	Pms2	Ptgfr	Ripply2
Ifna14	Kcnip3	Leo1	March4	Mtap	Nr1d2	Pcdhb9	Pnck	Ptgfrn	Ripply3
Ifng	Kcnip4	Lepr	March7	Mtbp	Nr1h4	Pcf11	Pnisr	Pth2r	Rlbp1
Ift140	Kcnk2	Lgals2	Mas1	Mterf1b	Nr1i2	Pcgf5	Pnlip	Pthlh	Rmdn1
Ift57	Kcnk5	Lgi4	Mast4	Mterf2	Nr2f1	Pcgf6	Pnma3	Ptk6	Rmdn2
Ift80	Kcnmb1	Lgr6	Mastl	Mtf2	Nr4a3	Pcm1	Pnmal2	Ptpdc1	Rmnd5a
Ift88	Kcnmb4	Lhcgr	Matr3	Mtg1	Nrcam	Pcp4	Pnmt	Ptpn4	Rnaseh2b
Igbp1b	Kcnn2	Lhx6	Mbd3l2	Mtif2	Nrg3	Pcsk1	Pnpt1	Ptprm	Rnd1
Igf2bp2	Kcnn4	Lig3	Mbd5	Mtm1	Nrn1	Pcyt1b	Pnrc2	Ptprz1	Rnf128
Igfbp5	Kcnrg	Lim2	Mbip	Mtmr7	Nrxn3	Pde1c	Pold3	Pttg1	Rnf138
Igfbp6	Kcns1	Limch1	Mboat2	Mtss2	Nsg2	Pde3b	Polm	Ptx3	Rnf148
Igfl3	Kcns2	Lin28b	Mbtd1	Mtx3	Nsrp1	Pde4b	Poln	Ptx4	Rnf152
Igfn1	Kcns3	Lipn	Mc3r	Muc2	Nt5c3	Pde4d	Polr3f	Purb	Rnf170
Igsf11	Kcnu1	Lipo3	Mchr1	Muc4	Nt5e	Pde7b	Polr3h	Purg	Rnf217
Igsf9b	Kcnv2	Lmbrd2	Mcoln3	Mxd3	Ntn1	Pde8a	Pon2	Pus10	Rnf38
Iigp1	Kctd4	Lmntd1	Mcph1	Mybl1	Ntng1	Pde9a	Pop4	Pus3	Rngtt
Ikzf2	Kctd9	Lncpint	Mcts1	Mybpc3	Nudt12	Pdgfa	Pou2f1	Pvr	Rnpc3
Ikzf4	Kdm4d	Lnpep	Mcub	Mybphl	Nudt6	Pdgfd	Pou3f1	Pwwp3b	Ro60
Il12b	Kdm5a	Lnpk	Mdga2	Mycn	Oard1	Pdlim4	Pou4f1	Pxmp2	Rorc
Il15	Kdm6a	Lonrf3	Mecp2	Myef2	Oaz3	Pdzd3	Pou4f2	Pyroxd1	Rp1
Il17f	Kif18a	Lpar4	Med12l	Myh14	Obox8	Pdzd9	Ppa2	Qpct	Rp1l1
Il17rd	Kif21a	Lrat	Med30	Myl4	Odf2l	Pdzrn3	Ppara	Qrfprl	Rpa3
Il18r1	Kif24	Lrba	Med6	Myo1h	Odf3l1	Peg10	Ppil6	Rab27b	Rpgrip1
Il1b	Kif5c	Lrch1	Megf10	Myo9a	Odr4	Penk	Ppm1j	Rab30	Rps6ka5
Il1f6	Kirrel3	Lrguk	Mei4	Mzb1	Ofd1	Per3	Ppm1l	Rab36	Rsbn1
Il1f9	Kiz	Lrif1	Mertk	N4bp2	Ogdhl	Pex1	Ppox	Rab39b	Rsf1
Il1rap	Klf12	Lrmda	Mesp2	N4bp2l2	Oip5	Pex11g	Ppp1r14c	Rab3b	Rsph10b
Il1rapl1	Klf5	Lrp1b	Metap1d	Naalad2	Olig1	Pex2	Ppp1r1c	Rab6b	Rsph9
Il2	Klhdc9	Lrp4	Metrn	Naaladl2	Olig2	Pex3	Ppp1r2	Rab9b	Rtkn2
Il20rb	Klhl15	Lrrc1	Mettl11b	Nae1	Olig3	Pex5l	Ppp1r9a	Rabgap1l	Rtn4
Il23r	Klhl24	Lrrc18	Mettl18	Nat14	Omd	Pfn2	Ppp2r3a	Rabl3	Rtn4rl2
Il25	Klhl32	Lrrc36	Mettl21c	Nat8f4	Omg	Pgap2	Ppp3cc	Rad1	Runx1t1
Il7	Klhl34	Lrrc40	Mettl25	Nat8f6	Omp	Pggt1b	Ppp4r4	Rad50	Rwdd2a
Impa1	Klhl38	Lrrc4c	Mettl5	Nav2	Opn1mw	Pgr	Ppp6c	Rad51ap1	S100b
Impad1	Klhl42	Lrrc7	Mettl7b	Nav3	Osbpl3	Phactr1	Pqlc3	Rad51b	S100pbp
Inava	Klk11	Lrrc75b	Mettl9	Ncald	Oscar	Phf19	Pramef25	Radx	Samd5
Ing2	Klk12	Lrrc8e	Mga	Ncam1	Ostn	Phf8-ps	Pramel5	Ralgapb	Sapcd2
Inha	Klk13	Lrrcc1	Mgme1	Ncam2	Otogl	Phgdh	Prdm1	Ralgps1	Sarm1
Inhba	Klra10	Lrriq3	Mgmt	Nckap1	Otud7b	Phka1	Prelid2	Ranbp17	Sat1
Inka2	Klra2	Lrrk2	Micall2	Nckap5	Ovgp1	Phlda3	Prex2	Rap1a	Satb1
Inpp5f	Klra20	Lrrn3	Micu3	Ncr1	Oxr1	Phxr4	Prickle1	Rarb	Sbspon
Insl6	Klra23	Lrrtm2	Mid2	Ndp	P2rx3	Pi4k2b	Prim1	Rarres1	Sc5d
Insrr	Klra3	Lrrtm3	Mier1	Ndst3	P2ry1	Piezo2	Prkaa2	Rasa1	Scai
Insyn2a	Klra7	Lrsam1	Miga1	Ndufs5	P2ry12	Pigf	Prkci	Rasa2	Scaper
Ints6l	Klra8	Lsamp	Mill2	Necab1	P3h2	Pigh	Prkd1	Rasgef1c	Scarb2
Ints8	Klra9	Ltbp1	Mios	Nectin3	Pabpc1l	Pigl	Prl3d2	Rasl10a	Scd2
Ipp	Klrb1	Ltbp3	Mir23b	Negr1	Pabpc4l	Pigm	Prl8a9	Rbak	Scd3
Iqca1l	Klrb1a	Luc7l2	Mis18a	Neil3	Pacrg	Pign	Prm3	Rbbp6	Scd4
Iqcb1	Klrb1b	Luc7l3	Mis18bp1	Nek11	Pacrgl	Pigp	Prmt3	Rbm26	Scg3
Iqck	Klrb1c	Luzp2	Mkx	Nek3	Paics	Pigu	Prodh2	Rbm3	Scgb1a1

Supplementary Table 1 (3/3) | Upregulated genes in *B; p38α* vs. *B* tumors ($log_2FC \geq 0.265$) (n = 2214).

Upregulated genes in *B; p38α* vs. *B*						
Scgb1b3	Slc33a1	Srp54b	Tedc1	Tst	Xlr5c	Zfp825
Scgb2b6	Slc38a6	Srp54c	Teddm1a	Tsx	Xpa	Zfp827
Schip1	Slc41a2	Srsf5	Tefm	Tti2	Xrcc5	Zfp846
Sclt1	Slc4a7	Ss18l2	Tenm2	Ttll2	Xrn1	Zfp85
Scml2	Slc4a8	Ssbp1	Tet1	Ttll5	Yes1	Zfp850
Scml4	Slc4a9	Ssxb8	Tet2	Tubb3	Ylpm1	Zfp867
Scn8a	Slc5a10	St3gal6	Tex10	Tubgcp5	Ypel4	Zfp870
Scoc	Slc5a7	St6gal1	Tex16	Tulp2	Zbtb10	Zfp873
Scube3	Slc6a11	St8sia2	Tex21	Tut4	Zbtb18	Zfp879
Scx	Slc6a15	Stac2	Tex9	Txndc11	Zbtb20	Zfp93
Scyl3	Slc6a17	Stag3	Tfap4	Txndc16	Zbtb39	Zfp931
Sec22a	Slc7a14	Stap1	Tfdp2	Txnrd3	Zc3h14	Zfp933
Sele	Slc7a15	Stard10	Tgfb2	Tyro3	Zc3h6	Zfp934
Sema3e	Slc7a2	Stard6	Tgfbr1	U2surp	Zc4h2	Zfp935
Sema4g	Slc8a2	Stfa3	Thada	Ubap1l	Zcchc10	Zfp936
Sema6d	Slc9a7	Stk32a	Thbs4	Ubash3b	Zcchc18	Zfp937
Senp6	Slc9b2	Stk38l	Themis3	Ube2dnl2	Zcchc4	Zfp938
Sept10	Slf1	Stox2	Thnsl1	Ube2e2	Zdhhc15	Zfp939
Sept6	Slf2	Stra6l	Thoc2	Ube2q2	Zdhhc17	Zfp94
Serf1	Slfn3	Stx19	Thsd7a	Ube2u	Zdhhc19	Zfp945
Serinc4	Slit1	Stx1b	Thumpd2	Ubp1	Zeb1	Zfp947
Serpina16	Slitrk3	Styx	Thyn1	Ubxn11	Zfand1	Zfp952
Serpina3b	Slitrk5	Styxl1	Tial1	Ucn2	Zfc3h1	Zfp958
Serpina7	Smad5	Suco	Tigd4	Ugp2	Zfhx4	Zfp959
Serpinb3d	Smad7	Sugct	Timd2	Ugt2b35	Zfp101	Zfp960
Serpinb9c	Smarca5	Sult1b1	Timm21	Uimc1	Zfp11	Zfp964
Serpinb9e	Smarca5-ps	Sult1d1	Timm8a1	Umad1	Zfp119a	Zfp965
Serpinb9g	Smc3	Sult2a2	Timm8a2	Umodl1	Zfp119b	Zfp966
Sertad4	Smc5	Supt20	Tipin	Unc93a	Zfp174	Zfp97
Setdb2	Smchd1	Supt3	Tll2	Unc93a2	Zfp180	Zfp970
Setmar	Smco3	Supv3l1	Tlr12	Ung	Zfp182	Zfp971
Sfrp4	Smim23	Svip	Tlr3	Unkl	Zfp184	Zfp973
Sfrp5	Smim3	Svs6	Tm2d1	Upf3b	Zfp2	Zfp975
Sfswap	Smok2a	Syce2	Tm7sf3	Upk1a	Zfp229	Zfp976
Sftpc	Smok2b	Sycp1	Tma16	Upk1b	Zfp248	Zfp995
Sgce	Smr3a	Sycp3	Tmbim4	Uprt	Zfp267	Zgrf1
Sgcz	Sms	Syn3	Tmc1	Urgcp	Zfp273	Zhx1
Sgip1	Sncaip	Syndig1l	Tmc2	Uri1	Zfp28	Zic1
Sgms2	Snhg11	Syne2	Tmc3	Use1	Zfp280c	Zic4
Sh2d1b1	Snrpn	Syt11	Tmed8	Usp14	Zfp280d	Zkscan1
Sh2d2a	Sntg2	Syt4	Tmod2	Usp2	Zfp286	Zkscan16
Sh3kbp1	Snx16	Sytl2	Tmprss15	Usp20	Zfp292	Zkscan17
Sh3rf2	Snx22	T	Tmprss3	Usp53	Zfp326	Zkscan8
Sh3yl1	Snx27	Taar7f	Tmprss5	Usp6nl	Zfp329	Zmat1
Shc3	Socs6	Taar8c	Tmsb15b2	Ust	Zfp354c	Zmat4
Shc4	Sod3	Tab3	Tmtc2	Uvssa	Zfp365	Zmym4
Shprh	Sorbs1	Tac2	Tmx3	Vcan	Zfp37	Znhit6
Siah1a	Sorcs1	Tacr2	Tnfaip6	Vcpip1	Zfp385b	Znrf3
Siah1b	Sorcs2	Taf4b	Tnfrsf9	Vegfa	Zfp389	Zpbp
Sik3	Sorcs3	Taf5	Tnik	Veph1	Zfp438	Zrsr1
Sipa1l1	Sort1	Taf9	Tnmd	Vpreb1	Zfp442	Zscan18
Skil	Sos1	Tafa1	Tnn	Vpreb2	Zfp454	Zscan30
Skint11	Sos2	Tafa5	Tnni3k	Vpreb3	Zfp455	Zswim5
Skint7	Sox2	Tagap	Tnnt2	Vps13a	Zfp462	Zswim6
Skint9	Sox5	Tagap1	Tnp1	Vps26a	Zfp472	Zup1
Sla2	Sox6	Tal2	Togaram1	Vps50	Zfp51	Zw10
Slamf6	Sp4	Taok1	Tom1l1	Vrtn	Zfp521	
Slamf7	Spag16	Tarsl2	Tom1l2	Vsig2	Zfp523	
Slamf9	Spag4	Tas2r114	Top2b	Vtn	Zfp551	
Slc10a1	Spag9	Tas2r117	Tox	Vwa5a	Zfp560	
Slc12a2	Sparcl1	Tas2r119	Tpbpa	Vxn	Zfp58	
Slc13a5	Spata1	Tas2r135	Tph2	Wbp4	Zfp61	
Slc14a2	Spata48	Tas2r137	Tpmt	Wdhd1	Zfp619	
Slc15a2	Spc25	Tas2r139	Tprkb	Wdpcp	Zfp62	
Slc16a1	Spem2	Tas2r140	Tpsg1	Wdr20rt	Zfp641	
Slc18a1	Spg11	Tatdn1	Traf3ip2	Wdr31	Zfp644	
Slc19a3	Spib	Tbc1d10c	Traf5	Wdr34	Zfp65	
Slc22a15	Spin2d	Tbc1d19	Trappc2	Wdr35	Zfp654	
Slc22a17	Spink11	Tbc1d8b	Trappc6b	Wdr37	Zfp663	
Slc22a2	Spint1	Tbpl1	Trdmt1	Whrn	Zfp709	
Slc24a2	Spire1	Tcaim	Triqk	Wif1	Zfp74	
Slc24a5	Spo11	Tceal1	Trmt10b	Wnk3	Zfp763	
Slc25a23	Spon1	Tceanc	Trmt11	Wnk4	Zfp773	
Slc25a27	Spopl	Tcerg1	Trpc3	Wnt16	Zfp777	
Slc25a33	Spp1	Tcf12	Trpc4	Wnt8b	Zfp78	
Slc26a1	Sprr3	Tcf24	Trpm3	Wnt9a	Zfp788	
Slc26a4	Spryd7	Tcfl5	Trpm6	Wrn	Zfp791	
Slc26a8	Sptssa	Tcl1b4	Trps1	Wsb1	Zfp804b	
Slc26a9	Spx	Tcp11l1	Trub2	Wwc1	Zfp808	
Slc27a6	Spz1	Tdpoz4	Tsga10ip	Xiap	Zfp81	
Slc2a1	Sqle	Tdrd3	Tspan6	Xkr4	Zfp810	
Slc30a4	Srek1	Tdrkh	Tspan7	Xkr5	Zfp811	
Slc30a9	Srp54a	Tecta	Tspyl5	Xkr7	Zfp819	

Supplementary Table 2 (1/4) | Downregulated genes in *B; p38α* vs. *B* tumors ($log_2FC \leq -0.265$) (n = 3000).

Downregulated genes in *B; p38α* vs. *B*									
A2ml1	Adipoq	Aplp1	B020004J07Rik	Calr	Cd209g	Cited1	Cpt1a	Cyth4	Dock2
A4galt	Adm	Apoa1	B3gat1	Camk1d	Cd226	Cited2	Cpxm1	Cytl1	Dohh
Aacs	Adora2a	Apoa4	B3gat3	Camk2a	Cd248	Cited4	Cpz	Cyyr1	Dok1
Aadacl3	Adra2a	Apobec2	B3gnt9	Camk2n2	Cd300a	CK137956	Crat	D17H6S53E	Dok2
Aadacl4fm4	Adrb2	Apoc1	B430306N03Rik	Camp	Cd300e	Ckap4	Crct1	D2hgdh	Dpagt1
Aard	Adtrp	Apoc2	B4galt6	Camsap3	Cd300lb	Ckb	Creb3l1	Dab1	Dpep2
Aass	Aebp1	Apol11a	Bag3	Cant1	Cd300ld	Ckm	Crhr1	Dab2	Dpf3
Abca1	AF366264	Apol7a	Baiap3	Capn1	Cd300ld3	Ckmt2	Crip1	Daglb	Dpp10
Abca13	Agpat1	Apol8	Bak1	Capn11	Cd300ld4	Clca1	Crisp1	Dapk1	Dpp3
Abcb1a	Agpat4	Apol9a	Bank1	Capn8	Cd300lg	Cldn16	Crispld2	Dapl1	Dpp4
Abcb9	Agtr1a	Apol9b	Banp	Capsl	Cd33	Cldn20	Crlf3	Dbil5	Dpp7
Abcc3	Agtrap	Apold1	Basp1	Car1	Cd36	Cldn3	Crnn	Dbx2	Dpp9
Abcc9	Ahcyl2	Apom	Batf3	Car11	Cd37	Cldn34-ps	Crocc	Dchs1	Dpt
Abcd1	Ahsa1	Aqp1	BB019430	Car15	Cd38	Cldn4	Cryaa	Dclk1	Dqx1
Abcg1	Ak4	Aqp3	Bcan	Car3	Cd40	Cldn5	Cryba4	Dclre1c	Drc7
Abcg3	Ak7	Aqp5	Bcat1	Car4	Cd53	Cldn8	Crygb	Dcpp3	Dsc1
Abi3	Ak8	Aqp6	Bcl11a	Car5a	Cd55b	Cldn9	Crygf	Dcps	Dsc2
Abi3bp	Akp3	Aqp7	Bcl11b	Car7	Cd5l	Cldnd2	Csf1	Dct	Dsc3
Ablim3	Akr1c18	Aqp9	Bcl6b	Card10	Cd68	Clec10a	Csf1r	Dctn1	Dscam
Abo	Akr1c21	Ar	Bcl7c	Casp8	Cd82	Clec11a	Csf2ra	Dda1	Dse
Abra	Akr1cl	Areg	Bdh1	Casq1	Cd84	Clec18a	Csf2rb	Ddit4	Dsg1a
Abt1	Akt1	Arf5	Bex4	Cass4	Cd93	Clec2g	Csf2rb2	Ddn	Dsg1b
Acads	Akt1s1	Arg1	Bex6	Castor2	Cdc34	Clec3b	Csf3r	Ddo	Dsg2
Ace	Alad	Arhgap23	Bgn	Catsper4	Cdc42ep2	Clec4a1	Csk	Ddr2	Dsg4
Acer1	Alas2	Arhgap27	Bhlhe22	Catsperb	Cdc42ep4	Clec4a3	Csmd2os	Ddx28	Dsp
Acer2	Alb	Arhgap28	Bicdl2	Catsperd	Cdcp2	Clec4b1	Csrp3	Ddx3y	Dtnbp1
Ackr3	Alcam	Arhgap29	Bik	Cav1	Cdh1	Clec4n	Csta1	Defa-rs4	Dubr
Ackr4	Aldh1a2	Arhgap30	Birc5	Cavin1	Cdh13	Clhc1	Csta2	Defa17	Duox2
Acly	Aldh1l1	Arhgap45	Blnk	Cavin2	Cdh26	Clic5	Cstdc4	Defa23	Duoxa1
Acot3	Aldh2	Arhgap6	Blvrb	Cavin4	Cdh3	Clmn	Ctf2	Defa27	Duoxa2
Acot5	Aldh3b2	Arhgdib	Bmp2k	Cbfa2t3	Cdh4	Cln3	Cth	Defa28	Dupd1
Acot7	Aldoa	Arhgdig	Bmp7	Cbln1	Cdh5	Cln6	Ctla2a	Defa3	Dusp1
Acp7	Alg12	Arhgef17	Borcs6	Cbr2	Cdh9	Cln8	Ctnna2	Defa30	Dusp10
Acpp	Alg3	Arid5a	Bpifa1	Cc2d1a	Cdk18	Clstn2	Ctps	Defa34	Dusp18
Acsl1	Alox5	Armc2	Bpifa2	Ccdc106	Cdk2ap2	Clu	Cts6	Defa42	Dusp7
Acsm4	Alox5ap	Armc6	Bpifa3	Ccdc117	Cdk3	Cluh	Cts8	Defb1	Dynap
Acsm5	Alpk2	Arpc3	Bpifb6	Ccdc137	Cdo1	Cma1	Ctsa	Defb14	Dysf
Acss3	Alpl	Arpc4	Bpnt1	Ccdc142	Cdsn	Cmah	Ctsb	Defb25	E2f1
Acta1	Als2cl	Arrb2	Bsn	Ccdc153	Cdx2	Cmip	Ctsc	Defb36	Ear1
Acta2	Alyref2	Arrdc4	Bst1	Ccdc162	Cdyl2	Cmklr1	Ctsd	Defb41	Ear10
Actbl2	Amigo2	Arsi	Btbd35f2	Ccdc190	Ceacam1	Cmtm7	Ctse	Defb42	Ear12
Actg2	Amotl2	Art1	Btbd35f25	Ccdc51	Ceacam11	Cmtm8	Ctsh	Depdc1b	Ebf1
Actl10	Ampd1	Arvcf	Btbd35f3	Ccdc71l	Ceacam2	Cmya5	Ctsk	Deptor	Ebf3
Actl6b	Ampd3	Arxes1	Btbd35f4	Ccdc80	Ceacam9	Cndp2	Ctsll3	Des	Ebi3
Actn1	Ang6	Asah2	Btbd6	Ccdc85a	Cebpa	Cnfn	Ctsr	Desi2	Ebp
Actn2	Angel1	Asb14	Btnl2	Ccdc85c	Cebpb	Cnih2	Cx3cl1	Det1	Ece1
Actn3	Angpt2	Asb4	Btnl9	Ccdc87	Cemip	Cnnm1	Cxadr	Dffa	Ece2
Actrt1	Angpt4	Asb5	C130026I21Rik	Ccdc89	Cercam	Cnpy3	Cxcl12	Dffb	Ecel1
Acvr1c	Angptl4	Ascl2	C1qa	Ccdc96	Cerk	Cnr1	Cxcl3	Dgat2	Ecm1
Acvrl1	Ank1	Ascl4	C1qb	Cckbr	Ces1f	Cnr2	Cxcr1	Dhrs3	Ecrg4
Adam11	Ank3	Asgr2	C1qc	Ccl21a	Ces2c	Cntd1	Cxcr4	Dhrs9	Ecscr
Adam15	Ankk1	Asic2	C1qtnf1	Ccl21b	Ces2g	Cntfr	Cxcr5	Dhx58	Edaradd
Adam24	Ankle1	Asic5	C1qtnf3	Ccl21c	Cfap206	Cntn3	Cyb561	Diaph1	Edf1
Adam5	Ankmy1	Aspn	C1qtnf5	Ccl22	Cfap43	Col11a1	Cyb561d2	Dio3	Edn1
Adam8	Ankrd13a	Asprv1	C1qtnf6	Ccl24	Cfap74	Col14a1	Cyba	Dipk2b	Edn2
Adamts12	Ankrd2	Ass1	C1qtnf7	Ccl6	Cfd	Col1a1	Cybc1	Disp2	Ednrb
Adamts15	Ankrd35	Astl	C1ra	Ccl8	Cfp	Col1a2	Cybrd1	Dlk1	Eef1a2
Adamts18	Ankrd60	Asz1	C1rb	Ccl9	Cggbp1	Col3a1	Cygb	Dll1	Eef2k
Adamts2	Anks4b	Atf6b	C2cd4d	Ccm2l	Cgref1	Col4a1	Cyp11a1	Dll3	Eepd1
Adamts5	Ano1	Atmin	C3	Ccn3	Ch25h	Col4a2	Cyp1b1	Dll4	Efcab6
Adamts9	Ano2	Atox1	C5ar1	Ccn4	Chac1	Col5a1	Cyp26b1	Dlx3	Efemp1
Adamtsl4	Anpep	Atp13a2	C5ar2	Ccn5	Chadl	Col5a2	Cyp27a1	Dlx6os2	Efemp2
Adap1	Anxa3	Atp13a4	C6	Ccna1	Chchd10	Col6a1	Cyp2ab1	Dmac1	Efhc2
Adap2	Anxa7	Atp1a3	C8b	Ccnb3	Chd3	Col6a2	Cyp2b13	Dmkn	Efhd2
Adcy10	Anxa9	Atp1a4	C8g	Ccne1	Chek2	Col6a3	Cyp2b19	Dmpk	Efnb1
Adcy4	Aoah	Atp2a1	Cabcoco1	Ccno	Chil3	Col6a4	Cyp2c67	Dmrt1	Egfem1
Adcy5	Aoc2	Atp4a	Cabp1	Ccr1	Chil4	Col6a6	Cyp2c69	Dmrt2	Egfl7
Adcy7	Aoc3	Atp5d	Cabp7	Ccr2	Chil5	Colq	Cyp2d26	Dmrta2	Egfr
Adcyap1r1	Aox2	Atp6v1e2	Cachd1	Ccr3	Chp2	Commd9	Cyp2d34	Dmrtc2	Egln2
Adgrb1	Aox3	Atp6v1fnb	Cacna1b	Ccr5	Chpf	Comt	Cyp2e1	Dnah2	Egr2
Adgrd1	Aox4	Atp8b2	Cacna1s	Ccser1	Chrna1	Comtd1	Cyp2f2	Dnah8	Ehd1
Adgre1	Ap1b1	Atp8b4	Cacnb1	Cd163	Chrna2	Cops7b	Cyp2s1	Dnaic1	Ehd2
Adgre4	Ap1m2	Atpsckmt	Cacnb3	Cd1d2	Chrng	Coro1a	Cyp4a32	Dnaja3	Ehd3
Adgrf3	Ap1s1	Atxn7l3	Cacng1	Cd2	Chst1	Coro1b	Cyp4b1	Dnajb1	Ehd4
Adgrf4	Ap1s3	AU016765	Calb2	Cd200r1	Chst15	Cotl1	Cyp4b1-ps2	Dnajb13	Eif2s3y
Adgrf5	Ap2a2	AU018091	Calca	Cd200r2	Chst5	Cox4i2	Cyp4f14	Dnajb7	Eif3a
Adgrg1	Ap2s1	Avpr1a	Calcoco2	Cd200r4	Chst7	Cox6a2	Cyp4f39	Dnajc28	Eif4ebp1
Adgrg2	Apba1	AW551984	Calhm4	Cd209a	Chsy1	Cox8b	Cyp4f41-ps	Dnajc6	Eif4ebp2
Adgrg3	Apba3	Axdnd1	Calhm5	Cd209b	Ciart	Cpa3	Cypt12	Dnase1l2	Eif6
Adgrg7	Apbb1ip	Axin2	Calhm6	Cd209c	Cib4	Cpn1	Cypt14	Dnase2a	Elane
Adgrl4	Apcdd1	AY074887	Calm4	Cd209d	Cidec	Cpne4	Cysltr1	Dnd1	Elavl3
Adh1	Apln	AY358078	Calml3	Cd209e	Ciita	Cpne6	Cystm1	Dnm1	Elf4
Adh7	Aplnr	Azgp1	Calml4	Cd209f	Cish	Cpne9	Cyth3	Dnpep	Elf5

Supplementary Table 2 (2/4) | Downregulated genes in *B; p38α* vs. *B* tumors ($log_2FC \leq -0.265$) (n = 3000).

Downregulated genes in *B; p38α* vs. *B*									
Elmo1	Fank1	Fthl17a	Gp1bb	H4f16	Hspb6	Islr	Krt25	Ldlrap1	Lyg2
Elmod1	Fasn	Fthl17d	Gpat2	H6pd	Hspb7	Ism1	Krt26	Lemd2	Lyl1
Eln	Fat2	Fthl17e	Gpd1	Hacd4	Hspb8	Isyna1	Krt27	Lep	Lypd1
Eloa	Fat4	Ftl1	Gpha2	Hand2	Hspd1	Itga11	Krt28	Lfng	Lypd10
Elovl1	Fbln1	Fut1	Gpihbp1	Hao2	Hspg2	Itga5	Krt31	Lgals12	Lypd5
Elovl3	Fbln2	Fxyd2	Gpnmb	Hba-a1	Hsph1	Itga9	Krt32	Lgals3	Lypd6b
Elp5	Fbln5	Fxyd4	Gpr132	Hba-a2	Htr1b	Itgam	Krt33a	Lgals3bp	Lyve1
Emb	Fbln7	Fzd10	Gpr135	Hbb-bs	Htr6	Itgb2	Krt33b	Lgalsl	Lyz1
Emcn	Fbn1	Fzd4	Gpr141	Hbb-bt	Htr7	Itgb2l	Krt34	Lgi2	Lyz2
Emilin2	Fbn2	Fzd6	Gpr153	Hbb-y	Htra2	Itgb7	Krt35	Lgi3	Lzts1
En1	Fbp1	G6pd2	Gpr160	Hcar1	Htra3	Itgbl1	Krt36	Lgmn	Lzts3
En2	Fbxl13	G6pdx	Gpr176	Hcfc1r1	Hydin	Itpkc	Krt39	Lhx5	Maats1
Enah	Fbxo15	Gaa	Gpr179	Hck	Hyou1	Itprid1	Krt4	Lhx9	Mab21l4
Endou	Fbxo43	Gabra5	Gpr182	Hcls1	I0C0044D17Rik	Itprip	Krt71	Lilr4b	Macc1
Eno1	Fbxw21	Gabrp	Gpr35	Hcst	Ica1l	Itsn1	Krt72	Lilra5	Macrod1
Eno1b	Fbxw27	Gadd45g	Gpr39	Hdac11	Icam2	Ivl	Krt73	Lilra6	Macroh2a2
Eno3	Fcer1g	Gal	Gpr75	Hdac7	Id1	Jade1	Krt74	Lilrb4a	Madd
Eno4	Fcer2a	Gal3st2c	Gprc5c	Hdc	Id4	Jag2	Krt75	Lin28a	Maf
Enox2	Fcgr1	Galm	Gprc5d	Hddc3	Idua	Jak3	Krt80	Lingo2	Mafa
Enpep	Fcgr2b	Galns	Gpt	Hdhd3	Ier5	Jakmip1	Krt82	Lipa	Mafb
Enpp2	Fcgr3	Galnt15	Gpx1	Heatr9	Ifi202b	Jaml	Krt84	Lipe	Magea1
Entpd1	Fcgrt	Galnt16	Gpx3	Hebp1	Ifi207	Jcad	Krt86	Lipg	Magea10
Entpd2	Fcna	Galnt9	Gpx7	Hebp2	Ifi27l2a	Jhy	Krt87	Liph	Mageb3
Entpd3	Fcrls	Gapt	Grap	Hecw2	Ifi27l2b	Jup	Krtap1-3	Lipi	Mal2
Entpd5	Fdps	Gas6	Grb7	Heg1	Ifi30	Kank1	Krtap1-5	Lipk	Mall
Entpd6	Fermt3	Gask1a	Greb1	Hemgn	Ifitm5	Kazald1	Krtap11-1	Lipm	Maml1
Eomes	Fes	Gask1b	Grem1	Heph	Ifitm6	Kazn	Krtap12-1	Lman2	Man1b1
Epb41	Fetub	Gata3	Grem2	Hephl1	Ifngr1	Kbtbd6	Krtap13-1	Lmcd1	Man1c1
Epb42	Fez2	Gatm	Grhl1	Herpud1	Ifngr2	Kbtbd8	Krtap14	Lmo2	Man2a2
Epha3	Ffar1	Gba	Grhl2	Hes6	Ifnlr1	Kcna4	Krtap15	Lmod2	Man2b1
Epha4	Ffar2	Gbgt1	Grid1	Hey1	Igf2bp1	Kcnab1	Krtap16-1	Lmod3	Man2b2
Ephb1	Fga	Gbx1	Grin2d	Hfe	Igfals	Kcnab2	Krtap16-3	Lnx1	Maneal
Ephx2	Fgd2	Gcat	Grk2	Hhex	Igfbp2	Kcnab3	Krtap17-1	LOC100861615	Manf
Ephx3	Fgd3	Gch1	Grm3	Hhipl1	Igfbp4	Kcnb1	Krtap19-1	LOC547349	Maob
Epor	Fgd5	Gchfr	Grn	Hif3a	Igsf21	Kcnd3	Krtap19-2	Lox	Map2k3
Eps8	Fgd6	Gcm2	Grrp1	Hip1r	Igsf6	Kcnh2	Krtap19-3	Lpar5	Map3k21
Eps8l2	Fgf10	Gda	Gsdmc2	Hjv	Ikbkb	Kcnh3	Krtap19-4	Lpgat1	Map3k5
Erg	Fgf11	Gdf10	Gsdmc3	Hk2	Ikzf1	Kcnh6	Krtap19-5	Lpin3	Map3k6
Esp8	Fgf14	Gdf6	Gstm1	Hk3	Il10ra	Kcnip2	Krtap19-9b	Lpl	Map3k7cl
Esr1	Fgf18	Gdnf	Gstm2	Hlx	Il10rb	Kcnj6	Krtap22-2	Lratd1	Map4k1
Esrp1	Fgfr1	Gdpd3	Gstm3	Hmox1	Il11ra1	Kcnk15	Krtap24-1	Lratd2	Map7d1
Esrp2	Fgr	Gemin5	Gstm7	Hnf4a	Il17d	Kcnk18	Krtap26-1	Lrfn5	Mapk11
Esyt1	Fhl5	Gfi1b	Gsto1	Hnmt	Il17re	Kcnk6	Krtap27-1	Lrg1	Mapk4
Ets2	Fhod3	Gfra3	Gstt1	Hopx	Il18	Kcnk9	Krtap3-1	Lrmp	Mapt
Etv6	Ficd	Gga2	Gtpbp6	Hormad1	Il1f5	Kcnma1	Krtap31-1	Lrp10	March1
Eva1a	Fitm1	Ggt1	Guca1a	Hoxb2	Il1r1	Kcnn1	Krtap31-2	Lrp11	Mark1
Eva1b	Fkbp11	Ggt5	Gucy1a1	Hoxb4	Il1r2	Kcnq4	Krtap4-1	Lrp3	Masp1
Evpl	Fkbp15	Ghrh	Gucy2d	Hoxb5	Il1rapl2	Kctd11	Krtap4-13	Lrr1	Matk
Exd1	Fkbp6	Gimap3	Guk1	Hoxb6	Il1rl1	Kctd12	Krtap4-2	Lrrc15	Matn1
Eya2	Flacc1	Gimap6	Gusb	Hoxb7	Il1rn	Kdelr1	Krtap4-6	Lrrc17	Matn4
Eya4	Flcn	Gipc1	Gxylt2	Hoxb9	Il20	Kdelr3	Krtap4-7	Lrrc2	Mb
F13a1	Fli1	Gipc2	Gzmg	Hoxc10	Il22ra2	Kdm5d	Krtap4-8	Lrrc25	Mbnl3
F2rl2	Flnb	Gja4	H1f8	Hoxc6	Il27	Kdr	Krtap4-9	Lrrc29	Mboat1
F3	Flrt2	Gja8	H2-Ab1	Hoxc8	Il27ra	Keap1	Krtap5-1	Lrrc3	Mboat7
F5	Flt4	Gjb4	H2-Ea-ps	Hoxd10	Il2ra	Kel	Krtap5-2	Lrrc32	Mbp
F7	Fmn2	Gjb6	H2-K1	Hoxd11	Il2rg	Kera	Krtap5-4	Lrrc3b	Mc5r
F930015N05Rik	Fmnl1	Glb1l2	H2-L	Hoxd3	Il34	Kif19a	Krtap6-1	Lrrc59	Mcc
Fabp2	Fmod	Glipr1	H2-M10.4	Hp	Il4ra	Kif1c	Krtap6-2	Lrrc72	Mcf2
Fabp3	Fn1	Glra1	H2-M11	Hpcal1	Il5ra	Kif26b	Krtap6-5	Lrrd1	Mcf2l
Fabp4	Folr1	Glra2	H2-M5	Hps1	Il6ra	Kif4-ps	Krtap7-1	Lrrk1	Mcfd2
Fabp5	Folr2	Glt1d1	H2-M9	Hpse	Il9	Klf11	Krtap8-1	Lrrn2	Mcm2
Fabp6	Foxa1	Gltp	H2-Q1	Hr	Il9r	Klf13	Krtap9-3	Lrrn4cl	Mcpt4
Fads2b	Foxc1	Glul	H2-T-ps	Hrc	Ildr2	Klf14	Krtap9-5	Lrrtm1	Mdga1
Fads6	Foxc2	Glyatl3	H2-T23	Hrh1	Inhbb	Klf2	L3mbtl1	Lrwd1	Me1
Fah	Foxe1	Glyctk	H2ac15	Hrk	Inhbe	Klf4	Lactb	Lsm10	Mecom
Faim2	Foxi3	Gm1995	H2ac4	Hrnr	Inmt	Klf6	Lad1	Lsmem1	Mecr
Fam129a	Foxl1	Gm5124	H2afb2	Hs3st1	Inpp5d	Klf8	Lama3	Lsr	Med22
Fam13c	Foxn1	Gm6300	H2afx	Hs3st3a1	Inpp5j	Klhdc7b	Lamb3	Ltb	Megf11
Fam167b	Foxo3	Gm7104	H2al1b	Hs6st2	Ints3	Klhl2	Lancl3	Ltb4r1	Meikin
Fam186a	Foxo4	Gmfg	H2al1k	Hs6st3	Ints5	Klhl21	Lao1	Ltb4r2	Men1
Fam186b	Foxr2	Gml	H2al1n	Hsbp1l1	Ip6k3	Klhl31	Laptm5	Ltc4s	Mest
Fam214b	Foxs1	Gmnc	H2bc11	Hsd11b1	Iqsec3	Klhl40	Large2	Lurap1l	Met
Fam25c	Fpr1	Gna12	H2bc12	Hsd11b2	Irak4	Klhl41	Lat2	Lvrn	Metrnl
Fam43a	Frmd4b	Gna14	H2bc13	Hsd17b6	Irf4	Klk1b11	Layn	Ly6a	Mettl24
Fam43b	Frmpd1	Gna15	H2bc14	Hsf2bp	Irf8	Klk1b16	Lbp	Ly6c1	Mfap2
Fam53b	Fry	Gnao1	H2bc15	Hsfy2	Irgq	Klk1b22	Lbx2	Ly6c2	Mfap4
Fam57a	Fscn1	Gnmt	H2bc6	Hsh2d	Irs1	Klk1b8	Lcat	Ly6d	Mfap5
Fam71b	Fsd1	Gnpda1	H2bc7	Hspa12b	Irs3	Klra16	Lcn2	Ly6e	Mfge8
Fam71e2	Fsd2	Gns	H2bc8	Hspa1a	Irx1	Kmt5c	Lcp1	Ly6g2	Mfhas1
Fam78a	Fshr	Golga7b	H2bc9	Hspa1b	Irx2	Kndc1	Lctl	Ly6g6e	Mfng
Fam78b	Fsip2l	Golph3	H2bu2	Hspa1l	Irx3	Krt17	Ldb3	Ly6g6f	Mfsd12
Fam83h	Fstl1	Golt1a	H3c7	Hspa5	Irx4	Krt20	Ldhc	Ly6h	Mfsd2a
Fam90a1b	Ftcd	Got1	H4c9	Hspb1	Isg20	Krt23	Ldhd	Ly6k	Mfsd4b1

Supplementary Table 2 (3/4) | Downregulated genes in *B; p38α* vs. *B* tumors ($log_2FC \leq -0.265$) (n = 3000).

Downregulated genes in *B; p38α* vs. *B*									
Mgarp	Mup5	Nfatc4	Onecut2	Pgm5	Pop5	Ptp4a3	Rgs7bp	Scara3	Shisal2b
Mgat1	Mup6	Nfkbie	Oog1	Phf2	Popdc2	Ptpn18	Rhag	Scara5	Shkbp1
Mgat4b	Mup7	Nfya	Oog4	Phf21b	Pou3f2	Ptpn6	Rhbdl2	Scarf2	Shox2
Mgl2	Mup8	Ngfr	Opn3	Phlda2	Pou3f4	Ptprb	Rhobtb1	Scd1	Shpk
Mgll	Mustn1	Ngp	Orai3	Phldb2	Ppa1	Ptpro	Rhod	Scel	Shroom3
Mgst1	Mvp	Nhlrc1	Orm1	Phxr1	Pparg	Ptprq	Rhou	Scgb1b30	Shtn1
Micalcl	Myadm	Nhsl2	Orm2	Phyhd1	Ppef1	Ptprr	Rhox2g	Scgb2b3	Siglec1
Micall1	Myadml2	Nim1k	Ormdl3	Pi15	Ppfia4	Ptrhd1	Rhox2h	Scly	Siglece
Mief2	Mybl2	Ninj1	Osbpl11	Pi16	Ppfibp2	Pvalb	Rhox4b	Scn2a	Sigmar1
Mien1	Mybpc1	Nkd1	Osr1	Pid1	Ppif	Pygl	Rhox4c	Scn3a	Sim2
Mip	Mybpc2	Nkiras2	Otof	Piga	Ppm1h	Pygm	Rhox4d	Scn3b	Sirpa
Mir322	Myc	Nkx1-2	Otulinl	Pigz	Ppp1r14a	Pyurf	Rhox4f	Scnn1a	Six2
Mir692-3	Myct1	Nlrc4	Ovol1	Pik3cb	Ppp1r14d	Pyy	Rhox4g	Scnn1g	Six3os1
Mknk2	Myd88	Nlrp14	P2rx1	Pik3cd	Ppp1r15b	Qrich2	Rhpn1	Scp2	Skint5
Mkrn2os	Myf5	Nlrp4b	P2rx4	Pik3cg	Ppp1r1b	Qsox1	Rin1	Scrg1	Skor1
Mlana	Myf6	Nlrp9b	P2rx5	Pik3r5	Ppp1r27	Rab11fip1	Rin2	Scrn3	Skor2
Mlec	Myh1	Nmbr	P2rx6	Pik3r6	Ppp1r37	Rab11fip4	Rin3	Sct	Sla
Mllt1	Myh11	Nme6	P2ry2	Pin1	Ppp1r3a	Rab25	Rinl	Sdc1	Slain1
Mlph	Myh2	Nmrk2	P2ry6	Pinlyp	Ppp1r3c	Rab29	Ripk3	Sdc3	Slc10a5
Mmp12	Myh4	Nmu	P4ha1	Pip4k2a	Ppp1r3d	Rab32	Rit2	Sdf2l1	Slc11a1
Mmp13	Myh7	Nod2	P4ha3	Pip4k2b	Ppp1r9b	Rab35	Rln3	Sdhafl	Slc12a3
Mmp19	Myh7b	Nog	Pacs1	Pipox	Ppp2r1b	Rab37	Rmdn3	Sds	Slc12a7
Mmp23	Myh8	Nol9	Pacsin2	Pira1	Pqlc1	Rab38	Rnase11	Sec1	Slc12a8
Mmp27	Myl1	Nos2	Padi3	Pira6	Praf2	Rab3il1	Rnase13	Sec14l4	Slc13a3
Mmp3	Myl2	Nos3	Padi4	Pirb	Pramef17	Rab42	Rnase2a	Sec16b	Slc15a1
Mmp8	Mylk	Notch3	Pak4	Pirt	Prcp	Rab44	Rnf113a2	Sec61b	Slc15a4
Mmp9	Mylk2	Notch4	Palm	Pitpna	Prdm16	Rab5c	Rnf125	Sel1l3	Slc15a5
Mmrn1	Mylpf	Npas2	Palmd	Pitpnm2	Prdm6	Rab7b	Rnf144a	Selenbp1	Slc16a13
Mmrn2	Myo15	Npc1l1	Pamr1	Pitx2	Prdm8	Rac2	Rnf144b	Selenom	Slc16a3
Mob1a	Myo18b	Npdc1	Papln	Piwil2	Preb	Rad51ap2	Rnf151	Selenop	Slc16a6
Mob3a	Myo1c	Npl	Papss2	Pjvk	Prelp	Rad52	Rnf165	Selenov	Slc16a7
Mob3b	Myo1d	Npnt	Parm1	Pkdcc	Prf1	Rag2	Rnf183	Selp	Slc16a9
Mocos	Myo1f	Nppb	Parvb	Pkhd1l1	Prg3	Rai14	Rnf187	Selplg	Slc17a3
Mog	Myo1g	Npr1	Pawr	Pkp1	Prg4	Ralb	Rnf222	Sema3g	Slc17a4
Moxd1	Myo3a	Npr3	Pbld1	Pkp3	Prkacb	Ralgps2	Rnf32	Sema4a	Slc1a5
Mpo	Myo5b	Nptx1	Pbx2	Pkp4	Prkar1b	Raly	Rnf39	Sephs2	Slc22a14
Mpp1	Myocd	Nr0b1	Pcdh1	Pla1a	Prkcb	Ralyl	Rnf43	Sept1	Slc22a26
Mpp3	Myom1	Nr0b2	Pcdh12	Pla2g15	Prkcd	Ramp2	Rnh1	Sept3	Slc22a3
Mpped2	Myom2	Nr1h2	Pcdh18	Pla2g2a	Prkch	Rapgef5	Rnpep	Sept8	Slc22a4
Mpzl2	Myot	Nr1h3	Pck1	Pla2g2d	Prkcq	Rasgef1a	Rnpepl1	Serf2	Slc25a18
Mpzl3	Myoz1	Nrap	Pclo	Pla2g2e	Prkd2	Rasgrf2	Robo4	Serinc2	Slc25a19
Mrap	Myoz2	Nrg1	Pcnx2	Pla2g2f	Prl2c2	Rasgrp2	Ros1	Serinc5	Slc25a31
Mrc1	Mypn	Nrg4	Pcolce	Pla2g4d	Prl2c3	Rasgrp4	Rph3a	Serpina12	Slc25a37
Mrc2	Myrip	Nrgn	Pcolce2	Pla2g4f	Prlr	Rasl11a	Rpp25	Serpina1a	Slc25a39
Mrgpra5	Myt1	Nrip3	Pcsk5	Pla2g7	Prm1	Rassf10	Rprm	Serpina1b	Slc26a11
Mrgpra6	N4bp2l1	Nrk	Pcsk6	Plagl1	Prm2	Rassf5	Rps19bp1	Serpina1c	Slc27a2
Mrgprb1	Naa40	Nrp1	Pctp	Plau	Prnd	Rassf7	Rps4l	Serpina1e	Slc28a2
Mrgprb2	Naa60	Nrp2	Pcx	Plbd1	Proc	Rassf9	Rps6ka1	Serpina3c	Slc28a2b
Mrgprf	Naaa	Nrros	Pcyox1	Plcd1	Procr	Rbbp8nl	Rps6ka4	Serpina3f	Slc2a10
Mroh1	Naaladl1	Nrxn1	Pcyox1l	Plcg2	Prox1	Rbm11	Rps6kc1	Serpina3h	Slc2a12
Mrpl14	Nab2	Nsf	Pdcd11g2	Plch1	Prr14l	Rbm20	Rptn	Serpina3i	Slc2a3
Mrps11	Nabp1	Nt5c	Pde1a	Plch2	Prr30	Rbm24	Rrp12	Serpina3m	Slc30a1
Mrvi1	Naga	Nt5el	Pde1b	Plcl2	Prr5	Rbm47	Rsph1	Serpina3n	Slc30a2
Ms4a3	Nagpa	Ntf5	Pde2a	Plcxd3	Prr9	Rbmxl2	Rsph4a	Serpina5	Slc35a2
Ms4a4a	Naif1	Ntn4	Pde3a	Pld2	Prrg2	Rbp2	Rspo1	Serpina9	Slc35c1
Ms4a4d	Naip2	Ntng2	Pde4a	Pld4	Prrt4	Rbp4	Rtl3	Serpinb10	Slc35d3
Ms4a6b	Naip5	Ntpcr	Pde4c	Pld5	Prrx1	Rbp7	Rtl9	Serpinb11	Slc35e1
Ms4a6c	Nap1l5	Ntrk3	Pde6b	Plek2	Prss12	Rbpj	Rtn1	Serpinb1b	Slc35f3
Ms4a6d	Napsa	Nudt15	Pde6g	Plekhb2	Prss2	Rcan2	Rtn2	Serpinb2	Slc35f6
Ms4a7	Nat8f7	Nudt17	Pdgfc	Plekhf1	Prss23	Rce1	Rtp3	Serpinb5	Slc36a1
Ms4a8a	Nav1	Nudt18	Pdgfra	Plekhg5	Prss27	Rcsd1	Runx1	Serpinb6b	Slc36a2
Msantd1	Nceh1	Nudt4	Pdgfrb	Plin1	Prss34	Rdh16	Ruvbl2	Serpinb8	Slc37a2
Msr1	Ncf1	Nuggc	Pdgfrl	Plin2	Prss41	Rdm1	Rxra	Serpine1	Slc38a1
Msrb1	Ncf2	Nup62cl	Pdha2	Plin4	Prss53	Reg1	Ryr1	Serpinf1	Slc38a10
Msrb2	Ncf4	Nxn	Pdia5	Plk3	Prx	Reg3b	Ryr3	Serpinh1	Slc38a3
Mst1	Nckap1l	Nxnl1	Pdlim2	Plk5	Psap	Reg3d	S100a1	Serpini1	Slc38a4
Mst1r	Ncln	Nxpe2	Pdlim3	Plpp5	Psd	Rell1	S100a11	Sertm1	Slc39a11
Msx1	Ndn	Nxpe5	Pdxk	Plppr5	Psen2	Reln	S100a3	Sf3a2	Slc39a12
Msx2	Ndnf	Nxph2	Pdzd7	Pltp	Psg21	Ren1	S100a4	Sfn	Slc39a8
Msx3	Ndufa4l2	Oas1g	Pecam1	Plvap	Psmb5	Rep15	S100a7a	Sfrp2	Slc40a1
Mt3	Ndufb8	Oas1h	Peg12	Plxna1	Psmb8	Repin1	S100a8	Sgk1	Slc43a2
Mt4	Ndufs7	Oas2	Peg3	Pmel	Psmb9	Reps2	S1pr1	Sh2d3c	Slc44a3
Mtfr2	Neb	Oasl1	Pepd	Pnliprp1	Psors1c2	Rerg	Saa2	Sh2d4a	Slc45a2
Mtg2	Necab2	Ocel1	Per2	Pnpla2	Pstpip2	Retn	Sall2	Sh3bgr	Slc45a3
Mtmr4	Necap1	Ocstamp	Perp	Pnpla3	Ptafr	Retnla	Samd4b	Sh3bgrl2	Slc45a4
Mucl3	Nectin2	Odaph	Pf4	Pnpla5	Ptgdr2	Retnlg	Samhd1	Sh3bgrl3	Slc46a1
Mup12	Nectin4	Odf1	Pfkl	Pnpo	Ptgds	Rex1bd	Samt3	Sh3bp1	Slc46a2
Mup13	Nedd9	Odf3	Pfkp	Podn	Ptger2	Rflnb	Samt4	Sh3bp5	Slc47a2
Mup19	Nefh	Ogn	Pga5	Podnl1	Ptger4	Rfx8	Sash3	Sh3gl3	Slc48a1
Mup20	Nefm	Olah	Pgam1	Pof1b	Ptges	Rgs18	Sbk2	Sh3tc1	Slc52a2
Mup21	Nell2	Olfm1	Pgam2	Polr2c	Ptgis	Rgs19	Sbk3	Shb	Slc52a3
Mup3	Neo1	Olfm2	Pgd	Pom121l12	Ptgs1	Rgs4	Sbpl	She	Slc5a1
Mup4	Nfam1	Olfml2b	Pgm1	Pon1	Pth1r	Rgs7	Sbsn	Shisa9	Slc5a12

Supplementary Table 2 (4/4) | Downregulated genes in *B; p38α* vs. *B* tumors ($log_2FC \leq -0.265$) (n = 3000).

Downregulated genes in *B; p38α* vs. *B*						
Slc5a3	Srl	Tcf21	Tmem229b	Trpc6	Uty	Zfp985
Slc5a4b	Srm	Tcf7l1	Tmem233	Trpm1	Vamp1	Zfpm1
Slc5a8	Srms	Tchh	Tmem246	Trpm4	Vamp8	Zim1
Slc6a1	Srpx	Tchhl1	Tmem250-ps	Trpv2	Vangl2	Znrd2
Slc6a12	Srpx2	Tcn2	Tmem252	Trpv3	Vash1	Znrf4
Slc6a18	Ssbp3	Tcstv3	Tmem255a	Trpv4	Vat1	Zp3
Slc6a21	St3gal2	Tcte1	Tmem256	Trpv6	Vat1l	Zp3r
Slc6a3	St6galnac5	Tdo2	Tmem262	Tsc22d3	Vcam1	Zpbp2
Slc6a4	Stab1	Tdpoz2	Tmem267	Tsfm	Vdr	Zscan10
Slc7a10	Stac3	Tdrd5	Tmem35a	Tshr	Vegfd	Zscan20
Slc7a11	Stap2	Tdrd9	Tmem37	Tslp	Vgll4	Zscan22
Slc7a12	Stard8	Tek	Tmem40	Tspan12	Vill	Zscan4d
Slc7a7	Stat2	Tekt3	Tmem45a	Tspan13	Vit	
Slc7a8	Stat6	Tepsin	Tmem50b	Tspan2	Vldlr	
Slc8a1	Stc1	Terb1	Tmem51	Tspan32	Vmo1	
Slc9a3r1	Stc2	Tesc	Tmem54	Tspan4	Vps26b	
Slc9a5	Steap1	Tex12	Tmem56	Tspan5	Vsig4	
Slc9a9	Steap3	Tex13a	Tmem59l	Tspan8	Vsig8	
Slc9b1	Stip1	Tex26	Tmem79	Tspo	Vsir	
Slco1c1	Stk11	Tex45	Tmem8	Tssk2	Wbp2nl	
Slco3a1	Stk40	Tfap2a	Tmem88	Tssk3	Wdfy4	
Slco4a1	Stmn2	Tfap2b	Tmem98	Tstd1	Wdr38	
Slco6b1	Stmn4	Tfap2c	Tmie	Ttc16	Wdr54	
Slfn1	Stom	Tfec	Tmod4	Ttc22	Wdr66	
Slfn2	Stpg3	Tff2	Tmprss11e	Ttc24	Wdr91	
Slfn5	Strc	Tfr2	Tmprss11f	Ttc34	Wdr93	
Slit2	Strip2	Tgfb1	Tmprss13	Ttc6	Wfdc12	
Slit3	Stum	Tgfbr3	Tmtc1	Ttc7	Wfdc17	
Slx1b	Stx2	Tgm1	Tnfaip8l2	Ttc9	Wfdc18	
Smagp	Stxbp2	Tgm2	Tnfrsf11b	Ttll9	Wfdc21	
Smc1b	Sucnr1	Tgm3	Tnfrsf13b	Ttn	Wnt10a	
Smco1	Sult1c1	Them5	Tnfrsf17	Ttpal	Wnt10b	
Smim10l2a	Sult2a5	Themis2	Tnfrsf1a	Ttr	Wnt5b	
Smim12	Susd1	Thrsp	Tnfrsf1b	Ttyh3	Wnt8a	
Smim17	Susd2	Thy1	Tnfrsf21	Tuba4a	Wscd2	
Smim24	Susd3	Tiam1	Tnfsf18	Tuba8	Wt1	
Smlr1	Sval1	Tiam2	Tnfsf9	Tubb1	Xbp1	
Smpx	Svep1	Ticam1	Tnnc2	Tubb2a	Xdh	
Smyd1	Sybu	Ticam2	Tnni2	Tubb4a	Xirp1	
Snai1	Syce1	Tie1	Tnnt3	Tufm	Xirp2	
Sncg	Syk	Tifab	Tnp2	Tusc1	Xk	
Snx18	Syn2	Tigd3	Tns1	Twf2	Xkr6	
Snx3	Syndig1	Timd4	Tnxb	Twist1	Xkrx	
Snx30	Syngr3	Timm10b	Top1mt	Twist2	Xlr4a	
Snx8	Syngr4	Timm17b	Tor3a	Txlnb	Xylb	
Soat2	Synpo2	Timm50	Tpbg	Txndc8	Xylt2	
Sohlh2	Synpr	Timp3	Tph1	Txnip	Yif1b	
Sord	Sypl2	Tk1	Tpi1	Txnl4a	Yipf7	
Sostdc1	Syt17	Tldc2	Tpm2	Tyr	Ypel2	
Sox1	Syt2	Tlnrd1	Tpo	Tyrobp	Ywhag	
Sox14	Syt6	Tlr5	Tppp	Tyrp1	Zar1l	
Sox17	Sytl1	Tlr8	Tpsab1	Ube2c	Zbed4	
Sox18	Syvn1	Tm6sf1	Tpsb2	Ube2g2	Zbtb16	
Sp6	Szrd1	Tmc8	Trabd2b	Ube2l6	Zbtb3	
Sp7	Taar6	Tmcc2	Traf4	Ube2ql1	Zbtb34	
Spaca9	Taar9	Tmed6	Trarg1	Ubl4a	Zbtb5	
Spata32	Tacstd2	Tmeff1	Trdn	Ubl4b	Zbtb7c	
Spata4	Taf10	Tmeff2	Trem2	Ubqln2	Zbtb9	
Spc24	Taf7l	Tmem104	Trem3	Ubtd2	Zcchc12	
Spdye4a	Tafa2	Tmem106a	Treml1	Ubtfl1	Zdhhc14	
Speer4a	Tanc2	Tmem119	Treml4	Ucp2	Zdhhc22	
Speer4b	Taok3	Tmem129	Trex2	Ucp3	Zdhhc23	
Speer4f2	Tap2	Tmem132a	Trf	Ugt1a2	Zfp185	
Spert	Tapbp	Tmem132b	Trhde	Ugt2a2	Zfp213	
Spesp1	Tas2r103	Tmem144	Trhr2	Ugt2a3	Zfp296	
Spg20	Tas2r105	Tmem14c	Trim12c	Ulk4	Zfp36l1	
Spi1	Tas2r120	Tmem150a	Trim14	Umps	Zfp36l2	
Spint2	Tas2r134	Tmem150b	Trim16	Unc45a	Zfp385a	
Spns2	Tbc1d2b	Tmem150c	Trim29	Unc45b	Zfp420	
Spock2	Tbc1d9	Tmem151a	Trim30c	Unc93b1	Zfp423	
Spock3	Tbkbp1	Tmem154	Trim30e-ps1	Uox	Zfp526	
Spon2	Tbx15	Tmem169	Trim32	Upk2	Zfp575	
Spopfm2	Tbx18	Tmem173	Trim46	Upp1	Zfp600	
Spred3	Tbx2	Tmem177	Trim54	Uqcrc1	Zfp612	
Sprr2e	Tbx21	Tmem178	Trim62	Urah	Zfp623	
Sprr2h	Tbx5	Tmem178b	Trim63	Uroc1	Zfp628	
Spsb4	Tbxas1	Tmem182	Trim65	Usf1	Zfp697	
Sptb	Tcap	Tmem184b	Trim67	Ushbp1	Zfp703	
Sptbn2	Tcea3	Tmem185b	Trim75	Usp19	Zfp750	
Sptssb	Tceal3	Tmem189	Triobp	Usp29	Zfp764	
Sqor	Tceal7	Tmem212	Trmo	Usp51	Zfp771	
Srd5a1	Tcf15	Tmem215	Trnp1	Utf1	Zfp979	
Srgn	Tcf19	Tmem229a	Trp63	Uts2b	Zfp981	

Supplementary Table 3 (1/3) | Published gene signatures associated with good response to immune checkpoint inhibitors (ICIs). Human gene symbols and the homologous mouse gene symbols of the indicated published signatures associated with good response to ICIs. log_2FC and -log_{10} P.Value data in *B; p38α* vs. *B* tumors are indicated for each gene. Dark gray cells indicate missing homologous gene in mouse. Light gray cells indicate missing data for the corresponding gene in our model.

Good response to αPD-1 - *Riaz et al., Cell, 2017*

Human gene symbol	Mouse gene symbol	log_2FC	-log_{10} P.Value
CCL16			
CCL4	Ccl4	0.442	0.495
CCL4L			
CCL4L1			
CCL5	Ccl5	0.313	0.253
CCL8	Ccl8	-0.850	0.709
CD2	Cd2	-0.598	0.660
CD247	Cd247	-0.169	0.212
CD3D	Cd3d	0.181	0.161
CD3G	Cd3g	0.168	0.124
CD7	Cd7	0.155	0.113
CD8A	Cd8a	0.192	0.132
CD8B	Cd8b1	0.278	0.242
CHGA	Chga	0.032	0.038
CTLA4	Ctla4	0.409	0.224
CXCL2	Cxcl2	0.067	0.030
CXCL9	Cxcl9	1.170	1.473
CXCR6	Cxcr6	0.564	0.421
DBH	Dbh	0.428	0.603
FASLG	Fasl	0.090	0.109
GBP1	Gbp2b	0.154	0.222
GNLY			
GZMA	Gzma	0.113	0.095
GZMB	Gzmb	0.466	0.423
GZMH			
ICOS	Icos	0.202	0.121
IDO1	Ido1	0.470	1.079
IFNG	Ifng	0.457	0.460
KLRC2	Klrc2	0.262	0.258
LAG3	Lag3	0.524	0.599
LCK	Lck	-0.042	0.034
LILRA3			
MPO	Mpo	-0.284	0.235
PDCD1	Pdcd1	-0.024	0.022
PRF1	Prf1	-0.421	0.441
SIRPG			
SIT1	Sit1	0.030	0.039
SKAP1	Skap1	0.110	0.104
SLA2	Sla2	0.491	0.645
THEMIS	Themis	0.107	0.113
TNFRSF9	Tnfrsf9	0.356	0.410
ZAP70	Zap70	0.155	0.135

Up in responders to αPD-1 - *Gide et al., Cancer cell, 2019*

Human gene symbol	Mouse gene symbol	log_2FC	-log_{10} P.Value
BATF2	Batf2	0.228	0.475
BFSP2	Bfsp2	0.262	0.465
C4orf50			
CD274	Cd274	0.096	0.116
CD38	Cd38	-0.334	0.602
CD7	Cd7	0.155	0.113
CD79A	Cd79a	-0.065	0.054
CD8A	Cd8a	0.192	0.132
CD8B	Cd8b1	0.278	0.242
CXCL10	Cxcl10	0.620	1.140
CXCL11	Cxcl11	0.094	0.099
CXCL13	Cxcl13	0.613	0.282
CXCL9	Cxcl9	1.170	1.473
DBH	Dbh	0.428	0.603
DBH-AS1			
DTHD1	Dthd1	-0.076	0.123
FAIM3	Fcmr	0.091	0.189
FCRL6	Fcrl6	0.227	0.463
FRMPD3	Frmpd3	-0.241	0.336
GFI1	Gfi1	0.015	0.022
GPR114	Adgrg5	0.022	0.024
GZMA	Gzma	0.113	0.095
GZMK	Gzmk	0.070	0.053
HSH2D	Hsh2d	-0.327	0.528
IDO1	Ido1	0.470	1.079
IFNG	Ifng	0.457	0.460
IKZF3	Ikzf3	-0.118	0.072
IL12RB1	Il12rb1	0.241	0.430
IL18RAP	Il18rap	0.229	0.315
IL4I1	Il4i1b	-0.094	0.261
KIR2DL4			
LAG3	Lag3	0.524	0.599
LCK	Lck	-0.042	0.034
NCR1	Ncr1	0.307	0.165
NKG7	Nkg7	0.201	0.128
NLRP7			
NUGGC	Nuggc	-0.425	0.890
P2RY10	P2ry10	0.185	0.135
PDCD1	Pdcd1	-0.024	0.022
PLA2G2D	Pla2g2d	-0.349	0.181
PRF1	Prf1	-0.421	0.441
PYHIN1	Ifi209	0.400	0.283
RLTPR	Carmil2	0.301	0.790
SAMD3	Samd3	0.228	0.254
SIRPG			
SIT1	Sit1	0.030	0.039
SLAMF7	Slamf7	1.093	0.980
SLFN14	Slfn14	-0.101	0.132
SYNGR3	Syngr3	-0.329	0.888
TBX21	Tbx21	-0.378	0.582
TIGIT	Tigit	0.077	0.068
TMPRSS3	Tmprss3	0.274	0.703
TNFRSF9	Tnfrsf9	0.356	0.410
TNIP3	Tnip3	-0.065	0.087
TRAJ1	Traj1		
TRAJ36	Traj36		
TRAJ42	Traj42		
TRAJ43	Traj43		
TRAJ5	Traj5		
TRBV28	Trabv28		
TRBV7-6	Trbv7/Trbv6		
TRGV10			
UBD	Ubd	0.120	0.147
XIRP1	Xirp1	-0.373	1.103
ZBP1	Zbp1	-0.038	0.047
ZNF683	Zfp683		
ZNF831	Zfp831	0.068	0.088

Supplementary Table 3 (2/3) | Published gene signatures associated with good response to immune checkpoint inhibitors (ICIs). Human gene symbols and the homologous mouse gene symbols of the indicated published signatures associated with good response to ICIs. log_2FC and -log_{10} P.Value data in *B; p38α* vs. *B* tumors are indicated for each gene. Dark gray cells indicate missing homologous gene in mouse. Light gray cells indicate missing data for the corresponding gene in our model.

	Human gene symbol	Mouse gene symbol	log_2FC	-log_{10} P.Value
Up in responders to αCTLA-4+αPD-1 - *Gide et al., Cancer cell, 2019*	ABCB1	Abcb1a	-0.380	0.423
	ADAM28	Adam28	0.786	1.872
	AK9	Ak9		
	AMICA1	Jaml	-0.299	0.369
	APOBEC3H			
	APOL1			
	ARRDC5	Arrdc5	0.078	0.123
	BIN2	Bin2	-0.262	0.263
	BIRC3	Birc3	-0.135	0.197
	BTLA	Btla	0.171	0.172
	C10orf131			
	C1orf204			
	C5orf56			
	C7orf31			
	CADM3-AS1			
	CADPS2	Cadps2	0.086	0.127
	CCDC186	Ccdc186	-0.098	0.276
	CCDC69	Ccdc69	-0.175	0.363
	CCL4	Ccl4	0.442	0.495
	CCL5	Ccl5	0.313	0.253
	CCNDBP1	Ccndbp1	0.153	0.277
	CCR5	Ccr5	-0.981	0.989
	CD247	Cd247	-0.169	0.212
	CD274	Cd274	0.096	0.116
	CD38	Cd38	-0.334	0.602
	CD79A	Cd79a	-0.065	0.054
	CD84	Cd84	-0.743	0.861
	CD8A	Cd8a	0.192	0.132
	CD96	Cd96	0.287	0.214
	CDH24	Cdh24	-0.069	0.114
	CLEC4E	Clec4e	-0.144	0.135
	COL20A1	Col20a1	0.326	0.303
	CSMD3	Csmd3	-0.126	0.104
	CSRNP3	Csrnp3	0.169	0.169
	CTSW	Ctsw	0.110	0.088
	CXCL9	Cxcl9	1.170	1.473
	CYTIP	Cytip	0.011	0.008
	DAPP1	Dapp1	-0.195	0.269
	DCHS2	Dchs2		
	DLK1	Dlk1	-1.233	2.165
	EOMES	Eomes	-0.307	0.215
	EPS8L2	Eps8l2	-0.438	0.473
	FAIM3	Fcmr	0.091	0.189
	FAM177B	Fam177b		
	FAM26F	Calhm6	-0.354	0.409
	FAM65B	Ripor2	0.282	0.328
	FASLG	Fasl	0.090	0.109
	FCRL3			
	FDCSP			
	FGR	Fgr	-0.624	0.952
	FMO3	Fmo3	0.583	0.921
	GBP1	Gbp2b	0.154	0.222
	GBP5	Gbp5		
	GCH1	Gch1	-0.586	1.401
	GFOD1	Gfod1	0.414	1.182
	GNAS-AS1			
	GPR114	Adgrg5	0.022	0.024
	GPSM1	Gpsm1	0.000	0.000
	GTF3C5	Gtf3c5	-0.152	0.506
	GZMK	Gzmk	0.070	0.053
	HID1	Hid1	-0.219	0.342
	HLA-F-AS1			
	HS3ST3B1	Hs3st3b1	0.216	0.348
	IGDCC3	Igdcc3	-0.272	0.843
	IGDCC4	Igdcc4	-0.106	0.234
	IKZF1	Ikzf1	-0.303	0.284
	IKZF3	Ikzf3	-0.118	0.072
	IL2RG	Il2rg	-0.279	0.276
	IL32			
	IPCEF1	Ipcef1	0.254	0.244
	ITPR1	Itpr1	0.036	0.048

	Human gene symbol	Mouse gene symbol	log_2FC	-log_{10} P.Value
Up in responders to αCTLA-4+αPD-1 - *Gide et al., Cancer cell, 2019*	JAK2	Jak2	0.260	0.763
	LGR5	Lgr5	-0.114	0.233
	LPHN2	Adgrl2	0.186	0.210
	LRRC18	Lrrc18	0.404	0.610
	LYN	Lyn	-0.069	0.116
	MCTP2	Lynx1	-0.247	0.321
	MMP12	Mctp2	-0.196	0.239
	MTM1	Mmp12	-0.295	0.152
	MUC16	Mtm1	0.374	0.852
	NLRC3	Nlrc3	-0.011	0.017
	NUGGC	Nuggc	-0.425	0.890
	OR2B6	Olfr11	0.020	0.017
	P2RX5	P2rx5	-0.461	0.728
	PATL2	Patl2	0.073	0.098
	PCDH11X	Pcdh11x	0.195	0.265
	PIK3CG	Pik3cg	-0.359	0.330
	PITRM1-AS1			
	PLAC8	Plac8	0.040	0.038
	PLCG2	Plcg2	-0.517	0.524
	PLEKHG1	Plekhg1	-0.029	0.041
	PRKCQ	Prkcq	-0.380	0.418
	PSD4	Psd4	-0.210	0.189
	PTPN22	Ptpn22	0.111	0.064
	PTPRC	Ptprc	-0.157	0.122
	PTTG2	Ptprcap	-0.027	0.037
	RAB11FIP3	Rab11fip3	0.127	0.356
	RASSF5	Rassf5	-0.423	0.778
	RCSD1	Rcsd1	-0.307	0.786
	RELN	Reln	-0.699	0.794
	RFC3	Rfc3	0.108	0.113
	RLTPR	Carmil2	0.301	0.790
	RNF144B	Rnf144b	-0.757	1.496
	SAMD12	Samd12	0.214	0.262
	SAMD3	Samd3	0.228	0.254
	SAMSN1	Samsn1	-0.052	0.030
	SIDT1	Sidt1	0.151	0.194
	SIGLEC6			
	SKAP1	Skap1	0.110	0.104
	SLAMF6	Slamf6	0.484	0.554
	SLAMF7	Slamf7	1.093	0.980
	SLFN12L	Slfn3	0.486	0.460
	SLFN12L	Slfn4	-0.011	0.016
	SLFN13	Slfn8	0.029	0.030
	SLFN13	Slfn9	-0.141	0.215
	SP140	Sp140	-0.098	0.218
	SQRDL	Sqor	-0.322	1.037
	SRSF4	Srsf4	0.018	0.051
	STRA6	Stra6	0.042	0.025
	SUMO4			
	SYTL2	Sytl2	0.829	1.271
	TEAD2	Tead2	0.016	0.018
	TESPA1	Tespa1	0.014	0.011
	TIGIT	Tigit	0.077	0.068
	TLX2	Tlx2	-0.047	0.110
	TMEM62	Tmem62	-0.054	0.124
	TMEM71	Tmem71	0.191	0.168
	TNFAIP3	Tnfaip3	0.076	0.048
	TNFRSF9	Tnfrsf9	0.356	0.410
	TRBC2	Trbc2		
	TRBV25-1	Trbv25		
	TRBV28	Trbv28		
	TRGC2	Trgc2		
	TRGV5	Trgv5		
	TRIM22			
	TRIM36	Trim36	0.177	0.294
	TSPAN7	Tspan7	0.327	0.533
	TTC24	Ttc24	-0.386	0.960
	UBASH3A	Ubash3a	0.013	0.015
	WWC1	Wwc1	0.370	0.305
	ZBP1	Zbp1	-0.038	0.047
	ZNF831	Zfp831	0.068	0.088

Supplementary Table 3 (3/3) | Published gene signatures associated with good response to immune checkpoint inhibitors (ICIs). Human gene symbols and the homologous mouse gene symbols of the indicated published signatures associated with good response to ICIs. log_2FC and $-log_{10}$ P.Value data in *B; p38α* vs. *B* tumors are indicated for each gene. Dark gray cells indicate missing homologous gene in mouse. Light gray cells indicate missing data for the corresponding gene in our model.

	Human gene symbol	Mouse gene symbol	log_2FC	$-log_{10}$ P.Value
Expanded IFNγ signature - *Ayers at al., JCI, 2017*	CCL5	Ccl5	0.313	0.253
	CD2	Cd2	-0.598	0.660
	CD3D	Cd3d	0.181	0.161
	CD3E	Cd3e	-0.054	0.034
	CIITA	Ciita	-0.344	0.346
	CXCL10	Cxcl10	0.620	1.140
	CXCL13	Cxcl13	0.613	0.282
	CXCL9	Cxcl9	1.170	1.473
	CXCR6	Cxcr6	0.564	0.421
	GZMB	Gzmb	0.466	0.423
	GZMK	Gzmk	0.070	0.053
	HLA-DRA	H2-Ea-ps	-1.118	0.381
	HLA-E	H2-T23	-0.280	0.306
	IDO1	Ido1	0.470	1.079
	IFNG	Ifng	0.457	0.460
	IL2RG	Il2rg	-0.279	0.276
	LAG3	Lag3	0.524	0.599
	NKG7	Nkg7	0.201	0.128
	STAT1	Stat1	0.053	0.079
	TAGAP	Tagap	0.349	0.345
Good response to αCTLA-4+αPD-1 - *Chen at al., Cancer Disc., 2016*	ACTB	Actb	-0.132	0.494
	AMIGO3	Amigo3	0.085	0.134
	ANGPT4	Angpt4	-0.800	1.347
	ARG2	Arg2	-0.137	0.114
	CALR	Calr	-0.279	1.221
	CCL25	Ccl25	0.019	0.040
	CD74	Cd74	-0.155	0.091
	CEACAM16	Ceacam16	0.029	0.046
	CTSB	Ctsb	-0.379	1.655
	CTSS	Ctss	-0.262	0.213
	CXCL12	Cxcl12	-0.715	0.800
	EPHA6	Epha6	0.119	0.174
	GRN	Grn	-0.671	2.153
	HLA-B			
	HLA-C			
	HLA-DMA	H2-Dma	-0.261	0.214
	HLA-DPA1			
	HLA-DPB1			
	HLA-DQA2			
	HLA-DQB1	H2-Ab1	-0.285	0.172
	HLA-DRA	H2-Ea-ps	-1.118	0.381
	HLA-DRB1			
	HLA-E	H2-T23	-0.280	0.306
	IFNA14	Ifna14	0.366	0.825
	IFNA16	Ifna16	0.186	0.414
	IL1F6	Il1f6	0.282	0.780
	IL23A	Il23a	-0.026	0.028
	MMP20	Mmp20	0.275	0.810
	MMP21	Mmp21	0.164	0.269
	OGDHL	Ogdhl	0.407	0.915
	S100A5	S100a5	0.082	0.129
	S100Z	S100z	0.177	0.243
	SSTR2	Sstr2	-0.127	0.130
	TIMP3	Timp3	-0.351	0.770
	TRIM46	Trim46	-0.339	0.630
	VTN	Vtn	0.301	0.236

Supplementary Table 4 (1/3) | Published gene signatures associated with bad response to immune checkpoint inhibitors (ICIs). Human gene symbols and the homologous mouse gene symbol of the indicated published gene signatures associated with bad response to ICIs. log_2FC and -log_{10} P.Value data in *B; p38α* vs. *B* tumors are indicated for each gene. Dark gray cells indicate missing homologous gene in mouse. Light gray cells indicate missing data for the corresponding gene in our model.

	Human gene symbol	Mouse gene symbol	log_2FC	-log_{10} P.Value
TIDE - *Jiang et al., Nat. Med., 2018*	ABCC3	Abcc3	-0.558	0.631
	ACRBP	Acrbp	0.041	0.084
	ACTN3	Actn3	-1.308	1.988
	ACY3	Acy3	-0.051	0.070
	ADAM19	Adam19	0.085	0.113
	ADGRG5	Adgrg5	0.022	0.024
	ALOX5AP	Alox5ap	-0.895	1.608
	AMPD3	Ampd3	-0.434	0.535
	ANKRD29	Ankrd29	-0.228	0.415
	ANTXR2	Antxr2	-0.001	0.003
	APBB1IP	Apbb1ip	-0.344	0.504
	ARHGAP22	Arhgap22	0.497	0.694
	ARHGAP25	Arhgap25	-0.055	0.050
	ARHGAP30	Arhgap30	-0.786	1.223
	ARHGAP45	Arhgap45	-0.630	0.944
	ARL4C	Arl4c	-0.192	0.530
	ASPN	Aspn	-0.345	0.482
	ATP9B	Atp9b	0.138	0.349
	AXL	Axl	-0.173	0.447
	B3GALT5	B3galt5	1.166	1.756
	BASP1	Basp1	-0.606	0.756
	BCL9L	Bcl9l	-0.153	0.263
	BLNK	Blnk	-0.285	0.328
	BMF	Bmf	-0.048	0.098
	C10orf54	Vsir	-0.558	1.159
	C14orf159	Dglucy	0.102	0.151
	C16orf54	AI467606	-0.450	0.540
	C18orf8	Rmc1	-0.002	0.004
	C20orf197			
	C2CD2L	C2cd2l	-0.182	0.401
	C3AR1	C3ar1	-0.120	0.073
	C5AR2	C5ar2	-0.374	0.586
	C7orf34	Llcfc1	-0.190	0.326
	CALHM2	Calhm2	-0.163	0.368
	CBL	Cbl	-0.207	0.514
	CCDC69	Ccdc69	-0.175	0.363
	CCIN	Ccin	-0.172	0.218
	CCL22	Ccl22	-0.615	0.650
	CCL24	Ccl24	-0.784	0.975
	CCRL2	Ccrl2	0.118	0.086
	CD14	Cd14	-0.019	0.013
	CD180	Cd180	-0.051	0.042
	CD1B			
	CD1E			
	CD300C	Cd300c	-0.008	0.013
	CD300LF	Cd300lf	0.043	0.074
	CD37	Cd37	-0.868	1.008
	CD4	Cd4	-0.057	0.055
	CD5	Cd5	0.811	1.156
	CD6	Cd6	-0.230	0.222
	CHST15	Chst15	-0.751	1.722
	CHST2	Chst2	-0.126	0.160
	CLMP	Clmp	0.284	0.565
	CMKLR1	Cmklr1	-0.289	0.293
	CMTM3	Cmtm3	-0.195	0.471
	CNGA3	Cnga3	0.251	0.417
	COL10A1	Col10a1	0.721	0.671
	COL8A2	Col8a2	-0.239	0.649
	CSF1Z			
	CXCL12	Cxcl12	-0.715	0.800
	CXCL16	Cxcl16	0.011	0.008
	CYTH4	Cyth4	-0.438	0.445
	DENND3	Dennd3	0.308	0.595
	DIAPH1	Diaph1	-0.340	1.098
	DIRC1			
	DNAH5	Dnah5	0.130	0.240
	DNAJC5B	Dnajc5b	-0.028	0.023
	DOK1	Dok1	-0.501	0.950
	DOK2	Dok2	-1.838	2.605
	EHBP1L1	Ehbp1l1	-0.209	0.408
	ELF4	Elf4	-0.579	1.007
	ELMO1	Elmo1	-0.417	1.158
	FAM171A1	Fam171a1	-0.102	0.176
	FAM20C	Fam20c	-0.003	0.005
	FAM30A			

	Human gene symbol	Mouse gene symbol	log_2FC	-log_{10} P.Value
TIDE - *Jiang et al., Nat. Med., 2018*	FAM46C	Tent5c	0.113	0.149
	FCHO1	Fcho1	0.143	0.139
	FERMT3	Fermt3	-0.741	0.686
	FGD3	Fgd3	-0.401	0.676
	FGF1	Fgf1	0.356	0.286
	FILIP1L	Filip1l	0.313	0.468
	FMNL3	Fmnl3	0.169	0.533
	FOLR2	Folr2	-1.558	1.567
	FUCA1	Fuca1	0.025	0.054
	GPR68	Gpr68	0.096	0.115
	GRK2	Grk2	-0.482	1.497
	HCK	Hck	-0.364	0.494
	HCLS1	Hcls1	-0.464	0.459
	HLA-C			
	HLA-DMA	H2-DMa	-0.261	0.214
	HLA-DPB1			
	HLA-DRB1			
	HLA-DRB5	H2-Eb1	0.028	0.011
	HSH2D	Hsh2d	-0.327	0.528
	HTRA1	Htra1	-0.106	0.095
	HVCN1	Hvcn1	0.165	0.278
	IKZF1	Ikzf1	-0.303	0.284
	IL17F	Il17f	0.369	0.677
	IL21R	Il21r	-0.084	0.087
	IL4R	Il4ra	-0.757	1.319
	INPP5D	Inpp5d	-0.410	0.463
	ITGA5	Itga5	-0.286	0.425
	ITGAL	Itgal	-0.214	0.209
	ITGAM	Itgam	-0.719	0.689
	ITGB2	Itgb2	-0.919	1.187
	JAML	Jaml	-0.299	0.369
	KCNA3	Kcna3	0.328	0.449
	KCNMA1	Kcnma1	-0.316	0.213
	KIF21B	Kif21b	0.058	0.086
	KLF13	Klf13	-0.318	0.803
	KLRB1	Klrb1	0.297	0.508
	LAIR1	Lair1	0.483	0.438
	LAPTM5	Laptm5	-0.853	0.831
	LAT	Lat	0.291	0.360
	LGALS2	Lgals2	0.943	1.292
	LGALS9	Lgals9	-0.107	0.205
	LGMN	Lgmn	-0.434	1.857
	LILRB4	Lilrb4a	-0.410	0.313
	LIMK1	Limk1	-0.270	0.743
	LINGO3	Lingo3	-0.102	0.139
	LOC145474			
	LPXN	Lpxn	-0.167	0.143
	LRRC15	Lrrc15	-0.925	0.925
	LRRC25	Lrrc25	-1.004	1.045
	LTBP2	Ltbp2	0.112	0.062
	LY9	Ly9	-0.078	0.070
	MAFB	Mafb	-0.494	0.708
	MBD1	Mbd1	0.003	0.009
	MFNG	Mfng	-0.352	0.758
	MGLL	Mgll	-0.287	0.302
	MID1IP1	Mid1ip1	-0.166	0.570
	MILR1	Milr1	-0.128	0.126
	MLKL	Mlkl	0.003	0.008
	MMP9	Mmp9	-0.630	0.778
	MPEG1	Mpeg1	-0.102	0.072
	MRGPRF	Mrgprf	-0.418	0.709
	MYO1F	Myo1f	-0.525	0.824
	NAAA	Naaa	-0.434	0.789
	NCF1	Ncf1	-0.605	0.748
	NCF1B			
	NCF1C			
	NCF4	Ncf4	-0.578	0.600
	NCKAP1L	Nckap1l	-0.471	0.472
	NFATC3	Nfatc3	0.061	0.148
	NLRP3	Nlrp3	-0.155	0.102
	NR1H3	Nr1h3	-0.579	1.271
	NT5E	Nt5e	0.803	0.554
	P2RY8			
	PCOLCE	Pcolce	-0.637	1.197
	PDPN	Pdpn	-0.264	0.421

Supplementary Table 4 (2/3) | Published gene signatures associated with bad response to immune checkpoint inhibitors (ICIs). Human gene symbols and the homologous mouse gene symbol of the indicated published gene signatures associated with bad response to ICIs. log_2FC and $-log_{10}$ P.Value data in *B; p38α* vs. *B* tumors are indicated for each gene. Dark gray cells indicate missing homologous gene in mouse. Light gray cells indicate missing data for the corresponding gene in our model.

	Human gene symbol	Mouse gene symbol	log_2FC	$-log_{10}$ P.Value
TIDE - *Jiang et al., Nat. Med., 2018*	PIK3R6	Pik3r6	-0.818	1.573
	PILRA	Pilra	0.240	0.348
	PIM1	Pim1	-0.174	0.185
	PIM2	Pim2	0.108	0.134
	PLAU	Plau	-0.308	0.508
	PLAUR	Plaur	0.221	0.233
	PLCG2	Plcg2	-0.517	0.524
	PLCL2	Plcl2	-0.367	0.605
	PODNL1	Podnl1	-0.445	0.498
	POU2AF1	Pou2af1	-0.016	0.016
	POU2F2	Pou2f2	-0.060	0.075
	PRR5L	Prr5l	-0.104	0.138
	PSD4	Psd4	-0.210	0.189
	PTAFR	Ptafr	-0.925	1.313
	PTK2B	Ptk2b	-0.148	0.154
	PVRIG	Pvrig		
	RAC2	Rac2	-0.818	0.954
	RASA4	Rasa4	0.019	0.022
	RHOF	Rhof	-0.124	0.155
	RNASE6	Rnase6	0.089	0.102
	RNF166	Rnf166	-0.042	0.065
	S100A16	S100a16	0.062	0.077
	S1PR4	S1pr4	0.066	0.100
	SASH3	Sash3	-0.555	0.740
	SELM	Selenom	-0.290	0.977
	SELPLG	Selplg	-0.638	0.800
	SEMA6B	Sema6b	-0.274	1.154
	SERPINA1	Serpina1a	-3.333	3.476
	SERPINA1	Serpina1b	-3.243	2.858
	SERPINA1	Serpina1c	-0.738	1.226
	SERPINA1	Serpina1d	-0.087	0.079
	SERPINA1	Serpina1e	-1.453	2.160
	SERPINA1	Serpina1f	0.258	0.418
	SIGLEC1	Siglec1	-1.410	1.692
	SIGLEC9	Siglec15	-0.178	0.376
	SIK3	Sik3	0.309	0.535
	SIRPB2			
	SLC12A6	Slc12a6		
	SLC12A8	Slc12a8	-0.531	0.956
	SLC43A2	Slc43a2	-0.676	1.728
	SLC7A7	Slc7a7	-0.647	1.671
	SLCO2B1	Slco2b1	-0.221	0.292
	SNX33	Snx33	-0.004	0.006
	SPI1	Spi1	-0.729	0.604
	SPN	Spn	0.175	0.217
	SPOCK2	Spock2	-0.749	1.136
	SUN2	Sun2	-0.215	0.477
	SYNDIG1	Syndig1	-0.555	0.705
	SYNJ2	Synj2	-0.172	0.360
	TBL1X	Tbl1x	-0.211	0.838
	TBXAS1	Tbxas1	-0.463	0.397
	TGFB1	Tgfb1	-0.312	0.629
	TGFBI	Tgfbi	0.197	0.382
	TLE3	Tle3	-0.081	0.146
	TMEM130	Tmem130	0.213	0.258
	TNFRSF1B	Tnfrsf1b	-0.376	0.651
	TNFRSF8	Tnfrsf8	-0.159	0.308
	TOX2	Tox2	-0.171	0.457
	TPD52L2	Tpd52l2	0.074	0.171
	TRERF1	Trerf1	0.107	0.192
	TRIM14	Trim14	-0.396	0.495
	TRIM8	Trim8	-0.073	0.177
	TTC7A	Ttc7	-0.470	1.268
	TXNDC11	Txndc11	0.272	0.625
	UBE2J1	Ube2j1	-0.170	0.611
	VAV1	Vav1	-0.127	0.096
	VOPP1	Vopp1	-0.141	0.224
	WDFY4	Wdfy4	-0.389	0.599
	WNT1	Wnt1	0.097	0.177
	XBP1	Xbp1	-0.366	1.297
	ZBTB32	Zbtb32	0.005	0.009
	ZBTB7A	Zbtb7a	-0.235	0.733
	ZMYND15	Zmynd15	0.223	0.286
	ZYX	Zyx	-0.232	0.351

	Human gene symbol	Mouse gene symbol	log_2FC	$-log_{10}$ P.Value
Up in resistant to αPD-1 – *Gide et al., Cancer cell, 2019*	AADAC	Aadac	-0.034	0.040
	CA9	Car9	-0.249	0.544
	GABRA2	Gabra2	0.046	0.061
	GRIA2	Gria2	-0.138	0.197
	GRIA4	Gria4	0.216	0.237
	GRIK3	Grik3	0.950	0.467
	ITIH5	Itih5	0.135	0.291
	LAMB4			
	NDST3	Ndst3	0.853	1.780
	RP1	Rp1	0.865	1.090
	SYTL5	Sytl5	0.010	0.010
	TMEM246	Tmem246	-0.384	0.552
	WNT3	Wnt3	0.046	0.087
Up in resistant to αCTLA-4+αPD-1 – *Gide et al., Cancer cell, 2019*	ANKRD22	Ankrd22	0.153	0.174
	CCDC64	Bicdl1	-0.015	0.025
	CDC42SE2	Cdc42se2	0.204	0.712
	CP	Cp	0.060	0.061
	DPH7	Dph7	0.137	0.383
	IRF1	Irf1	0.082	0.188
	SSFA2	Itprid2	0.220	0.577
	MEX3A	Mex3a	-0.087	0.135
	NABP1	Nabp1	-0.712	1.201
	P2RY13	P2ry13	0.244	0.354
	PHF21B	Phf21b	-0.284	0.574
	SLC12A3	Slc12a3	-0.606	1.743
	SOX11	Sox11	-0.213	0.408
	TRIL	Tril	0.214	0.203
	TSPAN33	Tspan33	0.066	0.093
IPRES - *Hugo et al., Cell, 2016*	AXL	Axl	-0.173	0.447
	CCL13			
	CCL2	Ccl2	0.072	0.063
	CCL7	Ccl7	-0.063	0.046
	CCL8	Ccl8	-0.850	0.709
	FAP	Fap	0.023	0.019
	IL10	Il10	0.003	0.002
	LOXL2	Loxl2	-0.033	0.035
	ROR2	Ror2	-0.094	0.142
	TAGLN	Tagln	0.104	0.063
	TWIST2	Twist2	-1.165	1.856
	VEGFA	Vegfa	0.323	0.545
	VEGFC	Vegfc	-0.224	0.529
	WNT5A	Wnt5a	-0.250	0.381
Up in resistant to αPD-1 - *Ascierto et al. Clin. Can.Res., 2017*	ARNT2	Arnt2	0.324	0.372
	CCM2L	Ccm2l	-0.489	0.680
	CST2			
	CXCR2	Cxcr2	-0.050	0.055
	DACT1	Dact1	-0.177	0.195
	DSC1	Dsc1	-1.114	0.736
	DSC3	Dsc3	-0.768	0.396
	EXO1	Exo1	-0.015	0.011
	FAM183B	Fam183b	0.483	0.957
	FLG2	Flg2	0.163	0.231
	GUSB	Gusb	-0.320	0.967
	KLK7	Klk7	-0.218	0.222
	KRT1	Krt1	-0.014	0.020
	KRT10	Krt10	0.165	0.212
	KRT15	Krt15	-0.066	0.046
	KRT5	Krt5	-0.085	0.031
	KRT78	Krt78	0.113	0.183
	LAMA3	Lama3	-0.360	0.358
	LGALS7	Lgals7	-0.222	0.234
	LOR	Lor	-0.106	0.173
	LOXL4	Loxl4	0.173	0.234
	NDUFA4L2	Ndufa4l2	-0.544	0.599
	PTPRC	Ptprc	-0.157	0.122
	SBSN	Sbsn	-0.651	1.123
	TSLP	Tslp	-0.595	0.888
	WNT3	Wnt3	0.046	0.087
	WNT5A	Wnt5a	-0.250	0.381

Supplementary Table 4 (3/3) | Published gene signatures associated with bad response to immune checkpoint inhibitors (ICIs). Human gene symbols and the homologous mouse gene symbol of the indicated published gene signatures associated with bad response to ICIs. log_2FC and -log_{10} P.Value data in *B; p38α* vs. *B* tumors are indicated for each gene. Dark gray cells indicate missing homologous gene in mouse. Light gray cells indicate missing data for the corresponding gene in our model.

T cell-induced CSF1 resistance signature - *Neubert et al., Sci. Trans. Med. 2018*

Human gene symbol	Mouse gene symbol	log_2FC	-log_{10} P.Value
ACSL1	Acsl1	-0.402	0.583
ADAP2	Adap2	-0.362	0.518
AIF1	Aif1	-0.051	0.024
APOC1	Apoc1	-1.025	1.927
BCL2A1	Bcl2a1a	0.554	0.621
BCL2A1	Bcl2a1b	0.546	0.467
BCL2A1	Bcl2a1c	0.115	0.113
BCL2A1	Bcl2a1d	0.693	0.713
C1QA	C1qa	-0.664	0.564
C1QB	C1qb	-0.553	0.380
C1QC	C1qc	-0.862	0.829
C3AR1	C3ar1	-0.120	0.073
C5AR1	C5ar1	-1.387	2.374
CCR1	Ccr1	-0.402	0.346
CD14	Cd14	-0.019	0.013
CD163	Cd163	-1.504	1.773
CD300E	Cd300e	-0.382	0.585
CD68	Cd68	-1.278	1.508
CD86	Cd86	-0.157	0.125
CLEC4A	Clec4a2	-0.209	0.154
CLEC7A	Clec7a	0.465	0.346
CPVL	Cpvl	0.063	0.080
CSF1R	Csf1r	-0.659	0.625
CSF3R	Csf3r	-0.353	0.349
CSTA	Csta1	-0.427	0.481
CXCL16	Cxcl16	0.011	0.008
F13A1	F13a1	-1.697	2.025
FCER1G	Fcer1g	-0.826	0.708
FCGR1A	Fcgr1	-0.321	0.305
FCGR1B			
FCGR1C			
FCGR2A	Fcgr3	-0.355	0.358
FCGR3A	Fcgr4	-0.051	0.033
FGL2	Fgl2	0.048	0.037
FGR	Fgr	-0.624	0.952
FRPR1			
FRR3			
FTL	Ftl1	-0.468	2.494
GK	Gk	0.529	1.223
GLUL	Glul	-0.824	1.856
GPX1	Gpx1	-0.342	1.195
HCK	Hck	-0.364	0.494
HK3	Hk3	-0.329	0.756
IFI30	Ifi30	-0.592	1.044
IL18	Il18	-0.407	0.629
IL4L1	Il4i1b	-0.094	0.261
ISGF6			
ITGAM	Itgam	-0.719	0.689
ITGAX	Itgax	0.503	0.451
LILRA1			
LILRA5	Lilra5	-0.296	0.383
LILRA6	Lilra6	-0.566	0.676
LILRB2			
LILRB4	Lilrb4a	-0.410	0.313
LIPA	Lipa	-0.327	0.979
LRRC25	Lrrc25	-1.004	1.045
LST1	Lst1	-0.056	0.040
LYZ	Lyz1	-1.373	2.064
LYZ	Lyz2	-0.647	0.508
MAFB	Mafb	-0.494	0.708
MNDA	Mndal	-0.113	0.114
MS4A4A	Ms4a4a	-0.939	0.759
MS4A6A	Ms4a6b	-0.533	0.550
MS4A6A	Ms4a6c	-0.755	0.951
MS4A6A	Ms4a6d	-0.973	1.186
MS4A7	Ms4a7	-0.290	0.235
MSR1	Msr1	-0.616	0.943
NCF2	Ncf2	-0.832	1.175
NINJ1	Ninj1	-0.582	1.674
NLRP3	Nlrp3	-0.155	0.102
NPL	Npl	-0.662	1.243
OLR1	Olr1	-0.147	0.142
PILRA	Pilra	0.240	0.348
PLAUR	Plaur	0.221	0.233
PLBD1	Plbd1	-0.302	0.211

T cell-induced CSF1 resistance signature – *Neubert et al., Sci. Trans. Med. 2018*

Human gene symbol	Mouse gene symbol	log_2FC	-log_{10} P.Value
PLIN2	Plin2	-0.538	1.722
PTAFR	Ptafr	-0.925	1.313
RAB20	Rab20	0.150	0.211
RASSF4	Rassf4	-0.089	0.148
RNF144B	Rnf144b	-0.757	1.496
S100A9	S100a9	-0.264	0.193
SERPINA1	Serpina1a	-3.333	3.476
SERPINA1	Serpina1b	-3.243	2.858
SERPINA1	Serpina1c	-0.738	1.226
SERPINA1	Serpina1d	-0.087	0.079
SERPINA1	Serpina1e	-1.453	2.160
SERPINA1	Serpina1f	0.258	0.418
SIGLEC1	Siglec1	-1.410	1.692
SIGLEC9			
SIRPB1	Sirpb1a/b/c		
SLAMF8	Slamf8	-0.220	0.181
SLC11A1	Slc11a1	-0.670	0.812
SLC31A2	Slc31a2	-0.005	0.005
SLC7A7	Slc7a7	-0.647	1.671
SLCO2B1	Slco2b1	-0.221	0.292
SPP1	Spp1	0.684	0.612
TBXAS1	Tbxas1	-0.463	0.397
TLR2	Tlr2	-0.070	0.073
TNFSF13	Tnfsf13b	0.166	0.151
TYMP	Tymp		
TYROBP	Tyrobp	-0.566	0.564
VSIG4	Vsig4	-0.886	0.916

Bad response to αPD-1 - *Riaz et al., Cell, 2017*

Human gene symbol	Mouse gene symbol	log_2FC	-log_{10} P.Value
ALX1	Alx1	0.178	0.168
BCAN	Bcan	-0.719	1.371
CITED1	Cited1	-0.799	1.015
DCT	Dct	-0.707	0.454
DLL3	Dll3	-0.338	0.502
DNER	Dner	0.269	0.360
DPF1	Dpf1	0.007	0.009
EN2	En2	-0.323	0.834
EPHA5	Epha5	0.187	0.333
ETV4	Etv4	0.279	0.329
FABP	Fabp1	-0.157	0.216
FABP7	Fabp7	0.281	0.275
FMN2	Fmn2	-1.204	1.454
FSTL4	Fstl4	0.348	0.784
GABRB3	Gabrb3	0.144	0.101
GPR143	Gpr143	0.304	0.639
HCN1	Hcn1	0.045	0.044
HILS1	Hils1	0.077	0.088
MAGEC1			
MCOLN3	Mcoln3	0.495	1.250
MDGA2	Mdga2	0.577	0.937
MLANA	Mlana	-0.442	0.522
MYH14	Myh14	0.560	1.362
MYT1	Myt1	-0.307	0.471
NRG3	Nrg3	0.574	1.231
NYAP	Nyap1	-0.160	0.272
NYAP1	Nyap2	0.082	0.113
PAX3	Pax3	0.122	0.102
PRAME	Prame	0.073	0.084
RGS20	Rgs20	-0.053	0.073
RIMS2	Rims2	0.257	0.785
S100A1	S100a1	-0.466	0.626
SLC45A2	Slc45a2	-0.496	0.594
SLC6A17	Slc6a17	0.384	0.915
SOX10	Sox10	0.181	0.240
SOX6	Sox6	0.541	0.819
TEX15	Tex15	-0.039	0.077
TFAP2A	Tfap2a	-0.444	0.678
TYR	Tyr	-0.491	0.519
TYRP1	Tyrp1	-0.600	0.372
ZIC2	Zic2	0.044	0.074

BIBLIOGRAPHY

1. World Health Organization. https://www.who.int.
2. Esteva, A. *et al.* Dermatologist-level classification of skin cancer with deep neural networks. *Nature* **542**, 115–118 (2017).
3. National Health Service (NHS). https://www.nhs.uk.
4. American Cancer Society. https://www.cancer.org.
5. Apalla, Z., Nashan, D., Weller, R. B. & Castellsagué, X. Skin Cancer: Epidemiology, Disease Burden, Pathophysiology, Diagnosis, and Therapeutic Approaches. *Dermatol Ther (Heidelb)* **7**, 5–19 (2017).
6. Bolick, N. L. & Geller, A. C. Epidemiology of Melanoma. *Hematol Oncol Clin North Am* **35**, 57–72 (2021).
7. Sung, H. *et al.* Global Cancer Statistics 2020: GLOBOCAN Estimates of Incidence and Mortality Worldwide for 36 Cancers in 185 Countries. *CA Cancer J Clin* **71**, 209–249 (2021).
8. European Cancer Information System (ECIS). https://ecis.jrc.ec.europa.eu/.
9. Schwartz, M. R., Luo, L. & Berwick, M. Sex Differences in Melanoma. *Curr Epidemiol Rep* **6**, 112–118 (2019).
10. Rastrelli, M., Tropea, S., Rossi, C. R. & Alaibac, M. Melanoma: Epidemiology, Risk Factors, Pathogenesis, Diagnosis and Classification. *In Vivo (Brooklyn)* **28**, 1005–1012 (2014).
11. Davis, L. E., Shalin, S. C. & Tackett, A. J. Current state of melanoma diagnosis and treatment. *Cancer Biol Ther* **20**, 1366–1379 (2019).
12. National Cancer Institute Melanoma of the Skin — Cancer Stat Facts. https://seer.cancer.gov/statfacts/html/melan.html.
13. De Fabo, E. C., Noonan, F. P., Fears, T. & Merlino, G. Ultraviolet B but not ultraviolet A radiation initiates melanoma. *Cancer Res* **64**, 6372–6376 (2004).
14. Sample, A. & He, Y.-Y. Mechanisms and prevention of UV-induced melanoma. *Photodermatol Photoimmunol Photomed* **34**, 13–24 (2018).
15. Emri, G. *et al.* Ultraviolet radiation-mediated development of cutaneous melanoma: An update. *J Photochem Photobiol B* **185**, 169–175 (2018).
16. Shah, P. & He, Y.-Y. Molecular Regulation of UV-Induced DNA Repair. *Photochem Photobiol* **91**, 254–264 (2015).
17. de Jager, T. L., Cockrell, A. E. & Du Plessis, S. S. Ultraviolet Light Induced Generation of Reactive Oxygen Species. *Adv Exp Med Biol* **996**, 15–23 (2017).
18. Mark Elwood, J. & Jopson, J. Melanoma and sun exposure: An overview of published studies. *Int J Cancer* **73**, 198–203 (1997).
19. Oliveria, S. A., Saraiya, M., Geller, A. C., Heneghan, M. K. & Jorgensen, C. Sun exposure and risk of melanoma. *Arch Dis Child* **91**, 131 (2006).
20. Whiteman, D. C., Whiteman, C. A. & Green, A. C. Childhood sun exposure as a risk factor for melanoma: a systematic review of epidemiologic studies. *Cancer Causes Control* **12**, 69–82 (2001).
21. Li, Y., Wu, J. & Cao, Z. Childhood sunburn and risk of melanoma and non-melanoma skin cancer: a Mendelian randomization study. *Environ Sci Pollut Res Int* **30**, 122011–122023 (2023).
22. Lergenmuller, S. *et al.* Lifetime Sunburn Trajectories and Associated Risks of Cutaneous Melanoma and Squamous Cell Carcinoma Among a Cohort of Norwegian Women. *JAMA Dermatol* **158**, 1367–1377 (2022).
23. Green, A. *et al.* The association of use of sunbeds with cutaneous malignant melanoma and other skin cancers: A systematic review. *Int J Cancer* **120**, 1116–1122 (2007).
24. Lazovich, D. *et al.* Indoor tanning and risk of melanoma: a case-control study in a highly exposed population. *Cancer Epidemiology, Biomarkers & Prevention* **19**, 1557–1568 (2010).
25. Dessinioti, C., Antoniou, C., Katsambas, A. & Stratigos, A. J. Melanocortin 1 receptor variants: Functional role and pigmentary associations. *Photochem Photobiol* **87**, 978–987 (2011).
26. Mort, R. L., Jackson, I. J. & Patton, E. E. The melanocyte lineage in development and disease. *Development* **142**, 620–632 (2015).
27. Rees, J. L. Genetics of Hair and Skin Color. *Annu Rev Genet* **37**, 67–90 (2003).
28. Bevona, C. *et al.* Cutaneous Melanomas Associated with Nevi. *Arch Dermatol* **139**, 1620–1624 (2003).
29. Gandini, S. *et al.* Meta-analysis of risk factors for cutaneous melanoma: I. Common and atypical naevi. *Eur J Cancer* **41**, 28–44 (2005).
30. Soura, E., Eliades, P., Shannon, K., Stratigos, A. & Tsao, H. Hereditary Melanoma: Update on Syndromes and Management - Genetics of familial atypical multiple mole melanoma syndrome. *J Am Acad Dermatol.* **74**, 395–407 (2017).
31. Rabbie, R., Ferguson, P., Molina-Aguilar, C., Adams, D. J. & Robles-Espinoza, C. D. Melanoma subtypes: genomic profiles, prognostic molecular markers and therapeutic possibilities. *Journal of Pathology* **247**, 539–551 (2019).
32. Sharouni, M.-A. El *et al.* Subtyping Cutaneous Melanoma Matters. *JNCI Cancer Spectr* **4**, (2020).

33. Clark Jr., W. H., From, L., Bernardino, E. A. & Mihm, M. C. The Histogenesis and Biologic Behavior of Primary Human Malignant Melanomas of the Skin. *Cancer Res* **29**, 705–726 (1969).
34. Miller, A. J. & Mihm, M. C. Melanoma. *N Engl J Med* **355**, 51–65 (2006).
35. Shain, A. H. & Bastian, B. C. From melanocytes to melanomas. *Nat Rev Cancer* **16**, 345–358 (2016).
36. Pollock, P. M. *et al.* High frequency of BRAF mutations in nevi. *Nat Genet* **33**, 19–20 (2003).
37. Michaloglou, C. *et al.* BRAFE600-associated senescence-like cell cycle arrest of human naevi. *Nature* **436**, 720–724 (2005).
38. Shain, A. H. & Bastian, B. C. From melanocytes to melanomas. *Nat Rev Cancer* **16**, 345–358 (2016).
39. Gershenwald, J. E. & Scolyer, R. A. Melanoma Staging: American Joint Committee on Cancer (AJCC) 8th Edition and Beyond. *Ann Surg Oncol* **25**, 2105–2110 (2018).
40. The Cancer Genome Atlas Network. Genomic Classification of Cutaneous Melanoma. *Cell* **161**, 1681–1696 (2015).
41. Hayward, N. K. *et al.* Whole-genome landscapes of major melanoma subtypes. *Nature 2017 545:7653* **545**, 175–180 (2017).
42. Sabbah, M. *et al.* RTK Inhibitors in Melanoma: From Bench to Bedside. *Cancers (Basel)* **13**, 1685 (2021).
43. Van Raamsdonk, C. D. *et al.* Frequent somatic mutations of GNAQ in uveal melanoma and blue nevi HHS Public Access. *Nature* **457**, 599–602 (2009).
44. Inamdar, G. S., Madhunapantula, S. V & Robertson, G. P. Targeting the MAPK Pathway in Melanoma: Why some approaches succeed and other fail. *Biochem Pharmacol* **80**, 624–637 (2010).
45. Ascierto, P. A. *et al.* The role of BRAF V600 mutation in melanoma. *J Transl Med* **10**, (2012).
46. Wan, P. T. C. *et al.* Mechanism of activation of the RAF-ERK signaling pathway by oncogenic mutations of B-RAF. *Cell* **116**, 855–867 (2004).
47. Fedorenko, I. V, Gibney, G. T. & Smalley, K. S. M. NRAS mutant melanoma: biological behavior and future strategies for therapeutic management. *Oncogene* **32**, 3009–3018 (2013).
48. Kiuru, M. & Busam, K. J. The NF1 gene in tumor syndromes and melanoma. *Laboratory Investigation* **97**, 146–157 (2017).
49. Handolias, D. *et al.* Mutations in KIT occur at low frequency in melanomas arising from anatomical sites associated with chronic and intermittent sun exposure. *Pigment Cell Melanoma Res* **23**, 210–215 (2010).
50. Davies, M. A. The Role of the PI3K-AKT Pathway in Melanoma. *The Cancer Journal* **18**, 142–147 (2012).
51. Hartman, M. L. & Czyz, M. MITF in melanoma: Mechanisms behind its expression and activity. *Cellular and Molecular Life Sciences* **72**, 1249–1260 (2015).
52. Shain, A. H. *et al.* The Genetic Evolution of Melanoma from Precursor Lesions. *New England Journal of Medicine* **373**, 1926–1936 (2015).
53. Sharpless, N. E. & Chin, L. The INK4a/ARF locus and melanoma. *Oncogene* **22**, 3092–2098 (2003).
54. Fernandez, M. F., Choi, J. & Sosman, J. New Approaches to Targeted Therapy in Melanoma. *Cancers (Basel)* **15**, 3224 (2023).
55. Chapman, P. B. *et al.* Improved survival with vemurafenib in melanoma with BRAF V600E mutation. *N Engl J Med* **364**, 2507–2516 (2011).
56. Hauschild, A. *et al.* Dabrafenib in BRAF-mutated metastatic melanoma: a multicentre, open-label, phase 3 randomised controlled trial. *Lancet* **380**, 358–365 (2012).
57. Manzano, J. L. *et al.* Resistant mechanisms to BRAF inhibitors in melanoma. *Ann Transl Med* **4**, 1–9 (2016).
58. Whittaker, S. R. *et al.* A genome-scale RNA interference screen implicates NF1 loss in resistance to RAF inhibition. *Cancer Discov* **3**, 350–362 (2013).
59. Nazarian, R. *et al.* Melanomas acquire resistance to B-RAF(V600E) inhibition by RTK or N-RAS upregulation. *Nature* **468**, 973–977 (2010).
60. Heidorn, S. J. *et al.* Kinase-Dead BRAF and Oncogenic RAS Cooperate to Drive Tumor Progression through CRAF. *Cell* **140**, 209–221 (2010).
61. Villanueva, J. *et al.* Acquired resistance to BRAF inhibitors mediated by a RAF kinase switch in melanoma can be overcome by cotargeting MEK and IGF-1R/PI3K. *Cancer Cell* **18**, 683–695 (2010).
62. Girotti, M. R. *et al.* Inhibiting EGF receptor or SRC family kinase signaling overcomes BRAF inhibitor resistance in melanoma Europe PMC Funders Group. *Cancer Discov* **3**, 158–167 (2013).
63. Shi, H. *et al.* Melanoma whole-exome sequencing identifies V600EB-RAF amplification-mediated acquired B-RAF inhibitor resistance. *Nature Communications 2012 3:1* **3**, 1–8 (2012).
64. Poulikakos, P. I. *et al.* RAF inhibitor resistance is mediated by dimerization of aberrantly spliced BRAF(V600E). *Nature* **480**, 387–390 (2011).
65. Montagut, C. *et al.* Elevated CRAF as a potential mechanism of acquired resistance to BRAF inhibition in melanoma. *Cancer Res* **68**, 4853–4861 (2008).

66. Emery, C. M. *et al.* MEK1 mutations confer resistance to MEK and B-RAF inhibition. *Proc Natl Acad Sci U S A* **106**, 20411–20416 (2009).
67. Marusiak, A. A. *et al.* Mixed lineage kinases activate MEK independently of RAF to mediate resistance to RAF inhibitors. *Nat Commun* **5**, (2014).
68. Johannessen, C. M. *et al.* COT/MAP3K8 drives resistance to RAF inhibition through MAP kinase pathway reactivation. *Nature* **468**, 972 (2010).
69. Paraiso, K. H. T. *et al.* PTEN loss confers BRAF inhibitor resistance to melanoma cells through the suppression of BIM expression. *Cancer Res* **71**, 2750–2760 (2011).
70. Smith, M. P. *et al.* Inhibiting Drivers of Non-mutational Drug Tolerance Is a Salvage Strategy for Targeted Melanoma Therapy. *Cancer Cell* **29**, 270–284 (2016).
71. Flaherty, K. T. *et al.* Combined BRAF and MEK Inhibition in Melanoma with BRAF V600 Mutations. *N Engl J Med* **367**, 1703 (2012).
72. King, A. J. *et al.* Dabrafenib; preclinical characterization, increased efficacy when combined with trametinib, while BRAF/MEK tool combination reduced skin lesions. *PLoS One* **8**, (2013).
73. Long, G. V. *et al.* Increased MAPK reactivation in early resistance to dabrafenib/trametinib combination therapy of BRAF-mutant metastatic melanoma. *Nature Communications 2014 5:1* **5**, 1–9 (2014).
74. Randic, T., Kozar, I., Margue, C., Utikal, J. & Kreis, S. NRAS mutant melanoma: Towards better therapies. *Cancer Treat Rev* **99**, 102238 (2021).
75. Whyte, D. B. *et al.* K- and N-Ras are geranylgeranylated in cells treated with farnesyl protein transferase inhibitors. *Journal of Biological Chemistry* **272**, 14459–14464 (1997).
76. Ascierto, P. A. *et al.* MEK162 for patients with advanced melanoma harbouring NRAS or Val600 BRAF mutations: A non-randomised, open-label phase 2 study. *Lancet Oncol* **14**, 249–256 (2013).
77. Carvajal, R. D. *et al.* KIT as a Therapeutic Target in Metastatic Melanoma. *JAMA* **305**, 2327–2334 (2011).
78. Carvajal, R. D. *et al.* Phase II study of nilotinib in melanoma harboring KIT alterations following progression to prior KIT inhibition. *Clinical Cancer Research* **21**, 2289–2296 (2015).
79. Lee, N., Zakka, L. R., Mihm, M. C. & Schatton, T. Tumour-infiltrating lymphocytes in melanoma prognosis and cancer immunotherapy. *Pathology* **48**, 177–187 (2016).
80. Rosenberg, S. A. A new era for cancer immunotherapy based on the genes that encode cancer antigens. *Immunity* **10**, 281–287 (1999).
81. Schumacher, T. N. & Schreiber, R. D. Neoantigens in cancer immunotherapy. *Science* **348**, 69–74 (2015).
82. Wang, R. F., Appella, E., Kawakami, Y., Kang, X. & Rosenberg, S. A. Identification of TRP-2 as a human tumor antigen recognized by cytotoxic T lymphocytes. *J Exp Med* **184**, 2207–2216 (1996).
83. Kawakami, Y. *et al.* Cloning of the gene coding for a shared human melanoma antigen recognized by autologous T cells infiltrating into tumor. *Proc Natl Acad Sci U S A* **91**, 3515 (1994).
84. Huang, S. K. S., Okamoto, T., Morton, D. L. & Hoon, D. S. B. Antibody responses to melanoma/melanocyte autoantigens in melanoma patients. *J Invest Dermatol* **111**, 662–667 (1998).
85. Kalaora, S., Nagler, A., Wargo, J. A. & Samuels, Y. Mechanisms of immune activation and regulation: lessons from melanoma. *Nat Rev Cancer* **22**, 195–207 (2022).
86. Mellman, I., Chen, D. S., Powles, T. & Turley, S. J. The cancer-immunity cycle: Indication, genotype, and immunotype. *Immunity* **56**, 2188–2205 (2023).
87. Khong, H. T., Wang, Q. J. & Rosenberg, S. A. Identification of Multiple Antigens Recognized by Tumor-Infiltrating Lymphocytes From a Single Patient: Tumor Escape by Antigen Loss and Loss of MHC Expression. *Journal of immunotherapy* **27**, 184 (2004).
88. Maeurer, M. J. *et al.* Tumor Escape from Immune Recognition Lethal Recurrent Melanoma in a Patient Associated with Downregulation of the Peptide Transporter Protein TAP-1 and Loss of Expression of the Immunodominant MART-1/Melan-A Antigen. *J. Clin. Invest* **98**, 1633–1641 (1996).
89. Gorelink, L. & Flavell, R. A. Immune-mediated eradication of tumors through the blockade of transforming growth factor-β signaling in T cells. *Nature Medicine 2001 7:10* **7**, 1118–1122 (2001).
90. Nicolaou, A., Estdale, S. E., Tsatmali, M., Herrero, D. P. & Thody, A. J. Prostaglandin production by melanocytic cells and the effect of α-melanocyte stimulating hormone. *FEBS Lett* **570**, 223–226 (2004).
91. Walunas, T. L., Bakker, C. Y. & Bluestone, J. A. CTLA-4 ligation blocks CD28-dependent T cell activation. *J Exp Med* **183**, 2541–2550 (1996).
92. Parry, R. V. *et al.* CTLA-4 and PD-1 receptors inhibit T-cell activation by distinct mechanisms. *Mol Cell Biol* **25**, 9543–9553 (2005).
93. Obeid, J. M. *et al.* PD-L1, PD-L2 and PD-1 expression in metastatic melanoma: Correlation with tumor-infiltrating immune cells and clinical outcome. *Oncoimmunology* **5**, (2016).
94. Jiang, Y., Li, Y. & Zhu, B. T-cell exhaustion in the tumor microenvironment. *Cell Death Dis* **6**, (2015).
95. Smith, F. O. *et al.* Treatment of Metastatic Melanoma Using Interleukin-2 Alone or in Conjunction with Vaccines. *Clin Cancer Res* **14**, 5610 (2008).

96. Hodi, F. S. *et al.* Improved survival with ipilimumab in patients with metastatic melanoma. *N Engl J Med* **363**, 711–723 (2010).
97. Robert, C. *et al.* Nivolumab in previously untreated melanoma without BRAF mutation. *N Engl J Med* **372**, 320–330 (2015).
98. Robert, C. *et al.* Pembrolizumab versus ipilimumab in advanced melanoma (KEYNOTE-006): post-hoc 5-year results from an open-label, multicentre, randomised, controlled, phase 3 study. *Lancet Oncol* **20**, 1239–1251 (2019).
99. Robert, C. *et al.* Pembrolizumab versus Ipilimumab in Advanced Melanoma. *N Engl J Med* **372**, 2521–2532 (2015).
100. Wolchok, J. D. *et al.* Long-Term Outcomes With Nivolumab Plus Ipilimumab or Nivolumab Alone Versus Ipilimumab in Patients With Advanced Melanoma. *J Clin Oncol* **40**, 127–137 (2022).
101. Long, G. V. *et al.* Standard-dose pembrolizumab plus alternate-dose ipilimumab in advanced melanoma: KEYNOTE-029 cohort 1C, a phase 2 randomized study of two dosing schedules. *Clinical Cancer Research* **27**, 5280–5288 (2021).
102. Huang, A. C. & Zappasodi, R. A decade of checkpoint blockade immunotherapy in melanoma: understanding the molecular basis for immune sensitivity and resistance. *Nat Immunol* **23**, 660–670 (2022).
103. Graydon, C. G., Mohideen, S. & Fowke, K. R. LAG3's Enigmatic Mechanism of Action. *Front Immunol* **11**, (2020).
104. Tawbi, H. A. *et al.* Relatlimab and Nivolumab versus Nivolumab in Untreated Advanced Melanoma. *New England Journal of Medicine* **386**, 24–34 (2022).
105. Waldman, A. D., Fritz, J. M. & Lenardo, M. J. A guide to cancer immunotherapy: from T cell basic science to clinical practice. *Nat Rev Immunol* **20**, 651–668 (2020).
106. Tang, W., Chen, J., Ji, T. & Cong, X. TIGIT, a novel immune checkpoint therapy for melanoma. *Cell Death & Disease 2023 14:7* **14**, 1–9 (2023).
107. Chauvin, J. M. *et al.* TIGIT and PD-1 impair tumor antigen–specific CD8+ T cells in melanoma patients. *J Clin Invest* **125**, 2046 (2015).
108. Mooradian, M. J. & Sullivan, R. J. Immunotherapy in Melanoma: Recent Advancements and Future Directions. *Cancers (Basel)* **15**, (2023).
109. Jenkins, R. W., Barbie, D. A. & Flaherty, K. T. Mechanisms of resistance to immune checkpoint inhibitors. *British Journal of Cancer 2018 118:1* **118**, 9–16 (2018).
110. Curran, M. A. & Allison, J. P. Tumor Vaccines Expressing Flt3-Ligand Synergize with CTLA-4 Blockade to Reject Pre-Implanted Tumors. *Cancer Res* **69**, 7747 (2009).
111. Plaksin, D. *et al.* Effective anti-metastatic melanoma vaccination with tumor cells transfected with MHC genes and/or infected with Newcastle disease virus (NDV). *Int J Cancer* **59**, 796–801 (1994).
112. Ott, P. A. *et al.* An Immunogenic Personal Neoantigen Vaccine for Melanoma Patients. *Nature* **547**, 217 (2017).
113. Sahin, U. *et al.* Personalized RNA mutanome vaccines mobilize poly-specific therapeutic immunity against cancer. *Nature* **547**, 222–226 (2017).
114. Das, A. *et al.* Advances in adoptive T-cell therapy for metastatic melanoma. *Curr Res Transl Med* **71**, 103404 (2023).
115. Robbins, P. F. *et al.* A pilot trial using lymphocytes genetically engineered with an NY-ESO-1-reactive T cell receptor: Long term follow up and correlates with response. *Clin Cancer Res* **21**, 1019 (2015).
116. Yee, C. *et al.* Adoptive T cell therapy using antigen-specific CD8+ T cell clones for the treatment of patients with metastatic melanoma: in vivo persistence, migration, and antitumor effect of transferred T cells. *Proc Natl Acad Sci U S A* **99**, 16168–16173 (2002).
117. Morrison, D. K. MAP Kinase Pathways. *Cold Spring Harb Perspect Biol* **4**, (2012).
118. Wei, Z. & Liu, H. T. MAPK signal pathways in the regulation of cell proliferation in mammalian cells. *Cell Research 2002 12:1* **12**, 9–18 (2002).
119. Drew, B. A., Burow, M. E. & Beckman, B. S. MEK5/ERK5 Pathway: The first fifteen years. *Biochim Biophys Acta* **1825**, 37 (2012).
120. Han, J., Lee, J. D., Bibbs, L. & Ulevitch, R. J. A MAP Kinase Targeted by Endotoxin and Hyperosmolarity in Mammalian Cells. *Science (1979)* **265**, 808–811 (1994).
121. Lee, J. C. *et al.* A protein kinase involved in the regulation of inflammatory cytokine biosynthesis. *Nature 1994 372:6508* **372**, 739–746 (1994).
122. Rouse, J. *et al.* A novel kinase cascade triggered by stress and heat shock that stimulates MAPKAP kinase-2 and phosphorylation of the small heat shock proteins. *Cell* **78**, 1027–1037 (1994).
123. Freshney, N. W. *et al.* Interleukin-1 activates a novel protein kinase cascade that results in the phosphorylation of hsp27. *Cell* **78**, 1039–1049 (1994).
124. Canovas, B. & Nebreda, A. R. Diversity and versatility of p38 kinase signalling in health and disease. *Nat Rev Mol Cell Biol* **22**, 346–366 (2021).

125. Cuenda, A., Cohen, P., Buée-Scherrer, V. & Goedert, M. Activation of stress-activated protein kinase-3 (SAPK3) by cytokines and cellular stresses is mediated via SAPKK3 (MKK6); comparison of the specificities of SAPK3 and SAPK2 (RK/p38). *EMBO J* **16**, 295–305 (1997).
126. Lechner, C., Zahalka, M. A., Giot, J. F., Møller, N. P. H. & Ullrich, A. ERK6, a mitogen-activated protein kinase involved in C2C12 myoblast differentiation. *Proc Natl Acad Sci U S A* **93**, 4355–4359 (1996).
127. Jiang, Y. *et al.* Characterization of the structure and function of a new mitogen-activated protein kinase (p38beta). *J Biol Chem* **271**, 17920–17926 (1996).
128. Cuadrado, A. & Nebreda, A. R. Mechanisms and functions of p38 MAPK signalling. *Biochemical Journal* **429**, 403–417 (2010).
129. Patel, S. B. *et al.* The three-dimensional structure of MAP kinase p38beta: different features of the ATP-binding site in p38beta compared with p38alpha. *Acta Crystallogr D Biol Crystallogr* **65**, 777–785 (2009).
130. Adams, R. H. *et al.* Essential role of p38α MAP kinase in placental but not embryonic cardiovascular development. *Mol Cell* **6**, 109–116 (2000).
131. Mudgett, J. S. *et al.* Essential role for p38α mitogen-activated protein kinase in placental angiogenesis. *Proc Natl Acad Sci U S A* **97**, 10454 (2000).
132. Beardmore, V. A. *et al.* Generation and Characterization of p38 (MAPK11) Gene-Targeted Mice. *Mol Cell Biol* **25**, 10454–10464 (2005).
133. Sabio, G. *et al.* p38γ regulates the localisation of SAP97 in the cytoskeleton by modulating its interaction with GKAP. *EMBO J* **24**, 1134–1145 (2005).
134. Gao, L. *et al.* Genome-wide promoter methylation analysis identifies epigenetic silencing of MAPK13 in primary cutaneous melanoma. *Pigment Cell Melanoma Res* **26**, 542–554 (2013).
135. Tanoue, T., Adachi, M., Moriguchi, T. & Nishida, E. A conserved docking motif in MAP kinases common to substrates, activators and regulators. *Nat Cell Biol* **2**, 110–116 (2000).
136. Ter Haar, E., Prabakhar, P., Liu, X. & Lepre, C. Crystal structure of the p38 alpha-MAPKAP kinase 2 heterodimer. *J Biol Chem* **282**, 9733–9739 (2007).
137. White, A., Pargellis, C. A., Studts, J. M., Werneburg, B. G. & Farmer, B. T. Molecular basis of MAPK-activated protein kinase 2:p38 assembly. *Proc Natl Acad Sci U S A* **104**, 6353–6358 (2007).
138. Hasegawa, M. *et al.* Stress-activated protein kinase-3 interacts with the PDZ domain of alpha1-syntrophin. A mechanism for specific substrate recognition. *J Biol Chem* **274**, 12626–12631 (1999).
139. Sabio, G. *et al.* p38γ regulates the localisation of SAP97 in the cytoskeleton by modulating its interaction with GKAP. *EMBO J* **24**, 1134 (2005).
140. Zarubin, T. & Han, J. Activation and signaling of the p38 MAP kinase pathway. *Cell Research 2005 15:1* **15**, 11–18 (2005).
141. Zhang, S. *et al.* Rho family GTPases regulate p38 mitogen-activated protein kinase through the downstream mediator Pak1. *J Biol Chem* **270**, 23934–23936 (1995).
142. Enslen, H., Raingeaud, J. & Davis, R. J. Selective activation of p38 mitogen-activated protein (MAP) kinase isoforms by the MAP kinase kinases MKK3 and MKK6. *J Biol Chem* **273**, 1741–1748 (1998).
143. Alonso, G., Ambrosino, C., Jones, M. & Nebreda, A. R. Differential activation of p38 mitogen-activated protein kinase isoforms depending on signal strength. *J Biol Chem* **275**, 40641–40648 (2000).
144. Jiang, Y. *et al.* Characterization of the structure and function of the fourth member of p38 group mitogen-activated protein kinases, p38δ. *Journal of Biological Chemistry* **272**, 30122–30128 (1997).
145. Ge, B. *et al.* MAPKK-independent activation of p38alpha mediated by TAB1-dependent autophosphorylation of p38alpha. *Science* **295**, 1291–1294 (2002).
146. Sakurai, H., Miyoshi, H., Mizukami, J. & Sugita, T. Phosphorylation-dependent activation of TAK1 mitogen-activated protein kinase kinase kinase by TAB1. *FEBS Lett* **474**, 141–145 (2000).
147. Salvador, J. M. *et al.* Alternative p38 activation pathway mediated by T cell receptor-proximal tyrosine kinases. *Nat Immunol* **6**, 390–395 (2005).
148. Mittelstadt, P. R., Yamaguchi, H., Appella, E. & Ashwell, J. D. T Cell Receptor-mediated Activation of p38α by Mono-phosphorylation of the Activation Loop Results in Altered Substrate Specificity. *J Biol Chem* **284**, 15469 (2009).
149. Tomida, T., Takekawa, M. & Saito, H. Oscillation of p38 activity controls efficient pro-inflammatory gene expression. *Nature Communications 2015 6:1* **6**, 1–9 (2015).
150. Cargnello, M. & Roux, P. P. Activation and Function of the MAPKs and Their Substrates, the MAPK-Activated Protein Kinases. *Microbiol Mol Biol Rev* **75**, 50 (2011).
151. McLaughlin, M. M. *et al.* Identification of mitogen-activated protein (MAP) kinase-activated protein kinase-3, a novel substrate of CSBP p38 MAP kinase. *J Biol Chem* **271**, 8488–8492 (1996).
152. Tan, Y. *et al.* FGF and stress regulate CREB and ATF-1 via a pathway involving p38 MAP kinase and MAPKAP kinase-2. *EMBO J* **15**, 4629 (1996).
153. Stein, B. *et al.* p38-2, a novel mitogen-activated protein kinase with distinct properties. *J Biol Chem* **272**, 19509–19517 (1997).

154. Huang, C., Ma, W. Y., Maxiner, A., Sun, Y. & Dong, Z. p38 kinase mediates UV-induced phosphorylation of p53 protein at serine 389. *J Biol Chem* **274**, 12229–12235 (1999).
155. Wang, X. Z. & Ron, D. Stress-induced phosphorylation and activation of the transcription factor CHOP (GADD153) by p38 MAP Kinase. *Science* **272**, 1347–1349 (1996).
156. Geest, C. R. *et al.* p38 MAP kinase inhibits neutrophil development through phosphorylation of C/EBPalpha on serine 21. *Stem Cells* **27**, 2271–2282 (2009).
157. Zhao, M. *et al.* Regulation of the MEF2 family of transcription factors by p38. *Mol Cell Biol* **19**, 21–30 (1999).
158. Yee, A. S. *et al.* The HBP1 transcriptional repressor and the p38 MAP kinase: Unlikely partners in G1 regulation and tumor suppression. *Gene* **336**, 1–13 (2004).
159. Giannì, M. *et al.* P38MAPK-dependent phosphorylation and degradation of SRC-3/AIB1 and RARalpha-mediated transcription. *EMBO J* **25**, 739–751 (2006).
160. Li, J. C. B. & Lau, A. S. Y. A role for mitogen-activated protein kinase and Ets-1 in the induction of interleukin-10 transcription by human immunodeficiency virus-1 Tat. *Immunology* **121**, 337–348 (2007).
161. Janknecht, R. Cell type-specific inhibition of the ETS transcription factor ER81 by mitogen-activated protein kinase-activated protein kinase 2. *J Biol Chem* **276**, 41856–41861 (2001).
162. Janknecht, R. & Hunter, T. Convergence of MAP kinase pathways on the ternary complex factor Sap-1a. *EMBO J* **16**, 1620 (1997).
163. Ramsauer, K. *et al.* p38 MAPK enhances STAT1-dependent transcription independently of Ser-727 phosphorylation. *Proc Natl Acad Sci U S A* **99**, 12859–12864 (2002).
164. Pramanik, R. *et al.* p38 isoforms have opposite effects on AP-1-dependent transcription through regulation of c-Jun. The determinant roles of the isoforms in the p38 MAPK signal specificity. *J Biol Chem* **278**, 4831–4839 (2003).
165. Mikkola, I., Bruun, J. A., Bjørkøy, G., Holm, T. & Johansen, T. Phosphorylation of the transactivation domain of Pax6 by extracellular signal-regulated kinase and p38 mitogen-activated protein kinase. *J Biol Chem* **274**, 15115–15126 (1999).
166. Mansky, K. C., Sankar, U., Han, J. & Ostrowski, M. C. Microphthalmia transcription factor is a target of the p38 MAPK pathway in response to receptor activator of NF-kappa B ligand signaling. *J Biol Chem* **277**, 11077–11083 (2002).
167. Bode, A. M. & Dong, Z. Mitogen-Activated Protein Kinase Activation in UV-Induced Signal Transduction. *Science STKE* **167**, (2003).
168. Jinlian, L., Yingbin, Z. & Chunbo, W. p38 MAPK in regulating cellular responses to ultraviolet radiation. *J Biomed Sci* **14**, 303–312 (2007).
169. Manke, I. A. *et al.* MAPKAP kinase-2 is a cell cycle checkpoint kinase that regulates the G 2/M transition and S phase progression in response to UV irradiation. *Mol Cell* **17**, 37–48 (2005).
170. Jin, S. *et al.* GADD45-induced cell cycle G2-M arrest associates with altered subcellular distribution of cyclin B1 and is independent of p38 kinase activity. *Oncogene* **21**, 8696–8704 (2002).
171. Gräb, J. & Rybniker, J. The Expanding Role of p38 Mitogen-Activated Protein Kinase in Programmed Host Cell Death. *Microbiol Insights* **12**, 117863611986459 (2019).
172. Galibert, M. D., Carreira, S. & Goding, C. R. The Usf-1 transcription factor is a novel target for the stress-responsive p38 kinase and mediates UV-induced Tyrosinase expression. *EMBO J* **20**, 5022–5031 (2001).
173. Corre, S. *et al.* UV-induced expression of key component of the tanning process, the POMC and MC1R genes, is dependent on the p-38-activated upstream stimulating factor-1 (USF-1). *J Biol Chem* **279**, 51226–51233 (2004).
174. Smalley, K. & Eisen, T. The involvement of p38 mitogen-activated protein kinase in the alpha-melanocyte stimulating hormone (alpha-MSH)-induced melanogenic and anti-proliferative effects in B16 murine melanoma cells. *FEBS Lett* **476**, 198–202 (2000).
175. Saha, B. *et al.* Activation of the Mitf promoter by lipid-stimulated activation of p38-stress signalling to CREB. *Pigment Cell Res* **19**, 595–605 (2006).
176. Kim, A. L. *et al.* Role of p38 MAPK in UVB-Induced Inflammatory Responses in the Skin of SKH-1 Hairless Mice. *Journal of Investigative Dermatology* **124**, 1318–1325 (2005).
177. Koul, H. K., Pal, M. & Koul, S. Role of p38 MAP Kinase Signal Transduction in Solid Tumors. *Genes Cancer* **4**, 342–359 (2013).
178. Zonneville, J. *et al.* Blockade of p38 kinase impedes the mobilization of protumorigenic myeloid populations to impact breast cancer metastasis. *Int J Cancer* **147**, 2279–2292 (2020).
179. Gui, J. *et al.* Activation of p38α stress-activated protein kinase drives the formation of the pre-metastatic niche in the lungs. *Nat Cancer* **1**, 603 (2020).
180. Katlinski, K. V. *et al.* Inactivation of interferon receptor promotes the establishment of immune privileged tumor microenvironment. *Cancer Cell* **31**, 194 (2017).

181. Wang, W. *et al.* Sequential activation of the MEK-extracellular signal-regulated kinase and MKK3/6-p38 mitogen-activated protein kinase pathways mediates oncogenic ras-induced premature senescence. *Mol Cell Biol* **22**, 3389–3403 (2002).
182. Iwasa, H., Han, J. & Ishikawa, F. Mitogen-activated protein kinase p38 defines the common senescence-signalling pathway. *Genes Cells* **8**, 131–144 (2003).
183. Bulavin, D. V. *et al.* Amplification of PPM1D in human tumors abrogates p53 tumor-suppressor activity. *Nat Genet* **31**, 210–215 (2002).
184. Bulavin, D. V., Kovalsky, O., Hollander, M. C. & Jr., A. J. F. Loss of Oncogenic H-ras-Induced Cell Cycle Arrest and p38 Mitogen-Activated Protein Kinase Activation by Disruption of Gadd45a. *Mol Cell Biol* **23**, 3859 (2003).
185. Kodama, R. *et al.* ROS-generating oxidases Nox1 and Nox4 contribute to oncogenic Ras-induced premature senescence. *Genes to Cells* **18**, 32–41 (2013).
186. Lee, A. C. *et al.* Ras proteins induce senescence by altering the intracellular levels of reactive oxygen species. *Journal of Biological Chemistry* **274**, 7936–7940 (1999).
187. Di Micco, R. *et al.* Oncogene-induced senescence is a DNA damage response triggered by DNA hyper-replication. *Nature* **444**, 638–642 (2006).
188. Bartkova, J. *et al.* Oncogene-induced senescence is part of the tumorigenesis barrier imposed by DNA damage checkpoints. *Nature* **444**, 633–637 (2006).
189. Passos, J. F. *et al.* Feedback between p21 and reactive oxygen production is necessary for cell senescence. *Mol Syst Biol* **6**, 347 (2010).
190. Ogrunc, M. *et al.* Oncogene-induced reactive oxygen species fuel hyperproliferation and DNA damage response activation. *Cell Death & Differentiation 2014 21:6* **21**, 998–1012 (2014).
191. Kwong, J. *et al.* Induction of p38δ Expression Plays an Essential Role in Oncogenic ras-Induced Senescence. *Mol Cell Biol* **33**, 3780 (2013).
192. Kwong, J. *et al.* p38α and p38γ Mediate Oncogenic ras-induced Senescence through Differential Mechanisms. *J Biol Chem* **284**, 11237 (2009).
193. Li, H. *et al.* Transcriptional factor HBP1 targets P16(INK4A), upregulating its expression and consequently is involved in Ras-induced premature senescence. *Oncogene* **29**, 5083–5094 (2010).
194. Sun, P. *et al.* PRAK is essential for ras-induced senescence and tumor suppression. *Cell* **128**, 295–308 (2007).
195. Martínez-Limón, A., Joaquin, M., Caballero, M., Posas, F. & de Nadal, E. The p38 Pathway: From Biology to Cancer Therapy. *Int J Mol Sci* **21**, (2020).
196. Igea, A. & Nebreda, A. R. The stress kinase p38α as a target for cancer therapy. *Cancer Res* **75**, 3997–4002 (2015).
197. Gialeli, C., Theocharis, A. D. & Karamanos, N. K. Roles of matrix metalloproteinases in cancer progression and their pharmacological targeting. *FEBS J* **278**, 16–27 (2011).
198. Dange, M. C., Agarwal, A. K. & Kalraiya, R. D. Extracellular galectin-3 induces MMP9 expression by activating p38 MAPK pathway via lysosome-associated membrane protein-1 (LAMP1). *Mol Cell Biochem* **404**, 79–86 (2015).
199. Simon, C. *et al.* The p38 SAPK pathway regulates the expression of the MMP-9 collagenase via AP-1-dependent promoter activation. *Exp Cell Res* **271**, 344–355 (2001).
200. Mukhopadhyay, S. *et al.* Calcium-induced matrix metalloproteinase 9 gene expression is differentially regulated by ERK1/2 and p38 MAPK in oral keratinocytes and oral squamous cell carcinoma. *J Biol Chem* **279**, 33139–33146 (2004).
201. Hong, I. K., Kim, Y. M., Jeoung, D. I. I., Kim, K. C. & Lee, H. Tetraspanin CD9 induces MMP-2 expression by activating p38 MAPK, JNK and c-Jun pathways in human melanoma cells. *Exp Mol Med* **37**, 230–239 (2005).
202. Lin, M. L. *et al.* Down-regulation of MMP-2 through the p38 MAPK-NF-kappaB-dependent pathway by aloe-emodin leads to inhibition of nasopharyngeal carcinoma cell invasion. *Mol Carcinog* **49**, 783–797 (2010).
203. Guarneri, C. *et al.* NF-κB inhibition is associated with OPN/MMP-9 downregulation in cutaneous melanoma. *Oncol Rep* **37**, 737 (2017).
204. Lee, K. R., Lee, J. S., Kim, Y. R., Song, I. G. & Hong, E. K. Polysaccharide from Inonotus obliquus inhibits migration and invasion in B16-F10 cells by suppressing MMP-2 and MMP-9 via downregulation of NF-κB signaling pathway. *Oncol Rep* **31**, 2447–2453 (2014).
205. Houle, F. & Huot, J. Dysregulation of the endothelial cellular response to oxidative stress in cancer. *Mol Carcinog* **45**, 362–367 (2006).
206. Pagès, G., Berra, E., Milanini, J., Levy, A. P. & Pouysségur, J. Stress-activated protein kinases (JNK and p38/HOG) are essential for vascular endothelial growth factor mRNA stability. *J Biol Chem* **275**, 26484–26491 (2000).

207. Naffa, R. *et al.* P38 MAPK Promotes Migration and Metastatic Activity of BRAF Mutant Melanoma Cells by Inducing Degradation of PMCA4b. *Cells* **9**, (2020).
208. Suarez-Lopez, L. *et al.* MK2 contributes to tumor progression by promoting M2 macrophage polarization and tumor angiogenesis. *Proc Natl Acad Sci U S A* **115**, E4236–E4244 (2018).
209. Zheng, T. *et al.* Protein kinase p38α signaling in dendritic cells regulates colon inflammation and tumorigenesis. *Proc Natl Acad Sci U S A* **115**, E12313–E12322 (2018).
210. Youssif, C. *et al.* Myeloid p38α signaling promotes intestinal IGF-1 production and inflammation-associated tumorigenesis. *EMBO Mol Med* **10**, (2018).
211. Barančík, M. *et al.* SB203580, a specific inhibitor of p38-MAPK pathway, is a new reversal agent of P-glycoprotein-mediated multidrug resistance. *European Journal of Pharmaceutical Sciences* **14**, 29–36 (2001).
212. Kuma, Y. *et al.* BIRB796 inhibits all p38 MAPK isoforms in vitro and in vivo. *Journal of Biological Chemistry* **280**, 19472–19479 (2005).
213. Laufer, S. & Lehmann, F. Investigations of SCIO-469-like compounds for the inhibition of p38 MAP kinase. *Bioorg Med Chem Lett* **19**, 1461–1464 (2009).
214. Duffy, J. P. *et al.* The discovery of VX-745: A novel and selective p38α kinase inhibitor. *ACS Med Chem Lett* **2**, 758–763 (2011).
215. Triantaphyllopoulos, K. *et al.* In vitro target validation and in vivo efficacy of p38 MAP kinase inhibition in established chronic collagen-induced arthritis model: A pre-clinical study. *Clin Exp Rheumatol* **28**, 176–185 (2010).
216. Selness, S. R. *et al.* Discovery of PH-797804, a highly selective and potent inhibitor of p38 MAP kinase. *Bioorg Med Chem Lett* **21**, 4066–4071 (2011).
217. Campbell, R. M. *et al.* Characterization of LY2228820 Dimesylate, a Potent and Selective Inhibitor of p38 MAPK with Antitumor Activity. *Mol Cancer Ther* **13**, 364–374 (2014).
218. Kudaravalli, S., den Hollander, P. & Mani, S. A. Role of p38 MAP kinase in cancer stem cells and metastasis. *Oncogene 2022 41:23* **41**, 3177–3185 (2022).
219. Pereira, L., Igea, A., Canovas, B., Dolado, I. & Nebreda, A. R. Inhibition of p38 MAPK sensitizes tumour cells to cisplatin-induced apoptosis mediated by reactive oxygen species and JNK. *EMBO Mol Med* **5**, 1759–1774 (2013).
220. Rudalska, R. *et al.* In vivo RNAi screening identifies a mechanism of sorafenib resistance in liver cancer. *Nat Med* **20**, 1138–1146 (2014).
221. Zarczynska, I. *et al.* p38 Mediates Resistance to FGFR Inhibition in Non-Small Cell Lung Cancer. *Cells* **10**, (2021).
222. Ohkusu-Tsukada, K., Toda, M., Udono, H., Kawakami, Y. & Takahashi, K. Targeted inhibition of IL-10-secreting CD25− Treg via p38 MAPK suppression in cancer immunotherapy. *Eur J Immunol* **40**, 1011–1021 (2010).
223. Gurusamy, D. *et al.* Multi-phenotype CRISPR-Cas9 Screen Identifies p38 Kinase as a Target for Adoptive Immunotherapies. *Cancer Cell* **37**, 818 (2020).
224. Chen, S. *et al.* p38 inhibition enhances TCR-T cell function and antagonizes the immunosuppressive activity of TGF-β. *Int Immunopharmacol* **98**, (2021).
225. Henson, S. M., Macaulay, R., Riddell, N. E., Nunn, C. J. & Akbar, A. N. Blockade of PD-1 or p38 MAP kinase signaling enhances senescent human CD8(+) T-cell proliferation by distinct pathways. *Eur J Immunol* **45**, 1441–1451 (2015).
226. Montagna, D. R. *et al.* Inhibition of hyperprogressive cancer disease induced by immune-checkpoint blockade upon co-treatment with meta-tyrosine and p38 pathway inhibitor. *BMC Cancer* **22**, (2022).
227. Lu, Y. *et al.* p38 MAPK-inhibited dendritic cells induce superior antitumour immune responses and overcome regulatory T-cell-mediated immunosuppression. *Nature Communications 2014 5:1* **5**, 1–14 (2014).
228. Kühnöl, C., Herbarth, M., Föll, J., Staege, M. S. & Kramm, C. CD137 stimulation and p38 MAPK inhibition improve reactivity in an in vitro model of glioblastoma immunotherapy. *Cancer Immunology, Immunotherapy* **62**, 1797–1809 (2013).
229. Wang, C. *et al.* Selective inhibition of the p38α MAPK-MK2 axis inhibits inflammatory cues including inflammasome priming signals. *J Exp Med* **215**, 1315–1325 (2018).
230. Reinhardt, H. C., Aslanian, A. S., Lees, J. A. & Yaffe, M. B. p53-deficient cells rely on ATM- and ATR-mediated checkpoint signaling through the p38MAPK/MK2 pathway for survival after DNA damage. *Cancer Cell* **11**, 175–189 (2007).
231. Donoghue, C. *et al.* Optimal linker length for small molecule PROTACs that selectively target p38α and p38β for degradation. *Eur J Med Chem* **201**, (2020).
232. Casadomé-Perales, Á. *et al.* Inhibition of p38 MAPK in the brain through nasal administration of p38 inhibitor loaded in chitosan nanocapsules. *Nanomedicine (Lond)* **14**, 2409–2422 (2019).

233. Maik-Rachline, G., Zehorai, E., Hanoch, T., Blenis, J. & Seger, R. The nuclear translocation of the kinases p38 and JNK promotes inflammation-induced cancer. *Sci Signal* **11**, (2018).
234. McGrail, K. *et al.* Loss of Lkb1 cooperates with BrafV600E and UV radiation increasing melanoma multiplicity and neural-like dedifferentiation. *bioRxiv* Preprint at https://doi.org/10.1101/2024.03.29.587140 (2024).
235. Mann, M. B. *et al.* Transposon mutagenesis identifies genetic drivers of Braf V600E melanoma. *Nat Genet* **47**, 486–495 (2015).
236. Viros, A. *et al.* Ultraviolet radiation accelerates BRAF-driven melanomagenesis by targeting TP53. *Nature* **511**, 478–482 (2014).
237. González Sánchez, E. Study of the cooperative effect of UVR, BRAF and LKB1 in Melanoma. (Universitat Autònoma de Barcelona, 2019).
238. De Fabo, E. C., Noonan, F. P., Fears, T. & Merlino, G. Ultraviolet B but not ultraviolet A radiation initiates melanoma. *Cancer Res* **64**, 6372–6376 (2004).
239. Luo, C. *et al.* Loss of ARF sensitizes transgenic BRAFV600E mice to UV-induced melanoma via suppression of XPC. *Cancer Res* **73**, 4337 (2013).
240. Recio, J. A. *et al.* Ink4a/Arf Deficiency Promotes Ultraviolet Radiation-induced Melanomagenesis 1. *Cancer Res* **62**, 6724–6730 (2002).
241. Noonan, F. P. *et al.* Neonatal sunburn and melanoma in mice. *Nature* **413**, 271–272 (2001).
242. Dankort, D. *et al.* BrafV600E cooperates with Pten loss to induce metastatic melanoma. *Nat Genet* **41**, 544–552 (2009).
243. Damsky, W. *et al.* mTORC1 activation blocks BrafV600E-induced growth arrest but is insufficient for melanoma formation. *Cancer Cell* **27**, 41–56 (2015).
244. Kravtsov, D. S., Erbe, A. K., Sondel, P. M. & Rakhmilevich, A. L. Roles of CD4+ T cells as mediators of antitumor immunity. *Front Immunol* **13**, (2022).
245. Raskov, H., Orhan, A., Christensen, J. P. & Gögenur, I. Cytotoxic CD8+ T cells in cancer and cancer immunotherapy. *Br J Cancer* **124**, 359–367 (2021).
246. Restifo, N. P. & Gattinoni, L. Lineage relationship of effector and memory T cells. *Curr Opin Immunol* **25**, 556–563 (2013).
247. Golubovskaya, V. & Wu, L. Different subsets of T cells, memory, effector functions, and CAR-T immunotherapy. *Cancers (Basel)* **8**, (2016).
248. Mahnke, Y. D., Brodie, T. M., Sallusto, F., Roederer, M. & Lugli, E. The who's who of T-cell differentiation: Human memory T-cell subsets. *Eur J Immunol* **43**, 2797–2809 (2013).
249. Han, J., Khatwani, N., Searles, T. G., Turk, M. J. & Angeles, C. V. Memory CD8+ T cell responses to cancer. *Semin Immunol* **49**, 101435 (2020).
250. Ohue, Y. & Nishikawa, H. Regulatory T (Treg) cells in cancer: Can Treg cells be a new therapeutic target? *Cancer Sci* **110**, 2080–2089 (2019).
251. Wolf, N. K., Kissiov, D. U. & Raulet, D. H. Roles of natural killer cells in immunity to cancer, and applications to immunotherapy. *Nat Rev Immunol* **23**, 90–105 (2023).
252. Juelke, K. *et al.* CD62L expression identifies a unique subset of polyfunctional CD56dim NK cells. *Blood* **116**, 1299–1307 (2010).
253. Liu, Y. *et al.* Increased expression of programmed cell death protein 1 on NK cells inhibits NK-cell-mediated anti-tumor function and indicates poor prognosis in digestive cancers. *Oncogene* **36**, 6143 (2017).
254. Sague, S. L., Tato, C., Puré, E. & Hunter, C. A. The regulation and activation of CD44 by natural killer (NK) cells and its role in the production of IFN-gamma. *J Interferon Cytokine Res* **24**, 301–309 (2004).
255. Terabe, M. & Berzofsky, J. A. The Role of NKT Cells in Tumor Immunity. *Advanced Cancer Research* **101**, 277–348 (2008).
256. Tian, G. *et al.* CD62L+ NKT cells have prolonged persistence and antitumor activity in vivo. *Journal of Clinical Investigation* **126**, 2341–2355 (2016).
257. Gabrilovich, D. I., Ostrand-Rosenberg, S. & Bronte, V. Coordinated regulation of myeloid cells by tumours. *Nature Reviews Immunology 2012 12:4* **12**, 253–268 (2012).
258. Veglia, F., Sanseviero, E. & Gabrilovich, D. I. Myeloid-derived suppressor cells in the era of increasing myeloid cell diversity. *Nature Reviews Immunology 2021 21:8* **21**, 485–498 (2021).
259. Mandruzzato, S. *et al.* IL4Ralpha+ myeloid-derived suppressor cell expansion in cancer patients. *Journal of immunology* **182**, 6562–6568 (2009).
260. Engblom, C., Pfirschke, C. & Pittet, M. J. The role of myeloid cells in cancer therapies. *Nature Reviews Cancer 2016 16:7* **16**, 447–462 (2016).
261. Wculek, S. K. *et al.* Dendritic cells in cancer immunology and immunotherapy. *Nature Reviews Immunology 2019 20:1* **20**, 7–24 (2019).
262. Nagarsheth, N., Wicha, M. S. & Zou, W. Chemokines in the cancer microenvironment and their relevance in cancer immunotherapy. *Nature Reviews Immunology 2017 17:9* **17**, 559–572 (2017).

263. Kryczek, I. *et al.* Phenotype, distribution, generation, and functional and clinical relevance of Th17 cells in the human tumor environments. *Blood* **114**, 1141 (2009).
264. Horton, L. W., Yu, Y., Zaja-Milatovic, S., Strieter, R. M. & Richmond, A. Opposing roles of murine duffy antigen receptor for chemokine and murine CXC chemokine receptor-2 receptors in murine melanoma tumor growth. *Cancer Res* **67**, 9791–9799 (2007).
265. Cai, Q., Dozmorov, M. & Oh, Y. IGFBP-3/IGFBP-3 Receptor System as an Anti-Tumor and Anti-Metastatic Signaling in Cancer. *Cells* **9**, (2020).
266. Koyama, N. *et al.* Identification of IGFBP-6 as an effector of the tumor suppressor activity of SEMA3B. *Oncogene 2008 27:51* **27**, 6581–6589 (2008).
267. Longhitano, L. *et al.* The Crosstalk between GPR81/IGFBP6 Promotes Breast Cancer Progression by Modulating Lactate Metabolism and Oxidative Stress. *Antioxidants* **11**, (2022).
268. Shurin, M. R. Osteopontin controls immunosuppression in the tumor microenvironment. *J Clin Invest* **128**, 5209 (2018).
269. Ribatti, D. Immunosuppressive effects of vascular endothelial growth factor. *Oncol Lett* **24**, (2022).
270. Neubert, N. J. *et al.* T cell-induced CSF1 promotes melanoma resistance to PD1 blockade. *Sci Transl Med* **10**, 86–109 (2018).
271. Maldonado, M. del M., Schlom, J. & Hamilton, D. H. Blockade of tumor-derived colony-stimulating factor 1 (CSF1) promotes an immune-permissive tumor microenvironment. *Cancer Immunology, Immunotherapy* **72**, 3349 (2023).
272. Giannoni, P., Cutrona, G. & de Totero, D. Survival and Immunosuppression Induced by Hepatocyte Growth Factor in Chronic Lymphocytic Leukemia. *Curr Mol Med* **17**, 24–33 (2017).
273. Palle, J. *et al.* Targeting HGF/c-Met Axis Decreases Circulating Regulatory T Cells Accumulation in Gastric Cancer Patients. *Cancers (Basel)* **13**, (2021).
274. Hallett, R. M. *et al.* Therapeutic Targeting of LIF Overcomes Macrophage-mediated Immunosuppression of the Local Tumor Microenvironment. *Clinical Cancer Research* **29**, 791–804 (2023).
275. Kim, W. T. *et al.* Secretory SERPINE1 Expression Is Increased by Antiplatelet Therapy, Inducing MMP1 Expression and Increasing Colon Cancer Metastasis. *Int J Mol Sci* **23**, (2022).
276. Chen, S. *et al.* SERPINE1 Overexpression Promotes Malignant Progression and Poor Prognosis of Gastric Cancer. *J Oncol* **2022**, (2022).
277. Wang, S., Pang, L., Liu, Z. & Meng, X. SERPINE1 associated with remodeling of the tumor microenvironment in colon cancer progression: a novel therapeutic target. *BMC Cancer* **21**, 1–13 (2021).
278. Karagiannidis, I., Salataj, E., Said Abu Egal, E. & Beswick, E. J. G-CSF in tumors: Aggressiveness, tumor microenvironment and immune cell regulation. *Cytokine* **142**, 155479 (2021).
279. Kim, M. J. *et al.* CXCL16 positively correlated with M2-macrophage infiltration, enhanced angiogenesis, and poor prognosis in thyroid cancer. *Scientific Reports 2019 9:1* **9**, 1–10 (2019).
280. Rašková, M. *et al.* The Role of IL-6 in Cancer Cell Invasiveness and Metastasis—Overview and Therapeutic Opportunities. *Cells* **11**, (2022).
281. Riaz, N. *et al.* Tumor and Microenvironment Evolution during Immunotherapy with Nivolumab. *Cell* **171**, 934-949.e15 (2017).
282. Gide, T. N. *et al.* Distinct Immune Cell Populations Define Response to Anti-PD-1 Monotherapy and Anti-PD-1/Anti-CTLA-4 Combined Therapy. *Cancer Cell* **35**, 238-255.e6 (2019).
283. Chen, P. L. *et al.* Analysis of Immune Signatures in Longitudinal Tumor Samples Yields Insight into Biomarkers of Response and Mechanisms of Resistance to Immune Checkpoint Blockade. *Cancer Discov* **6**, 827–837 (2016).
284. Ayers, M. *et al.* IFN-γ–related mRNA profile predicts clinical response to PD-1 blockade. *J Clin Invest* **127**, 2930–2940 (2017).
285. Jiang, P. *et al.* Signatures of T cell dysfunction and exclusion predict cancer immunotherapy response. *Nat Med* **24**, 1550–1558 (2018).
286. Hugo, W. *et al.* Genomic and Transcriptomic Features of Response to Anti-PD-1 Therapy in Metastatic Melanoma. *Cell* **165**, 35–44 (2016).
287. Ascierto, M. L. *et al.* Transcriptional mechanisms of resistance to anti-PD-1 therapy. *Clinical Cancer Research* **23**, 3168–3180 (2017).
288. Chen, Z. *et al.* TIGER: A Web Portal of Tumor Immunotherapy Gene Expression Resource. *Genomics Proteomics Bioinformatics* **21**, 337–348 (2023).
289. Robert, C. *et al.* Improved Overall Survival in Melanoma with Combined Dabrafenib and Trametinib. *New England Journal of Medicine* **372**, 30–39 (2015).
290. Eddy, K. & Chen, S. Overcoming Immune Evasion in Melanoma. *Int J Mol Sci* **21**, 1–48 (2020).
291. Lopez-Bergami, P. The role of mitogen-and stress-activated protein kinase pathways in melanoma. *Pigment Cell Melanoma Research* **24**, 902–921 (2011).
292. Lopez-Bergami, P. *et al.* Re-wired ERK-JNK signaling pathways in melanoma. *Cancer Cell* **11**, 447 (2007).

293. Puujalka, E. *et al.* Opposing Roles of JNK and p38 in Lymphangiogenesis in Melanoma. *J Invest Dermatol* **136**, 967–977 (2016).
294. Wen, S. Y. *et al.* Roles of p38α and p38β mitogen-activated protein kinase isoforms in human malignant melanoma A375 cells. *Int J Mol Med* **44**, 2123–2132 (2019).
295. Quail, D. F. & Joyce, J. A. Microenvironmental regulation of tumor progression and metastasis. *Nat Med* **19**, 1423 (2013).
296. Gupta, J. *et al.* Dual Function of p38α MAPK in Colon Cancer: Suppression of Colitis-Associated Tumor Initiation but Requirement for Cancer Cell Survival. *Cancer Cell* **25**, 484–500 (2014).
297. Linnskog, R., Jönsson, G., Axelsson, L., Prasad, C. P. & Andersson, T. Interleukin-6 drives melanoma cell motility through p38α-MAPK-dependent up-regulation of WNT5A expression. *Mol Oncol* **8**, 1365–1378 (2014).
298. Chen, L. *et al.* Inhibition of the p38 Kinase Suppresses the Proliferation of Human ER-Negative Breast Cancer Cells. *Cancer Res* **69**, 8853 (2009).
299. Dickinson, S. E. *et al.* p38 MAP Kinase Plays a Functional Role in UVB-Induced Mouse Skin Carcinogenesis. *Mol Carcinog* **50**, 469 (2011).
300. Liu, K. *et al.* Sunlight UV-induced skin cancer relies upon activation of the p38α signaling pathway. *Cancer Res* **73**, 2181 (2013).
301. Uxa, S. *et al.* Ki-67 gene expression. *Cell Death & Differentiation 2021 28:12* **28**, 3357–3370 (2021).
302. Estrada, Y., Dong, J. & Ossowski, L. Positive crosstalk between ERK and p38 in melanoma stimulates migration and in vivo proliferation. *Pigment Cell Melanoma Res* **22**, 66–76 (2009).
303. Ventura, J. J. *et al.* p38α MAP kinase is essential in lung stem and progenitor cell proliferation and differentiation. *Nature Genetics 2007 39:6* **39**, 750–758 (2007).
304. Ahmadzadeh, M. *et al.* Tumor antigen-specific CD8 T cells infiltrating the tumor express high levels of PD-1 and are functionally impaired. *Blood* **114**, 1537–1544 (2009).
305. Inozume, T. *et al.* Selection of CD8+PD-1+ lymphocytes in fresh human melanomas enriches for tumor-reactive T-cells. *J Immunother* **33**, 956 (2010).
306. Simon, S. *et al.* PD-1 expression conditions T cell avidity within an antigen-specific repertoire. *Oncoimmunology* **5**, (2015).
307. Gros, A. *et al.* PD-1 identifies the patient-specific $CD8^+$ tumor-reactive repertoire infiltrating human tumors. *J Clin Invest* **124**, 2246–2259 (2014).
308. Sakuishi, K. *et al.* Targeting Tim-3 and PD-1 pathways to reverse T cell exhaustion and restore anti-tumor immunity. *J Exp Med* **207**, 2187 (2010).
309. Tumeh, P. C. *et al.* PD-1 blockade induces responses by inhibiting adaptive immune resistance. *Nature* **515**, 568–571 (2014).
310. Manjarrez-Orduño, N. *et al.* Circulating T cell subpopulations correlate with immune responses at the tumor site and clinical response to PD1 inhibition in non-small cell lung cancer. *Front Immunol* **9**, 1613 (2018).
311. Garofalo, C., De Marco, C. & Cristiani, C. M. NK Cells in the Tumor Microenvironment as New Potential Players Mediating Chemotherapy Effects in Metastatic Melanoma. *Front Oncol* **11**, (2021).
312. McKay, K., Moore, P. C., Smoller, B. R. & Hiatt, K. M. Association between natural killer cells and regression in melanocytic lesions. *Hum Pathol* **42**, 1960–1964 (2011).
313. Barry, K. C. *et al.* A natural killer-dendritic cell axis defines checkpoint therapy-responsive tumor microenvironments. *Nat Med* **24**, 1178–1191 (2018).
314. Falleni, M. *et al.* M1 and M2 macrophages' clinicopathological significance in cutaneous melanoma. *Melanoma Res* **27**, 200–210 (2017).
315. Zhao, Z., Chung, Y. H. & Steinmetz, N. F. Melanoma immunotherapy enabled by M2 macrophage targeted immunomodulatory cowpea mosaic virus. *Mater Adv* **5**, 1473 (2024).
316. Pender, A. *et al.* Genome and transcriptome biomarkers of response to immune checkpoint inhibitors in advanced solid tumors. *Clinical Cancer Research* **27**, 202–212 (2021).
317. Weber, J. *et al.* Phase I/II Study of Metastatic Melanoma Patients Treated with Nivolumab Who Had Progressed after Ipilimumab. *Cancer Immunol Res* **4**, 345–353 (2016).
318. Meyer, C. *et al.* Frequencies of circulating MDSC correlate with clinical outcome of melanoma patients treated with ipilimumab. *Cancer Immunology, Immunotherapy* **63**, 247–257 (2014).
319. Abdul-Rahman, T. *et al.* The paradoxical role of cytokines and chemokines at the tumor microenvironment: a comprehensive review. *European Journal of Medical Research 2024 29:1* **29**, 1–19 (2024).
320. Harlin, H. *et al.* Chemokine expression in melanoma metastases associated with CD8 + T-CeII recruitment. *Cancer Res* **69**, 3077–3085 (2009).
321. House, I. G. *et al.* Macrophage-Derived CXCL9 and CXCL10 Are Required for Antitumor Immune Responses Following Immune Checkpoint Blockade. *Clin Cancer Res* **26**, 487–504 (2020).

322. Lim, R. J. *et al.* CXCL9/10-engineered dendritic cells promote T cell activation and enhance immune checkpoint blockade for lung cancer. *Cell Rep Med* **5**, 101479 (2024).
323. Chow, M. T. *et al.* Intratumoral activity of the CXCR3 chemokine system is required for the efficacy of anti- PD-1 therapy. *Immunity* **50**, 1498 (2019).
324. Reschke, R. *et al.* Immune cell and tumor cell-derived CXCL10 is indicative of immunotherapy response in metastatic melanoma. *J Immunother Cancer* **9**, (2021).
325. Croft, M., So, T., Duan, W. & Soroosh, P. The Significance of OX40 and OX40L to T cell Biology and Immune Disease. *Immunol Rev* **229**, 173 (2009).
326. Gramaglia, I. *et al.* The OX40 Costimulatory Receptor Determines the Development of CD4 Memory by Regulating Primary Clonal Expansion. *The Journal of Immunology* **165**, 3043–3050 (2000).
327. Xi, G. *et al.* GSDMD is required for effector CD8+ T cell responses to lung cancer cells. *Int Immunopharmacol* **74**, (2019).
328. Lou, X. *et al.* Pyroptosis correlates with tumor immunity and prognosis. *Commun Biol* **5**, (2022).
329. Ménasché, G. *et al.* A newly identified isoform of Slp2a associates with Rab27a in cytotoxic T cells and participates to cytotoxic granule secretion. *Blood* **112**, 5052–5062 (2008).
330. Pascual-García, M. *et al.* LIF regulates CXCL9 in tumor-associated macrophages and prevents CD8+ T cell tumor-infiltration impairing anti-PD1 therapy. *Nat Commun* **10**, (2019).
331. Humbert, L., Ghozlan, M., Canaff, L., Tian, J. & Lebrun, J. J. The leukemia inhibitory factor (LIF) and p21 mediate the TGFβ tumor suppressive effects in human cutaneous melanoma. *BMC Cancer* **15**, (2015).
332. Kumar, V., Patel, S., Tcyganov, E. & Gabrilovich, D. I. The nature of myeloid-derived suppressor cells in the tumor microenvironment. *Trends Immunol* **37**, 208 (2016).
333. Chia, T. Y. *et al.* The CXCL16-CXCR6 axis in glioblastoma modulates T-cell activity in a spatiotemporal context. *Front Immunol* **14**, (2024).
334. Palakurthi, B. *et al.* Targeting CXCL16 and STAT1 augments immune checkpoint blockade therapy in triple-negative breast cancer. *Nature Communications 2023 14:1* **14**, 1–17 (2023).
335. Anfray, C., Ummarino, A., Andón, F. T. & Allavena, P. Current Strategies to Target Tumor-Associated-Macrophages to Improve Anti-Tumor Immune Responses. *Cells* **9**, (2020).
336. Linde, N. *et al.* Vascular endothelial growth factor-induced skin carcinogenesis depends on recruitment and alternative activation of macrophages. *J Pathol* **227**, 17–28 (2012).
337. Qian, B. Z. *et al.* CCL2 recruits inflammatory monocytes to facilitate breast-tumour metastasis. *Nature* **475**, 222–225 (2011).
338. Lim, G. Y. *et al.* IFI16/Ifi202 released from breast cancer induces secretion of inflammatory cytokines from macrophages and promotes tumor growth. *J Cell Physiol* **238**, 1507–1519 (2023).
339. Wee, W. K. J. *et al.* Single-cell analysis of skin immune cells reveals an Angptl4-ifi20b axis that regulates monocyte differentiation during wound healing. *Cell Death & Disease 2022 13:2* **13**, 1–9 (2022).
340. Dinesh, R., Hahn, B. H., La Cava, A. & Singh, R. P. Interferon-inducible gene 202b controls CD8+ T cell-mediated suppression in anti-DNA Ig peptide-treated (NZB × NZW) F1 lupus mice. *Genes & Immunity 2011 12:5* **12**, 360–369 (2011).
341. Leonardi, G. C. *et al.* Cutaneous melanoma: From pathogenesis to therapy (Review). *Int J Oncol* **52**, 1071–1080 (2018).
342. Wai, P. Y. & Kuo, P. C. The role of Osteopontin in tumor metastasis. *J Surg Res* **121**, 228–241 (2004).
343. Van Den Steen, P. E., Husson, S. J., Proost, P., Van Damme, J. & Opdenakker, G. Carboxyterminal cleavage of the chemokines MIG and IP-10 by gelatinase B and neutrophil collagenase. *Biochem Biophys Res Commun* **310**, 889–896 (2003).
344. Dankort, D. *et al.* A new mouse model to explore the initiation, progression, and therapy of BRAFV600E-induced lung tumors. *Genes Dev* **21**, 379–384 (2007).
345. González-Sánchez, E. *et al.* Lkb1 Loss Promotes Tumor Progression of BRAFV600E-Induced Lung Adenomas. *PLoS One* **8**, (2013).
346. Zhou, Y. *et al.* Metascape provides a biologist-oriented resource for the analysis of systems-level datasets. *Nat Commun* **10**, (2019).